CLASSIFICATION [redacted] CANCELLED

N63-20524

Copy 27 (26)

NASA TM X-28

See attached letter

NASA TM X-28

TECHNICAL MEMORANDUM

X-28

DESIGN ANALYSIS OF A SUBSONIC NUCLEAR-POWERED LOGISTIC AIRPLANE WITH HELIUM-COOLED REACTOR

By R. H. Cavicchi, H. H. Ellerbrock, E. W. Hall, H. J. Heppler, J. N. B. Livingood, and F. C. Schwenk

Lewis Research Center
Cleveland, Ohio

OTS PRICE

XEROX $ 16.00

MICROFILM $ 7.70

RESTRICTED DATA

THIS DOCUMENT CONTAINS RESTRICTED DATA AS DEFINED IN THE ATOMIC ENERGY ACT OF 1954. ITS TRANSMITTAL OR DISCLOSURE OF ITS CONTENTS IN ANY MANNER TO AN UNAUTHORIZED PERSON IS PROHIBITED.

Declassified 1-24-1963

UMENT - TITLE UNCLASSIFIED

g the National Defense of the United States within the meaning s. 793 and 794, the transmission or revelation of which in any manner to an unauthorized person is prohibited by law.

NATIONAL AERONAUTICS AND SPACE ADMINISTRATION

WASHINGTON October 23, 1959

CL[redacted] CANCELLED

CLAS[redacted]ED

THIS DOCUMENT CONSISTS OF 251 PAGES
NO. 27 OF 360 COPIES, SERIES A

E-288

This document released to Category C-84, Reactors-Special Features of Aircraft Reactors; and C-85, Reactors-Aircraft Nuclear Propulsion Systems (M-3679, 23rd Ed.)

[redacted]
Declassified 1-24-1963

DATA AS DEFINED IN THE ATOMIC ENERGY ACT OF 1954. ITS TRANSMITTAL OR DISCLOSURE OF ITS CONTENTS IN ANY MANNER TO AN UNAUTHORIZED PERSON IS PROHIBITED.

CLASSIFICATION [redacted]LED

SECRET
Declassified 1-24-1963

E-288

TABLE OF CONTENTS

	Page
SUMMARY	1
INTRODUCTION	2
SYMBOLS	3
GENERAL REQUIREMENTS	6
GENERAL ASSUMPTIONS AND TYPICAL AIRPLANE	8
AIRPLANE	11
Analysis	12
Effect of Design Flight Conditions and Landing Speed	12
Design flight Mach number	13
Design flight altitude	13
Design landing speed	14
Effect of Airplane Gross Weight	14
Effect of Design Aspect Ratio	16
Effect of Crew Dose Rate	16
ENGINE	17
Selection of Engine Design Parameters	17
Effect of Engine Design Parameters on Component Weights	19
Effect of turbine-inlet temperature	19
Effect of compressor pressure ratio	20
HEAT EXCHANGERS, PUMPS, AND LINES	20
Heat Exchanger	21
Materials considerations	21
Type of heat exchanger	21
Heat exchanger for typical airplane	22
Effect of compressor pressure ratio	23
Helium Pumps	23
Helium Lines	24
REACTOR	25
Considerations Leading to Selection of Reactor	25
Design Procedure	26
Fuel Element	27
Materials	27
Shape	28
Analytical methods used in design	29
Tube design	29

Declassified 1-24-1963
SECRET

Declassified 1-24-1963

Page

Core and Reflector 32
Preliminary nuclear characteristics 32
Core-structure nuclear effects 32
Final nuclear characteristics 33
Power and uranium distributions 35
Moderator characteristics 37
Reflector characteristics 37
Thermal Shields and Pressure-Shell Characteristics 38
Control 40
Poisoning effects 40
Temperature effects 42
Fuel burnup 43
Control rods 43
Reactor Structure 45
Core structure 45
Reflector structure 46
Thermal shields and pressure-shell structure 47
Control-rod structure 47
Reactor Assembly and Stresses 48

BIOLOGICAL SHIELD 49
Primary Biological Shield 49
Additional Shielding Required for Streaming Through Ducts and for Voids 52
Additional Weight Required to Provide for Shield Cooling 52
Adjustment of Primary Shield Weight for the Typical Airplane . . . 52
Total Shield and Reactor Weight 52
Structural Features 53
Construction 53
Mounting in fuselage 53

AIRPLANE OPERATION 54
Propulsion-System Control 54
Startup and Shutdown Procedure 55
Off-Design Performance 56
Performance at various altitudes 57
Takeoff and climb 57
Emergency range 58

FABRICATION AND DESIGN FEATURES 59

CONCLUDING REMARKS 60

APPENDIXES

A - AIRPLANE AERODYNAMIC PERFORMANCE AND STRUCTURAL WEIGHT 62

B - ENGINE DESIGN AND WEIGHT 73

E-288

Declassified 1-24-1963

Declassified 1-24-1963

Page

C - HEAT EXCHANGER, HEADERS, AND LINES 76

D - AXIAL-FLOW HELIUM PUMP 84

E - ANALYSIS OF TEMPERATURE DISTRIBUTION AND PRESSURE DROP IN FUEL ELEMENTS AND MODERATOR BLOCKS 91

F - ANALYSIS OF STRESSES IN FUEL ELEMENT AND MODERATOR BLOCK . . 109

G - ANALYSIS OF NUCLEAR CRITICAL REQUIREMENTS 125

H - ANALYSIS OF SIDE-REFLECTOR, THERMAL-SHIELD, AND PRESSURE-SHELL TEMPERATURES 132

I - REACTOR COMPONENTS AND ASSEMBLY PROCEDURE, By D. W. Drier . 140

J - REACTOR BIOLOGICAL SHIELD 146

K - ADDITIONAL SHIELD WEIGHTS TO COMPENSATE FOR DUCTS 159

REFERENCES 161

TABLES 165

FIGURES 177

E-288

Declassified 1-24-1963

Declassified 1-24-1963

NATIONAL AERONAUTICS AND SPACE ADMINISTRATION

TECHNICAL MEMORANDUM X-28

DESIGN ANALYSIS OF A SUBSONIC NUCLEAR-POWERED LOGISTIC AIRPLANE WITH HELIUM-COOLED REACTOR*

By R. H. Cavicchi, H. H. Ellerbrock, E. W. Hall, H. J. Heppler, J. N. B. Livingood, and F. C. Schwenk

E-288

CA-1

SUMMARY

A detailed design analysis of a nuclear-powered turboprop logistic airplane with a helium-cooled reactor was made to determine how the nuclear and engine components might look, whether any unforeseen difficulties might arise in the design, and what research is most needed to support such a system. A 400,000-pound-gross-weight airplane designed for 0.72 flight Mach number at 30,000 feet was selected as the reference airplane. The resulting wingspread and fuselage length are 250 and 175 feet, respectively; and reactor power of 98.5 megawatts is required. Chemical fuel is provided for thrust augmentation for takeoff, landing, and emergency use. For emergency, part of the neutron shield is assumed to be chemical fuel. Each of eight 4600-horsepower turboprop engines required is supplied with air at 1800° R turbine-inlet temperature from its separate heat exchanger. Mounted in the wings, the heat exchangers receive helium at 2250° R from the reactor. A helium pump, absorbing about 24 percent of the engine power, is required with each heat-exchanger unit.

The airplane can be either logistic (carrying passengers and/or freight) or patrol type. A unit shield designed to limit the dose rate in the crew compartment to 0.025 rem per hour is provided. This limit allows approximately 40 hours of flight every 2 weeks. On the basis of the assumptions of the analysis, the following weight breakdown seems reasonable: Aircraft structure, 108,000; equipment, 22,000; powerplants, 83,000; shield and reactor, 120,000; payload, 63,000; and chemical fuel for takeoff and landing, 4000 pounds. The heat-exchanger temperature limits the performance. Research on the reactor (especially the fuel elements), the heat exchangers, the pumps, and the helium leakage problem is required.

*Title, Unclassified.

RESTRICTED DATA
Declassified 1-24-1963

THIS DOCUMENT CONTAINS RESTRICTED DATA AS DEFINED IN THE ATOMIC ENERGY ACT OF 1954. ITS TRANSMITTAL OR DISCLOSURE OF ITS CONTENTS IN ANY MANNER TO AN UNAUTHORIZED PERSON IS PRO-

Declassified 1-24-1963

Declassified 1-24-1963

INTRODUCTION

The direct-air, liquid-metal, and circulating-fuel reactor cooling systems for aircraft nuclear powerplants have been under investigation for several years. However, studies of the gas-cooled reactor in a closed cycle have mainly been limited to cycle analyses. As a gaseous coolant, helium is very attractive because it is inert and has excellent properties for heat transfer. Analysis of the performance of direct-air, liquid-metal, and helium-cooled systems for supersonic, turbojet-powered, logistic aircraft indicates that helium compares very favorably with the other systems (ref. 1). However, no known detailed study was available on which to base many of the assumptions that were required in this analysis. Therefore, it was decided to make a more detailed design study of a helium-cooled aircraft nuclear powerplant to determine how the components might look, whether any unforeseen difficulties might arise in the design, and what research is needed most to support a system of this kind.

E-288

The choice of airplane type lay between a supersonic airplane and a subsonic airplane that may have less value but would be considerably easier to design and operate. The power requirements for a supersonic airplane are several times those of a subsonic airplane so that the weights and performance of the power system are much more critical in a supersonic design. The first nuclear-powered airplane, regardless of the type, will have many problems that cannot now be anticipated in the design. Accordingly, a conservative approach appeared to be justified, and a subsonic airplane was selected for the design analysis.

For subsonic speeds, unless speeds near Mach 1 are required, the turboprop engine is much more efficient than the turbojet engine (see ref. 2). Furthermore, the turboprop engine and propeller characteristics provide increasing thrust with decreasing speed, so that, if the engine lacks sufficient power to fly at the design speed, flight may still be possible at a lower speed. The characteristics of the turbojet engine, however, are such that it would be in more serious trouble under similar conditions. In addition, the turboprop has better takeoff characteristics. Therefore, the turboprop engine was selected for the nuclear-powered airplane of this study.

The present analysis is a design study of the airplane and the various components, rather than a cycle study of the effects of changing various parameters. In most instances the parameters are arbitrarily

Declassified 1-24-1963

Declassified 1-24-1963

chosen and in only a few cases are the effects of changing these parameters investigated. The report is divided into discussions of the major airplane components, and the effects of changes in design or operating conditions investigated are discussed in connection with each component.

All methods used to calculate performance are reported in appendixes. Whenever existing methods are available, they are referenced. In many cases these methods are extended or revised to fit the conditions of this analysis. In some cases they are generalized to cover a wider range of conditions; these general analyses are included in the appendixes. The reactor components and assembly procedure are described in appendix I, by D. W. Drier.

E-288

CA-1 back

SYMBOLS

The following symbols are used in the body of this report:

A_T	turbine frontal area, sq ft
AFD1,2,3,4	annular flow dividers
AR1,2,3,4	annular reflectors
AS	annular support
AS1,2,3,4,5,6	annular shields
D	airplane drag, lb
d	reactor core diameter, in.
E	energy, ev
F	net jet thrust, lb
FS1,2,3,4,5	front support shields
HP	shaft horsepower
ISP1,2,3,4,5	inner shield plates
k_{eff}	effective multiplication factor
LCFPP	low cross-section fission products poison
l	reactor core length, in.

Declassified 1-24-1963

Declassified 1-24-1963

M_0	flight Mach number
OSP1,2	outer shield plates
P	helium pressure, lb/sq ft
p_o	equilibrium poison (during operation)
p(t)	poisoning at time t (during operation)
Q	volumetric heat source, Btu/(sec)(cu in.)
RAS1,2,3,4,5	rear annular shields
RS1,2,3,4	rear shields
T_a	temperature of inner cladding surface of circular hole through fuel element (see fig. 25), °R
T_d	temperature of cladding surface at inner radius of annular passage through fuel element (see fig. 25), °R
T_e	temperature of moderator block surface at outer radius of annular passage through fuel element (see fig. 25), °R
T_f	temperature at outer boundary of moderator block (see fig. 25), °R
T_{He}	temperature of helium, °R
T_m	maximum temperature of fuel-element meat, °R
t	time, sec
V_r	uranium volume content per unit volume of compound
W	weight, lb
w_a	rate of airflow through engine, lb/sec
w_{an}	rate of helium flow in annular passage through fuel element, lb/sec
w_{He}	rate of helium flow through reactor, lb/sec

Declassified 1-24-1963

Declassified 1-24-1963

E-288

w_h	rate of helium flow in circular passages through fuel element, lb/sec
Xe_o	xenon concentration at equilibrium, nuclei of xenon/(sec)(cu cm)
γ	fission yield
δk	reactivity
λ	decay constant, sec^{-1}
Σ_a	macroscopic absorption cross section, cm^{-1}
Σ_f	macroscopic fission cross section, cm^{-1}
σ_a	microscopic absorption cross section, barns
σ_f	microscopic fission cross section, barns
φ_o	equilibrium neutron flux, neutrons/(sec)(cm^2)
φ_r	relative neutron flux, neutrons/(sec)(cm^2)
$\varphi_{1,2,3,4,5,6}$	neutron flux for group 1, 2, 3, 4, 5, and 6, neutrons/(sec)(cm^2)
ψ	turbine blade metal taper factor

Subscripts:

D	decalin
eq	equipment
G	gross
I	iodine 135
n	neutron shield
P	payload
Pm	promethium 149
pp	powerplant
R	reactor

Declassified 1-24-1963

Declassified 1-24-1963

S	shield
st	structure
t	total
th	thermal
U	uranium 235
Xe	xenon 135
γ,i	inner gamma shield
γ,o	outer gamma shield

Superscript:

FPP	fission products poison

GENERAL REQUIREMENTS

The mission for which this nuclear-powered airplane is considered is logistic, for carrying heavy loads of either equipment or personnel over long distances. The increase in thrust with decrease in flight speed of the turboprop engine chosen for the airplane provides a performance margin that would be available if required. Thus, if the engine is designed for a fairly high subsonic flight Mach number, flight might still be possible at a reduced speed if less than design power is available from the engine or more than design power is required for the airplane. The design flight Mach number for this mission is therefore 0.70 or higher. From considerations of desired Mach number, wing loading, and ambient air temperature, the design altitude was arbitrarily selected early in the investigation as 30,000 feet. Later, the effects of changing design altitude were investigated. The results are included in a later discussion.

The characteristics of the nuclear-powered airplane and shield are such that the payload fraction of the gross weight increases rapidly with increasing gross weight for airplanes near the size and weight of existing ones. Nevertheless, in spite of the increased carrying efficiency with increased size, it is desirable to limit the size and weight to even less than those of some existing airplanes, provided that at least a reasonable payload can be carried. Larger gross weights would seriously limit the number of fields from which the airplane can operate; and, with the usual growth factors that accompany the design and use of an airplane, the gross weight would become prohibitive. Furthermore, in keeping with the conservative approach, more knowledge is available for

Declassified 1-24-1963

Declassified 1-24-1963

the design and construction of airplanes within the existing size class. For these reasons the design gross weight is to be kept under 400,000 pounds if a payload of the order of 50,000 to 100,000 pounds can be carried.

For similar reasons, the engine size is kept within the size of existing engines. Although this probably results in more engines on the airplane than is generally desirable, the reliability obtained from engines within the existing size class probably more than offsets the disadvantages of multiengine installations. Engine size is based on the sea-level airflow. A value of 140 pounds per second at standard sea-level conditions was chosen as the maximum allowable airflow for an engine. For the assumed turbine-inlet temperature (1800° R), this airflow limit ensures that shaft power will not exceed 5900 horsepower. For a 400,000-pound airplane with the speed and altitude considered, this limitation in size results in a requirement of eight engines.

E-288

Except for the reactor, the heat exchangers are probably the most critical items in the airplane. The maximum turbine-inlet temperature of the engines is limited by the heat exchangers to considerably less than that employed in some existing engines. The engines then are conservatively designed with respect to turbine-inlet temperature, which should contribute to their reliability.

The payload-carrying ability of the airplane might also be increased by using a lighter-weight divided shield rather than a unit shield. However, because of the increased radiation in the cargo compartment, its use would seriously restrict the usefulness of the airplane by limiting the payload to materiel or equipment and by complicating the transfer or loading operations and the airplane and engine maintenance and overhaul procedures. Since not enough is known about handling procedures, it was decided to concentrate on a unit shield.

Some proposals for nuclear-powered airplanes are based on the use of two reactors to improve the safety. Providing the airplane with twice the power required to fly it imposes a serious penalty, since the two reactors must be independent; that is, each must be capable of critical operation without the other, and this results in increased shield weight. When power in only one of the reactors is inadequate to fly the airplane, sustained flight would be possible only by using chemical fuel to provide the additional heat to the air.

A more reliable system for the same weight, but which possibly provides less emergency range, is obtained by eliminating the second reactor and shield and replacing them with an equivalent weight of chemical fuel. There are probably many instances, and perhaps even whole flights, where flight on chemical fuel alone is desirable (e.g., takeoff or landing, training, ferrying, etc.). Furthermore, this chemical fuel could replace

Declassified 1-24-1963

Declassified 1-24-1963

part of the reactor shield, because, if the reactor were shut down, full reactor shielding would no longer be necessary. Because of the added complication of two-reactor design and operation, a single reactor is used in this airplane, and chemical fuel is used for emergency flight. The amount of emergency fuel is limited to that required in the reactor shield. Some additional chemical fuel is provided for takeoff and landing.

It would, of course, be desirable to have to refuel the reactor as infrequently as possible. Refueling will involve dismantling the reactor and shield and removing many radioactive components from the reactor. This operation should be avoided as much as possible. On the other hand, designing for a large fuel burnup not only makes the design more difficult, but also leads to more uneven power distributions and therefore more severe operating conditions. Since the reactor, like the other airplane components, should be inspected within reasonable intervals to forestall any failure, an operating time of about 1000 hours at full power was selected as the burnup time for the fuel elements. On a structural basis the reactor lifetime was taken as a minimum of 10,000 hours. Although the reactor would probably not be operated for this length of time (10 refuelings), this tends to provide some margin of safety from a structural standpoint.

The missions to which this airplane is best suited are exceptionally long range, perhaps beyond those normally possible with chemically fueled airplanes. If a total range of 16,000 nautical miles is assumed, the trip would require about 40 hours. One large unknown is the waiting and turnaround time; but, if it is further assumed that one such trip could be made every 9 days to 2 weeks, then about 30 to 50 weeks would elapse between refuelings of the reactor. Therefore, it is estimated that the reactor should be refueled once each year, after it has operated about 1000 hours and has flown about 400,000 nautical miles.

Although the calculation of crew dose rates is an uncertain procedure at the present time, an attempt was made to calculate the shield requirements, and a choice of allowable dose rates was therefore necessary. For an assumed dose rate of 600 millirems per week, which is double the allowable laboratory dose rate of 300 millirems per week, the previously assumed 40 hours of flight every 9 days to 2 weeks results in an allowable dose rate during flight of between 20 and 30 millirems per hour. For the present case a dose rate of 0.025 rem per hour was assumed.

GENERAL ASSUMPTIONS AND TYPICAL AIRPLANE

Throughout this study many arbitrary assumptions had to be made because there was insufficient time to investigate all parameters and combinations of parameters. Thus, even though the effects of varying many

Declassified 1-24-1963

Declassified 1-24-1963

conditions were studied, it was necessary to set standard or reference conditions fairly early in the investigation in order to establish a basis for comparison and to study in greater detail the design of the reactor and the heat exchanger. Considerably more effort was therefore spent on the design of this reference airplane than on any other; however, this should not be taken to mean that the design and the operating conditions for this particular airplane are considered superior to others that may or may not have been investigated. In fact, later analyses showed improved performance for other values of several parameters.

E-288

Because the design is considered to be fairly representative of the type of airplanes and conditions investigated, this reference airplane will hereafter be referred to as the typical airplane. The principal assumptions, specifications, and operating conditions for this typical airplane are given in table I. The weight breakdown of the various components is given in table II. An artist's sketch of the airplane is presented in figure 1, and a picture of a model showing the location and arrangement of equipment is presented in figure 2. The general over-all picture of the design and performance of the typical airplane is presented here in order to provide orientation for later discussions of the various components.

CA-2

The airplane is a conventional subsonic type with control surfaces on the tail in the rear. The reactor and shield are housed in the rearward part of the fuselage, with helium lines running through the wings to eight heat exchangers located in the wings, each directly over an engine. Eight turboprop engines are located on the underside of the wings. The engine and heat-exchanger layout is shown in figure 3. Air is collected behind the engine compressor, ducted upward and through the heat exchanger in the wing, then through an afterburner-type combustor, and thence down and is delivered to the turbine. No fuel is burned in the combustor during normal operation, but the combustor is provided to allow for emergency or off-design operation. An afterburner-type combustor is used so that very small pressure losses will be incurred. Therefore, air can be passed through the combustor at all times and no bypass ducting or valving need be provided.

By locating the heat exchangers in the wings away from the engines, the engines can be dismounted or changed without disrupting the helium system by disconnecting the air ducts and helium-pump drive shafts. The helium pump is located beside the heat exchanger and driven from the engine shaft. The helium lines between the heat exchanger and reactor are concentric, with the hot line coming from the reactor located inside the annular passage carrying the cooled helium back to the reactor. Heat transfer between the passages is reduced by using a multiple-walled duct with a corrugated inner wall between two smooth outer walls. A sketch of the inner pipe showing the corrugations between the two walls is shown in figure 4.

Declassified 1-24-1963

Declassified 1-24-1963

Each engine has a sea-level airflow of about 110 pounds per second (which is below the limit of 140 lb/sec established previously) and a sea-level shaft power (including helium pump power) of 4600 horsepower at the rated turbine-inlet temperature of 1800° R. Six engines could be used if engines were available having a sea-level airflow of about 150 pounds per second and a shaft power of over 6000 horsepower. Temperatures higher than 1800° R could be used in the engine except for the added difficulty in the design of the heat exchanger. The engine is a one-spool type with the propeller, helium pump, and compressor all driven by one turbine with three stages. The compressor has 11 stages and a design-point pressure ratio of 11, which was selected on the basis that this is the highest value that can be obtained practically in a one-spool engine.

E-288

The reactor is of two-pass construction, having a flow divider surrounding the core. An outline of the reactor is shown in figures 5 and 6 (plan views) and 7 (which is section C-C of fig. 5). Helium enters the reactor through the shield at the rear face, passes through the reflectors and thermal shields for cooling, then reverses and flows through the core containing the fuel elements and moderator, and thence back out the rear face of the reactor in the center of two concentric helium ducts. Figures 8 and 9 show closeup pictures of the reactor pressure shell in the airplane model with the external shield indicated.

The reactor was originally designed on the basis of 100 megawatts of heat given up to the coolant. Later it developed that about 98.5 megawatts were required at the design point. Helium enters the reactor at 1250° R (pump outlet temperature), is heated to about 1300° R in cooling the reflector and shields, and is further heated to the final temperature of 2250° R in the core. The helium pressure entering the reactor is assumed to be 180,000 pounds per square foot. A total-pressure loss of 4 percent was assumed for the helium in passing through the reactor; of this loss, 2.6 percent occurs in the core.

The fuel elements consist of tubes containing a total of 153.2 pounds of uranium carbide UC (129.7 lb U^{235}) in a molybdenum matrix with a molybdenum cladding both inside and outside. Helium flows both inside the tube and outside through the annulus between the tube and the moderator. The moderator consists of hexagonal blocks of beryllium oxide. Molybdenum is used as the supporting structure for the core. The side-reflector material is assumed to be beryllium metal, and the end reflector beryllium oxide. The thermal shields and pressure shell are made of mild steel and type 347 stainless steel, respectively. The outside diameter of the pressure shell is about 64 inches. Further details of the reactor are given in a later section.

There are 13 control rods of the following types located as shown in figure 7: two regulating rods, six shim rods, three shim-safety rods, and two scram rods. The six shim rods are placed in three pairs, each

Declassified 1-24-1963

Declassified 1-24-1963

pair operated so that the two rods move in opposite directions with a variable loading in each rod, thus tending to maintain an undistorted axial flux distribution. The six shim and two regulating rods are actuated by electric motors. The three shim-safety rods are hydraulically operated, and the two scram rods are pneumatically operated.

The biological shield (see figs. 8 and 9) surrounding the pressure shell consists of an inner gamma shield of iron or borated steel and an outer neutron shield consisting of lithium hydride and decalin (used for emergency chemical fuel) located as shown in the figures. Tanks of decalin are also used to reduce duct streaming. Chemical fuel for use in takeoff and landing is stored in tanks in the wings; the shielding decalin is used for emergency only.

E-288

The payload is considered to consist of two parts: one part having a high density, such as materiel or equipment, and the other part having a low density, such as personnel or very bulky but lightweight objects. The high-density part is located near the center of gravity of the airplane just ahead of the reactor and shield. Ahead of this is located the compartment that carries the low-density payload. Figure 1 shows the airplane equipped with two decks of seats in the low-density compartment arranged for carrying personnel.

CA-2 back

For the assumed 400,000-pound airplane, the aircraft structure weighs about 108,000 pounds or 27 percent of the gross weight. In addition, there are 22,000 pounds or about 5 percent for equipment weight, which includes the crew, instruments, and so forth. The powerplant system, including the engines, heat exchangers, lines, and so forth, weighs about 83,000 pounds or 21 percent of the gross weight. Of this weight about one-third is attributed to the heat exchangers and lines. Four thousand pounds of chemical fuel for takeoff and landing are contained in tanks in the wings. The reactor and shield weigh 120,000 pounds or 30 percent. The remaining weight is available for a payload of 63,000 pounds.

AIRPLANE

Only a cursory analysis was made before the design conditions for the typical airplane were selected. During the time that the typical airplane was being studied in detail, analyses were made to determine to what extent the typical airplane payload could be increased through the choice of different design conditions for the airplane and its components. In the case of certain of the design conditions, it was possible to incorporate better choices into the typical airplane design without disturbing previously completed work; however, most of the design conditions remained fixed at the initially assumed values. This section presents the results of the design-point studies that are related to the performance of the airplane.

Declassified 1-24-1963

Declassified 1-24-1963

Analysis

The lift-drag ratios were computed by conventional methods. These are described in appendix A along with the methods for determining the structural weights. As mentioned in appendix A, structural weights depend on the distribution of the loads between the wing and fuselage. Consequently, the variation of structural weight with the load distribution was calculated and plotted for each airplane geometry. These curves were used to determine the structural weight after calculations of the weights of the components attached to the wings (engines, nacelles, heat exchangers, lines, and wing-mounted landing gear) were completed. Methods for calculating component weights are given in the appendixes. Payload is defined as the portion of the gross weight W_G remaining after all component and structure weights are accounted for.

The results of the analyses are presented as the variation of component weights and payload with one particular design variable, as in figure 10. All other conditions remain fixed at the values selected for the typical airplane. The airplane weights are divided into four main categories: (1) structure and equipment weight W_{st+eq}, including crew, instruments, and controls; (2) powerplant weight W_{pp}, including engines, nacelles, propellers, heat exchangers, lines, gearboxes, and helium pumps; (3) reactor and shield weight W_{R+S}; and (4) payload weight W_P.

Part of the shield consists of a chemical fuel that would be available for use in the combustors for emergency operation (reactor shutdown). The weight of the fuel portion of the shield W_D is also indicated in figure 10, since this quantity determines the endurance under emergency conditions. The emergency flight duration is discussed later.

A small amount of fuel (1 percent of gross weight) to be used during takeoff and climb is allowed for and is shown in the figures ($W_{D,climb}$). This fuel is not part of the reactor shield; therefore it is accounted for apart from the emergency fuel supply.

Effect of Design Flight Conditions and Landing Speed

As mentioned previously, it was decided that the airplane should be designed for flight at a Mach number greater than 0.70 and at an arbitrarily assigned altitude of 30,000 feet. Some preliminary calculations indicated that an airplane of 400,000-pound gross weight would require approximately 100 megawatts of reactor power for these flight conditions. Accordingly, reactor calculations and design were based on this power output. More refined airplane performance calculations showed that the required reactor power would be 98.5 megawatts at a flight Mach number of 0.72.

Declassified 1-24-1963

Declassified 1-24-1963

The effects on payload of variations in both the design Mach number and altitude (each independently) were studied. An intrinsic factor in these variations is the constraint placed on the design wing area by the allowed landing speed and lift coefficient at landing. For the typical airplane, the landing speed was set at 175 feet per second, and the lift coefficient at landing was 1.75. These two values remained constant during the studies of the effects of design altitude and Mach number. In fact, the landing-speed requirement instead of the flight condition established the wing area for most of the cases studied. The effects of varying landing speed are also presented.

E-288

Design flight Mach number. - The effects of variations in design flight Mach number on the component and payload weights are shown in figure 10. There is a decrease in payload from 93,000 to 8000 pounds as the Mach number is increased from 0.60 to 0.85. It appears that the greatest payload could be carried at a design Mach number somewhat less than 0.60. At the design Mach number for the typical airplane (0.72), the payload is about 63,000 pounds.

The decrease in payload is due to an increase in powerplant and reactor and shield weights. These weights depend on the required power, which increases from 74 to 138 megawatts as the Mach number varies from 0.60 to 0.85. The increase in required power can be traced to two causes. First, even with a constant drag, the power required varies directly with flight speed. Second, the airplane drag increases with increasing Mach number, because the wing area cannot be decreased. Wing area is specified by the landing conditions and not by flight Mach number in these cases. Consequently, at 30,000 feet and in the Mach number range considered, the lift-drag ratio is never optimum. Lift-drag ratio decreases from 22.8 to 15.7 as the Mach number changes from 0.60 to 0.85. At a higher altitude the situation would be modified, because an increase in altitude requires an increase in the wing area for optimum lift-drag ratio.

Design flight altitude. - The effect of changing design altitude, at a flight Mach number of 0.72, on the weights of the airplane components is shown in figure 11. The large variation in powerplant weight with changes in altitude is a result of several effects. The maximum lift-drag ratio (minimum thrust and power) occurs at an altitude of approximately 40,000 feet. However, because of higher air density at lower altitude, the engine weight is a minimum at 30,000 feet. Minimum heat-exchanger weight occurs at 35,000 feet. As a result, the total weight of the powerplant (which consists of engines, nacelles, heat exchangers, manifolds, pumps, and helium lines) is minimum at 35,000 feet. The lowest reactor and shield weight occurs at the altitude for minimum reactor power (40,000 ft) in spite of the reduction of air-scattered dose rate at higher altitudes. A maximum payload of nearly 70,000 pounds

Declassified 1-24-1963

Declassified 1-24-1963

occurs at an altitude of just above 35,000 feet compared with a payload of 63,000 pounds for the 30,000-foot design altitude selected for the typical airplane.

The optimum altitude (maximum payload) depends, of course, on the design flight speed. Maximum payload would occur at a lower design altitude if a lower design speed were selected. Performance for simultaneous variations in design speed and altitude was not determined.

Design landing speed. - Figure 12 shows the variation with design landing speed of the weights of the airplane components for a design altitude of 30,000 feet and a design Mach number of 0.72. The range of landing speeds presented varies from 140 to 250 feet per second. Design landing speed for the typical airplane was 175 feet per second.

The payload increases from 25,000 pounds at a design landing speed of 140 feet per second to a maximum of 82,000 pounds at a design landing speed of 230 feet per second. For the range of landing speeds shown in figure 12, wing area depends on landing speed and not the flight conditions. Therefore, structure weight decreases with increasing landing speed. The maximum design lift-drag ratio occurs at a landing speed of 220 feet per second; and, at the same speed, the weights of the powerplant, reactor, and shield are a minimum.

For a design landing speed of 250 feet per second or more, the wing area is determined by the design flight conditions. Therefore, no further variations in the component weights with landing speed will occur for speeds above 250 feet per second.

Effect of Airplane Gross Weight

The effects of changing the airplane design gross weight on the component weights are shown in figure 13. Flight conditions were taken at the typical values of Mach number (0.72) and altitude (30,000 ft). As might be expected, the sum of the powerplant and structure weights is nearly a constant fraction of gross weight. At a gross weight of 300,000 pounds, the structure, equipment, and powerplant account for 53.6 percent of the gross weight. These items represent 55.2 percent of an 800,000-pound airplane. Specifically, the powerplant weight decreases from 21 to 20 percent, the equipment weight decreases from 6.3 to 4.2 percent, and the structure weight increases from 26 to 31 percent of gross weight as the gross weight increases from 300,000 to 800,000 pounds.

As a consequence of these variations, the sum of the reactor, shield, and payload weights is also nearly a constant fraction (45 percent) of the gross weight. The weights of these items increase from 136,000 to

Declassified 1-24-1963

Declassified 1-24-1963

348,000 pounds for the range of airplane gross weights shown in figure 13. Compared with this large variation, the reactor and shield weight varies only a small amount with gross weight. Of course, the reactor and shield weights depend on the power and on the crew-reactor separation distance, which are related to gross weight.

The methods used for calculating reactor and shield weights as a function of power and of crew-reactor separation distance are presented in detail in appendix J. Very briefly, the reactor core length was maintained constant, the core frontal area was assumed to be proportional to the power, and reflector and thermal-shield thicknesses were held constant. Based on these assumptions, the fuel-element - moderator-block geometry will not depend on reactor power, and the number of fuel elements will vary directly with power. In addition, it is expected that the amount of U^{235} required for each fuel element will not vary significantly with power; however, no calculations were made to determine fuel loadings for the large-size reactors.

E-288

An increase in gross weight from 300,000 to 800,000 pounds requires a change in reactor power from 86.5 to 182.4 megawatts. The associated increase in reactor and shield weight is from 110,000 to 146,000 pounds, which is a decrease in the fraction of gross weight from 37 to 18 percent. The net result is that the payload increases from 28,000 to over 200,000 pounds for the gross-weight variation considered. However, the percentage of gross weight available for payload changes from 9.5 to over 25 percent. This result illustrates a fundamental characteristic of nuclear-powered aircraft, that a large increase in payload-carrying efficiency results from an increase in gross weight of the airplane.

In the selection of design gross weight for a logistic airplane, some consideration should be given to the growth potential of the airplane. The gross weight of many airplanes designed in the past has grown by as much as 30 percent of the initial weight. The growth in gross weight has usually been accomplished without increasing the structural weight of the airplane, through redesign and refinement of the structure. Therefore, as the airplane structure is developed, an increase in gross weight results in a large increase in payload-carrying ability. Such improvements are greater than the variations of payload with design gross weight shown in figure 13.

It is expected that a similar growth potential exists for nuclear-powered aircraft. Therefore, in order to take advantage of the improvements mentioned, the design gross weight of the typical airplane was set at 400,000 pounds. At this weight the payload-carrying efficiency is low compared with what could be achieved at the higher gross weights. However, with past experience as an indication, the 400,000-pound airplane would grow in gross weight and payload-carrying ability. The

Declassified 1-24-1963

Declassified 1-24-1963

gross weight of the developed airplane would not be excessive for currently available manufacturing and runway facilities.

The improvements due to structural refinements leading to increased gross weight and payload of particular airplanes in the past have led to an erroneous belief that the same effect could be achieved simply by increasing the design gross weight of the airplane. However, structural improvements are available for any of the initial design gross weights.

If the airplane gross weight is to be increased after design, adequate thrust must be provided for flight with the increased gross weight. Adequate thrust can be provided by designing oversized engines or by operation at other than design flight conditions. In the present typical airplane, added thrust is available at flight speeds below the design Mach number of 0.72. Since the design wing area of the typical airplane is larger than that required for optimum lift-drag ratio, flight at the design altitude of 30,000 feet could be maintained with an increase in gross weight and some decrease in flight Mach number.

Effect of Design Aspect Ratio

The effects of design aspect ratio on the airplane component weights are shown in figure 14 for a range of aspect ratios from 6 to 15. Design aspect ratio for the typical airplane is 10.

The payload maximizes at a design aspect ratio of 8 for this airplane; however, only a small variation of payload with aspect ratio is indicated. The variation in payload is due to several factors. Structural weight increases with increasing aspect ratio. The powerplant and reactor and shield weights decrease with increasing aspect ratio because an increase in aspect ratio improves the lift-drag ratio and effects a decrease in required power.

Since aspect ratio has a relatively small effect on payload and since the heat exchangers can be located in the wings as shown in figure 2, the final choice of aspect ratio may depend on the space required for the heat exchanger.

Effect of Crew Dose Rate

For the typical airplane the total weight of reactor, shield, and payload is 183,000 pounds. A decrease in crew dose rate results in a heavier shield and a correspondingly lighter payload. Figure 15 shows the change in shield and payload weights with a change in crew dose rate. The shield weights shown were calculated according to the methods

Declassified 1-24-1963

Declassified 1-24-1963

given in appendix J. No claim is made for the accuracy of these calculations; the trends, however, are believed correct. A discussion of the calculations is given later.

A tenfold change in crew dose rate from the nominal value of 0.025 rem per hour causes a change in shield weight, and therefore payload weight, of about 35,000 pounds. A decrease in dose rate to the currently allowable laboratory rate of 0.3 rem per week (40-hr week) or 0.0075 rem per hour would require a decrease in payload of 17,000 pounds.

E-288

ENGINE

As indicated in the INTRODUCTION, turboprop engines were chosen for the airplane. This type of engine is well suited for driving the typical airplane, which is designed for 0.72 Mach number at 30,000 feet. The section GENERAL REQUIREMENTS has explained the selection of eight engines to drive the 400,000-pound airplane. A shaft power of 5900 horsepower per engine approximates that obtainable from turboprop engines in current production in the United States (e.g., Pratt & Whitney T34 and Allison T40).

CA-3

In line with the conservative mission selected for the first nuclear aircraft, the engine design was also made conservative. As a consequence, it was felt unnecessary to make detailed designs of the engine components, since the magnitude of their problems should not be great. This section will, however, discuss some of the parameters of the compressor and turbine designs.

Selection of Engine Design Parameters

A range of theoretical turboprop engine designs is presented in reference 3. For flight conditions approximating those of the typical airplane, this reference indicates that a compressor pressure ratio of 11 and a turbine pressure ratio of 9 would yield low specific fuel consumption in a chemically powered engine. Low specific fuel consumption is indicative of high propulsive efficiency. Therefore, it was reasonably expected that a combination of design parameters that result in low specific fuel consumption would likewise result in a requirement of low reactor power.

Preliminary design-point calculations were then made for a compressor pressure ratio of 11 and also for 8 and 15. For the latter two values, turbine pressure ratios of 6.7 and 12 were used, respectively. A turbine-inlet temperature of 1800° R was specified. Figure 16 shows that, although net jet thrust per unit airflow F/w_a decreases, airflow

Declassified 1-24-1963

Declassified 1-24-1963

per unit turbine frontal area w_a/A_T and shaft horsepower per unit airflow HP/w_a both rise with increasing compressor pressure ratio. Higher propulsive efficiency is a further advantage of the higher compressor pressure ratios. On the other hand, pressure ratios greater than about 12 are not considered feasible for a one-spool compressor. On the basis of these considerations, a one-spool compressor with a pressure ratio of 11 was selected for design of the engine of the typical airplane. Subsequent calculations indicate that a value of compressor pressure ratio of 11 yields maximum payload.

E-288

Figure 17 was also used in the preliminary design in selecting the turbine-inlet temperature. This figure shows that F/w_a and w_a/A_T decrease while HP/w_a rises with increasing turbine-inlet temperature. A turbine-inlet temperature of 1800° R was chosen for the typical airplane. Subsequent calculations, discussed later in this section, show that maximum payload is obtainable at 1900° R temperature.

The performance of an experimental eight-stage compressor with a pressure ratio of 10 is presented in reference 4. This reference shows that such a high pressure ratio is obtainable in a one-spool machine that will operate with an adiabatic efficiency of 0.84. This value corresponds to a polytropic efficiency of 0.88 at the pressure ratio of 10. With an equivalent tip speed of 1100 feet per second and an inlet hub-tip radius ratio of 0.48, this experimental compressor had a weight-flow capacity of about 30 pounds per second per square foot of frontal area. The corresponding values for the compressor design of the present report are 1000 feet per second equivalent tip speed, 0.5 hub-tip radius ratio, and 20.9 pounds per second per square foot equivalent weight flow. The compressor tip diameter is 29.4 inches. Eleven conservative compressor stages are required for the pressure ratio of 11. Compressor and turbine design parameters are summarized in table III.

The turbine is designed for 30,000-psi centrifugal stress at the rotor-exit hub radius. This is a conservative value for a turboprop engine because of the low stagnation temperature at the rotor exit (1103° R for the typical airplane). Reference 5 indicates that the life of the turbine blade metal should well exceed 1000 hours.

Use of a design turbine-inlet relative Mach number of 0.6 at the hub radius, 0.6 exit hub-tip radius ratio, the required enthalpy drop of 183.1 Btu per pound, and the tip speed corresponding to 30,000-psi stress result in a requirement of three turbine stages. This determination was obtained with the aid of reference 6. With such conservative design, there should be no difficulty in realizing a turbine polytropic efficiency of 0.85. Turbine tip diameter is 34.9 inches.

Declassified 1-24-1963

Declassified 1-24-1963

The methods of calculating design-point thrust, weight flow, horsepower, and engine component weights are given in appendix B.

Effect of Engine Design Parameters on Component Weights

Effect of turbine-inlet temperature. - The effect of turbine-inlet temperature on airplane component weights is presented in figure 18(a). Design-point flight Mach number, altitude, and compressor pressure ratio were maintained at 0.72, 30,000 feet, and 11, respectively. Of prime interest on this plot is the increase in payload with temperature up to about 1900° R, above which the payload decreases. For the conditions of figure 18(a), reactor power decreases with rising turbine-inlet temperature because of improved cycle efficiency. As shown in figure 18(a), this results in decreasing reactor plus shield weight by about 10 percent over the range studied.

Additional explanation for the payload variation with turbine-inlet temperature is provided by the variation in powerplant weight. Figure 18(a) shows that powerplant weight decreases to a minimum, then increases as turbine-inlet temperature rises. A breakdown of powerplant component weight variation with temperature as presented in figure 18(b) is instructive. Total powerplant weight, according to this figure, is a minimum at about 1880° R. The weight of the engines decreases with rising turbine-inlet temperature because of the decrease in airflow requirements. The increase in heat-exchanger weight with rising temperature has a major effect on powerplant weight. With constant temperature of the helium entering the heat exchanger, in order for turbine-inlet temperature to rise, additional surface area must be provided in the heat exchanger. Furthermore, the resulting higher heat-exchanger wall temperatures as turbine-inlet temperature rises pose a more serious stress problem. The walls must therefore be thicker. These two factors cause heat-exchanger weight to rise continuously with increasing turbine-inlet temperature.

Figure 18(b) thus shows that, up to about 1880° R, the decrease in engine weight offsets rising heat-exchanger weight so that powerplant weight decreases. Above this temperature, the heat exchangers become so heavy that they cause powerplant weight to rise.

Returning to figure 18(a), it will be noticed that structure and equipment weight increases to a maximum at approximately the temperature at which powerplant weight is a minimum. This is to be expected, for as powerplant weight is decreased, the distributed lift forces on the airplane wings cause greater bending moments at the roots of the wings. The structure must be made stronger and thus heavier.

E-288

CA-3 back

Declassified 1-24-1963

Declassified 1-24-1963

The net result of the variations in these airplane component weights with turbine-inlet temperature is that payload is a maximum at approximately 1900° R. At this temperature the payload is 6000 pounds greater than that at the 1800° R temperature used in the final design.

Effect of compressor pressure ratio. - Figure 19(a) presents the effect of varying compressor pressure ratio on airplane component weights. Turbine-inlet temperature remains at 1800° R and flight conditions remain at their design values in this figure. Payload is essentially constant at compressor pressure ratios of 8 and higher. For the conditions of this figure, it can be shown that reactor power decreases as compressor pressure ratio rises because of increases in cycle efficiency. Figure 20 shows that this results in decreasing weight of reactor plus shield.

E-288

Figure 19(a) also shows that powerplant weight decreases to a minimum and then rises as compressor pressure ratio is increased. Variation in powerplant component weights with compressor pressure ratio is shown in figure 19(b). For the conditions of this figure, airflow first decreases and then increases with rising compressor pressure ratio. This accounts for the minimum in the curve of engine weight.

In figure 19(b) heat-exchanger weight decreases with rising compressor pressure ratio up to a value of about 9.5. Further increase in compressor pressure ratio results in heavier heat exchangers. This effect is discussed in the section on heat exchangers.

Reference to figure 19(a) shows that the weight of structure and equipment is essentially insensitive to change in compressor pressure ratio. The previously discussed variations in reactor plus shield and powerplant weights result in little variation in payload above a compressor pressure ratio of about 8. Maximum payload occurs at a pressure ratio of approximately 11.

HEAT EXCHANGERS, PUMPS, AND LINES

In order to deliver the energy developed in the reactor to the turboprop engines, a helium-to-air heat exchanger is required, as well as helium lines, air ducts, and pumps for the helium. Figure 3 shows the arrangement of these components. Each heat exchanger is located close to its engine so that the length of relatively large-diameter air ducts can be made as small as possible. The helium pumping power is extracted from the engine shafts, and there is one helium pump for each engine.

The primary reason for separating the heat exchanger from the engine was to permit engine handling and maintenance without any disruption

Declassified 1-24-1963

Declassified 1-24-1963

of the helium system. In addition, calculations showed that the heat exchangers can be designed to be stowed in the wings as shown in figure 3.

Heat Exchanger

E-288

Materials considerations. - As mentioned previously, the turbine-inlet temperature and helium temperature at the reactor outlet for the typical airplane were set largely by materials limitations in the heat exchanger. Strength and oxidation resistance at high temperatures are required of the material used in the heat exchanger. Some nickel-base alloys are suitable for this application. Figure 21 shows 1000-hour stress-rupture data for a nickel-base alloy. The stress values assumed for the various heat-exchanger designs are also shown in figure 21 at metal temperatures corresponding to the peak temperature in the heat exchanger. Corresponding turbine-inlet temperatures are also indicated (refer to discussion of effects of turbine-inlet temperature in ENGINE section).

Type of heat exchanger. - A shell-and-tube heat exchanger with the helium contained in the tubes was selected for this airplane. On the basis of size and weight considerations, it was also decided to use multiple passes of the helium tubes with counter crossflow of the air-stream. Calculations showed that a four-pass heat exchanger (including shells and structure) was somewhat lighter than a three-pass type and that the resulting size allowed stowage of the heat exchanger in the wings. Circular tubes were chosen for reasons of mechanical strength.

There are many other items to consider in the design of the heat exchanger. Some of these are the size of the tubes, the spacing and arrangement of the tubes, the desirability of finning, the fin material, fin spacing and thickness, and allowable pressure drop in each fluid or gas. In addition, theoretical or empirical relations for the heat-transfer coefficients are required. The calculation of heat-transfer coefficients for flow inside tubes is well established (e.g., refs. 7 and 8); however, the situation is much different for flows across banks of tubes. It appears that the dependence of heat-transfer coefficient and pressure losses on factors such as tube and fin geometry has not been established for all cases. Therefore, it was decided to limit the heat exchangers considered to those specifically given in the compilation of reference 9. Such a decision restricts the study of heat exchangers and prohibits a complete optimization of all variables; however, through the use of empirical heat-transfer and pressure-loss data, the heat exchangers can be accurately designed. Design calculations were done on an IBM 653 computer, as outlined in appendix C.

Declassified 1-24-1963

Declassified 1-24-1963

Finned- and plain-tube heat exchangers were designed for identical conditions in order to determine the value of finning in the application. Figures 48 and 100 of reference 9 provided the geometry and heat-transfer characteristics for the plain-tube and the finned-tube heat exchangers, respectively. It was assumed that the fins and tubes were made from the same alloy. Although the sizes of these two types of heat exchanger were not equal, each type would fit into the wing. It was found that the finned heat exchanger was heavier than the plain-tube type; consequently, the plain-tube heat-exchanger was selected. The simplicity of fabricating a plain-tube heat-exchanger appeared to be an advantage, also. Of course, the use of fins might have proved worthwhile with other fin-and-tube geometries or with fins constructed of a material having a high thermal conductivity such as copper. Copper fins would require oxidation protection for this application, however.

The pressure losses of the air and helium are important in the heat-exchanger design, since the weights of many components are influenced by these quantities. Actually, the selection of optimum pressure losses for the heat-exchanger requires a complete analysis of the airplane system, because the helium and air pressure losses affect heat-exchanger weights, engine and nacelle weights, and reactor and shield weights. Analysis showed that very low pressure loss was required in the helium flow to keep pumping power to a reasonable level. For the typical airplane, 834 horsepower per engine were required to pump the helium with a pressure ratio of 1.085. The corresponding helium pressure ratio across the heat exchanger (outlet to inlet) is 0.99, a value that is probably near the optimum for this system. Efforts were made to minimize the pressure losses on the air side of the heat exchanger. The analysis showed that the desirable value of outlet-to-inlet pressure ratio for the heat exchanger is approximately 0.92. The design ratio of turbine-inlet pressure to compressor-outlet pressure is 0.85 including pressure losses in the air ducts and burner.

Heat exchanger for typical airplane. - The heat exchanger for the typical airplane was designed according to the geometry and data given in figure 48 of reference 9. The following are some of the features of the heat exchanger that meets the design specifications given in table I. Approximately 530 tubes of 0.32-inch inside diameter are required for each heat exchanger. For an allowed stress of 7000 psi, the outside diameter of the tubes must be 0.372 inch. The peak metal temperature is estimated to be 1690° F with a turbine-inlet temperature of 1340° F (1800° R). The total length of each tube is 30.3 feet, and the dimensions of each heat exchanger are 7.6 feet long, 1.4 feet high, and 3.3 feet wide. (The width is measured in direction of airflow in fig. 3.) It is estimated that the total weight of each heat exchanger will be 2000 pounds, 1500 pounds for the tubes and 500 pounds for shell, tube supports, structure, and headers. Figure 22 shows the arrangement of

Declassified 1-24-1963

Declassified 1-24-1963

the helium headers on the heat exchanger. The helium that leaves the pump is ducted around the high-temperature header mainly to reduce the pressure differential from the hot metal and thereby reduce greatly the header weights.

In this design, pressure loads are carried by the cool outer jacket. Some additional discussion of the header design is given in appendix C.

E-288

Effect of compressor pressure ratio. - The effect on airplane component weights of varying design compressor pressure ratio has been discussed previously, but some additional information on the heat exchanger is required. Furthermore, a discussion of the effects on the heat exchanger of varying pressure ratio will serve to illustrate the analyses of heat exchangers that were made for all design variations considered in the AIRPLANE and ENGINE sections of this report.

The variations of some of the important heat-exchanger parameters with compressor pressure ratio are shown in figure 23 for a reference airflow rate of 100 pounds per second. Helium inlet and outlet temperatures and turbine-inlet temperature were constant and equal to the values assigned for the typical airplane. Constant percentage pressure losses were also assumed. Figure 23 shows that the tubing weight, which is directly related to the heat-transfer surface area, minimizes at a pressure ratio of 10.5. The variation in weight (surface area) results from a combination of effects. The increase in inlet air density with pressure ratio provides higher heat-transfer coefficients and lower weight. However, the increase in inlet air temperature associated with increasing pressure ratio requires increased effectiveness of the heat exchanger, which in turn means larger surface area and weight. The observed decrease in air inlet Mach number with increasing pressure ratio also increases the surface area and weight through a lowering of the heat-transfer coefficient. The inlet Mach number variation is required to maintain constant percentage pressure losses in view of the variation in the airflow length (width of heat exchanger).

All heat-exchanger designs were calculated on the basis of 100 pounds per second of airflow and then were properly scaled for the correct engine airflow. The number of tubes, the weight of tubes, and the depth measured perpendicularly to the airflow all vary directly with airflow.

Helium Pumps

Since the helium pumping power is quite large (834 hp of the 3410 hp developed by each engine at design flight condition), pump efficiency is important in this cycle, because a decrease in pump efficiency will

Declassified 1-24-1963

Declassified 1-24-1963

require an increase in engine size and weight and reactor and shield weight. In view of the importance of pump efficiency, an axial-flow pump was chosen over the centrifugal type to take advantage of the potentially high efficiencies of axial-flow compressors. Furthermore, since the pumps are very small and low in weight, any weight advantages of either type of pump are unimportant.

The design of the axial-flow pump is given in appendix D along with an estimation of the pump performance map. Some of the features of this pump are as follows. Three identical stages can produce a pressure ratio of 1.085 with an estimated pump adiabatic efficiency of 0.80. The design tip speed is 1500 feet per second, the tip diameter is 5.23 inches, and the rotational speed is 65,800 rpm. Inlet relative Mach numbers are less than 0.4. The aerodynamic design is straightforward; conventional techniques and blading can be used. However, the high rotational speeds and high temperature of the helium (800° F) will pose problems in bearing and shaft seal design.

The bearing problem can be solved through the use of small, high-quality ball bearings, provided that they are well lubricated and installed carefully. The shaft sealing problem requires more attention. Preliminary calculations showed that labyrinth seals would allow excessive leakage of helium. Face-type seals will keep leakage to a low value; however, the combined effects of high rubbing speed, temperature, and pressure differential make their design difficult. A possible solution to the sealing and bearing problem is shown in figure 24. This proposal utilizes lubricating oil at a pressure of 600 pounds per square inch to reduce the pressure differential across the helium seal and to provide some cooling. The arrangement shown in figure 24 appeared reasonable to a manufacturer of face-type seals.

Helium Lines

Two problems are associated with the design of the helium lines. Sufficient mechanical strength must be provided (1) to hold the high-pressure helium and (2) to prevent destructive heating of the airplane structure. Both of these problems can be solved if concentric lines are used with the inner line containing the high-temperature (1790° F) helium. The cool helium (790° F) flows in the annulus and removes the high-pressure loads from the hot metal parts. As a result, the inner liner of the concentric ducts can be made thinner. The weight of a concentric line will be approximately one-fifth the weight of two single lines.

Heat transfer between the two helium streams in the concentric lines was investigated, and it was found that the temperature of the

Declassified 1-24-1963

Declassified 1-24-1963

helium decreased approximately 50° F in transit from the reactor to the outboard engines if the inner pipe was uninsulated. However, the heat loss from the high-temperature helium can be reduced significantly by using a lightweight, three-layer construction for the walls of the hot pipe. Typically, the hot pipe can be built from a tube having corrugated walls placed between two smooth-walled tubes as shown in figure 4. The insulating effect of this construction reduces the heat transfer to the extent that the temperature of the helium decreases only 2° F in flowing from the reactor to the outboard engine.

E-288

REACTOR

Considerations Leading to Selection of Reactor

The reactor designed for the typical airplane has already been described briefly. The reactor layout is shown in figures 5 to 7. Many considerations enter into the selection of the reactor type to use, some of which will be discussed in this section.

CA-4

As mentioned previously, this study was made using a helium-cooled reactor. Helium has several advantages:

(1) Has good heat-transfer characteristics

(2) Does not become radioactive by neutron bombardment, obviating an intermediate heat exchanger and shielding of external circuitry

(3) Is chemically inert; consequently the materials it contacts will suffer no corrosion nor mass-transfer difficulties

Reference 10 points out that "the only contamination in the helium system would be due to the leakage of radioactive materials from the reactor into the helium stream." Helium has the disadvantage that it diffuses readily through imperfections in the containment system; hence a great deal of care in fabrication is required.

The use of the inert gas, helium, leads to the use of high-temperature refractory materials such as molybdenum, columbium, and so forth, that cannot be used with air without cladding because of oxidation and corrosion effects. The strengths of these materials are generally adequate for reactor design up to temperatures of approximately 3500° R. A solid-core reactor was chosen for the present study to take advantage of the characteristics of these materials. The limiting temperature in the reactor - heat-exchanger system with helium as the reactor coolant will be the heat-exchanger wall temperature. Materials

Declassified 1-24-1963

Declassified 1-24-1963

must be used in the heat exchanger that are compatible with the air from the engine, which is on one side of the heat-exchanger walls.

A helium temperature of 2250° R out of the reactor was set as the design value from considerations of the heat-exchanger limitations. A temperature of 1250° R into the reactor was determined from consideration of heat-exchanger size and the transfer of the heat to the engine air. The helium is required to be at high pressure to reduce the void in the reactor as well as to increase the heat-transfer coefficient. A high pressure also makes the heat exchanger and helium lines more amenable to fabrication with respect to size. A value of 1250 pounds per square inch into the reactor was used.

E-288

The high pressure of the gas in the reactor leads to the problem of containing the gas. A pressure shell was chosen for the following reasons:

(1) It avoids use of headers for the fuel tubes with large pressure differentials across them.

(2) It removes pressure loads from high-temperature (fuel element) region.

(3) A high-density gamma shield is needed anyway.

Thermal shields, located between the reactor core and the pressure shell, were required to reduce the rate of heat generation and consequently the thermal stresses in the pressure shell. A cylindrical geometry was chosen for the core shape. One benefit of the cylindrical geometry is that all fuel-element tubes are the same length.

A small reactor size permits the design of a low shield weight, an item that can make or break nuclear airplane feasibility. To obtain small reactors, the fuel must be highly enriched. The performance gain due to the relatively small reactor will be of enough advantage to offset the extra cost of the fuel. For the present reactor the fuel chosen was 92.5 percent U^{235} and 7.5 percent U^{238}.

Design Procedure

The main steps in the design of the reactor are as follows: From the known values of reactor-coolant inlet and outlet temperatures and reactor power distribution and assumed values of fuel-element length, moderator-to-reactor volume ratio, and heat generation,

(a) Determine the fuel-element and moderator-block dimensions to meet specified temperature and coolant pressure-drop limitations. From

Declassified 1-24-1963

Declassified 1-24-1963

these calculations the ratio of moderator cross-sectional area to frontal area and power per fuel element are obtained.

(b) From the power of the reactor and the dimensions determined in the first step, determine the number of fuel elements and get the reactor diameter.

(c) For an estimated excess reactivity, from nuclear calculations determine the fuel quantity required for the reactor obtained in steps (a) and (b). Excess reactivity is built in because of the effects of poisons and burnup.

E-288

The first calculations made along the foregoing lines are of a preliminary nature, because the structure and control rods are omitted for simplicity. The calculations are repeated with other fuel-element and moderator dimensions, as required, until a satisfactory design is achieved. Then the nuclear calculations are continued with these final dimensions and with the items that were omitted.

CA-4 back

After the core and reflector aspects of the reactor are finalized, the thermal shields, pressure shell, supporting structure, and control-rod mechanisms are designed. The process requires much iteration, as can be inferred from the preceding discussion.

Fuel Element

A solid-core reactor can be constructed from parts made in numerous ways and of differing shapes, sizes, and materials. The choices made and some reasons for the choices of the parts used in the reactor are given in this section on the fuel element and following sections of the report.

Materials. - The use of helium leads to possibilities of using molybdenum or other refractory metals in the fuel elements. To minimize radiation damage in fuel elements, the fuel is contained in a matrix of nonfissile material, and superposed on the matrix is cladding consisting of only the nonfissile material. Matrix materials with melting points above 4000° F are about the only ones of interest in an application such as the one considered herein. Even though the outlet helium temperature is only 1800° F, the maximum fuel-element temperature will be much higher. If the refractory materials that appear to be scarce and expensive are omitted, the metals that are left for consideration are tungsten, tantalum, molybdenum, and columbium. Considerations of the strength, ductility, ease of fabrication, thermal conductivity, neutron absorption cross section, and state of development of these four materials led to the

Declassified 1-24-1963

Declassified 1-24-1963

choice of molybdenum as the best material to use for the fuel elements. This choice was mainly based on the state of development of molybdenum compared with the other materials. The choice does not mean that molybdenum is superior in all the properties mentioned. Consideration of the materials at a later date might lead to another choice, but this would not greatly affect the results.

The dispersant fuel phase (or the uranium compound) of a fuel element should be chemically stable with regard to its environment at the operating temperature. It should contain the highest possible density of uranium per unit volume. Among possible fuel dispersants, uranium dioxide UO_2 and uranium carbide UC or UC_2 are the most promising. Some properties are as follows:

E-288

Compound	V_r (a)	Melting point, °F
U	1.0	2072
UC	.69	4132
UC_2	.56	4352
UO_2	.53	4532

[a]Uranium content per unit volume of dispersed phase relative to density of uranium.

The table shows that the several uranium compounds permit much higher operating temperatures than does natural uranium. Uranium dioxide stands out because its technology and handling are well understood, although all the compounds listed have relatively high density of uranium, UC being better than UO_2 in this respect. It was decided to use UO_2 in the reactor fuel elements, and calculations were made using this material. Later considerations caused a change to UC. These considerations will be taken up later in the report.

Shape. - In choosing the fuel-element shape, considering the most general types used (i.e., solid cylindrical rods, hollow cylinders, and plate type), the hollow cylinder or tube type was finally chosen. The basis of this choice is that it is strong and that it can be cooled by forced convection by passing coolant through the hole in the element as well as through an annulus formed by the outer radius of the fuel element and the inner radius of a moderator block. In order to get a large surface-to-volume ratio for good heat transfer, the element must be small.

Declassified 1-24-1963

Declassified 1-24-1963

E-288

Analytical methods used in design. - The analytical methods used for determining the temperatures and stresses in the fuel elements and the pressure drops in the coolant passages are given in detail in appendixes E and F. In the temperature analysis the fuel element was assumed to be composed entirely of molybdenum, because the amount of uranium in each element was unknown at the start of the calculations, and to include the thermal conductivity of UO_2 in the analysis would have complicated it unduly. The conductivity of UO_2 is much less than that of molybdenum, so that the results of the temperature analysis used herein would be optimistic for the fuel elements where large amounts of UO_2 are used. The power distribution assumed for the heat-transfer calculations at first was constant in a radial direction and "chopped" 2/3-cosine law in the axial direction (see appendix E). Consequently, the fuel elements near the reactor core periphery contain the most fuel, and the calculated temperatures would be more in error for these elements than for the elements near the center of the core. It was assumed that 90 percent of the reactor power was generated in the fuel elements.

The assumption was also made in the stress analysis that the fuel element was made of one material only, or the cladding and matrix can be represented by one ring. If the element had been divided into two cladding rings and one "meat" ring, each would have to be treated separately. Such a stress theory development was considered beyond the scope of this report. Consequently, stresses were calculated using the analysis and assuming that the fuel element was made entirely of molybdenum. In this way some idea of the upper limit of the strength of the element could be obtained.

Tube design. - The fuel element used in the reactor is shown in figure 25. It consists of a sandwich of three concentric tubes, the tubes being continuous through the core and the end reflectors as shown in figure 6. The middle tube contains molybdenum plus the uranium compound through the core length; it is only molybdenum through the end reflector lengths. The two outer tubes form the cladding. The cross section shown in figure 25 is section D-D of figure 5. Also shown in this figure, besides the fuel element and moderator block, are a molybdenum spring spacer for positioning the fuel element within the moderator block and a molybdenum bushing on which the spacer bears rather than on the fairly brittle BeO moderator block. A number of these spacers and bushings are placed along the fuel-element length as shown in figure 6. The dimensions of the fuel element, moderator block, and other parts are included in figure 25. The inner coolant passage is 0.25 inch, the cladding thicknesses 0.007 inch, and the "meat" thickness about 0.030 inch. The outer coolant passage, the annulus, has a spacing of 0.071 inch.

The reactor was designed on the basis of 100 megawatts (95 Mw of heat in core, 5 Mw of heat in side reflector and thermal shields), as

Declassified 1-24-1963

Declassified 1-24-1963

stated previously. Because the coolant picks up heat from the thermal shields and side reflectors and then passes through the core, the total heat picked up by the coolant is 100 megawatts. On the basis of some simple preliminary calculations, it was decided to cool the fuel element on both sides with helium as shown in figure 25. The temperatures of the fuel element were calculated with an allowable pressure drop of approximately 2.5 percent of the inlet pressure (which was 1250 lb/sq in.), helium temperature in and out of the core of 1300° and 2250° R, respectively, core length of 24 inches, and end reflector thickness of 4 inches. (There is a rise of 50° F in helium temperature through the thermal shields and side reflectors, which is the reason for the 1300° R temperature into the core.) The helium flow rate to the reactor had been determined to be 76 pounds per second. The number of fuel elements finally used was 640. Eighteen positions where fuel elements would be are occupied by through-bolts. Some of the coolant flows along the control rods and through-bolts. This flow was estimated, on the basis of obtaining the same temperature rise of the coolant or 950° F, to be roughly 2 percent. The flow through each fuel-element - moderator-block assembly is then about 0.1143 pound per second.

E-288

Axial temperature variations of coolant, meat, and cladding are given in figure 26. The pressure drop through the core is about 2.6 percent, a value considered satisfactory with regard to the pressure drop allowable for the whole helium system, with flows of 0.0459 and 0.0684 pound per second through the hole and annulus, respectively, of a fuel-element - moderator-block assembly. The maximum fuel-element temperature was 3235° R (fig. 26). The temperatures and pressure drop being considered satisfactory, the next step was to determine the stresses for this design.

The temperatures given in figure 26 were then used to evaluate the properties in the stress equations for the case when the fuel element is considered to be entirely molybdenum. Built into the stress equation are the effects of the thermal gradients resulting from using a particular material. These effects are separate from the property terms appearing in the equations. The sources of data for the properties of Mo required in the calculation of the stresses are given in appendix F. Since relatively long life is required of the Mo, the stress-rupture strength was considered the best criterion to use. The allowable strength data for Mo at 1000-hour rupture life are shown in figure 27 and were extrapolated from data for Mo plus 0.45 percent titanium in reference 11. These allowable data were used because adding the small amount of titanium increased the strength of Mo appreciably.

The results of the stress calculations with only Mo in the fuel element are shown in figure 28, where the allowable and actual stresses

Declassified 1-24-1963

Declassified 1-24-1963

are plotted against the axial distance along the fuel element. For quite some distance along the fuel element it is apparent that the calculated actual stresses are greater than the allowable stresses. It should be pointed out that the theory in appendix F is for the elastic case and plastic flow is not included. It might be expected that plastic flow would relieve the stresses and the fuel element would be safe even in the regions indicated as unsafe in figure 28. It would be much better to have a fuel element that is safe along the entire length using elastic stress theory; then plastic flow would provide a further margin of safety.

E-288

A means of changing both the allowable and calculated axial stress distribution is to vary the axial volumetric heat-source distribution, and thus the axial power distribution, in some manner different from the cosine distribution used to obtain the results shown thus far. Such a different heat-source distribution will result, of course, in a different temperature distribution from that presented in figure 26. Consequently, calculations were made of the fuel-element temperatures, heat-source distribution, and stresses for a case that would result in the actual stress curve paralleling the allowable stress curve. The calculations were obtained using methods given in appendixes E and F and from a simplified analysis not included herein.

The axial variations in the fuel element and helium temperatures are shown in figure 29 for the case described previously. The axial variation of the volumetric heat-source distribution for this case compared with the distribution for the 2/3 "chopped cosine" law is shown in figure 30. The resulting stresses are shown in figure 31. The conditions used result in a "safe" fuel element from consideration of the calculated thermal stresses. The fact that the curves in figure 31 are not parallel may be attributed to the simplifying assumptions in the analysis. The distribution of fuel required to obtain the variation of volumetric heat source resulting in the stresses of figure 31 will be taken up in a later section of the report with the nuclear characteristics.

No calculations were made considering the fuel element made up entirely of the uranium compound, because of the results described previously. All efforts should be made to keep the volume of compound in an element as small as possible. Therefore, it was decided in the final design to change from UO_2 to UC on the basis of the table previously presented. If some fuel elements do have large amounts of UC in them, the calculations presented will be rather meaningless with regard to the stresses, for reasons explained before. In any event, experiment alone will determine whether the fuel elements are satisfactory.

Declassified 1-24-1963

Declassified 1-24-1963

Core and Reflector

Preliminary nuclear characteristics. - For the application of nuclear power to airplanes, it is important to design the reactor as small as possible so that the shield will not be overly heavy. Consequently, preliminary calculations of the uranium investment, fission spectrum, and flux for a series of reactors of varying core diameters and side-reflector thicknesses were made to determine how small a reactor seemed feasible. The smallest core diameter chosen was 17 inches. The control rods and structure were not included in the calculations. The analysis used for these nuclear calculations, and those to be presented later, are given in appendix G, with the exception of a few details that will be discussed in connection with some characteristics as they arise. The length-diameter ratio l/d of the reactor core was chosen to be a little less than 1.0 for all cases because, on the basis of equations in reference 12, it can be shown that this results in minimum amount of fuel needed for a required effective multiplication factor k_{eff}.

E-288

The results showed that to keep the uranium investment from getting too high, the reactor (including side reflector) should be at least 38 inches in diameter, as shown in figure 32. No values are shown on the figure ordinate on the amount of uranium because of the factors that were omitted. The trend of the curve is probably valid for reactors that include all the factors omitted. Another result was that the small reactors were in the high epithermal range, and in keeping with the idea of conservatism for the whole project this was not desirable. In addition, there are doubts about the accuracy of the nuclear theory for such reactors, and the resulting calculations could be doubtful. Thus, even though smaller diameters would be desirable with respect to shield weight, these preliminary calculations indicated that the reactor should be greater than 38 inches in diameter (including reflector) on the basis of designing a more conservative reactor.

Core-structure nuclear effects. - A few nuclear calculations were made after those just described in order to find out the effects of using different materials in the structure of the reactor. A calculation was made in which it was assumed that the structure would increase the frontal area of the reactor by 20 percent, and the multiplication factor was determined first assuming ZrC as the structural material and then Mo. The conditions used in the calculations are as follows:

Declassified 1-24-1963

Declassified 1-24-1963

E-288

Reactor power = 100 Mw

Fuel amount = 70 lb uranium (92.5 percent U^{235})

Number of fuel elements = 528

Pressure drop of helium through reactor = 4 percent

Diameter of reactor ≈ 32 in.

Length of reactor = 24 in.

No end reflector

Side reflector = 4 in.

Structure = 20 percent of total volume (increases frontal area)
With ZrC structure, k_{eff} = 1.06
With Mo structure, k_{eff} = 0.74

CA-5

The result showed that ZrC would give a much higher multiplication factor, 1.06 as compared with 0.74 for Mo, for the conditions used. Again from the standpoint of conservatism it was decided not to use a cermet for the structure, even though it gave a much better k_{eff}, because of possible brittleness. It was decided to use molybdenum for the same reasons given previously in connection with the choice of material for the fuel element. Columbium could probably be used equally as well at some future time when its development is advanced to the point where molybdenum is now. This would probably make considerable changes in reactor characteristics compared with molybdenum, but the over-all airplane results would probably remain unchanged.

It should be pointed out that the percent structure in the final core was much less than that used in these calculations, so that the difference between using a cermet like ZrC and a refractory metal will not be as great as that determined in the calculations.

Final nuclear characteristics. - The foregoing calculations led to a final reactor with the characteristics presented in table IV and the general design features given in figure 6. The core radius was 17.36 inches, and the core length 24 inches. To meet specified coolant pressure-drop limitations of the helium, 640 fuel elements were used. The result was a 2.6-percent pressure drop discussed previously in the fuel-element design. Both mechanical and control-rod structure (the sizes of the latter were roughly estimated) were included in the reactor to obtain the nuclear characteristics. In table IV, UC is the fuel.

Declassified 1-24-1963

Declassified 1-24-1963

From the calculations made without the structure, it was estimated that 130 pounds of uranium would be required to obtain the estimated required k_{eff} and that there would be 10 pounds of fuel burnup in the estimated 1000 hours of operation proposed for the reactor. In making the calculations, it was estimated that the moderator and core structure would be operating at about 1400° F; and, since this structure is about 90 percent of the reactor, the reactor core would not be operating at a temperature much higher than this. Since temperatures up to 1800° F, as compared with 1400° F, did not affect the cross sections appreciably, it was decided to use 1800° F in determining the thermal energy. Calculations were made of k_{eff} for the startup both cold and hot, and at 1000 hours for a "clean" reactor and for one including poisons effects. The latter will hereafter be called "dirty" reactor. The calculation for the "clean" reactor at 1000 hours was made to determine the effect of fuel burnup alone on k_{eff}. For the cold startup calculation the thermal macroscopic cross sections were determined at E_{th} of 0.025 electron volt. During the operation of the reactor there will be a buildup of xenon, samarium, and other fission product poisons which must be accounted for. They will reduce the k_{eff}. To make the calculation in a rigorous manner, the nuclear calculations would be done over the entire operating time in steps corresponding to the "cycle" of operation from the start of a flight to the start of another flight. This would be very tedious and was thought to be unnecessary for this investigation. It was assumed that the reactor would be operating without shutdown over the entire period of operation of 1000 hours; this would result in a pessimistic value of k_{eff} for the dirty reactor. In the calculation, the thermal macroscopic absorption cross sections of the fission product poisons $\Sigma^{FPP}_{a,th}$, of the xenon $\Sigma^{Xe}_{a,th}$, and of the samarium $\Sigma^{Sm}_{a,th}$ were added to the thermal macroscopic absorption cross section used for the clean reactor at 1000 hours. The microscopic fission product poisons cross section $\sigma^{FPP}_{a,th}$, used to get $\Sigma^{FPP}_{a,th}$, was obtained from reference 13. The cross sections $\Sigma^{Xe}_{a,th}$ and $\Sigma^{Sm}_{a,th}$ were obtained by methods given in reference 12 (pp. 332 and 338, respectively). The microscopic cross section $\sigma^{Xe}_{a,th}$ used in $\Sigma^{Xe}_{a,th}$ was obtained from reference 14.

The resulting values of k_{eff} from these calculations are shown in figure 33. At startup, k_{eff} of 1.18 was obtained for the cold reactor and 1.12 for the hot reactor. After 1000 hours, the value of k_{eff} for the hot clean reactor was 1.11 and for the dirty reactor was 1.08. A dashed line is drawn between the hot condition at startup and the dirty condition at 1000 hours because, as stated before, unless the cycle of operation for a flight is decided, this curve cannot be drawn. These

E-288

Declassified 1-24-1963

Declassified 1-24-1963

results will be discussed in relation to their effect on the control problem in a later section on reactor control. The values of neutron flux obtained for the six energy groups used in the calculations for hot startup are shown in figures 34 and 35 for flux along a radius at the midplane of the reactor and for that along the axial centerline, respectively. In order to plot the fluxes of all six groups on one figure, some of the flux values were multiplied by a factor shown on the curves. For instance, the fluxes of group 1, φ_1, were multiplied by 20. The 20 φ_1 were plotted on the ordinate. The resulting numbers are labeled relative flux φ_r.

E-288

The percentage fissions in the fourth, fifth, and thermal groups, the average flux of each group, and the energy range of each group are shown in table V for the hot startup and "clean" reactor at 1000 hours. The methods of obtaining these data and their use are discussed in appendix G. The code discussed in this appendix permits fissions to occur only in the fourth, fifth, and thermal groups. The resulting k_{eff} for these conditions is pessimistic. The values of the flux at thermal energy are useful in determining time to start up the reactor after a shutdown and will be discussed more fully in the reactor control section. The number of fissions is generally well divided among the lower three energy groups as shown in the table, which indicates an epithermal reactor. To obtain a thermal reactor, an increase in size would probably be necessary. Such an increase would be detrimental to airplane performance.

CA-5 back

The weights of the constituents in the core, the core weight, and the core constituent atomic densities are given in table VI. The moderator amounts to a little over 70 percent of the weight of the core, the latter being about 2500 pounds.

Power and uranium distributions. - The nuclear calculations were made assuming a uniform fuel distribution, as discussed previously. The fuel-element and moderator temperatures were based on uniform radial power distribution, which results from a nonuniform radial fuel distribution. In the axial direction, these temperatures were based on a "chopped" 2/3-cosine-law power distribution, which results from an approximately uniform axial fuel distribution. Calculations were made to determine the radial fuel distribution for the uniform radial power distribution assumed in the first temperature calculations with UO_2 and then with UC as the fuel. The reactor core was divided into 10 radial segments, the thickness of each being the same. The required volume of UO_2 (or of UC) in each segment for the startup case (140.5 lb of uranium) was calculated and compared with the available volume in the "meat" of the fuel elements in each segment. The details of the calculations are

Declassified 1-24-1963

Declassified 1-24-1963

not included herein except to note that the assumption was made that the radial flux distribution for constant radial power was the same as that for uniform fuel distribution. The flux for the latter was part of the nuclear results obtained with the computing program.

The results of these calculations are shown in table VII. In the center of the reactor core (reactor sector 1) there is no volume available because no fuel elements are in this part. The two central control rods and through-bolts occupy the space near the core center. Comparison of available and required volume for the fuel shows that except at reactor sector 1 there is enough volume to handle the UC. This is not the case for the UO_2. It was for this reason that it was finally decided to use UC in the reactor. Because less volume would be required by the UC than by the UO_2, a stronger fuel element would result. The conductivity of UC is much higher than that of UO_2; hence the use of UC will improve the dissipation of heat. Reference to table VII shows that the UC required in sector 1 could be put into sector 2 in addition to that already in sector 2.

E-288

Comparison of the core composition using UC with that using UO_2 (the nuclear calculations were made using the latter fuel) showed little difference. Consequently the nuclear calculations are considered adequate for UC. It is also thought that these nuclear calculations, from which k_{eff} was obtained and which were made for a uniform fuel distribution, are a fair approximation with regard to uranium required for uniform radial power distribution.

In addition to determining the fuel distribution for the conditions used for table VII, the fuel distribution using UC only was determined for a uniform radial power distribution and for the axial distribution resulting in satisfactory fuel-element stresses. Because no nuclear calculations were made with these power distributions, the radial and axial flux distributions for this case were again assumed to be the same as those for uniform fuel distribution. The results are shown in figure 36. The sketch at the top shows an end view of half the reactor core and the available volume for UC in each of the 10 radial segments. The reactor was divided into 20 axial segments. Thus each outer semicircular segment of 1.2-inch length has a volume of 2.255 cubic inches available for UC. The volumes required in each segment are shown at the bottom of the figure. The numbers apply to the entire semicircle and for this reason were not repeated in the right half of the bottom sketch. The segments for which the volumes available are not adequate to hold the UC required are cross-hatched in the figure. The available volume at the center of the reactor is zero for the same reason as that discussed in connection with table VII. It appears from the figure that many segments are inadequate, and some of the fuel in these segments must be

Declassified 1-24-1963

Declassified 1-24-1963

shifted to near segments. Some of the available volumes have no apparent pattern radially because of control rods occupying positions in which fuel elements might be placed.

No nuclear calculations were made with this fuel distribution. The total amount of uranium in figure 36 is 140.5 pounds, the amount determined as required for the startup with uniform fuel distribution. It would be expected that, for the power distributions used to obtain figure 36, the effective multiplication factor would not be appreciably different from the values shown in figure 33. These values were determined for uniform fuel distribution. It is expected, however, that the total fuel quantity required would be much greater than the 140.5-pound total of figure 36. Further nuclear analysis of this reactor will be required if future work is to be done on this project.

E-288

Moderator characteristics. - The moderator blocks in the core were made of BeO, and the shape and size are given in figure 25. Temperatures and stresses of the blocks were calculated using the methods in appendixes E and F. The outside wall temperature T_f and inside wall temperature T_e of the moderator blocks and the helium temperatures T_{He} axially through the core are given in figure 37 for the power distribution that resulted in the satisfactory fuel-element stresses of figure 31. The temperatures continue to rise axially through the core, the highest temperature being about 2370° R. These are "safe" absolute temperatures, being far below the melting point.

Figure 38 shows the tensile strength of BeO as a function of temperature as obtained from reference 15 (p. 843). This was used with the temperatures T_f of figure 37 to determine the allowable axial stress variation through the core shown in figure 39. The actual thermal stresses calculated using the temperature results of figure 37 are also shown in figure 39. The results show that there is a large margin of safety between the calculated allowable and actual moderator stresses.

Reflector characteristics. - The side reflector was made of Be for strength reasons, as mentioned previously. The methods used for determining the temperatures in the reflector pieces are given in appendix H. The side reflectors can be considered shields for the pressure shell, because the radiation is attenuated through them. Five percent of the reactor power was considered to be dissipated outside the core. From this value, the heat flux could be obtained as a starting value from which the heat source in each reflector piece could be obtained as shown in appendix H. It was assumed that the coolant flows through each passage, including thermal shield passages, will be metered so that the coolant temperature in each passage at a given axial position from the inlet will be equal. This will result in a fixed ratio of coolant weight

Declassified 1-24-1963

Declassified 1-24-1963

SECRET

flows in adjacent passages throughout the length of passage, and the maximum temperature in a part will remain at the same radial position for all axial positions.

The general method of design was to assume the temperature of the reflector pieces at the coolant exit (because this is where the highest temperatures will occur) and to calculate the thicknesses of the slabs from a thermal stress consideration. Only thermal stresses were considered, because these members carry small loads and can be designed with no restraints. After the thicknesses were determined, the temperatures were calculated to see if the temperatures were satisfactory (i.e., below the 1000° F assumed for the stress calculations). The properties, thermal conductivity, gamma radiation absorption coefficient, modulus of elasticity, coefficient of thermal expansion, and Poisson's ratio, of the Be reflector pieces used in the calculations were obtained from references 15 and 16.

E-288

The side reflector must be divided into a series of concentric cylinders to provide for reflector cooling and to limit the thermal stresses. In addition, the inner portion of the side reflector is used also as a framework for the core structure (fig. 6). Therefore, the inner reflector must not distort in service and should be designed for low thermal stresses. A design stress of 1000 psi was selected for the inner reflector piece. The corresponding creep rate is much less than 0.001 percent per hour (p. 76, ref. 16) at a temperature of 1000° F, which is the highest temperature expected in the reflector. Based on the simplified calculations of heat generation given in appendix H and flat-plate thermal-stress theory (ref. 15, p. 703), the allowed thickness of the inner portion of the side reflector is 0.50 inch. The remainder of the side reflector is made from cylinders having wall thicknesses of 0.75, 1.00, and 1.50 inches. The largest thermal stress (5000 psi) occurs in the 1.50-inch piece. This stress value will be relieved by plastic deformation at the operating temperature.

A sketch of a plan view of the four side-reflector pieces showing the channels between them is given in figure 40. The coolant-flow rates in each passage, the helium in and out temperatures, and the reflector temperatures at the coolant exit are shown. The latter are shown as curves on each piece with the temperature scale to the left. The highest temperature shown is about 1380° R (920° F), which is below the 1000° F used for the properties calculations in the determination of the stresses.

Thermal Shields and Pressure-Shell Characteristics

The pressure shell must be designed to contain the high-pressure helium and to withstand thermal stresses due to neutron and gamma

SECRET
Declassified 1-24-1963

Declassified 1-24-1963

heating. Consequently, the pressure shell and internal thermal shield must be considered as a system in the design. Furthermore, since the internal thermal shield and pressure shell will serve as a part of the total biological shield, the weights of these components are not primary design criterions (except for handling problems) in a unit shield configuration.

E-288

Since the pressure shell is the basic structural member of the core assembly, it must be constructed of a material with good creep properties at operating temperatures of about 1000° F. An austenitic stainless steel (type 347) will creep at a rate of approximately 1 percent in 10,000 hours at a stress of 25,000 psi and 1000° F temperature (ref. 16). This material was chosen for the pressure shell. Because of the chromium in this steel, it will be radioactive when the reactor is shut down. An alloy such as Hastelloy alloy B could probably be used with less radioactive effect. Creep data on this metal, however, are scarce. Mild steel was selected for thermal shielding.

On the basis of the simplified calculations of neutron and gamma heating rates described in appendix H, it was determined that 6.5 inches of steel thermal shielding would limit the total stress in the pressure shell to 25,000 psi if the pressure-shell thickness was 1.75 inches. (The properties of type 347 stainless steel were taken from ref. 16.) The same limiting stress in the pressure shell could be obtained with less thermal shielding and a thinner pressure shell. However, since iron is also required for the biological shield exterior to the pressure shell, no detailed analysis to determine the minimum stress or minimum thicknesses of the thermal shields and pressure shell was made.

Plain carbon steel (SAE 1040) can serve as material for most of the thermal shielding, because corrosion is not a problem, and adequate creep strength can be achieved at the expected peak operating temperature of 1000° F. Molybdenum is used as thermal shielding in the hot gas stream at the outlet of the reactor. The cylindrical thermal shield, which is 6.5 inches in thickness, must be divided into six concentric cylinders (fig. 7) to allow for cooling and to reduce thermal stresses. The thicknesses of the individual cylinders are 0.5, 0.75, 1.00, 1.25, 1.50, and 1.50 inches. Thermal stresses are less than 8000 psi, and the resulting creep rates are less than 1 percent per 1000 hours for SAE 1040 steel operated at 1000° F. Cooling of the thermal shielding located at the ends of the core is provided by the holes shown in the shields in figure 6.

The results of calculations of the cylindrical thermal-shield temperatures are shown in figure 41 for the final reactor design conditions. This figure is a sketch similar to that for the side reflectors in figure 40. The shield temperatures shown are those at the helium outlet, because this is where the highest values occur. The methods of calculation are given in appendix H. The helium flow rate w_{He} is shown in

Declassified 1-24-1963

Declassified 1-24-1963

each passage, the criterions of design being the same as that for the side reflectors discussed before. The highest temperature, which occurred in the second thermal shield, was about 1390° R (930° F), and then there was a general reduction in temperature to an average of about 880° F in the shield next to the pressure shell. Since the stresses given previously were based on properties at 1000° F and were satisfactory, these temperatures will provide a greater margin of safety.

Control

The reactor control primarily regulates the source energy required by the turboprop powerplants. That is, the nuclear components should provide performance and stability consistent with the over-all system demands. Other important considerations in the nuclear control design are reliability and safety. Normal operation results in components operating continuously over extended periods of time. During operation the safety of the personnel and the vehicle demands a minimum of dangerous excursions or reactor scrams.

A potential for large excursions exists in this reactor design, since the fuel loading results in a large excess reactivity. The excess reactivity to be controlled varies substantially with operating conditions. Table V, discussed in the analysis of the nuclear characteristics, shows a change of reactivity of 6 percent from a cold clean to a hot clean configuration. This variation in reactivity, added to lesser amounts from fission product poisoning and fuel depletion, results in the need for continuous shim control of the reactor.

A block diagram showing the more important parameters that affect reactivity is shown in figure 42. The forward path has a transfer function composed of the basic reactor kinetics with power or neutron flux as an output and reactivity as an input. Power changes, in turn, affect reactivity and are shown by the feedback paths that close the loop. The feedback paths according to their environment are classed in two groups: (1) the internal feedback path that is inherent in the core design and (2) the external feedback paths composed of the control rods and the reactor load. A more complete discussion of nuclear control loops is given in references 12 and 17.

Poisoning effects. - Calculations were made for the individual worth of poisoning resulting from equilibrium and peak xenon-135, equilibrium and peak samarium-149, and the other fission products. These calculations supplement the steady-state lumped values obtained in the nuclear characteristics section.

The methods of calculating xenon concentration as described in reference 12 were applied to this high-temperature epithermal reactor.

Declassified 1-24-1963

E-288

Declassified 1-24-1963

Equilibrium xenon poisoning, a balance between the rates of formation and loss, can be calculated from the following equation:

$$p_o = \frac{Xe_o \sigma_{a,Xe}}{\Sigma_{a,U}} = \frac{\sigma_{a,Xe}(\gamma_I + \gamma_{Xe}) \frac{\Sigma_f}{\Sigma_{a,U}} \varphi_o}{(\lambda_{Xe} + \sigma_{a,Xe}\varphi_o)} \tag{1}$$

The development of the equilibrium poison equation can be found in reference 12. Several of the parameters of equation (1) vary with energy, namely the xenon cross section, the ratio of the fuel fission to total cross sections, and the neutron flux. The xenon cross section varies greatly with energy in the region of interest, as shown in reference 18. Thermal energy associated with the high moderator temperature at rated power is 0.102 electron volt. At this energy, the xenon cross section is at a threshold of sharp reduction and has a Maxwellian average of 1.32×10^6 barns. The next energy level, group 5, covers the energy range from 0.411 to 50.6 electron volts, with a corresponding xenon cross-section variation from 8.5×10^4 to 28.5 barns. The average xenon cross section in the fifth group is several orders of magnitude below that of the thermal group. This results in negligible poison contributions from the epithermal group.

Equilibrium xenon poisoning was calculated for two conditions: (1) a freshly loaded core and (2) a partially depleted core with neutron flux shown in table V. The values of poisoning equivalent to reactivity of -0.0107 and -0.0112, respectively, were obtained. These values are adjusted to consider that approximately one-third of the fissions occur at thermal energy.

Xenon peak poisoning results when the xenon formation rate exceeds its loss rate because of rapid decreases in the neutron flux. Neutron capture by xenon becomes ineffective, causing xenon to build up through a maximum as a function of time. The time variation of xenon from equilibrium conditions for a step decrease in neutron flux as derived in reference 12 is as follows:

$$p(t) = \left[\frac{\sigma_{a,Xe}\varphi_o \gamma_I}{(\lambda_{Xe} - \lambda_I)} \frac{\Sigma_f}{\Sigma_{a,U}} \left(e^{-\lambda_I t} - e^{-\lambda_{Xe} t}\right) + p_o e^{-\lambda_{Xe} t}\right] \tag{2}$$

The xenon buildup affects the thermal region only, as in the equilibrium xenon calculations. Since the thermal flux is relatively low, with approximately one-third of the fissions in this region, the peak xenon is limited to small values. Under the most stringent conditions (i.e., a step decrease in neutron flux from rated power), the negative reactivity remains below 2 percent. Figure 43 shows the xenon time

E-288

CA-6

SECRET

Declassified 1-24-1963

Declassified 1-24-1963

variations for these conditions with a freshly loaded core and a partially depleted core. The maximum values are reached in about $7\frac{1}{2}$ hours.

The over-all xenon poisoning is greatly reduced in this high-temperature epithermal reactor over what would be expected from a low-temperature thermal reactor. A slight additional fuel inventory in the core provides the ability to override xenon, resulting in a safer and more flexible system. Since xenon "buildup" is limited to small values, the related problem of "burnout" upon restart at peak values is also of a minor nature.

E-288

The effect of samarium poisoning is calculated in a manner similar to xenon poisoning. The equilibrium poison equation is simplified, since there is no direct samarium yield from fission and no decay of samarium. Therefore, the equilibrium equation reduces to the following equation, which is independent of neutron flux and samarium cross section:

$$p_o = \gamma_{Pm} \frac{\Sigma_f}{\Sigma_{a,U}} \tag{3}$$

The equilibrium poisoning results in a negative reactivity of 0.0114 and reaches equilibrium in approximately 35 days. Since the time to reach equilibrium is long, the effect on criticality is fairly negligible.

Samarium poisoning as a function of time for a step decrease in flux is very small and can be neglected.

Temperature effects. - The temperature variations within the reactor have an important effect on reactivity. These temperature changes are caused by local variations in the fission energy and variations in the coolant parameters. The helium coolant is a non-neutron absorber and has a relatively small moderating value. Therefore, the coolant does not directly influence reactivity. Changes in coolant-flow parameters and in the heat-exchanger load do affect reactivity by varying reactor temperature, but in a more gradual manner.

A change in reactor temperature alters the multiplication factor in two ways. The change in the mean energy of the thermal neutrons affects the thermal cross sections, and density changes affect buckling and leakage. The first effect, which is called the nuclear temperature coefficient (ref. 12), is the stronger and quicker and therefore the more important. Table V shows a 6-percent drop in k_{eff} from the cold clean to the hot clean configuration. This amounts to an over-all temperature coefficient of -3.76×10^{-5} $\delta k/^{o}F$. Although there are other factors affecting the total-temperature coefficient, this value should be representative and contribute toward the inherent stability of the reactor.

Declassified 1-24-1963

Declassified 1-24-1963

E-288

CA-6 back

Fuel burnup. - The calculations presented in the nuclear characteristics section based on an estimated 1000-hour load life resulted in effective multiplication factors as shown in figure 33. The following analysis shows the rate of fuel burnup and the expected operating time before reloading.

The following equation gives the fuel burnup rate per megawatt of power:

$$U^{235}\ \frac{\text{Burnup rate}}{\text{Unit energy}} = 1.044\ \frac{\sigma_{a,U}}{\sigma_f}\ \frac{\text{grams}}{\text{Mw-day}}$$

$$= 2.29\times10^{-3}\ \frac{\sigma_{a,U}}{\sigma_f}\ \frac{\text{lb}}{\text{Mw-day}} \qquad (4)$$

The ratio $\sigma_{a,U}/\sigma_f$ varies somewhat with energy, and the average value at thermal energy 1.228 was used in the calculations. The rate of U^{235} burnup per megawatt adjusted for nonfission capture is 2.81×10^{-3} lb/Mw-day. At this rate it takes 37.4 days (approximately 900 hr) of continuous operation at rated power to burn up 10.5 pounds of fuel. In this time the reduction of k_{eff} from fuel burnup is 1.0 percent, as shown in figure 44. Loss of reactivity from poisoning reduces k_{eff} another 3 percent to a value of 1.08. Considering that peak xenon contributes less than 1-percent negative reactivity at this point, there is a margin of reactivity of better than 7 percent. A rough extrapolation indicates that reloading of the reactor will be required after 195 days of operation at full power. This extrapolation does not take into account the fission spectrum shift towards a more thermal reactor and the associated increase in xenon and samarium poisoning. The actual flight plan does not call for continuous operation and will affect the burnup rate also. Therefore, the reloading time is an approximate number to be adjusted when more exact calculations are made.

Control rods. - The maximum excess reactivity that occurs with the cold clean configuration is 18 percent. This excess reactivity considered with a shutdown reactivity of 10 percent results in a total worth of 28 percent. Therefore, the design of the control rods has a worth of 28 percent distributed between the shim and safety systems.

The tentative control-rod system is composed of two scram rods, three combination shim-scram rods, three pairs of shim rods, and two regulating rods. Figure 7, which is the end view of the reactor, shows the radial position of the various rod types. The actuators used to drive the control rods are powered by electric motors, hydraulic servos, or pneumatic servos. Table VIII lists the drive mechanisms and worth of each rod when all the rods are in the core.

Declassified 1-24-1963

Declassified 1-24-1963

Two regulating rods with a worth of 0.005 each are located at the center of the reactor. One of the regulating rods will normally be in a standby position fully withdrawn from the core. In the event of a malfunction, the standby rod is used with an effective worth of 0.005 or less, depending on the shadowing of the primary rod. The regulating rods have individual drive mechanisms located within external thimbles, as shown in figure 5. Linear reluctance motors similar to those described in reference 17 provide the drive motion directly without the need of gearing.

E-288

Shim control during operation at power level is attained by three pairs of rods located 120° apart and half the radial distance from the center to the reflector, as shown in figure 7. Each pair of rods has a worth of 0.04 and is motivated by a common synchronous reluctance motor. The rotary motion of the motor is transformed by gearing, screw, and a movable nut to provide linear motion of opposite directions to the individual rods. The boron loading of each rod varies in a linear manner over its length but in opposite directions, as shown in figure 5. This results in a worth of the pair of rods that is equal at all times along the length of the reactor core, therefore minimizing axial power distortion normally associated with a rod partially inserted in the core. Variation in total worth is accomplished as the rod pairs are simultaneously inserted and extracted.

Dual-purpose rods used for both shim control and scram are located equidistant between the shim-rod pairs. These three rods have individual worths of 0.04 each and are used as shim rods for starting. Upon reaching power level, the rods are almost completely extracted from the core and can be used as scram rods exclusively. The drive mechanism can be hydraulic or pneumatic with slow speed operation in or out in conjunction with a special dump port to provide fast insertion for scram. The pneumatic system seems more advantageous because it can make use of the same inert gas, helium, used as the coolant. The high temperatures, radioactive field, and possibility of contaminating the coolant by leaks make the hydraulic system less favorable. Individual rods have their own drive that can be externally connected to work in unison or singly.

Two scram rods of relatively small worth, 0.02 each, are located 180° apart at a radius larger than the shim and shim-scram rods, as shown in figure 7. These rods are pneumatically operated with slow extraction and very fast insertion speeds. The position of these rods from start to shutdown will be fully extracted.

All the control rods are cooled by helium bled off the main supply and passed through an external air heat exchanger. This cooled helium at 950° R enters the control-rod sleeves near the actuators, passes through the sleeve around the control rod, and mixes with the primary coolant to flow through the reactor core.

Declassified 1-24-1963

Declassified 1-24-1963

Automatic control in the power range is obtained by varying the regulating rod, with followup shim-rod control when the regulating rod reaches a limit.

Reactor Structure

E-288

Core structure. - The geometry of the 640 fuel elements and the moderator blocks has been described, and figure 45 shows a section (E-E of fig. 5) of them through the core. Figures 5 and 7 show plan and end views of their assembly in the reactor, and figure 25 shows cross section D-D of figure 5. Figure 46 shows a complete assembly of a fuel element and moderator block. The fuel element is continuous, but the moderator block is divided into six lengths, as shown in figure 6. The lengths between the outer moderator block and fuel-element support plates OSP1 and OSP2 (see fig. 6) and the inner moderator block and fuel-element support plates ISP1 and ISP5 form the end reflectors. Five of these inner support plates are used in the core, as shown in figure 6. The detail of these plates is shown in figure 47. The outer support plates are similar, except that larger holes (1-in. diam.) are in them to give more area for the flow of greater volume of hot helium at the reactor exit.

The principal problem encountered in the pressure-vessel-enclosed reactor design was the differential radial expansion between the core, reflector, thermal shield, and pressure vessel. This incompatible differential expansion results from the varying expansion rates of the dissimilar materials used in these structures and the high negative radial temperature gradient from the core to the pressure vessel, especially during startup.

To eliminate this radial expansion problem and the stresses resulting from expansion interferences, the supporting structure of the core, reflector, and shields was designed to allow these parts to expand freely radially. This was accomplished without leaving these parts free to cause impact loading between each other during periods of acceleration or deceleration. It was especially important to protect the brittle BeO moderator blocks of the core from any type of impact loading.

In the core the BeO moderator blocks are individually supported by the molybdenum plates shown in figure 47 and similar ones at the outlet, so that clearances for cooling are provided between the blocks. The Mo plates are each supported by 24 radial pins around their circumference as shown in the figure. These radial pins fit into radial holes in the plates and the first Be side reflector (AR1 of fig. 6), which is also used as a support housing for the core. These radial pins allow free radial expansion between the core structure and the side reflector, and

Declassified 1-24-1963

Declassified 1-24-1963

SECRET

also the horizontal and near-horizontal pins allow the first reflector to help support the core weight. The pins finally fit into slots in the second reflector (see fig. 6, reflector AR2), which also helps to support the core weight. Similarly, in the core the moderator blocks and support plates are held together axially by low-stressed through-bolts, making it possible to use thin plates (1/8 in. thick) to support the weight of the moderator blocks and fuel elements. The moderator blocks held together in this manner act as stiffeners for the support plates.

E-288

The control rods are supported independently from the core with necessary clearances to isolate them from the core. Further details of this structure will be given later.

The fuel elements are positioned in the core in the following manner: Each element is attached to an end positioning block by a Mo spring spacer as shown in figure 48. The spacer is brazed to both the positioning block and to the fuel element. The positioning blocks fit into holes in support plate OSP2 as shown in figure 6. The remaining spring spacers that support the fuel element (fig. 25) are brazed to the Mo support bushings shown in figure 46. The five inner support bushings are positioned axially by the moderator blocks, while the end support bushing at support plate OSP1 is positioned axially by a pin through the moderator block. The fuel-tube - positioning-block assembly is slid through the spring spacers and is positioned axially by the block, which has a protuberance as shown in figure 48. The protuberance bears on the shield plate RS1. The positioning block is held between the moderator block and the plate RS1.

The core assembly is surrounded by a thin molybdenum cylindrical flow divider as shown in figure 6. This divider separates the helium flowing through the side reflectors and thermal shields in one direction from the helium flowing through the core in the other direction.

Reflector structure. - The structural features of the first side-reflector cylinder AR1 have been discussed in the preceding section. The weight of the core is further supported through the Be reflector cylinders AR2, AR3, and AR4 by means of spacers between them, as shown in figure 6. The four reflector cylinders are centered and supported by four radial vanes, in both the front and rear of the reactor, over which the cylinders slide (see fig. 6). The vanes at the rear of the reactor are shown in figure 49. The four front radial vanes are attached to the front support shield FS5, and the four rear vanes to the rear support shield RS4 (see figs. 5 and 49). FS5 is centered and supported by the centering pin in the front, and RS4 by the centering collar in the rear.

SECRET
Declassified 1-24-1963

Declassified 1-24-1963

E-288

Thermal shields and pressure-shell structure. - The internal shielding consists of the six side cylindrical shields AS1, 2, 3, 4, 5, and 6 for which the stresses and temperatures were previously given, four circular front shields FS1, 2, 3, and 4 (fig. 6), front shield FS5 (fig. 6) which has been described, three circular rear shields RS1, 2, and 3, (fig. 6), five rear annular shields RAS1, 2, 3, 4, and 5 (fig. 6), and rear shield RS4 (figs. 6 and 49) which has also been described. The front shield FS1 and rear annular shield RAS1 are shown in figures 50 and 51, respectively. The other shields are similar to the two types shown in these figures except that they vary in thickness. Included between RS3 and RS4 are a plenum and ducts for the helium leaving the reactor. The thin cylindrical flow separator around the core butts against this plenum chamber. A cylindrical annular support AS (fig. 6) is placed between the rear circular and annular shields.

The radial vanes described before (the rear ones are shown in fig. 49) also center and support the iron shields. These supports are such that they will give positive location at assembly and allow relative expansions during startup and shutdown. The shield structure is axially positioned by four clamping bars that are axially fixed in the pressure-vessel head. Some details of the shields, ducts, vanes, and clamping bars are shown in figures 7 and 52, which are sections C-C and B-B, respectively, of figure 5.

It is expected that the shield structure and pressure vessel will creep because of the weight and pressure loads at the design operating temperatures. For this reason spacers have been placed on the annular shields to maintain minimum cooling-passage openings and control-rod housing clearances.

Axial motion is not considered serious, since the axial accelerations are not expected to be as high as the vertical and turning accelerations. Provision to prevent axial impact loads due to creep loosening have therefore not been made; they could be incorporated, however, if necessary.

Further details of the way the foregoing structure is supported and assembled in the pressure shell can best be obtained from appendix I, which gives a complete listing of the reactor components and a step-by-step assembly procedure. Following the procedure will clarify the structural picture of figure 6.

Control-rod structure. - The control rods are loaded with $(Mo)_2B_5$ and have a cladding of molybdenum around this material, as shown in figure 53. Each three-layer rod is attached to a molybdenum cylinder by means of molybdenum spring spacers as shown in figure 53. The latter cylinder then slides in a stationary molybdenum sleeve shown in figures

Declassified 1-24-1963

Declassified 1-24-1963

5 and 45. As mentioned, low-temperature helium flows through a hole in each rod as well as around the rod in the annulus formed by the rod outer cladding and the cylinder to which it is attached. Higher-temperature helium also flows through an annulus formed by the support sleeve and the moderator blocks. Details of the helium flow can be obtained from figure 5.

The control rods are independently supported from the core with necessary clearances to isolate them from the core. The sleeves are supported in front by knife-edge supports in FS5 (see fig. 5) and in the rear by similar supports on split positioning rings, shown in figure 5, in the pressure-shell head. The positioning rings are held in place by housings in which the control-rod mechanisms are placed. This type of support for the control rods ensures that the control-rod housings will not be loaded by the core expansions and movements and cause the control rods to jam.

E-288

Reactor Assembly and Stresses

The reactor structural features have been discussed in some detail in a previous section of the report. The method of assembly of the reactor is given in appendix I. This appendix augments the discussion given previously so that a clear picture can be obtained of the reactor structural aspects from it and the material presented herein. A detail worth mentioning is that the fuel-element tubes are designed for removal from the rear end of the core. Replacement is possible by removing the pressure-vessel head and the rear reactor shield assembly. After these are removed, the fuel tubes can be slid in or out for replacement or checking. The fuel tubes are held in place in the reactor by positioning blocks attached to the fuel tubes and clamped between OSP2 and RS1 (see fig. 5). This positioning arrangement permits the tubes to expand freely and also facilitates the replacement of the tubes.

Calculations of some reactor stresses were made, and the results are shown in table IX. They do not include internal stresses due to high internal thermal gradients. The major stresses tabulated for the pressure-vessel wall and flanges are due to the internal helium pressure. Gussets were added to flanges to reduce bending stresses and to reduce maximum combined stresses to 25,000 psi or less for low creep rates.

The primary stresses tabulated in table IX for the reactor core, control rod, and shield components are for weight loads, the assembly of these components being such that no thermal-interference stresses occur between mating parts. The weight loads were based on the operation of a logistic airplane with low maneuvering and landing accelerations during normal operations. The assumed normal maximum acceleration

Declassified 1-24-1963

Declassified 1-24-1963

in the vertical direction was 3 g's. Side and longitudinal accelerations are expected to be less. The normal maximum angular acceleration about the longitudinal axis was assumed to be 6 radians per second^2. Six radians per second^2 is equivalent to a vertical acceleration of 3 g's about the longitudinal axis of a point on the wing 16 feet from the fuselage centerline.

The maximum deflection for the control-rod housing tube is given for a 3-g acceleration load for a shim-scram rod in the most unfavorable position. With this low deflection, these rods should be able to move freely during normal maximum expected accelerations.

E-288

BIOLOGICAL SHIELD

Primary Biological Shield

The determination of the size and weight of a unit biological shield was accomplished by use of the procedure discussed in appendix J.

CA-7

For the typical airplane considered herein, flying at 0.72 Mach number at an altitude of 30,000 feet, calculations revealed a required power of 98.5 megawatts. The dimensions of the reactor, cylindrical in shape, were found to be 24 inches in length and 34.66 inches in diameter. A 4-inch BeO reflector surrounded the reactor. Thermal shields, with provision for cooling, and a pressure shell of maximum 4-inch thickness surrounded the reactor and reflector. The thermal shields and pressure shell were considered part of the gamma shield. Additional required gamma and neutron shielding, exterior to the pressure shell, was determined so as to yield a crew-compartment dose rate of 0.025 rem per hour at a distance of 90 feet from the reactor-core center.

The configuration was divided into six 15° and four $22\frac{1}{2}°$ sectors, as shown in figure 54. The shield external to the pressure shell was shaped (the thicknesses of gamma and neutron shields varied for each sector) so that for the specified total dose rate of 0.025 rem per hour at the crew compartment (for air scattering and direct radiation), the shield weight is minimum. Initial calculations were made for 100 megawatts and a 100-foot separation distance; the results could then be adjusted for the 98.5-megawatt and 90-foot case.

The assumptions and approximations made in the shield evaluation are discussed in appendix J. Any attempt at an analytical evaluation of a shaped shield requires many simplifying assumptions, and at best the shield weights obtained are approximate. The shield method used is based on core radiations only, and the very important source of gammas from captures in the shield is not taken into account. It is hoped

Declassified 1-24-1963

Declassified 1-24-1963

that borated materials used in the shield will reduce these capture gammas to the extent that neglecting them does not cause considerable error in the shield-weight results.

The first set of calculations was made using various combinations of gamma and neutron shielding materials. The results of these calculations, for 100 megawatts and 100 feet, presented in table X in increasing order of total shield weight, reveal considerable differences in weight for the different combinations of materials. The combination Fe-Fe-decalin-LiH was selected for the present reactor shield. Reasons for this choice follow. The typical airplane is of a conservative design, and one which could be built almost immediately. Iron (or borated steel) was selected for use in the inner gamma shield, pressure shell, and outer gamma shield because this material can withstand the temperatures and pressures imposed, can be fabricated in the sizes necessarily required for such an application, is a reasonably good gamma shield, and is relatively inexpensive. Some other of the gamma materials considered would result in a lighter shield, but fabrication with these materials to the required sizes might require a long development program and their costs might be prohibitive. A second requirement imposed in the current design was the use of a chemical fuel as part of the neutron shield. This fuel could be burned in case of emergency. Decalin was chosen for this fuel, and lithium hydride for the remaining neutron shield. The total shield weight including the thermal shields and pressure shell for the chosen materials for the 100-megawatt 100-foot case was 103,000 pounds (see table X). Of this total, 23,000 pounds were decalin; this weight amounts to about 3100 gallons. Table XI presents the calculated exterior gamma- and neutron-shield thicknesses for each sector used in this weight determination. If depleted uranium were used for the gamma shield throughout and lithium hydride for the neutron shield, the weight could be reduced to 73,000 pounds (see table X).

E-288

After selection of the shielding materials (Fe-Fe-decalin-LiH), calculations were made for different reactor powers and different separation distances. The thermal-shield and pressure-shell thicknesses, reactor-core length, crew dose rate, and reflector thickness were all held fixed, but the core diameter was varied by the relation

$$\text{Core diameter} = 3.466\sqrt{\text{Reactor power in Mw}} \quad \text{in.}$$

The diameter is proportional to the square root of the power, since only the number of tubes and the flow through them varied. Reactor powers of 50, 100, 150, and 200 megawatts and separation distances of 50, 100, and 150 feet were considered. The results of the calculations are presented in table XII.

The variation of shield weight with altitude was calculated for the 100-megawatt, 100-foot, 0.025-rem-per-hour case. The scattered neutron

Declassified 1-24-1963

Declassified 1-24-1963

and gamma dose rates were altered by consideration of the variations in air density. The results are shown in figure 55.

The variation in shield weight with dose rate for the so-called standard condition (100 Mw, 100 ft, 30,000 ft) and for the chosen shield materials is given in figure 56.

Calculations were also made for the standard case with dimensions exterior to the reflector held constant, but with different reflector thicknesses and the corresponding variations in core size. For example, the following cases were considered:

Reflector thickness, in.	Core length, in.	Core diameter, in.
2	28	38.66
4	24	34.66
6	20	30.66

The total shield weights for these three cases differed by only 700 pounds.

Other calculations were made for the standard case with the reactor-core size fixed, but with reflector thicknesses of 2, 4, and 6 inches. The thicknesses of the thermal shields and pressure shell were held fixed, but the distance from the reactor-core center to the pressure shell varied as the reflector thickness was changed. The total shield weights obtained were as follows:

Reflector thickness, in.	Shield weight, lb
2	95,000
4	103,000
6	113,000

The final set of calculations was made, again for the standard conditions, but with the decalin replaced by either JP fuel, water, or void. For JP fuel or for H_2O, the dose rate remained at about 0.025 rem per hour. However, with the void, the dose rate increased to 295 rems per hour. Hence, once the reactor is off and the decalin is used for fuel, the reactor must not be restarted until the decalin tanks are refilled. However, if the plane happens to be in a location where decalin is not available, water can be used as a substitute. This, however, will remove the safety factor originally leading to the use of decalin and will also increase the shield weight, but it may make possible the return of the plane to a site where decalin can again be used.

Declassified 1-24-1963

E-288

CA-7 back

Declassified 1-24-1963

Additional Shielding Required for Streaming Through Ducts and for Voids

In addition to the primary biological shield, additional shielding is required to compensate for the presence of ducts and streaming through the ducts. As stated in appendix K, if considerations for these effects are made for neutrons, the resulting additional shielding will also be satisfactory for gamma shielding.

The geometrical considerations of the present problem prevented the use of optimum-sized ducts, and streaming calculations were made by the procedure described in appendix K. It was found that an additional shield weight of 3500 pounds was required to compensate for streaming. An additional 3000 pounds of shielding was also required to compensate for the void in the primary shield caused by the presence of the ducts. This combined additional shielding was added in the form of hemispherical tanks of decalin; about 900 additional gallons of decalin became available for emergency use.

Additional Weight Required to Provide for Shield Cooling

As yet, no discussion has been made regarding provision for cooling the biological shield exterior to the pressure shell. To allow for such cooling, the calculated diameter of the biological shield was increased 8 inches. The additional weight required to compensate for this arbitrarily selected void was calculated to be about 5000 pounds.

Adjustment of Primary Shield Weight for the Typical Airplane

It was previously stated that the so-called standard case (100 Mw, 100 ft, etc.) could be adjusted to the 98.5 megawatts and 90 feet necessary for the typical airplane. This was done, and the resulting weight of the primary biological shield increased from 103,000 to 104,000 pounds.

Total Shield and Reactor Weight

The total weight of the shield plus reactor for the typical airplane can now be found as follows:

Primary biological shield, lb	104,000
Weight for ducts and voids, lb	6,500
Weight for shield cooling voids, lb	5,000
Reactor and reflector weight (given previously in report), lb	4,500
Total, lb	120,000

Declassified 1-24-1963

Declassified 1-24-1963

E-288

Structural Features

The previous discussion of the shield has indicated the amount of gamma and neutron shielding required. Part of the gamma shield (thermal shields) is inside the pressure shell, which surrounds the reactor. A suggested method of constructing the shields exterior to the pressure shell is indicated in figure 9. This figure shows the reactor and shield mounted in the fuselage. Plan, elevation, and end views are presented. The plan view shows that the shield and reactor will occupy a large part of the fuselage width.

Construction. - The gamma shield on the exterior of the pressure shell is a part of the permanent airframe and is a circular yoke, as shown in the end view. This yoke is made of iron containing a small percentage of boron. A method of constructing the neutron shield, consisting of lithium hydride and decalin, is indicated in figure 9. Decalin was selected as the neutron shield forward of the reactor, and lithium hydride in the rear. The additional shielding required for streaming and void effects was chosen as decalin and located in tanks exterior to the primary shield and in direct line with the various duct legs. Figures 6 and 9 show the proposed ducting. The lithium hydride was placed in containers that are stacked, like bricks, in such a way that the joints of successive rows are staggered. The decalin was installed in a series of tanks, as shown. The lithium hydride containers and the decalin storage tanks around and forward of the iron-boron shield are installed permanently. The lithium hydride and the two decalin storage tanks at the rear of the reactor surrounding the flange, ducting, and control-rod actuators must be removable for reactor installation or replacement.

Mounting in fuselage. - The circular-yoke gamma shield, on which the reactor is designed to be mounted, is a permanent part of the airframe. It is attached to the airframe structure by means of the girders indicated in figure 9. The reactor is first attached to a lift outside the airplane. The rear flange of the reactor pressure vessel has a circumferential groove into which the hydraulic lift fixture is secured by hydraulically actuated pins in the lift fixture. The lift mechanism, supported from a railroad track alined with the airplane fuselage, lifts the reactor to its vertical position in the fuselage through bay doors that swing open from the fuselage bottom. The front of the reactor is then slid into the iron-boron shield yoke, with sufficient clearance allowed for cooling. The reactor is then positioned in front by a centering pin and around the flange by a circular I-beam. This I-beam is a part of the permanent airframe structure. An electrical drive mechanism then opens and closes the split ring that positions the reactor axially by fitting in a circumferential groove in the reactor center-

Declassified 1-24-1963

Declassified 1-24-1963

ing pin. The ducts are welded into place after the reactor is secured in the fuselage structure. The lithium hydride containers and the two decalin storage tanks at the rear of the reactor are then installed.

AIRPLANE OPERATION

Propulsion-System Control

The propulsion system is composed of eight turboprop engines with their individual heat exchangers and helium pumps, powered by a common reactor. Since the control scheme is the same for all engines, this section considers the operation of an individual engine.

E-288

Basically, the control system can be divided into three individual component control loops. They are the reactor nuclear control loop, the reactor coolant-flow system, and the turboprop engine control, as shown in the block diagram of figure 57. The nuclear and coolant-flow loops are coupled at the reactor, while the coolant-flow loop and engine are coupled at the heat exchanger and at the engine-driven coolant pump. Interaction between the loops is possible, even to the extent of an engine disturbance being reflected in a nuclear loop response.

The philosophy of the integrated control loop design is to minimize interaction between components without penalizing the component controls of the system; that is, to arrive at a complete system that has both stability and adequate dynamic response time.

The primary change from a conventional turboprop system is the replacement of the conventional fuel-metering valve and burner with a reactor heat source, coolant gas, and heat exchanger. A chemical fuel-burning engine normally uses engine parameters such as temperature and engine speed to vary propeller pitch and fuel flow for control. An analogous system could be used for the nuclear-powered engine. This system could control the heat source by nucleonic means, or use a controllable coolant bypass about the heat exchanger. Some disadvantages of these modes of operation are as follows: (1) Changes in engine power demand place the burden of control on the nuclear loop, increasing the possibility of discontinuous operation; and (2) the transient response to an engine power demand is dependent on the nuclear period, thermal lags in the reactor and heat exchanger, and transport time of the coolant lines.

A more desirable control scheme is shown in figure 58. The engine control consists of two loops, propeller blade pitch controlled by engine speed and power modulation from a turbine bleed control. Normal operation after startup is at a fixed engine speed and fixed reactor power. Fixed engine speed results in a constant airflow through the

Declassified 1-24-1963

Declassified 1-24-1963

compressor and heat exchanger. Since the coolant pump is driven by the engine, it also will operate at constant speed. Therefore, the load on the reactor is essentially constant, reducing the number of nuclear transients. Engine power variations are obtained by regulating the amount of heated airflow through the turbine and the turbine bypass. With the bypass valve fully closed, all the air flows through the turbine, producing rated engine thrust. As more air bypasses the turbine, the rotor speed tends to drop, but the automatic speed control varies the propeller pitch to maintain the desired speed at a loss of propeller power. Therefore, power settings are changed with a minimum of interaction between engine and reactor. Further detailed investigations are needed to study transient effects, loop stability, and automatic turbine bypass operation.

E-288

An additional fuel input is located between the heat exchanger and turbine bypass control where decalin can be metered with an afterburner type flameholder. This chemical fuel system can be used as the primary system when the reactor is inoperative or in conjunction with the reactor to increase turbine temperature up to its limiting value. The control of the chemical fuel, whether automatic or manual, depends on turbine-inlet temperature.

The heat exchanger operates near its critical temperature limit, and in certain phases of the flight plan it may overheat. Therefore, a temperature-limiting control is necessary to restrict reactor power to the temperature limit of the heat exchangers.

Since the integrated control system is a complex network with a reactor and eight turboprop engines, it is reasonable to assume that a crew including both a nuclear engineer and a powerplant engineer is needed to assist the pilots in operation.

Startup and Shutdown Procedure

The startup procedure is a matter of programming the various operations in the reactor, the coolant loop, and the engine to provide a safe, efficient operation. Until the power range of the reactor is reached, the coolant temperature is unchanged, essentially uncoupling the reactor from the engines. Therefore, initially the reactor flux can be increased to the power level and the engines started on chemical fuel independently. For reasons of safety, one or two of the engines should be operative during reactor startup. This provides circulation of the coolant to absorb an accidental overshoot into the power range.

Increasing reactor power through the power range to rated power is a more critical operation. Several reactor limitations restrict the

Declassified 1-24-1963

Declassified 1-24-1963

rate of increasing power. They are the reactor period, reactor temperature, and thermal shock to the reactor components.

The reactor period is governed by control-rod manipulations and is limited by the nucleonics of the system. During the positive reactor period, the reactor temperature will increase and must be maintained within limiting values. The coolant flow must increase with reactor power to maintain temperature below the temperature limit of the reactor. Since the coolant pumps are engine-driven, the engine speed loop control regulates the coolant flow through the reactor. Therefore, coolant flow or engine speed must maintain reactor temperature below its maximum value. Coordination is necessary between the nuclear variations and coolant-flow control to minimize sharp temperature changes. These quick, large temperature variations may cause reactor components to exceed their thermal stress limits.

As the usable power of the reactor becomes available at the heat exchangers, the chemical power can be decreased accordingly. When the reactor is delivering rated power, the engines are at rated speed, with the excess power bypassing the turbine. To take off, the turbine bypass is closed, increasing the propulsion power. Chemical power is used as needed to augment the nuclear power.

The shutdown process is comparatively simple. Insertion of the reactor control rods shuts down the reactor with a stable period of approximately 80 seconds. Chemical fuel is used as needed to maintain an adequate coolant pumping power to remove reactor afterheat.

Off-Design Performance

The design-point performance represents an important phase of airplane operation; however, the characteristics at off-design conditions must be satisfactory in a worthwhile airplane system. Furthermore, some of the demands on the control system can be uncovered by examining the off-design performance. Another important point to be considered is the emergency range supplied by the fuel used as shielding should the reactor become inoperative.

Information on the performance of the typical airplane at off-design flight conditions was determined by calculations based on the following assumptions. The calculations assumed constant shaft speed (engine and pump) type of operation, as mentioned in the discussion of the Propulsion-System Control. The temperature of the helium leaving the reactor was not allowed to exceed the design value of 2250° R, and the temperature of the air leaving the heat exchanger was limited to 1800° R. These temperature restrictions were imposed largely because

Declassified 1-24-1963

Declassified 1-24-1963

of properties of the heat-exchanger material. The compressor performance was estimated from the data of reference 4, and the pump performance map is given in appendix D.

Performance at various altitudes. - Calculated variations of thrust and drag with Mach number are shown in figure 59 for altitudes of 25,000, 30,000, and 35,000 feet. The thrust curves were calculated for purely nuclear operation. The curves show that the maximum flight Mach numbers at 25,000 and 35,000 feet are less than at the design altitude. This result is due to a combination of factors. At high Mach numbers, the drag of the typical airplane at 35,000 feet is less than the drag at 30,000 feet because of the large wing area, as discussed previously. On this basis alone, an increase in Mach number with increasing altitude would be expected. However, the reduction in engine airflow rate with increasing altitude requires that the helium temperature leaving the reactor be reduced below the design value to prevent the air temperature at the heat-exchanger outlet from exceeding the limiting value of 1800° R. As a result, the heat-exchanger material limitations do not allow the power potentialities of the reactor to be utilized at altitudes above design. A similar effect occurs at the design altitude (30,000 ft) for flight Mach numbers below the design value of 0.72. In this case, the engine airflow rate decreases with flight Mach number (changes in ram density ratio), and a decrease in reactor outlet temperature is again required. For example, at a flight Mach number of 0.46 at 30,000 feet, the reactor-outlet temperature must be 2170° R.

At lower than design altitude, the maximum Mach number decreases largely because of the reduction in lift-drag ratio (increase in drag). There is, however, an additional effect caused by temperature limitations. At 25,000 feet and with the maximum reactor-outlet temperature of 2250° R, the turbine-inlet temperature is lower than the design value of 1800° R because of an increased engine airflow rate at the lower altitude.

Takeoff and climb. - Chemical augmentation is required for takeoff and some phases of climb. Calculations showed that, with no burning, the power produced by the turbine was almost entirely absorbed by the compressor and helium pump at sea-level static (takeoff) conditions. At these conditions, the temperature of the air leaving the heat exchanger is only 1460° R because of the high engine airflow rate. If enough fuel is burned to raise the turbine-inlet temperature to 1800° R, an adequate takeoff thrust (86,000 lb) is achieved.

An estimate of the amount of fuel consumed during transition from a climb-out condition to the design flight condition was calculated. The climb was assumed to start from sea level at a Mach number of 0.22 and to progress at constant dynamic head up to 30,000 feet and a Mach

E-288

CA-8

Declassified 1-24-1963

Declassified 1-24-1963

number of 0.41. Subsequently, the airplane is accelerated to a Mach number of 0.72. During this maneuver, the turbine-inlet temperature is maintained at 1800° R by burning fuel at altitudes below 30,000 feet. At 30,000 feet, no fuel is used; in fact, the reactor-outlet temperature is, necessarily, reduced below the design value to meet the temperature limitations discussed previously.

The entire climb maneuver was divided into seven steps for calculation purposes, and the midpoint conditions of each step were used to compute rate of climb and fuel consumption. According to the approximate calculations, 6 minutes are required for the climb and 200 pounds of fuel are consumed. These results show that the 4000 pounds of chemical fuel allowed for takeoff and climb are sufficient.

E-288

Emergency range. - Calculations were made to determine the range provided by the fuel used as part of the neutron shield should the reactor become inoperative. The weight of fuel is about 30,500 pounds in the typical airplane. Time did not allow a complete survey of flight and operating conditions for the purpose of finding maximum emergency range, and only two flight conditions (a Mach number of 0.5 at altitudes of 25,000 and 30,000 ft) were studied. The Mach number of 0.5 was chosen because, at this condition, the airplane operates close to maximum lift-drag ratio or peak aerodynamic efficiency. A turbine-inlet temperature of 1546° R was selected for the emergency range calculations. It is at this inlet temperature that net thrust equals airplane drag.

The fuel used as shielding provides 1.73 hours of flying time and a range of 590 statute miles at 30,000 feet. At 25,000 feet, the time is 1.55 hours and the distance is 540 miles. Other flight or operating conditions may provide greater range; however, more fuel may be required in the interest of safety than is provided in the typical airplane.

The possibility of burning part of the neutron shield as a means of providing emergency propulsion raises several points for discussion. It might be supposed that the after-shutdown radiation may become intolerable because of removal of the decalin. Calculations have shown, however, that the decay of neutron flux is much more rapid than the decalin removal.

Another item of interest is the penalty in payload if the entire neutron shield consists of decalin. It can be shown that the entire shield would weigh an additional 10,000 pounds, with a corresponding decrease in payload. Nevertheless, the weight of decalin would then become 48,000 pounds. The extra amount of decalin would permit the airplane to fly an additional 61 minutes at 0.5 Mach number at 30,000 feet. The emergency range would then become 935 statute miles. It should be mentioned here that the typical airplane already suffers a 5400-pound

Declassified 1-24-1963

Declassified 1-24-1963

penalty in payload compared with that available if the entire neutron shield is lithium hydride.

As mentioned in the section BIOLOGICAL SHIELD, if all the decalin has been burned the reactor must not be restarted. It would be necessary to land the airplane and fill the decalin tanks with water (if no fuel is available) before starting up the reactor.

E-288

CA-3 back

FABRICATION AND DESIGN FEATURES

In the designs described in this report it has been stated that certain items would be fabricated, without indicating the means of fabrication. In addition, several items were not designed; it was merely stated that they were provided. The most important among the latter were several features of the control-rod design. No calculations were made of coolant-flow rates or control-rod temperatures nor was the radiator designed for cooling the low-temperature helium passing through the control rods. The amount of $(Mo)_2B_5$ required in each rod also was not calculated. Statements were also made that cooling is provided around the pressure shell and through the biological shield, but no detailed calculations were made of these temperatures. None of these problems are considered serious enough to prevent the attainment of the reactor design proposed, and consequently for this type of study they are not considered in detail.

In connection with the fuel elements, it was stated that they would be made of molybdenum and UC. Experience is lacking for mixtures of this nature. The following discussion is known to apply to UO_2 and Mo fuel elements, and it is expected that similar procedures would apply to the fuel elements used herein. The UO_2 and Mo, both in powder form, are mixed in proper proportions, blended, and cold-pressed in a die to form annular disks. The disks are then assembled to form tubes. The tubes are made in this way so that the fuel can be nonuniformly distributed both axially and radially, since the disks vary in fuel quantity. In the mixture of UO_2 and Mo, there is a tendency for the Mo to react with the oxygen. The pressed disk is heated to about 3500° F in a Mo furnace with hydrogen atmosphere. The cladding may be put onto the meat by the use of molybdenum hexacarbonyl $Mo(CO)_6$. The carbonyl is volatile at a low temperature. When passed over the fuel element, it decomposes, depositing Mo on the meat and releasing CO.

The stresses calculated for the fuel elements did not include pressures in the material caused by fission-product gases buildup. Uranium and its alloys tend to swell during irradiation because of such buildup (e.g., xenon and krypton). This tendency increases at high temperatures.

Declassified 1-24-1963

Declassified 1-24-1963

Fission-product gases produce excessive pressures in metal already weakened by high temperature.

UO_2 is free from the swelling and corrosion problems associated with uranium metal. When compacted to a high density, sintered, and irradiated at moderate temperatures, UO_2 can retain fission-product gases with no swelling at much higher burnups than metallic uranium elements. It is believed that extra space in the crystal lattice provides for the fission products. It appears that UC combines the best characteristics of U and UO_2. Furthermore, UC has excellent thermal conductivity and good irradiation stability. In the fabrication of the reactor, the fuel element proposed would first have to be developed to prove some of the expectations discussed.

E-288

Lithium hydride was proposed as a shielding material, and some of its physical properties will be reviewed in this section to indicate its probable feasibility as a shielding material. Lithium hydride LiH comes as a crystalline solid, but is also available as a powder. It is in the latter form that it is proposed herein to use it.

The finely divided powder is quite hazardous, since it is highly flammable if contacted with a small amount of water. In fact, powdered LiH ignites spontaneously upon exposure to air on a very humid day. At elevated temperatures, LiH reacts violently with oxygen and the halogens. In addition, LiH dust is irritating to nose, throat, and skin.

The container proposed for the powdered LiH must be impervious to hydrogen and capable of withstanding relatively high pressure. The container must also resist attack of LiH at high temperatures, have high tensile strength, and be sealed hermetically. The tensile strength should be about 50,000 psi at 1200° F. Low-carbon stainless steels are suitable and easily available container materials. Satisfactory canning techniques for preparing hydrides for shielding purposes are still in the development stage. Glass, quartz, and enameled containers should not be used, since LiH has the ability to crack these materials at low temperatures.

The fact that in the present reactor the LiH shield is out far from the core results in an environment in which heating and flux are not too high. In the present design, air-cooling has been provided for further reducing the heat to which the LiH is subjected.

CONCLUDING REMARKS

This study was made to determine the payload capacity and the design feasibility of a helium-cooled nuclear-powered turboprop subsonic

Declassified 1-24-1963

Declassified 1-24-1963

airplane. A gross weight of 400,000 pounds, comparable to some airplanes in current production, was selected; and conservative design principles were used whenever possible.

A 63,000-pound payload was obtained. This is about 16 percent of the gross weight and compares favorably with payloads of current conventional large airplanes.

E-288

This nuclear airplane appears feasible, subject to experimental confirmation of several components. The nuclear reactor will require the most research and development. Fuel-element fabrication and testing and control-rod fabrication, testing, and operation are of primary importance. Experimental data on the adequacy of the shielding are also required. In addition to reactor research and development, the heat exchangers and helium pumps require experimentation. The heat exchanger restricts the turbine-inlet temperature to 1800° R because of material limitations. Heat exchangers must be developed even for this low a value of turbine-inlet temperature. If the turbine-inlet temperature could be increased 100° R, a 6000-pound increase in payload would result. Although the aerodynamic design of the helium pumps is conservative, the high rotational speed (65,800 rpm) will pose problems in bearing and shaft seal design.

No problems are anticipated in the compressors and turbines because of their conservative designs. In addition, the weight and size of the airplane create no runway problems.

Lewis Research Center
National Aeronautics and Space Administration
Cleveland, Ohio, April 10, 1959

Declassified 1-24-1963

Declassified 1-24-1963

APPENDIX A

AIRPLANE AERODYNAMIC PERFORMANCE AND STRUCTURAL WEIGHT

The equations and methods that were used to calculate lift-drag ratios and structural weights of the airplanes are presented herein. In calculating the performance and weight it is assumed that the following items are either known or specified: flight conditions (Mach number and altitude), gross weight of airplane, fuselage size and geometry, wing cross section and taper ratio (but not sweep or area), and maximum landing speed. A photograph of a model of the typical airplane is shown in figure 2. The lift-drag ratio of the airplane is calculated first. In this calculation the geometry and size of all the parts are completely specified. This information is then used to calculate the structural weights.

E-288

Symbols

The following symbols are used in appendix A:

A	surface area factor; multiplier to define skin weight as a function of surface area
A_t	horizontal plus vertical plan-form tail area, sq ft
A_w	wing plan-form area, sq ft
$\mathscr{A}$	aspect ratio, b^2/A_w
B	bending structural factor; multiplier to define bending weight as a function of load transmitted
b	aerodynamic span, ft
b_s	structural span (distance from wing tip to tip along mid-chord), ft
C_D	total airplane drag coefficient, based on wing plan-form area
$C_{D,fr}$	friction drag coefficient, based on surface area
$C_{D,L}$	induced drag coefficient, based on wing plan-form area
C_L	wing lift coefficient, based on wing plan-form area
D	total airplane drag, qA_wC_D, lb

Declassified 1-24-1963

Declassified 1-24-1963

E-288

d_F	equivalent fuselage diameter, ft
f_1, f_2, f_3, f_4	functions defined by equations (A23), (A24), (A25), and (A26), respectively
K	ratio of design to optimum lift coefficient
K_{eq}	ratio of equipment weight to gross weight
K_{lg}	ratio of landing-gear weight to gross weight
L	wing lift, lb
l_F	fuselage length, ft
M	flight Mach number
M_{div}	drag-divergence Mach number (eq. (A5))
m	sweep efficiency factor, induced drag without sweep divided by induced drag with sweep
N	$1 - \frac{1.5}{\mathscr{A}}$
n	normal load factor, number of design g's divided by level-flight g of 1
q	dynamic pressure, $\frac{1}{2}\rho v^2$, lb/sq ft
Re	Reynolds number
S_F	fuselage surface area, sq ft
v	velocity, ft/sec
W_{eq}	equipment weight that is independent of gross weight, lb
W_F	fuselage structural weight, lb
$W_{F,avail}$	available load in fuselage, lb
$W_{F,l}$	total weight of fuselage and contents and tail, lb
W_G	airplane gross weight, lb
$W_{R,w}$	total weight on wing but excluding wing weight, lb

Declassified 1-24-1963

Declassified 1-24-1963

W_t	weight of tail or empennage surfaces, lb
W_w	wing weight, lb
$W_{w,avail}$	available load on wing, lb
γ	ratio of specific heats for air
Λ	wing leading-edge sweep
λ	taper ratio, ratio of tip chord to root chord
ρ	density, slugs/cu ft
τ	wing thickness ratio

Subscripts:

F	fuselage
max	maximum
opt	optimum
w	wing

Lift-Drag Ratio

The lift-drag ratio was calculated for the airplane without the powerplant or nacelles. The drag of these components is accounted for by subtracting their drag from the engine thrust. Thus the airplane drag, as hereafter referred to, does not include the engine or nacelle drag.

The airplane lift-drag ratio is taken to be the lift of the wing divided by the sum of all the drags of the airplane (except engine and nacelle).

For subsonic flight the pressure or wave drag is assumed to be zero in all cases. For the wing, the sweep is set to assure that this is true. The airplane drag, therefore, is composed only of skin-friction drag and the induced drag (drag due to lift) of the wing.

Skin-friction drag. - The skin-friction drag coefficient $C_{D,fr}$ is calculated from two different equations depending on whether the flow is laminar or turbulent. In either case the value 0.0005 is added to the

Declassified 1-24-1963

Declassified 1-24-1963

usual equations to account for skin roughness. When the Reynolds number Re is less than 2×10^5, the skin-friction drag coefficient is defined by the following laminar-flow equation (including the term for roughness):

$$C_{D,fr} = \frac{1.328}{\sqrt{Re}} + 0.0005 \tag{A1}$$

This equation, without the roughness correction term 0.0005, is given in reference 19. If Re is greater than 6×10^6, $C_{D,fr}$ is defined by the following turbulent-flow equation:

$$C_{D,fr} = \frac{0.0306}{(Re)^{1/7}\left(1 + \frac{\gamma - 1}{4} M^2\right)^{5/7}} + 0.0005 \tag{A2}$$

This equation, minus the roughness correction, is taken from reference 20 and is a flat-plate equation in which the temperature is the arithmetic average of the wall and free-stream temperatures. The Reynolds number is based on the fuselage length for the fuselage and on the root chord for the wing. For Reynolds numbers between 2×10^5 and 6×10^6, combined laminar and turbulent boundary layers are considered. That portion or surface of the fuselage or wing from the forward part to the distance that results in a Reynolds number of 2×10^5 is taken as laminar with Reynolds number of 2×10^5, and the remaining surface is assumed to have turbulent flow with Reynolds number based on the full length. With tapered wings (i.e., tip chord less than root chord), it was arbitrarily assumed that the same fraction of the wing surface was laminar for the entire wing as at the wing root, even though the root chord is longer than any other chord for tapered wings.

Induced drag. - The induced drag or drag due to lift is found from the parameter $C_{D,L}/C_L^2$. The theoretical value of $C_{D,L}/C_L^2$ for subsonic airplanes is $1/\pi\mathscr{A}$ for elliptical wings and elliptical pressure distribution. In practice, the induced drag is higher than this theoretical value. With appropriate values for the airplane type under consideration and some allowance for inefficiencies, the following equation was used:

$$\frac{C_{D,L}}{C_L^2} = \frac{1}{m}\left(\frac{1}{0.95\,\pi\mathscr{A}} + 0.006\right) \tag{A3}$$

where the value of the sweep efficiency factor m is a function of the sweep angle Λ and is given by

$$m = \sqrt{\cos\Lambda} \tag{A4}$$

Declassified 1-24-1963

E-288
CA-9

Declassified 1-24-1963

The induced drag coefficient $C_{D,L}$ is, of course, found by multiplying $C_{D,L}/C_L^2$ by the square of the lift coefficient.

Sweep angle. - The sweep angle of the wing is set so that the drag-divergence Mach number M_{div} of the wing is equal to or higher than the flight Mach number. The drag-divergence Mach number is defined by

$$M_{div} = \frac{1}{\cos^N \Lambda}\left[(0.75 - 0.1333\ C_L)\left(1 + \frac{0.24}{\mathscr{A}}\right) - 0.01\right] \tag{A5}$$

where

$$N = 1 - \frac{1.5}{\mathscr{A}} \tag{A6}$$

In order to provide some margin between M_{div} and the design flight Mach number M, the following equation was used to find the sweep angle Λ:

$$(\cos \Lambda - 0.02)^N = \frac{1}{(M + 0.02)}\left[(0.75 - 0.1333\ C_L)\left(1 + \frac{0.24}{\mathscr{A}}\right) - 0.01\right] \tag{A7}$$

Tail drag. - The tail surfaces are assumed to have no lift, so that there is no induced drag of the tail. The skin-friction drag coefficient of the tail surfaces is assumed to be the same as that for the main wing, regardless of the Reynolds number. Thus, the friction drag of the main wing is increased by the factor $\left(1 + \frac{A_t}{A_w}\right)$. The tail area A_t was assumed to be 0.40 times the wing area A_w.

Lift-drag ratio. - The lift-drag ratio is given by the ratio of lift coefficient to the total drag coefficient:

$$\frac{L}{D} = \frac{C_L}{C_D} \tag{A8}$$

where

$$C_D = C_{D,L} + 2\left(1 + \frac{A_t}{A_w}\right)C_{D,fr,w} + \frac{S_F}{A_w}\ C_{D,fr,F} \tag{A9}$$

and both C_L and C_D are based on the wing plan-form area. For simplicity, the wing and tail surface areas are taken to be twice the plan-form area. The surface of the fuselage S_F is, for simplicity, taken to be the surface of a cylinder (excluding the ends) having values for length and diameter equal to those of the fuselage. This is almost

Declassified 1-24-1963

Declassified 1-24-1963

exactly true for a fuselage having a main cylindrical section and ellipsoidal ends each with length-diameter ratio of 2.5.

Optimum wing area. - The wing lift is given by

$$L = qC_L A_w \tag{A10}$$

The dynamic pressure q is determined by the flight conditions (Mach number and altitude), and the lift L is equal to the airplane gross weight W_G. Thus, the product $C_L A_w$ is specified by the gross weight and flight conditions. The specification of the wing area A_w or alternatively the lift coefficient C_L is difficult; it is usually set to provide the best compromise of lift-drag ratio and structural weight of the airplane. The lift coefficient C_L is generally made larger than that for maximum lift-drag ratio, because this results in a smaller and therefore lighter wing. The optimum value of C_L for best over-all performance may vary considerably, depending on the flight conditions and many other factors. At the same time the lift coefficient for maximum lift-drag ratio also varies, and therefore it was found convenient to specify the ratio of lift coefficient C_L to the lift coefficient for maximum lift-drag ratio $C_{L,opt}$. The value of $C_{L,opt}$ can be calculated from known fuselage drag and flight conditions. Therefore, by specifying the ratio K, where

$$K = \frac{C_L}{C_{L,opt}} \tag{A11}$$

the wing area A_w can be determined. Various values of K can be tried to determine which value gives the best over-all performance.

The wing area for a given airplane also determines the landing speed. Thus, if the landing speed is not to exceed a certain value, the wing area must be greater than a certain minimum value for a given airplane gross weight. Consequently, the wing area is taken to be the larger of the values determined (1) by the maximum landing speed or (2) from the lift coefficient as determined by $C_{L,opt}$ and the specified value of K.

The wing area determined from this lift coefficient is found from the following equations. The wing area is given by

$$A_w = \frac{W_G}{qC_L} \tag{A12}$$

The lift coefficient is determined from equation (A11), where K is set arbitrarily by experience to give the best airplane performance. The

Declassified 1-24-1963

E-288

CA-9 back

Declassified 1-24-1963

optimum lift coefficient $C_{L,opt}$ is defined as that value which gives the maximum lift-drag ratio. From equations (A3), (A8), and (A9),

$$\frac{L}{D} = \frac{C_L}{\frac{C_L^2}{m}\left(\frac{1}{0.95\,\pi\mathscr{A}} + 0.006\right) + 2\left(1 + \frac{A_t}{A_w}\right)C_{D,fr,w} + \frac{S_F}{A_w}\,C_{D,fr,F}} \tag{A13}$$

Setting the derivative of L/D with respect to C_L equal to zero and solving for $C_{L,opt}$ result in

$$C_{L,opt} = \sqrt{\frac{2\left(1 + \frac{A_t}{A_w}\right)C_{D,fr,w}}{\frac{1}{m}\left(\frac{1}{0.95\,\pi\mathscr{A}} + 0.006\right)}} \tag{A14}$$

Combining equations (A11), (A12), and (A14) and solving for A_w yield

$$A_w = \sqrt{\frac{\left(\frac{W_G}{qK}\right)^2 \frac{1}{m}\left(\frac{1}{0.95\,\pi\mathscr{A}} + 0.006\right)}{2\left(1 + \frac{A_t}{A_w}\right)C_{D,fr,w}}} \tag{A15}$$

An iterative procedure is sometimes required, since m depends on C_L or A_w. In other cases, however, where the wing area is determined by landing speed, this iteration is avoided. From equation (A12), the minimum wing area for a given weight is determined by the maximum value of q (set by landing speed at sea level) and the maximum value of C_L (1.75).

Structural Weights

The total airplane gross weight is made up of (1) several known or assumed fixed weights, such as fixed equipment; (2) equipment weight that is proportional to or a function of the gross weight; (3) some weights not presently known but to be determined later, such as powerplant or shield weight, which can only be determined after the drag or required thrust is known; (4) structural weights; and (5) payload. Methods for calculating the structural weights will be discussed in this section.

The structural weights are, to some extent, dependent on the distribution of the loads in the airplane. Principally, removing loads from the fuselage and locating them on the wing, where the lift occurs, decreases the bending moments in both the wing and the fuselage. Since the

Declassified 1-24-1963

Declassified 1-24-1963

load distribution is not always known initially, the structural weights for each airplane were first determined for a range of load distributions.

The structural weights of both the wing and fuselage are assumed to consist of two parts: One part is a function of the surface area, and the other part is a function of the bending moments. The wing weight is given by

E-288

$$W_w = 1.5\ A_w + 0.03\ \frac{A_w^2}{b_s} + 2(10^{-6})\ \frac{b_s^3 n(1 + \lambda)}{\tau A_w}\ W_{F,l} \tag{A16}$$

For the fuselage,

$$W_F = 3d_F^2\ \frac{l_F}{d_F} + 2.72(10^{-5})nd_F\left(\frac{l_F}{d_F}\right)^2\ W_{F,l} \tag{A17}$$

In both equations (A16) and (A17) the last term is a function of the bending moments. The term $W_{F,l}$ is the total load causing bending moments at the wing root and is equal to the total load in the fuselage plus the weight of the fuselage and tail.

Equations (A16) and (A17) can be rewritten as

$$W_w = f_1(A_w) + W_{F,l}f_2(B_w) \tag{A18}$$

and

$$W_F = f_3(A_F) + W_{F,l}f_4(B_F) \tag{A19}$$

where all the factors except $W_{F,l}$ are determined by the geometry, size, and load factor n.

The weight of the empennage or tail is given by

$$W_t = \frac{A_t}{A_w}\ f_1(A_w) + \frac{n - 1}{n}\left(\frac{A_t}{A_w}\right)^{3/2}\ f_2(B_w)W_{F,l} \tag{A20}$$

The factor $\frac{n - 1}{n}$ accounts for the fact that in normal flight the tail was assumed to carry no load, so that during turns or climb when the angle of attack is above normal the lift coefficient on the horizontal tail surface is $\frac{n - 1}{n}$ times that of the main wing.

The structural-weight equations presented are not available in any reference. There are very few sources that present equations that are useful in a study of this type. In general, they are either much too

Declassified 1-24-1963

Declassified 1-24-1963

detailed to be used in a study that must consider the complete airplane or so simple that they do not include the trends or variations that are desired when considering airplanes of different sizes, types, geometry, and so forth. Those equations that have been given in the literature and are suitable for a study of this type are generally in agreement as to trends but seldom in agreement regarding the magnitude of the trends. In the equations presented herein, an attempt was made to include any significant trend that might affect the weight and to obtain values that are in general agreement with other available sources.

The structural weights and allowable loads can now be computed in the following manner. All required values are either known from the calculation of lift-drag ratio or selected. The aerodynamic span b is given by

$$b = \sqrt{A_w \mathscr{A}} \tag{A21}$$

The structural span (distance from wing tip to tip along the midchord) b_s is given by

$$b_s = \frac{b}{\cos \Lambda} \tag{A22}$$

Also,

$$f_1(A_w) = 1.5\ A_w + 0.03\ \frac{A_w^2}{b_s} \tag{A23}$$

$$f_2(B_w) = 2(10^{-6})\ \frac{b_s^3 n(1 + \lambda)}{\tau A_w} \tag{A24}$$

$$f_3(A_F) = 3d_F^2\ \frac{l_F}{d_F} \tag{A25}$$

and

$$f_4(B_F) = 2.72(10^{-5}) n d_F \left(\frac{l_F}{d_F}\right)^2 \tag{A26}$$

Various values are then assumed for $W_{R,w}$, the load that is placed on the wing but excluding the weight of the wing.

Then the wing weight is given by

$$W_w = \frac{f_1(A_w) + (W_G - W_{R,w}) f_2(B_w)}{1 + f_2(B_w)} \tag{A27}$$

Declassified 1-24-1963

Declassified 1-24-1963

and the total fuselage load $W_{F,l}$ as previously defined is

$$W_{F,l} = W_G - W_{R,w} - W_w \tag{A28}$$

Then the fuselage structural weight is

$$W_F = f_3(A_F) + W_{F,l} f_4(B_F) \tag{A29}$$

and the tail weight W_t (including the vertical fin) is given by equation (A20).

E-288

All equipment is assumed to be carried in the fuselage so that the remaining load available in the fuselage for payload, reactor, shielding, or powerplant is

$$W_{F,avail} = W_{F,l} - W_F - W_{eq} - K_{eq}W_G - K_{lg}W_{F,l} - W_t \tag{A30}$$

It is assumed that the landing-gear weight (which is $K_{lg}W_G$) is divided between the fuselage and the wing in proportion to the gross weight of these components. Thus, the landing-gear weight in the fuselage is $K_{lg}W_{F,l}$, and that on the wing is $K_{lg}(W_G - W_{F,l})$.

The load available on the wing, then, for powerplant or externally mounted reactor and shielding is

$$W_{w,avail} = W_{R,w} - K_{lg}(W_G - W_{F,l}) \tag{A31}$$

Values of $W_{F,avail}$ can be plotted as a function of $W_{w,avail}$ as $W_{R,w}$ is varied. When the load on the wing $W_{w,avail}$ is known, the weight available in the fuselage $W_{F,avail}$ can be determined.

Assumed Airplane Design Variables

Where not otherwise noted, the following values were used in the airplane analysis:

Fuselage fineness ratio, l_F/d_F	10.0
Aspect ratio, $\mathscr{A}$	10.0
Wing thickness ratio, τ	0.15
Taper ratio, λ	0.30
Maximum lift coefficient at landing, $C_{L,max}$	1.75
Maximum landing speed, v_{land}, ft/sec	175.00
Normal load factor, n	2.0
Landing-gear- to gross-weight ratio, K_{lg}	0.075
Equipment weight (independent of gross weight), W_{eq}, lb	10,000
Equipment weight factor, K_{eq}	0.030

Declassified 1-24-1963

Declassified 1-24-1963

In all cases investigated the wing area was determined by the landing speed.

E-288

Declassified 1-24-1963

Declassified 1-24-1963

E-288

CA-10

APPENDIX B

ENGINE DESIGN AND WEIGHT

The performance of the turboprop-engine type selected for this mission was calculated by conventional methods with the aid of references 6 and 21. Both engine weight and performance were calculated by methods which, as for the airplane, show the effects of changes in the design or operating conditions and give results that are in general agreement with the existing technology. As with the airplane, rather conservative performance and adequately heavy components were assumed, thus covering cases where changes have to be made to existing equipment or new engines must be built with a minimum of development time and effort.

Calculations were first made to determine the shaft power and net jet thrust for the assigned engine operating conditions, turbine-inlet temperature, compressor pressure ratio, and pressure losses. Sizes of the various engine components were next calculated for a range of engine airflows by assigning values to flow parameters of the compressor and turbine. Finally, engine weight and drag were calculated for the same range of engine sizes. The equations for calculating the engine weight are presented later. As described in appendix A, the engine drag was subtracted from the engine thrust instead of added to the airplane drag. In this way the engine size is not required when calculating airplane performance. The drag of the engine was calculated by the same methods as were used for the airplane fuselage.

As with the airplane, most calculations were made for a standard set of conditions. Variations were then made in some of these conditions, varying them one at a time, to determine their effect on over-all airplane performance. Conditions typical of those that were varied are compressor pressure ratio, turbine-inlet temperature, and heat-exchanger and line pressure losses. Other design conditions, such as efficiencies and flow parameters, were held constant throughout the analysis, and these values are listed in table III.

Symbols

The following symbols are used in appendix B:

d tip diameter, in.

ΔH change in total enthalpy, Btu/lb

l length, in.

Declassified 1-24-1963

Declassified 1-24-1963

SECRET

P_2/P_1 compressor pressure ratio

HP shaft horsepower

W weight, lb

Subscripts:

A accessories

C compressor

E engine

g reduction gear

m miscellaneous

N exhaust nozzle

nac nacelle

st structure

T turbine

E-288

Equations Used

In reference 22, empirical formulas are given for calculating the component weights of gas-turbine engines. These equations were modified to give slightly heavier components, and the resulting equations used in this analysis are given herein.

Compressor:

$$W_C = 0.133\ l_C d_C \tag{B1}$$

where

$$\frac{l_C}{d_C} = \ln \frac{P_2}{P_1} \tag{B2}$$

Turbine:

$$W_T = 0.0052(\Delta H)_T d_T^2 \tag{B3}$$

Declassified 1-24-1963

SECRET

Declassified 1-24-1963

Structure:

$$W_{st} = 3\left[50 + 0.1(W_C + W_T)\right] \tag{B4}$$

Accessories:

$$W_A = 125 + 0.02(W_C + W_T) \tag{B5}$$

Exhaust nozzle:

$$W_N = d_T^2\left(0.05 + 0.01\,\frac{P_2}{P_1}\right) \tag{B6}$$

Reduction gear:

$$W_g = 0.1\ HP \tag{B7}$$

Miscellaneous:

$$W_m = 0.2(W_C + W_T + W_{st} + W_A) \tag{B8}$$

The total engine weight W_E is equal to the sum of these component weights. In addition, a nacelle weight was added, taken to be

$$W_{nac} = 0.25\ W_E \tag{B9}$$

The nacelle dimensions were assumed to be defined by the following equations:

$$d_{nac} = 1.2\ d_T \tag{B10}$$

and

$$l_{nac} = 6.0\ d_{nac} \tag{B11}$$

E-288

CA-10 back

Declassified 1-24-1963

Declassified 1-24-1963

APPENDIX C

HEAT EXCHANGER, HEADERS, AND LINES

Heat-Exchanger Core Design

A program was devised for an IBM 653 computer for designing heat exchangers of a variety of configurations encompassing parallel-flow and crossflow geometries. References 8, 9, and 23 served as the bases for the heat-exchanger calculations.

Symbols

The following symbols are used in appendix C:

A,B	empirical constants
c_p	specific heat at constant pressure, Btu/(lb)(°R)
d	diameter, ft
d_h	hydraulic diameter, ft
f	friction factor
g	acceleration due to gravity, ft/sec^2
h	heat-transfer coefficient, Btu/(sq ft)(sec)(°R)
k	thermal conductivity, Btu/(sec)(ft)(°R)
l	length, ft
n	number of passes
P	pressure, lb/sq ft
Pr	Prandtl number, $c_p\mu/k$
Re	Reynolds number, $\rho vd/\mu$
S	wetted surface area, sq ft
St	Stanton number, $h/\rho vc_p$
T	temperature, °R

Declassified 1-24-1963

Declassified 1-24-1963

E-288

Tu	number of heat-transfer units
U	over-all heat-transfer coefficient, Btu/(sq ft)(sec)(^{o}R)
v	velocity, ft/sec
w	weight flow, lb/sec
Z	ratio of heat capacities
η_t	over-all heat-exchanger effectiveness
η_1	defined by eq. (C6)
$\eta_{1,1}$	defined by eq. (C7)
μ	absolute viscosity, lb/(ft)(sec)
ρ	density, lb/cu ft

Subscripts:

A	first fluid
B	second fluid
cir	circular
i	inner
max	maximum
min	minimum
n	number of passes
o	outer
1,2	stations

Superscripts:

a,b,c	empirical constants

Declassified 1-24-1963

Declassified 1-24-1963

Calculation Procedure

The relation employed in calculating heat-transfer coefficients was

$$(Re)(St) = A \frac{(Re)^a}{(Pr)^b} \tag{C1}$$

Friction factors for pressure-drop calculations were determined from

$$f = B(Re)^c \tag{C2}$$

E-288

In these two equations, A, B, a, b, and c are empirical constants applicable to a particular geometry. The quantities Re, Pr, and St are evaluated for average bulk or film properties depending on the type of data correlation used as source material for the empirical constants. For example, the data on compact heat exchangers in reference 9 are presented in terms of the bulk properties of the heat-exchanger fluid.

General method. - For this project, interest centered on multipass crossflow heat exchangers with the heating fluid, helium, contained in tubes. Air flows perpendicularly across the tubes, which are arranged to give multiple helium passes. Values of the empirical constants in equations (C1) and (C2) were taken from reference 8 for the helium side and from reference 9 for the air side of the heat exchanger.

Input to the heat-exchanger design calculations consisted of the following:

(1) Inlet and outlet total temperatures of both gases

(2) Inlet total pressures of both gases

(3) Weight-flow rate of air

(4) Allowable total-pressure losses for both gases

(5) Allowable tube wall stress

(6) Tube and fin metal thermal conductivities

(7) Geometrical data such as the spacings and diameter of the tubes and the pitch and thickness of fins

The design calculations then provided the weights of the tubes and the fins, the number of tubes required, and the dimensions of the heat exchanger. Header and shell weights were determined in a separate calculation.

Declassified 1-24-1963

Declassified 1-24-1963

E-288

Calculation details. - Reference 9 presents a partly graphical method for calculating multipass crossflow heat exchangers. For use in the automatic computer, some of the design curves in reference 9 were approximated by polynomials, and these details may be of interest.

The surface area of the exchanger is computed from

$$S = \frac{(Tu)_n (wc_p)_{min}}{U} \tag{C3}$$

The quantity $(wc_p)_{min}$ is the smaller of the two products of weight-flow rate and specific heat, and $(Tu)_n$ is the number of heat-transfer units for an n-pass exchanger. This latter quantity is a function of the over-all heat-exchanger effectiveness η_t, the number of passes n, and a ratio of heat capacities Z:

$$Z = \frac{(wc_p)_{min}}{(wc_p)_{max}}, \qquad Z \leq 1 \tag{C4}$$

The procedure for evaluating $(Tu)_n$ is as follows. The over-all heat-exchanger effectiveness is given by

$$\eta_t = \left| \frac{(wc_p)_A (T_{A,1} - T_{A,2})}{(wc_p)_{min} (T_{B,1} - T_{A,1})} \right| \tag{C5}$$

The calculation procedure then required that the over-all effectiveness be converted to an equivalent effectiveness η_1 of a single-pass heat exchanger:

$$\eta_1 = \frac{\left(\frac{\eta_t Z - 1}{\eta_t - 1}\right)^{1/n} - 1}{\left(\frac{\eta_t Z - 1}{\eta_t - 1}\right)^{1/n} - Z} \tag{C6}$$

A relation between the effectiveness $\eta_{1,1}$ of a single-pass heat exchanger for which $Z = 1$ and the effectiveness η_1 of a single-pass heat exchanger for which $Z \neq 1$ is

$$\eta_{1,1} = \frac{\eta_1}{1.37 - 0.37\,Z} \tag{C7}$$

Declassified 1-24-1963

Declassified 1-24-1963

Equation (C7) is an approximation determined from figure 5 in reference 9. The desired value for the number of heat-transfer units $(Tu)_n$ was obtained from

$$(Tu)_n = n(1.4\ \eta_{1,1} + 14\ \eta_{1,1}^5) \tag{C8}$$

This equation was also obtained from figure 5 in reference 9. The resulting value of $(Tu)_n$ permitted the calculation of heat-exchanger surface area by means of equation (C3).

Helium and air properties. - Helium properties were calculated from the following relations based on reference 24:

Absolute viscosity μ:

$$\mu = 2.3072\times10^{-7}(T)^{0.647}\ \text{lb/(ft)(sec)} \tag{C9}$$

Thermal conductivity k:

$$k = 4.085\times10^{-7}(T)^{0.650}\ \text{Btu/(sec)(ft)(}^{\circ}\text{R)} \tag{C10}$$

Specific heat of helium was taken constant at 1.25 Btu/(lb)($^{\circ}$R).

Air properties were based on reference 25 and were calculated from the following expressions:

Absolute viscosity μ:

$$\mu = 1.672\times10^{-7}(T)^{0.684}\ \text{lb/(sec)(ft)} \tag{C11}$$

Thermal conductivity k:

$$k = 2.055\times10^{-8}(T)^{0.846}\ \text{Btu/(sec)(ft)(}^{\circ}\text{R)} \tag{C12}$$

Specific heat c_p:

$$c_p = 0.117(T)^{0.112}\ \text{Btu/(lb)(}^{\circ}\text{R)} \tag{C13}$$

The temperature T in all the property equations is measured in degrees Rankine.

Helium Lines

As mentioned in the body of this report, concentric helium lines are used for transporting helium from the reactor to the engines and back again. The high-temperature helium flows through the inner lines,

Declassified 1-24-1963

Declassified 1-24-1963

and the low-temperature helium flows in an annulus surrounding the inner line. The method used for determining diameters of the lines will now be discussed.

An expression is derived for the required diameters of the helium lines for specified conditions of length l, pressure drop ΔP, and weight-flow rate w. The derivation assumes an incompressible, constant-temperature flow, which is satisfactory for this situation, since the allowed pressure drop is small and the heat flow from the lines can be reduced to relatively low values.

E-288

Circular cross section. - The equations necessary for determining the required inside diameter d of a circular pipe are as follows:

$$\Delta P = 4f \frac{l}{d} \frac{\rho v^2}{2g} \tag{C14}$$

$$w = \frac{\pi}{4} d^2 \rho v \tag{C15}$$

CA-11

$$4f = 0.316(Re)^{-1/4} \text{ (eq. (131), p. 81, ref. 7)} \tag{C16}$$

$$Re = \frac{\rho v d}{\mu} \tag{C17}$$

A combination of these equations yields for d:

$$d^{19} = \left(\frac{0.16}{g}\right)^4 \left(\frac{4}{\pi}\right)^7 \left(\frac{l}{\rho\ \Delta P}\right)^4 \mu w^7 \tag{C18}$$

or

$$d = 0.0115 \left(\frac{l}{\rho\ \Delta P}\right)^{4/19} \mu^{1/19}\ w^{7/19} \tag{C19}$$

Equation (C19) gives the diameter of a circular pipe required as a function of weight-flow rate w, length l, density of fluid ρ, allowable pressure drop ΔP, and viscosity μ.

Annulus formed by two concentric circles. - In this case, the inner diameter d_i of the annulus is taken as a known quantity, and the outer diameter d_o is determined from the following equations:

$$\Delta P = 4f \frac{l}{d_h} \rho \frac{v^2}{2g} \tag{C20}$$

$$w = \frac{\pi}{4} (d_o^2 - d_i^2) \rho v \tag{C21}$$

Declassified 1-24-1963

Declassified 1-24-1963

$$4f = 0.316(Re)^{-1/4} \tag{C22}$$

$$Re = \frac{\rho v d_h}{\mu} \tag{C23}$$

where d_h, the hydraulic diameter for an annulus, is given by

$$d_h = d_o - d_i \tag{C24}$$

Equations (C20) to (C24) yield

$$d_h^{12}(d_h + 2d_i)^7 = \left(\frac{0.16}{g}\right)^4 \left(\frac{4}{\pi}\right)^7 \left(\frac{l}{\rho\ \Delta P}\right)^4 \mu w^7 \tag{C25}$$

It is noted that the right side of equation (C25) is identical to the expression derived for the diameter of a circular pipe in equation (C18). Thus, the hydraulic diameter d_h of an annular pipe can be related to the diameter of an equivalent circular pipe d_{cir} by the following equation:

$$d_h^{12}(d_h + 2d_i)^7 = d_{cir}^{19} \tag{C26}$$

In terms of outside diameter d_o, equation (C26) becomes

$$\left(\frac{d_o}{d_i} - 1\right)\left(\frac{\frac{d_o}{d_i} + 1}{\frac{d_o}{d_i} - 1}\right)^{7/19} = \frac{d_{cir}}{d_i} \tag{C27}$$

This relation is plotted in figure 60 for convenience in determining annulus dimensions. Given fluid properties, length of line, flow rate, and allowable pressure loss, the diameter of an equivalent circular pipe d_{cir} is found from equation (C18). Then for a specified inside diameter d_i, the required outside diameter d_o of the annulus can be determined with the aid of figure 60.

Headers

Headers or manifolds are required to distribute helium to the heat-exchanger tubes and to collect the cooled helium into a single line for pumping. Both the inlet and outlet headers must have leak-proof connections with 540 tubes and must be stressed to withstand a helium pressure of nearly 1200 psi. The greater design problem is, of course, associated

E-288

Declassified 1-24-1963

Declassified 1-24-1963

with the inlet header, since the helium temperature at the inlet is 1790° F compared with the helium outlet temperature of 790° F. The inlet header described here is one solution to this design problem.

Figure 22 is a schematic sketch of the arrangement of the headers for the heat exchanger. The outlet header consists of three cylinders arranged for series flow. Helium flows to the pump and then to the inlet header, which is designed to allow the cool helium to flow around the inlet header.

One purpose for this type of design is to allow the high-temperature parts of the inlet header to be nearly free of pressure loading. Pressure loads are transferred to the outer pipe, which operates at relatively low temperature. Actually, the pressure of the low-temperature helium is approximately 100 psi greater than the pressure of the high-temperature helium.

In addition, a leak-proof seal is not required where the tubes are joined to the high-temperature inner shell, because leakage flow at these points would not cause any loss of helium from the system. Consequently, the design of a leak-proof system is eased, since only the low-temperature outer shell is involved. However, should a sizable leak develop in the inner shell, the mixing of the low- and high-temperature streams would reduce the cycle efficiency and power output.

E-288

CA-11 back

Declassified 1-24-1963

Declassified 1-24-1963

SECRET

APPENDIX D

AXIAL-FLOW HELIUM PUMP

As mentioned in the body of this report, either a centrifugal-flow or an axial-flow pump could be employed in the helium system; however, the axial-flow type was investigated for the typical airplane described herein. It was decided to use one helium pump for each engine. This appendix describes some features of the aerodynamic design of the pump.

Symbols

The following symbols are used in appendix D:

a	sonic velocity, ft/sec
c_p	specific heat at constant pressure, Btu/(lb)($^{\circ}$R)
D	diffusion factor
g	acceleration due to gravity, ft/sec^2
i	incidence angle, deg
J	mechanical equivalent of heat, ft-lb/(lb)($^{\circ}$R)
P	stagnation pressure, lb/sq ft
r	radius, ft
T	stagnation temperature, $^{\circ}$R
U	blade speed, ft/sec
v	flow velocity, ft/sec
w	weight flow, lb/sec
β	flow direction measured from axis of rotation, deg
γ	ratio of specific heats
δ	$P_1/P_{1,d}$
η_p	polytropic efficiency

Declassified 1-24-1963

SECRET

Declassified 1-24-1963

θ $T_1/T_{1,d}$

σ solidity, ratio of chord to spacing

φ flow coefficient

ψ_T dimensionless temperature-rise parameter

Subscripts:

d design point

h hub

m midspan

R rotor

S stator

t tip

z axial component

1 inlet

2 outlet

Superscript:

' relative to blade row

E-288

Aerodynamic Design

Specifications. - The helium pump was designed for the following specifications:

Weight-flow rate, w, lb/sec	9.5
Inlet stagnation pressure, P_1, lb/sq ft	166,000
Inlet stagnation temperature, T_1, $^{\circ}R$	1200
Over-all stagnation-pressure ratio, P_2/P_1	1.085
Expected polytropic efficiency, η_p	0.80
Design stagnation-temperature rise, ΔT, $^{\circ}F$	50

The low flow rate and high pressure require that the pump diameter be rather small. The sonic velocity in helium is 5000 feet per second

Declassified 1-24-1963

Declassified 1-24-1963

at 1200° R, and therefore the relative Mach numbers in the pump will be quite low for any practical blade speed and velocity diagram. Furthermore, the flow in the pump will be effectively incompressible because of the low Mach numbers and pressure ratio. As a result, the aerodynamic design is straightforward, and conventional techniques and blade shapes can be utilized.

Blade speed and pump size. - High blade speeds are required if few pump stages are desired. In this design, the blade speed is limited primarily by the allowable stresses. Other conditions that influence the choice of blade speed are the hub-tip radius ratio and the inlet velocity diagram of the pump. By compromising aerodynamic and mechanical considerations, the following parameters were selected:

E-288

Blade tip speed, U_t, ft/sec	1500
Hub-tip radius ratio, r_h/r_t	0.8
Inlet flow direction measured from axis of rotation, β_1, deg	0
Ratio of inlet flow velocity to inlet sonic velocity, v_1/a_1	0.1
Inlet velocity, v_1, ft/sec	500

For these conditions, the centrifugal stresses at the roots of untapered blades are estimated at 40,000 psi. Since the temperature of the pump blades will not exceed 800° F, no problems are anticipated in the selection of blade materials. Low-creep-rate materials would be required for the pump blading to prevent excessive radial growth and rubbing of the blades on the pump casing. Type 347 stainless steel would be suitable as a blade material.

The pump tip diameter is calculated as 5.23 inches for the prescribed conditions, and the required rotational speed is 65,800 rpm. The angle of the inlet relative velocity is 71.55° at the rotor tip.

One of the problems associated with small compressors for air is the occurrence of low Reynolds numbers and the resulting penalty in efficiency. The blade-chord Reynolds number for the helium pump considered herein will be on the order of 10^6, which is above the critical Reynolds number of 2×10^5 observed in compressor tests. Therefore, scale effects due to low Reynolds numbers are not expected in this helium pump.

Velocity-diagram calculations. - Velocity diagrams are calculated for the mean radius only, because of the short blade height. The blades have a slight twist; the mean line essentially represents the complete blade. The following assumptions are made:

(1) Equal temperature rise in each stage (ΔT_{ST})

Declassified 1-24-1963

Declassified 1-24-1963

(2) Constant annulus area; therefore, equal axial velocities at exit from each blade row (incompressible flow)

(3) Constant hub and tip radii

(4) No inlet guide vanes; axial flow leaving each set of stator blades

These assumptions simplify the design to the extent that all stages are identical. There does not seem to be any reason to complicate the design by using unlike stages other than to alter the range characteristics of the pump if this proves to be necessary.

A dimensionless temperature-rise parameter ψ_T is defined as

$$\psi_T = \frac{gJc_p\Delta T_{ST}}{U_m^2} \tag{D1}$$

Then, from equation (B7) of reference 26, ψ_T can be related to the relative flow direction at the rotor exit and the flow coefficient φ as

$$\psi_T = 1 - \varphi \tan \beta_2' \tag{D2}$$

and

$$\varphi = \frac{v_{z,1}}{U_m} = \frac{v_1}{U_m} \tag{D3}$$

It is necessary to design the pump so that the blade loadings do not exceed the values that experience has shown to produce good efficiency. The diffusion factor D of reference 27 is used as a measure of the blade loading and can be written, for this simplified design situation, for the rotors as

$$D_R = 1 - \frac{\sqrt{(1 - \psi_T)^2 + \varphi^2}}{\sqrt{1 + \varphi^2}} + \frac{\psi_T}{2\sigma_R\sqrt{1 + \varphi^2}} \tag{D4}$$

and for the stators as

$$D_S = 1 - \frac{\varphi}{\sqrt{\psi_T^2 + \varphi^2}} + \frac{\psi_T}{2\sigma_S\sqrt{\psi_T^2 + \varphi^2}} \tag{D5}$$

where σ_R and σ_S are the rotor and stator solidities for the midspan of the blade rows.

Declassified 1-24-1963

Declassified 1-24-1963

Typical airplane. - For the three-stage pump used in the typical airplane, the following values are taken:

$$U_t = 1500 \text{ ft/sec}$$

$$r_h/r_t = 0.8$$

$$v_1/a_1 = 0.1, \; a_1 = 5000 \text{ ft/sec}$$

$$\varphi = 0.37$$

$$\Delta T = 50^\circ \text{ R}, \; \Delta T_{ST} = 16.67^\circ \text{ R}$$

$$\psi_T = 0.286$$

$$\beta_1' = \cot^{-1}\varphi = 69.7^\circ$$

$$\beta_2' = \tan^{-1}\frac{1 - \psi_T}{\varphi} = 62.6^\circ$$

Turning angle in rotor, $\Delta\beta' = 7.1^\circ$

Solidity, $\sigma = 1$

$$D_R = 0.382$$

Flow direction entering stator $\beta_2 = \tan^{-1}\frac{\psi_T}{\varphi} = 37.7^\circ$
(equivalent to turning angle in stators for this design)

$$D_S = 0.515$$

The values of diffusion factor for the rotors and stators are within the range for which high efficiency might be expected. They are not so low as to allow for a two-stage pump.

Although little experimental data on small pumps are available, the assumed efficiency of 0.80 for the pump design is probably reasonable.

Estimated Off-Design Performance of Helium Pump

It was necessary to construct a performance map for the helium pump to allow for the calculation of powerplant performance at off-design conditions. Since the engine controls are devised to hold constant

Declassified 1-24-1963

Declassified 1-24-1963

mechanical speed for the engine shaft, the pump map was estimated for a constant actual blade speed.

In order to simplify the task of estimating the off-design performance of the helium pump, it was first hypothesized that only a small operating range (variation of incidence angles) would be required. Later calculations proved this hypothesis to be reasonable. Since the pump operates with low relative Mach numbers (<0.4), the limit on the operating range allowed the assumption of constant polytropic efficiency. This is practically equivalent to an assumption of constant blade-element losses, as is the case in low-speed cascades for a limited range of incidence angles greater than and less than the optimum incidence angle. It was also assumed that the flow direction leaving each blade was constant, a valid assumption for a limited operating range.

E-288

In order to match calculations for other portions of the powerplant, the pump map was computed using the following variables:

(1) Ratio of flow coefficients $\frac{\varphi}{\varphi_d} = \frac{w}{w_d}\frac{\theta}{\delta}$

(2) Inlet temperature ratio $\theta = \frac{T_1}{T_{1,d}}$

(3) Inlet pressure ratio $\delta = P_1/P_{1,d}$

(4) Over-all pressure ratio P_2/P_1

CA-12

The following equations are required for computing the pump map:

$$\Delta T = 3\,\Delta T_{ST} = \frac{3U_m^2\left[1 - \left(\frac{\varphi}{\varphi_d}\right)\varphi_d \tan \beta_2'\right]}{gJc_p} \tag{D6}$$

$$\frac{T_2}{T_1} = 1 + \frac{\Delta T}{\theta T_{1,d}} \tag{D7}$$

and

$$\frac{P_2}{P_1} = \frac{T_2}{T_1}^{\left(\frac{\eta_p \gamma}{\gamma - 1}\right)} \tag{D8}$$

The mean blade speed U_m and the rotor-outlet relative flow angle β_2' are constants and are equal to the design values.

Declassified 1-24-1963

Declassified 1-24-1963

The estimated pump performance map is shown in figure 61. The figure also gives high and low limits of flow-coefficient ratio φ/φ_d, which indicate the operating range for which the off-design calculation is expected to apply. These limits were determined from an estimation of the low-loss incidence-angle range (ref. 28) for the rotor blade elements.

E-288

Declassified 1-24-1963

Declassified 1-24-1963

E-288

CA-12 back

APPENDIX E

ANALYSIS OF TEMPERATURE DISTRIBUTION AND PRESSURE DROP IN FUEL ELEMENTS AND MODERATOR BLOCKS

The reactor fuel element is circular and consists of a fuel "meat" with inner and outer surfaces clad as shown in figure 25. The moderator block has a circular inner surface and a hexagonal outer surface. The coolant flows in the central hole of the fuel element and in the annulus formed by the inner surface of the moderator block and the outer surface of the fuel element.

For this fuel element, heat will flow from the "meat" to channel 1 and to channel 2 (see fig. 62). Because of flow differences in the channels, T_d and T_a will be different and there will be some maximum temperature T_m at radius R_m in the "meat." If T_2 and T_1, the coolant temperatures in the channels, are different, R_m will vary axially. For one set of conditions, call them on-design, radius e can be determined when radii a and d are known, so that T_2 and T_1 will be the same and R_m will remain fixed axially. The coolant is also considered to be flowing between the moderator blocks but at very slow speed. Its heat-transfer effect is neglected, and dT/dr at the equivalent radius f is assumed equal to zero. The equivalent radius f is the radius of a circle whose area is equivalent to that of the hexagon in a moderator block.

The "on-design" method of analysis involves, as mentioned, the determination of the radius e so that the coolant temperatures are equal in both channels at a given axial station for a given total coolant flow. An equation for R_m is required, and then the coolant temperatures and fuel-element temperatures can be obtained. The design must also consider the coolant pressure drops allowable through the reactor and the amount of heat that must be picked up by the coolant from the reactor to provide the power for the engine.

The "off-design" method of analysis takes a given fuel-element design and determines the coolant conditions for a given total coolant flow through the fuel element. In this case the coolant temperatures in the channels at a given axial station will be practically the same, and the radius R_m will also remain practically unchanged axially.

The following analysis develops equations for use in both design methods, and further details on how to use them will be given after the equations are developed.

Declassified 1-24-1963

Declassified 1-24-1963

Symbols

The following symbols are used in appendix E:

A	values given in table XIII to be applied to eqs. (E49) and (E50), (cu ft)(sec)($^{\circ}$R)/Btu
a	radius of hole in fuel element, ft
B	values given in table XIII to be applied to eqs. (E49) to (E51), (cu ft)(sec)($^{\circ}$R)/Btu
b	inner radius of fuel element, ft
C_1,C_2,C_3	constants, Btu/(sec)(ft^5), Btu/(sec)(ft^4), and Btu/(sec)(cu ft), respectively
c	inner radius of outer cladding of fuel element, ft
c_p	specific heat of coolant, Btu/(lb)($^{\circ}$R)
D	values given in table XIII to be applied to eqs. (E49) and (E50), $^{\circ}$R
d	outer radius of fuel element, ft
d_h	hydraulic diameter in eqs. (E57), (E61), and (E63), ft
E	values given in table XIII to be applied to eqs. (E49) and (E50), $^{\circ}$R
e	inner radius of moderator block, ft
F	values given in table XIII to be applied to eq. (E51), $^{\circ}$R
f	equivalent radius for outer hexagonal surface of moderator block, ft (πf^2 = area of hexagonal block)
$\bar{f}$	friction factor in eqs. (E61) and (E62)
G	ratio of coolant mass-flow rate, w, to cross-sectional area of channel, lb/(sec)(sq ft)
g	gravitational constant, 32.2 ft/sec^2

E-288

Declassified 1-24-1963

Declassified 1-24-1963

E-288

h	convective heat-transfer coefficient, Btu/(sec)(sq ft)($^{\circ}$R)
K_{en}	coefficient for entrance pressure loss into reactor passages, see eq. (E65)
k	thermal conductivity, Btu/(sec)(ft)($^{\circ}$R)
l	length, ft
N	number of fuel elements
P	total pressure of coolant, lb/sq ft
$\mathscr{P}_{pp}$	power or heat picked up by coolant in reactor core and required by powerplants, Mw
p	static pressure, lb/sq ft
Q	volumetric heat source at any axial position x, Btu/(sec)(cu ft)
$\overline{Q}$	average of axial heat sources, Btu/(sec)(cu ft)
q	heat transferred radially, Btu/sec
R_m	radius to point of maximum temperature in fuel-element meat, ft
Re	Reynolds number
r	any radius in fuel-element - moderator-block assembly, ft
S	surface area, sq ft
T	total temperature, $^{\circ}$R
t	thickness, ft
U	over-all heat-transfer coefficient, Btu/(sec)(sq ft)($^{\circ}$R)
w	coolant-flow rate, lb/sec
X	defined by eq. (E26), Btu/(sec)(sq ft)
x	axial distance from core entrance, ft
Y	defined by eq. (E27), Btu/(sec)(sq ft)

Declassified 1-24-1963

Declassified 1-24-1963

α	defined by eq. (E66)
μ	viscosity of coolant, lb/(ft)(sec)
ρ	density of coolant, lb/cu ft

Subscripts:

a	radius a
av	average
B	bulk
b	radius b
c	radius c
cl	cladding
d	radius d
e	radius e
eff	effective
F	film
f	radius f
in	into reactor upstream end reflector
m	radius R_m
mod	moderator
mt	meat
out	out of reactor downstream end reflector
r	reflector
w	wall
1	hole
2	annulus

E-288

Declassified 1-24-1963

Declassified 1-24-1963

Required Data and Assumptions

The following data are assumed known before making a fuel-element design:

(1) Total pressure of coolant flowing into reactor, P_{in}

(2) Total pressure of coolant flowing out of reactor, P_{out}

(3) Total temperature of coolant flowing into reactor, T_{in}

(4) Total temperature of coolant flowing out of reactor, T_{out}

(5) Total coolant flow through reactor, w

(6) Power required by powerplant including pumping power or power required from reactor to heat coolant (does not include power dissipation from reactor core to reflector, thermal shields, and pressure shell), $\mathscr{P}_{pp}$

(7) Dimensions of fuel element (radii a, b, c, and d)

(8) Ratio of moderator area to frontal area

(9) Reactor-core length, l

(10) Reflector thickness, t_r

The following general assumptions are made:

(1) There is constant radial heat distribution in the core. Therefore, each fuel element picks up the same amount of heat, and only one fuel element need by analyzed.

(2) There is no heat transfer between moderator blocks. Therefore, as mentioned before, dT/dr at radius f is zero, and all heat from the moderator flows to the coolant in the annulus.

(3) 90 Percent of total reactor heat is released "locally" in the fuel element. This heat originates from fission fragments and beta particles (see ref. 15, p. 638).

(4) 5 Percent of total reactor heat is released "nonlocally" in core or in moderator. This heat derives from gammas and neutrons (see ref. 15).

(5) 5 Percent of total reactor heat is released "nonlocally" in reflector, thermal shields, and pressure shell. This heat originates mostly from gamma radiation (see ref. 15). These values apply to "thermal" reactors but are assumed for the present reactor.

Declassified 1-24-1963

E-288

Declassified 1-24-1963

(6) No internal sources of heat from nuclear reactions exist in the coolant.

Heat-Transfer Analysis

The development of the heat-transfer equations is similar to that in two special problems of reference 29 (pp. 130-138). Some repetition of that work is included herein in order to obtain continuity in the various analyses of the present project. The development could also have proceeded from heat-transfer equations given in reference 15 (pp. 657 and 662).

"Meat" temperatures. - For $r > R_m$ (see fig. 62), the heat generated between R_m and r in distance dx is

$$dq = \int_{R_m}^{r} Q_{mt}\, dx\, 2\pi r\, dr \tag{E1}$$

where Q_{mt} is the volumetric heat source in the "meat" at station x from the entrance.

For the assumption that Q_{mt} is constant radially, equation (E1) integrates to

$$dq = \pi Q_{mt}(r^2 - R_m^2)dx \tag{E2}$$

By Fourier's law,

$$dq = -k_{mt}\, 2\pi r\, dx \frac{dT}{dr} \tag{E3}$$

Equating equations (E2) and (E3) and integrating from radius R_m to radius c give

$$T_m - T_c = \frac{Q_{mt}}{2k_{mt}}\left(\frac{c^2 - R_m^2}{2} - R_m^2 \ln \frac{c}{R_m}\right) \tag{E4}$$

At the outer boundary (from eq. (E2)),

$$dq_c = \pi Q_{mt}(c^2 - R_m^2)dx \tag{E5}$$

When $r < R_m$, a corresponding development will result in the following equations:

$$T_m - T_b = \frac{Q_{mt}}{2k_{mt}}\left(R_m^2 \ln \frac{R_m}{b} - \frac{R_m^2 - b^2}{2}\right) \tag{E6}$$

$$dq_b = \pi Q_{mt}(R_m^2 - b^2)dx \tag{E7}$$

Declassified 1-24-1963

Declassified 1-24-1963

E-288

Cladding temperatures. - The cladding is very thin, and the assumption is made that heat generation in it can be neglected. Then the heat from the meat passes through the cladding by a pure conduction process. Also, because of the thinness of the cladding, the assumption is made that the conduction of heat through it can be represented by the equation

$$q = -kS \frac{\Delta T}{\Delta r} \tag{E8}$$

and for S the mean area will be used. Then, for the outer cladding the difference between the temperatures at radii c and d becomes, using equation (E8),

$$T_c - T_d = \frac{(d - c)(dq_c/dx)}{2\pi\left(c + \frac{d - c}{2}\right)k_{cl}} \tag{E9}$$

CA-13

The difference between the temperatures at radii a and b becomes

$$T_b - T_a = \frac{(b - a)(dq_b/dx)}{2\pi\left(b - \frac{b - a}{2}\right)k_{cl}} \tag{E10}$$

Surface-to-coolant temperature differences. - The differences in temperature between the fuel-element surfaces and the coolant are

$$T_d - T_2 = \frac{dq_c/dx}{2\pi d\ h_2} \tag{E11}$$

and

$$T_a - T_1 = \frac{dq_b/dx}{2\pi a\ h_1} \tag{E12}$$

where h_1 and h_2 are the convective heat-transfer coefficients of the channels.

Temperature change from maximum meat temperature to coolant. - The temperature difference from radius R_m to the coolants in channels 1 and 2 can be obtained by combining equations (E6), (E7), (E10), and (E12) and equations (E4), (E5), (E9), and (E11), respectively. The results are as follows:

$$T_m - T_2 = \frac{Q_{mt}}{2k_{mt}}\left(\frac{c^2 - R_m^2}{2} - R_m^2 \ln \frac{c}{R_m}\right) + \frac{Q_{mt}(c^2 - R_m^2)}{2U_2 d} \tag{E13}$$

Declassified 1-24-1963

Declassified 1-24-1963

$$T_m - T_1 = \frac{Q_{mt}}{2k_{mt}}\left(R_m^2 \ln\frac{R_m}{b} - \frac{R_m^2 - b^2}{2}\right) + \frac{Q_{mt}(R_m^2 - b^2)}{2U_1 a} \tag{E14}$$

where

$$U_2 = \left[\frac{d - c}{\left(\frac{c + \frac{d - c}{2}}{d}\right)k_{cl}} + \frac{1}{h_2}\right]^{-1} \tag{E15}$$

$$U_1 = \left[\frac{b - a}{\left(\frac{b - \frac{b - a}{2}}{a}\right)k_{cl}} + \frac{1}{h_1}\right]^{-1} \tag{E16}$$

Determination of radius R_m. - By subtracting equation (E14) from equation (E13) and solving the resulting equation for R_m, the following equation is obtained:

$$R_m = \sqrt{\frac{\frac{2(T_2 - T_1)}{Q_{mt}} + \frac{c^2 - b^2}{2k_{mt}} + \frac{c^2}{U_2 d} + \frac{b^2}{U_1 a}}{\frac{\ln\frac{c}{b}}{k_{mt}} + \frac{1}{U_2 d} + \frac{1}{U_1 a}}} \tag{E17}$$

Because the cladding is so thin, $c \approx d$ and $b \approx a$; therefore,

$$R_m \approx \sqrt{\frac{\frac{2(T_2 - T_1)}{Q_{mt}} + \frac{c^2 - b^2}{2k_{mt}} + \frac{d}{U_2} + \frac{a}{U_1}}{\frac{\ln\frac{c}{b}}{k_{mt}} + \frac{1}{U_2 d} + \frac{1}{U_1 a}}} \tag{E18}$$

Moderator temperatures. - On the basis of the assumption that all the heat in the moderator flows to the coolant in the annulus, and therefore $dT/dr = 0$ at radius f, the temperature difference between radii f and e can be represented by equation (E6) with changes appropriate to the moderator block:

$$T_f - T_e = \frac{Q_{mod}}{2k_{mod}}\left[f^2 \ln\left(\frac{f}{e}\right) - \frac{f^2 - e^2}{2}\right] \tag{E19}$$

Declassified 1-24-1963

E-288

Declassified 1-24-1963

In a manner analogous to getting dq_b, dq_e becomes

$$dq_e = \pi Q_{mod}(f^2 - e^2)dx \tag{E20}$$

The temperature drop from the surface at radius e to the coolant is

$$T_e - T_2 = \frac{dq_e/dx}{2\pi e\ h_2} \tag{E21}$$

Combining these equations gives

$$T_f - T_2 = \frac{Q_{mod}}{4k_{mod}}\left(2f^2 \ln \frac{f}{e} + e^2 - f^2\right) + \frac{Q_{mod}(f^2 - e^2)}{2h_2 e} \tag{E22}$$

Axial temperature variations. - From equations (E11), (E12), (E13), or (E14), (E21), and (E22), the maximum and surface temperatures of the fuel element or the moderator block, respectively, can be obtained for any axial position x. Before solving the equations, the coolant temperatures at the various axial positions must be determined. For any position x the coolant temperatures depend on the equations

$$w_2 c_p\left[T_2(x) - T_{2,in}\right] = \int_0^x dq_c + \int_0^x dq_e \tag{E23}$$

$$w_1 c_p\left[T_1(x) - T_{1,in}\right] = \int_0^x dq_b \tag{E24}$$

Using equations (E11), (E12), (E13), (E21), (E22), (E5), (E7), (E20), (E23), and (E24), it can be shown that

$$T_2(x) = T_{2,in} + \frac{\pi(c^2 - R_m^2)}{w_2 c_p} X + \frac{\pi(f^2 - e^2)}{w_2 c_p} Y \tag{E25}$$

where

$$X = \int_0^x Q_{mt}(x)dx \tag{E26}$$

and

$$Y = \int_0^x Q_{mod}(x)dx \tag{E27}$$

Declassified 1-24-1963

E-288

CA-13 back

Declassified 1-24-1963

Also,

$$T_1(x) = T_{1,in} + \frac{\pi(R_m^2 - b^2)}{w_1 c_p} X \tag{E28}$$

$$T_a(x) = T_1(x) + \frac{Q_{mt}(x)(R_m^2 - b^2)}{2h_1 a} \tag{E29}$$

$$T_d(x) = T_2(x) + \frac{Q_{mt}(x)(c^2 - R_m^2)}{2h_2 d} \tag{E30}$$

$$T_e(x) = T_2(x) + \frac{Q_{mod}(x)(f^2 - e^2)}{2h_2 e} \tag{E31}$$

$$T_m(x) = T_2(x) + Q_{mt}(x)\left[\frac{1}{2k_{mt}}\left(\frac{c^2 - R_m^2}{2} - R_m^2 \ln \frac{c}{R_m}\right) + \frac{(c^2 - R_m^2)}{2U_2 d}\right] \tag{E32}$$

$$T_f(x) = T_2(x) + \frac{Q_{mod}(x)}{2}\left[\frac{1}{k_{mod}} f^2 \ln \frac{f}{e} + \frac{e^2 - f^2}{2k_{mod}} + \frac{f^2 - e^2}{h_2 e}\right] \tag{E33}$$

The next step in the solution of the equations is to determine the axial heat-source variation in the reactor.

Axial distribution of heat source. - For a uniform axial fuel distribution, reference 15 (p. 643) shows that the heat distribution in a cylindrical unreflected reactor follows a cosine law. Because the reactor has end reflectors, a modified power distribution is used. This is

$$Q_{mt}(x) = Q_{mt}\left(\frac{l}{2}\right)\cos\left(\frac{2\pi x}{3l} - \frac{\pi}{3}\right) \tag{E34}$$

where $Q_{mt}(l/2)$ is the maximum flux that occurs at the center of the core. This distribution is called the "chopped" 2/3-cosine distribution. The flux is not zero at the core-reflector interface.

Now, the average heat source in the core equals

$$\overline{Q}_{mt} = \frac{\int_0^l Q_{mt}\left(\frac{l}{2}\right)\cos\left(\frac{2\pi x}{3l} - \frac{\pi}{3}\right)dx}{l} \tag{E35}$$

Declassified 1-24-1963

Declassified 1-24-1963

Integrating and solving for $Q_{mt}(l/2)$ result in

$$Q_{mt}\left(\frac{l}{2}\right) = 1.21\ \overline{Q}_{mt} \tag{E36}$$

Then

$$Q_{mt}(x) = 1.21\ \overline{Q}_{mt} \cos\left(\frac{2\pi x}{3l} - \frac{\pi}{3}\right) \tag{E37}$$

From a similar development,

$$Q_{mod}(x) = 1.21\ \overline{Q}_{mod} \cos\left(\frac{2\pi x}{3l} - \frac{\pi}{3}\right) \tag{E38}$$

E-288

Combining equations (E26) and (E37), and (E27) and (E38), gives the following equations for X and Y:

$$X = 1.21\ \overline{Q}_{mt} \frac{3l}{2\pi}\left[\sin\left(\frac{2\pi x}{3l} - \frac{\pi}{3}\right) + \frac{\sqrt{3}}{2}\right] \tag{E39}$$

$$Y = 1.21\ \overline{Q}_{mod} \frac{3l}{2\pi}\left[\sin\left(\frac{2\pi x}{3l} - \frac{\pi}{3}\right) + \frac{\sqrt{3}}{2}\right] \tag{E40}$$

A constant or uniform axial distribution of fuel, which generally results in a heat-source distribution approximately like the one just derived, will cause the temperatures of the reactor core to vary in a manner that will be quite different from that desired when the allowable stress curve is considered. It would be advantageous to design reactors so that the temperature resulting would be more nearly like those desired from allowable stress considerations. The following is an analysis of the heat-source distribution required for any arbitrarily selected temperature distribution (which could be selected on the basis of the stress desired). From the heat-source distribution so determined, the fuel distribution would then be determined, if it is assumed that the neutron-flux distribution is the same as for the case of uniform fuel distribution.

Suppose the heat-source distribution in fuel element or moderator to be represented by an equation of the following type:

$$Q(x) = C_1x^2 + C_2x + C_3 \tag{E41}$$

Then

$$Q(0) = C_3 \tag{E42}$$

$$Q\left(\frac{l}{2}\right) = C_1\frac{l^2}{4} + C_2\frac{l}{2} + C_3 \tag{E43}$$

$$Q(l) = C_1l^2 + C_2l + C_3 \tag{E44}$$

Declassified 1-24-1963

Declassified 1-24-1963

Also,

$$\int_0^x Q(x)dx = C_1 \frac{x^3}{3} + C_2 \frac{x^2}{2} + C_3 x \tag{E45}$$

Therefore,

$$\int_0^0 Q(x)dx = 0 \tag{E46}$$

$$\int_0^{l/2} Q(x)dx = C_1 \frac{l^3}{24} + C_2 \frac{l^2}{8} + C_3 \frac{l}{2} \tag{E47}$$

$$\int_0^l Q(x)dx = C_1 \frac{l^3}{3} + C_2 \frac{l^2}{2} + C_3 l \tag{E48}$$

Any three values of the fuel-element or moderator temperature can now be set; for example, $T(0)$, $T\left(\frac{l}{2}\right)$, and $T(l)$ can be selected at any one of the radii a, d, e, m, or f. Suppose T_m is chosen. Then three equations based on equation (E32) are available with known temperatures into which equation (E25), for the appropriate axial position, is first substituted; and then into the three resulting equations the equations (E26), (E27), (E42), (E43), (E44), (E46), (E47), and (E48) are substituted; again for the appropriate axial position. Three equations result with three unknowns, the constants C_1, C_2, and C_3 in the heat-distribution equation (E41). These equations can be solved for the constants; and thus, for the chosen temperature distribution, the required heat-source distribution is known. In like manner, C_1, C_2, and C_3 can be determined for any set of temperatures T_a, T_d, and so forth. Of course only one set can be chosen, and from the resulting $Q(x)$ variation the other temperatures will automatically result. By performing the algebraic manipulations mentioned, the equations for C_1, C_2, and C_3 resulting from choosing T_m, T_a, T_d, T_e, or T_f variations are

$$C_1 = \frac{6}{l^2}\left[\frac{4(A + 2B)D - (A + 4B)E}{(A + 6B)(A + 2B) - 2(A + 3B)(A + 4B)}\right] \tag{E49}$$

$$C_2 = \frac{2}{l}\left[\frac{(A + 6B)E - 8(A + 3B)D}{(A + 6B)(A + 2B) - 2(A + 3B)(A + 4B)}\right] \tag{E50}$$

$$C_3 = \frac{F - T_{in}}{B} \tag{E51}$$

E-288

Declassified 1-24-1963

Declassified 1-24-1963

where A, B, D, E, and F have the values given in table XIII depending upon which temperature distribution is chosen as the desired one.

The foregoing analysis depends on the selection of one set of temperatures at $x = 0$, $x = l/2$, and $x = l$, but it does not indicate what values to choose or limitations on values that can be chosen. From equation (E48) it can be shown that

$$\overline{Q} = C_1 \frac{l^2}{3} + C_2 \frac{l}{2} + C_3 \tag{E52}$$

and, as will be shown in the following section, $\overline{Q}_{mt}$ and $\overline{Q}_{mod}$ have fixed values depending on the power required of the reactor. Therefore, temperatures must be chosen so that, when C_1, C_2, and C_3 are calculated and substituted into equation (E52), the average volumetric heat source will not be exceeded. Temperatures can be picked at random until such a result occurs, but some guidance to the selection of temperatures would save computation. A method of doing this would be to substitute into equation (E52) for the temperature selected as known, values of corresponding C_1, C_2, and C_3 obtained from equations (E49), (E50), and (E51). Then one equation results with $\overline{Q}$ in it, which is known. (The method of determining $\overline{Q}$ is discussed later.) For example, for getting $Q_{mt}(x)$ for known T_m values, the resulting equation is

$$\frac{T_m(l)}{T_m(0)} + K_1 \frac{T_m\left(\frac{l}{2}\right)}{T_m(0)} = \frac{\overline{Q}_{mt} - K_2 T_{in}}{K_3 T_m(0)} - K_4 \tag{E53}$$

where the K are known terms. From the allowable stress curve, some idea of the ratio of temperatures can be obtained, and then $T_m(0)$ can be obtained from the preceding equation. Knowing $T_m(0)$, then, and the temperature ratios, enough information is available to get the $Q_{mt}(x)$ variation from the analysis presented. The same type of equation will result for the other temperatures listed in table XIII.

Average volumetric heat source. - According to the assumptions outlined previously, 90 percent of the total reactor power or heat is in the fuel elements and 5 percent in the moderator blocks. Also, 5 percent is lost to the outside of the core. If the power in megawatts required by the powerplant is denoted by $\mathscr{P}_{pp}$, then the total heat produced by the reactor on the basis of the percentages quoted is $948.1\ \mathscr{P}_{pp}/0.95$ Btu per second. The heat given up by each fuel-element - moderator-block assembly is then

$$(w_1 + w_2)c_p(T_{out} - T_{in}) = \frac{948.1\ \mathscr{P}_{pp}}{N} \tag{E54}$$

Declassified 1-24-1963

E-288

Declassified 1-24-1963

SECRET

where w_1 and w_2 are coolant-flow rates through one assembly. The heat given off by a fuel element will then be

$$\frac{0.9(w_1 + w_2)c_p(T_{out} - T_{in})}{0.95}$$

and by a moderator block,

$$\frac{0.05(w_1 + w_2)c_p(T_{out} - T_{in})}{0.95}$$

and the average volumetric heat sources consequently are

$$\overline{Q}_{mt} = \frac{0.9}{0.95} \frac{(w_1 + w_2)c_p(T_{out} - T_{in})}{\pi l(c^2 - b^2)} \tag{E55}$$

$$\overline{Q}_{mod} = \frac{0.05}{0.95} \frac{(w_1 + w_2)c_p(T_{out} - T_{in})}{\pi l(f^2 - e^2)} \tag{E56}$$

Heat-transfer coefficient. - The convective heat-transfer coefficients in the two channels of the fuel-element - moderator-block assembly are required in the solution of the equations. Average turbulent-flow forced-convection coefficients have been experimentally obtained over a wide range of Reynolds numbers, surface temperatures, heat fluxes, entrance conditions, and l/d_h ratios, as reported in reference 30. Evaluating the properties of the fluid and density at the film temperature gave good correlations. The empirical equation resulting was

$$h = \frac{0.0216\ k_F}{d_h} \left(\frac{GT_B d_h}{\mu_F T_F}\right)^{0.8} \left(\frac{c_{p,F}\mu_F}{k_F}\right)^{0.4} \tag{E57}$$

where d_h is the hydraulic diameter. For the hole in the fuel element, $d_h = 2a$; and for the annulus, $d_h = 2(e - d)$. The subscript B refers to the bulk temperature of the fluid, assumed equal to the arithmetic mean of T_{in} and T_{out}, and F refers to film temperature conditions. The film temperature is

$$T_F = \frac{T_B + T_{w,eff}}{2} \tag{E58}$$

where $T_{w,eff}$ is the effective wall temperature of the entire channel. The equation for it is

Declassified 1-24-1963

SECRET

Declassified 1-24-1963

$$T_{w,eff} = T_{in}\left(\frac{\frac{T_{out}}{T_{in}} e^{Sh/wc_p} - 1}{e^{Sh/wc_p} - 1}\right) \tag{E59}$$

where e in this equation is the base for Napierian logarithms, and S is equal to $2\pi a l$ for the hole in the fuel element and $2\pi(e + d)l$ for the annulus around the fuel element. For the coolant used in this project (helium), c_p is 1.25 Btu/(lb)(°R), and the viscosity and conductivity (obtained from ref. 24) are

E-288

$$\mu_F = 2.3072(T_F)^{0.647}\times10^{-7} \text{ lb/(ft)(sec)}$$

$$k_F = 4.085(T_F)^{0.650}\times10^{-7} \text{ Btu/(sec)(ft)(°R)}$$

The determination of h requires iteration, because it depends on $T_{w,eff}$, which in turn is calculated for a known value of h.

CA-14

Pressure-Drop Analysis

The decrease in pressure of the coolant through the end reflectors and the fuel-element - moderator-block assemblies in the core was kept below a specified minimum value. The calculation of the coolant pressure change through two channels of the assemblies (the end reflectors having the same geometry as the core but with no uranium in the circular elements) was thus required. It was assumed that there was no heat pickup by the coolant in the end reflectors and thus no change in total temperature in passing through the reflectors.

The static-pressure drops through the channels were calculated using normal momentum and friction pressure-drop formulas for turbulent flow through pipes. Or, for momentum pressure drop,

$$\Delta p = \frac{G^2}{g}\left(\frac{1}{\rho_{out}} - \frac{1}{\rho_{in}}\right) \tag{E60}$$

and for friction pressure drop,

$$\Delta p = 4\bar{f}\,\frac{l}{d_h}\,\frac{G^2}{2g\rho_{av}} \tag{E61}$$

Declassified 1-24-1963

Declassified 1-24-1963

where ρ_{av} is the arithmetic mean of ρ_{in} and ρ_{out}. The friction coefficients used were those given by Reynolds' analogy as

$$\frac{\bar{f}}{2} = 0.023(Re)^{-0.2} \tag{E62}$$

which are in good agreement with Kármán-Nikuradse values for the Reynolds number range most frequently used. The correlation of friction coefficients also depends, as in the case of heat-transfer coefficients, on the heat flux and the temperature at which the fluid properties are evaluated. Making use of this fact, and combining equations (E61) and (E62),

$$\Delta p = \frac{0.184}{\left(\frac{G d_h T_B}{\mu_F T_F}\right)^{0.2}} \frac{T_B}{T_F} \frac{l}{d_h} \frac{G^2}{2g\rho_{av}} \tag{E63}$$

For the holes in the fuel elements, the hydraulic diameter d_h in equation (E63) is equal to $2a$; and for the annulus between the fuel element and moderator block, it is $2(e - d)$. When the end-reflector passages are being considered, l in equation (E63) is the end-reflector thickness t_r; and, when the core passages are considered, l is the core length.

Contraction and expansion losses into and out of the end-reflector passages were also considered. The change in total pressure from the inlet duct to the passage inlets was calculated from

$$P_{in} - P_{passage\ inlet} = K_{en} \frac{G^2}{(\rho_{passage\ inlet})^2 g} \tag{E64}$$

where K_{en} was obtained from reference 9 and is given by the equation

$$K_{en} = 0.5\left[\frac{Re_{inlet\ passage}}{3000}\right]^{0.077} - 0.4\alpha \tag{E65}$$

where

$$\alpha = \frac{a^2 + (e^2 - d^2)}{f^2} \tag{E66}$$

The change in total pressure from the passage outlets to the outlet duct was obtained from

$$P_{passage\ outlet} - P_{out} = (1 - \alpha)^2 \frac{G^2}{(\rho_{passage\ outlet})^2 g} \tag{E67}$$

Declassified 1-24-1963

E-288

Declassified 1-24-1963

Each part of the pressure-drop calculation requires iteration, because the densities used to get the Δp or ΔP values depend on the downstream pressures being calculated.

General Method of Design

There is some radius e, as brought out at the beginning of this analysis, for which R_m will remain constant axially and $T_1(x)$ will equal $T_2(x)$ at each axial position. By assuming some value of radius a and values of the coolant-flow rates (knowing total coolant flow through a fuel element and the ratio of w_1/w_2 obtained as explained in the following sentence), various values of e can be assumed until such a condition occurs. An approximate formula for e to start the calculation can be determined by equating equations (E25) and (E28), solving for the flow ratio w_1/w_2 from the resulting equation, then equating this ratio to $a^2\sqrt{a}/\left[(e^2 - d^2)\sqrt{(e - d)}\right]$. This expression was obtained by assuming that the only pressure drops in the two channels were those due to friction, and of course must be equal. As a consequence the flow ratio is roughly proportional to the ratio of the cross-sectional areas of the channels multiplied by the ratio of the square root of the hydraulic diameters of the channels. After determining the pressure drops, the temperatures are calculated and iteration is required because the pressure drops are dependent on the surface temperatures of the fuel element and moderator block.

The calculations are made for various assumed values of radii a and e and flow rates w_1 and w_2 until the conditions of (1) the same coolant temperature rise in both channels, (2) the same over-all pressure drop in both channels with a value below the required limit, and (3) the required hardware surface temperature limitations are met. Because of the numerous iterative processes involved, computations were carried out on an IBM 653 computing machine.

For the present study the fuel elements and moderator blocks were designed by the foregoing method for a given set of conditions. These conditions were later changed, but no change was made in the individual fuel elements and moderator blocks. More fuel elements and moderator blocks were added to the core, thus changing the flow rates. A new IBM 653 program was made to calculate this "off-design" case, which was also briefly discussed at the beginning of this analysis. The problem is to find the resulting fuel-element and moderator-block temperatures and, for a given total amount of coolant flowing through each assembly, the amount flowing through each channel that gives the same pressure drop. It can be shown that, because the ratio of $a^2\sqrt{a}/\left[(e^2 - d^2)\sqrt{(e - d)}\right]$

Declassified 1-24-1963

E-288

CA-14 back

Declassified 1-24-1963

is the same as for the on-design case, then w_1/w_2 is about the same; and thus using equations (E25) and (E28) the temperature of the coolant out of the annulus and hole will be about the same as for the on-design case. Thus, a very good estimate of w_1 and w_2 can be made when the sum of the two values for the off-design case is known.

SECRET
Declassified 1-24-1963

Declassified 1-24-1963

E-288

APPENDIX F

ANALYSIS OF STRESSES IN FUEL ELEMENT AND MODERATOR BLOCK

A theory for the stresses in a circular fuel element is available in reference 31 (pp. 169 to 182) for conditions not quite the same as for the fuel element used here. One assumption in the reference is that no external or surface forces are exerted on the heated tube. Another assumption is that there is no heat flow across the outer boundary of the fuel element and therefore the maximum temperature occurs at this radius. In the present fuel element the heat is dissipated to the coolant at the inner and outer radii of the element, and the temperature reaches a maximum (or no heat flow occurs) at some radius within the fuel-element "meat." Some initial equations of reference 31 could be used, and the reader is referred to the reference for their development. These equations are then further developed in the following analysis for the particular conditions mentioned in the foregoing discussion.

Symbols

The following symbols are used in appendix F:

A	integration constant, (Btu)(in.)/sec
A'	integration constant (see eq. (F36))
a	inner radius of fuel element, in.
B	integration constant, Btu/(in.)(sec)
B'	integration constant (see eq. (F37))
b	outer radius of inner cladding of fuel element, in.
C'	integration constant (see eq. (F42))
C_1	integration constant (see eq. (F3)), $^{\circ}R$
C_2	integration constant (see eq. (F6)), $^{\circ}R$
c	inner radius or outer cladding of fuel element, in.
c_p	specific heat of coolant, Btu/(lb)($^{\circ}R$)
d	outer radius of fuel element, in.

Declassified 1-24-1963

Declassified 1-24-1963

E	modulus of elasticity of material in tube, lb/sq in.
e	inner radius of moderator block, in.
$F_1(\xi)$	defined by eq. (F29)
$F_2(\xi)$	defined by eq. (F30)
$F_3(\xi)$	defined by eq. (F31)
f	equivalent outer radius of moderator block, in. (πf^2 = area of the block with hexagonal boundary)
k	thermal conductivity, Btu/(sec)(°R)(in.)
l	length of core of reactor, in.
m	$= (R_m - a)$ or $(R_m - R)$, in.
p	static pressure of coolant, lb/sq in.
Q	volumetric heat source in material at a radial and an axial point in tube, Btu/(sec)(cu in.)
$\overline{Q}$	equivalent average volumetric heat source for solid tube of radius equal to outer diameter of tube at an axial position x, Btu/(sec)(cu in.), see eq. (F25) and its derivation
R	= a, in. (used for convenience in expanding $\sigma_\theta(a/d)$ equation)
R_m	radius at which maximum tube temperature occurs, in. (determined from temperature analysis of appendix E)
r	any radius in tube, in.
T	total temperature, °R
W	defined by equation (F32), lb/sq in.
w_1	coolant flow through hole of fuel element, lb/sec
w_2	coolant-flow rate through annulus of fuel-element - moderator-block assembly, lb/sec
x	axial position from coolant inlet to reactor core, in.
α	coefficient of thermal expansion of material in tube, in./(in.)(°R)

E-288

Declassified 1-24-1963

Declassified 1-24-1963

E-288

β	= (b - a) or (b - R), in.
γ	$= Q/Q_o$
δ	= (d - a) or (d - R), in.
ϵ	longitudinal strain, in./in.
ν	Poisson's ratio
ξ	= r/d
ρ	= (c - a) or (c - R), in.
σ	stress, psi
σ_{eq}	equivalent stress, psi (see eq. (F52))

Subscripts:

ad	adjusted
d	radius d
eq	equivalent
in	into reactor core
mod	moderator
mt	meat
o	reference
out	out of reactor core
r	radial
z	axial
θ	tangential
1,2,3	used with r and ξ when double or triple integrals are used

Declassified 1-24-1963

Declassified 1-24-1963

Fuel Element

Development of general stress equations. - The fuel element and the sketch used for the analysis are shown in figures 25 and 62. The maximum temperature occurs at radius R_m in figure 62. Then

$$\left(\frac{dT}{dr}\right)_{r=R_m} = 0 \tag{F1}$$

From reference 31 (p. 170) for steady-state conditions for a tube,

$$\frac{1}{r}\frac{d}{dr}\left(r\frac{dT}{dr}\right) + \frac{Q}{k} = 0 \tag{F2}$$

where Q is the volumetric heat-source strength, which varies with location.

Integrating equation (F2) once,

$$r\frac{dT}{dr} + \frac{1}{k}\int_a^r Qr_1\,dr_1 + C_1 = 0 \tag{F3}$$

Using equation (F1) in equation (F3),

$$C_1 = -\frac{1}{k}\int_a^{R_m} Qr_1\,dr_1 \tag{F4}$$

Combining equations (F3) and (F4),

$$r\frac{dT}{dr} + \frac{1}{k}\int_{R_m}^r Qr_1\,dr_1 = 0 \tag{F5}$$

Integrating equation (F5),

$$T + \frac{1}{k}\int_a^r \frac{dr_1}{r_1}\int_{R_m}^{r_1} Qr_2\,dr_2 + C_2 = 0 \tag{F6}$$

At $r = d$,

$$T_d + \frac{1}{k}\int_a^d \frac{dr_1}{r_1}\int_{R_m}^{r_1} Qr_2\,dr_2 + C_2 = 0 \tag{F7}$$

Declassified 1-24-1963

Declassified 1-24-1963

Subtracting equation (F7) from equation (F6),

$$T - T_d + \frac{1}{k} \int_d^r \frac{dr_1}{r_1} \int_{R_m}^{r_1} Qr_2 \, dr_2 = 0 \tag{F8}$$

Let

$$\xi = \frac{r}{d} \tag{F9}$$

and

$$\gamma = \frac{Q}{Q_o} \tag{F10}$$

where Q_o is the power or heat-source density at some reference point. Then equation (F8) becomes

$$T - T_d + \frac{Q_o d^2}{k} \int_1^{\xi} \frac{d\xi_1}{\xi_1} \int_{R_m/d}^{\xi_1} \gamma \xi_2 \, d\xi_2 = 0 \tag{F11}$$

The fuel element is made of three rings, two cladding rings and the "meat" ring containing the uranium. For stress analysis, the assumption was made that the fuel element consisted of one material only, or the cladding and matrix could be represented by one ring. If the element had been divided into two cladding rings and one "meat" ring, each would have to be treated separately. Because of the complexity of the analysis, it was considered beyond the scope of the present study. Therefore, the modulus of elasticity E, the coefficient of thermal expansion α, and Poisson's ratio ν were considered constant in the radial direction. For these conditions, reference 31 (p. 177) arrives at the following equation for radial stress in the tube:

$$\frac{d}{dr}\left(r^3 \frac{d\sigma_r}{dr}\right) + \frac{E\alpha r^2}{1 - \nu} \frac{dT}{dr} = 0 \tag{F12}$$

Substituting in this equation the value of dT/dr from equation (F5),

$$\frac{d}{dr}\left(r^3 \frac{d\sigma_r}{dr}\right) = \frac{E\alpha}{(1 - \nu)k} \, r \int_{R_m}^{r} Qr_1 \, dr_1 \tag{F13}$$

This is a differential equation for the radial thermal stress in terms of properties of the tube and the distributed heat source Q. It is to be integrated twice subject to appropriate boundary conditions.

Declassified 1-24-1963

Declassified 1-24-1963

Integrating it once, including an arbitrary constant that depends on the slope of the stress curve at $r = d$,

$$\frac{d\sigma_r}{dr} = \frac{E\alpha}{k(1 - \nu)} \frac{1}{r^3} \left(\int_d^r r_1 \, dr_1 \int_{R_m}^{r_1} Qr_2 \, dr_2 + 2A \right) \tag{F14}$$

Integrating again, including a second constant that depends on the stress at $r = d$,

$$\sigma_r = \frac{E\alpha}{k(1 - \nu)} \left\{ \int_d^r \left[\frac{dr_1}{r_1^3} \int_d^{r_1} \left(r_2 \, dr_2 \int_{R_m}^{r_2} Qr_3 \, dr_3 \right) \right] + A\left(\frac{1}{d^2} - \frac{1}{r^2}\right) + B \right\} \tag{F15}$$

From reference 31 (p. 177), the tangential stress is

$$\sigma_\theta = r \frac{d\sigma_r}{dr} + \sigma_r \tag{F16}$$

Substituting equations (F14) and (F15) into this equation,

$$\sigma_\theta = \frac{E\alpha}{k(1 - \nu)} \left\{ \frac{1}{r^2} \int_d^r \left(r_1 \, dr_1 \int_{R_m}^{r_1} Qr_2 \, dr_2 \right) \right.$$

$$\left. + \int_d^r \left[\frac{dr_1}{r_1^3} \int_d^{r_1} \left(r_2 \, dr_2 \int_{R_m}^{r_2} Qr_3 \, dr_3 \right) \right] + A\left(\frac{1}{d^2} + \frac{1}{r^2}\right) + B \right\} \tag{F17}$$

Also from reference 31 (p. 176), the axial stress may be written

$$\sigma_z = \nu(\sigma_r + \sigma_\theta) - E\alpha(T - T_o) + \epsilon_z E \tag{F18}$$

where T_o is a reference temperature that is eliminated in the analysis.

Substituting equations (F15) and (F17) into equation (F18),

$$\sigma_z = \frac{E\alpha\nu}{k(1 - \nu)} \left\{ \frac{1}{r^2} \int_d^r \left(r_1 \, dr_1 \int_{R_m}^{r_1} Qr_2 \, dr_2 \right) \right.$$

$$\left. + 2 \int_d^r \left[\frac{dr_1}{r_1^3} \int_d^{r_1} \left(r_2 \, dr_2 \int_{R_m}^{r_2} Qr_3 \, dr_3 \right) \right] + \frac{2A}{d^2} + 2B \right\} - E\left[\alpha(T - T_o) - \epsilon_z\right] \tag{F19}$$

Declassified 1-24-1963
E-288

Declassified 1-24-1963

E-288

CA-15 back

From equation (F8),

$$T = T_d - \frac{1}{k} \int_d^r \frac{dr_1}{r_1} \int_{R_m}^{r_1} Qr_2 \, dr_2 \tag{F20}$$

Putting equation (F20) into (F19) gives

$$\sigma_z = \frac{E\alpha\nu}{k(1 - \nu)} \left\{ \frac{1}{r^2} \int_d^r \left(r_1 \, dr_1 \int_{R_m}^{r_1} Qr_2 \, dr_2 \right) \right.$$

$$+ 2 \int_d^r \left[\frac{dr_1}{r_1^3} \int_d^{r_1} \left(r_2 \, dr_2 \int_{R_m}^{r_2} Qr_3 \, dr_3 \right) \right]$$

$$\left. + \frac{1 - \nu}{\nu} \int_d^r \left(\frac{dr_1}{r_1} \int_{R_m}^{r_1} Qr_2 \, dr_2 \right) + \frac{2A}{d^2} + 2B \right\} - E\left[\alpha(T_d - T_o) - \epsilon_z\right] \tag{F21}$$

Define, as in reference 31, the following:

$$F_1(\xi) = \int_1^\xi \left[\frac{d\xi_1}{\xi_1^3} \int_1^{\xi_1} \left(\xi_2 \, d\xi_2 \int_{R_m/d}^{\xi_2} \gamma\xi_3 \, d\xi_3 \right) \right] \tag{F22}$$

$$F_2(\xi) = \frac{1}{\xi^2} \int_1^\xi \left(\xi_1 \, d\xi_1 \int_{R_m/d}^{\xi_1} \gamma\xi_2 \, d\xi_2 \right) \tag{F23}$$

$$F_3(\xi) = \frac{1 - \nu}{\nu} \int_1^\xi \left(\frac{d\xi_1}{\xi_1} \int_{R_m/d}^{\xi_1} \gamma\xi_2 \, d\xi_2 \right) \tag{F24}$$

As before, let

$$\xi = r/d \tag{F9}$$

and

$$\gamma = Q/Q_o \tag{F10}$$

The average power density $\overline{Q}$ for the space occupied by the tube can be related to the reference value Q_o by the following integral (the same as in ref. 31):

Declassified 1-24-1963

Declassified 1-24-1963

$$\overline{Q}\pi d^2 = \int_a^d Q 2\pi r \, dr = \int_a^d \gamma Q_o 2\pi r \, dr$$

$$\overline{Q} = -2Q_o \int_d^a \gamma \frac{r}{d} \, d\left(\frac{r}{d}\right)$$

or

$$\overline{Q} = -2Q_o \int_1^\xi \gamma \xi_1 \, d\xi_1 \tag{F25}$$

Using equations (F22) to (F25) in equations (F15), (F17), and (F21), the latter three equations become the same as those in reference 31 except for the limits of integration in equations (F22), (F23), and (F24). The final equations are

$$\sigma_r(\xi) = -\frac{E\alpha\overline{Q}d^2}{2k(1-\nu)\int_1^{a/d} \gamma\xi \, d\xi}\left[F_1(\xi) + A'\left(1 - \frac{1}{\xi^2}\right) + B'\right] \tag{F26}$$

$$\sigma_\theta(\xi) = -\frac{E\alpha\overline{Q}d^2}{2k(1-\nu)\int_1^{a/d} \gamma\xi \, d\xi}\left[F_1(\xi) + F_2(\xi) + A'\left(1 + \frac{1}{\xi^2}\right) + B'\right] \tag{F27}$$

$$\sigma_z(\xi) = -\frac{E\alpha\overline{Q}d^2\nu}{2k(1-\nu)\int_1^{a/d} \gamma\xi \, d\xi} \times \left[2F_1(\xi) + F_2(\xi) + F_3(\xi) + 2A' + 2B' + C'\right] \tag{F28}$$

where

$$A' = \frac{A}{Q_o d^4}$$

$$B' = \frac{B}{Q_o d^2}$$

and

Declassified 1-24-1963

E-288

Declassified 1-24-1963

$$C' = \frac{E\left[\alpha(T_d - T_o) - \epsilon_z\right]}{\dfrac{E\alpha\bar{Q}\nu d^2}{2k(1 - \nu)\displaystyle\int_1^{a/d} \gamma\xi_1 \, d\xi_1}}$$

Solution of general stress equations. - The first step in the solution of the radial, tangential, and longitudinal thermal stress equations is to integrate the $F_1(\xi)$, $F_2(\xi)$, and $F_3(\xi)$ equations. The results are

E-288

$$F_1(\xi) = \frac{1}{2}\left(\ln \xi - \frac{1}{2}\right)\int_{R_m/d}^{\xi} \gamma\xi \, d\xi - \frac{1}{2}\int_1^{\xi} \gamma\xi \ln \xi \, d\xi + \frac{1}{4\xi^2}\int_{R_m/d}^{1} \gamma\xi \, d\xi + \frac{1}{4\xi^2}\int_1^{\xi} \gamma\xi^3 \, d\xi \qquad \text{(F29)}$$

$$F_2(\xi) = \frac{1}{2}\int_{R_m/d}^{\xi} \gamma\xi \, d\xi - \frac{1}{2\xi^2}\int_{R_m/d}^{1} \gamma\xi \, d\xi - \frac{1}{2\xi^2}\int_1^{\xi} \gamma\xi^3 \, d\xi \qquad \text{(F30)}$$

$$F_3(\xi)\frac{\nu}{1 - \nu} = \ln \xi \int_{R_m/d}^{\xi} \gamma\xi \, d\xi - \int_1^{\xi} \gamma\xi \ln \xi \, d\xi \qquad \text{(F31)}$$

Now the boundary conditions are

$$\sigma_r\left(\frac{a}{d}\right) = -p$$

$$\sigma_r(1) = -p$$

where p is the coolant static pressure.

Let

$$W = \frac{E\alpha\bar{Q}d^2}{2k(1 - \nu)\displaystyle\int_1^{a/d} \gamma\xi \, d\xi} \qquad \text{(F32)}$$

Then applying the boundary conditions to equation (F26),

$$-p = -W\left[F_1\left(\frac{a}{d}\right) + A'\left(1 - \frac{d^2}{a^2}\right) + B'\right] \qquad \text{(F33)}$$

Declassified 1-24-1963

Declassified 1-24-1963

$$-p = -W\left[F_1(1) + A'(1 - 1) + B'\right] \tag{F34}$$

From equation (F29),

$$F_1(1) = -\frac{1}{4}\int_{R_m/d}^{1} \gamma\xi \, d\xi + \frac{1}{4}\int_{R_m/d}^{1} \gamma\xi \, d\xi = 0 \tag{F35}$$

Using this in equation (F34) and solving the resulting equation and equation (F33) for A' and B', the result is

$$A' = \frac{a^2}{d^2 - a^2} F_1\left(\frac{a}{d}\right) \tag{F36}$$

$$B' = \frac{p}{W} \tag{F37}$$

In the cladding it is assumed that there is no heat source; therefore, $\gamma = 0$. In the meat, the heat source is assumed constant radially and equal to Q_o (at any axial station), so that $\gamma = 1$. Then, in the stress equations,

$$\int_{1}^{a/d} \gamma\xi \, d\xi = \int_{c/d}^{b/d} \xi \, d\xi = \frac{1}{2}\left(\frac{b^2 - c^2}{d^2}\right) \tag{F38}$$

The remaining terms required before the stress equations can be solved for a particular radial position are C' and $F_1(a/d)$, the latter being required in equation (F36).

Using equation (F29) and the variation of γ just noted, it can be shown that

$$F_1\left(\frac{a}{d}\right) = \frac{1}{4}\left[\ln\left(\frac{a}{d}\right) - \frac{1}{2}\right]\frac{b^2 - R_m^2}{d^2} - \frac{1}{8}\left\{\left(\frac{b}{d}\right)^2\left[\ln\left(\frac{b}{d}\right)^2 - 1\right] - \left(\frac{c}{d}\right)^2\left[\ln\left(\frac{c}{d}\right)^2 - 1\right]\right\} + \frac{c^2 - R_m^2}{8a^2} + \frac{b^4 - c^4}{16a^2d^2} \tag{F39}$$

The third boundary condition is that the total force exerted over a cross section normal to the axis is zero (there are no end restraints and no acceleration), or

$$\int_{a}^{d} \sigma_z 2\pi r \, dr = 0$$

Declassified 1-24-1963

Declassified 1-24-1963

or

$$2\pi d^2 \int_{a/d}^{d/d} \sigma_z \frac{r}{d} d\left(\frac{r}{d}\right) = 0$$

$$2\pi d^2 \int_{a/d}^{1} \sigma_z \xi \, d\xi = 0 \qquad \text{(F40)}$$

E-288

Using equations (F28) and (F32) in equation (F40),

$$-2\pi W d^2 \int_{a/d}^{1} \left[2F_1(\xi) + F_2(\xi) + F_3(\xi) + 2A' + 2B' + C'\right] \xi \, d\xi = 0$$

or

$$C' = -2(A' + B') - \frac{2d^2}{d^2 - a^2} \int_{a/d}^{1} \left[2F_1(\xi) + F_2(\xi) + F_3(\xi)\right] \xi \, d\xi \qquad \text{(F41)}$$

Using equations (F29) to (F31) and knowing the variation of γ previously noted, the expression under the integral sign can be integrated so that

$$C' = -2(A' + B') - \frac{2d^2}{d^2 - a^2} \left[\frac{1}{8\nu} \frac{R_m^2 - c^2}{d^2} + \frac{1}{8\nu} \left(\frac{a}{d}\right)^2 \left(\frac{b^2 - R_m^2}{d^2}\right)\right.$$

$$+ \frac{1}{16\nu} \frac{c^4 - b^4}{d^4} - \frac{1}{8\nu} \left(\frac{a}{d}\right)^2 \frac{b^2 - c^2}{d^2} - \frac{1}{4\nu} \left(\frac{a}{d}\right)^2 \left(\frac{b^2 - R_m^2}{d^2}\right) \ln \frac{a}{d}$$

$$\left. + \frac{1}{4\nu} \left(\frac{a}{d}\right)^2 \left(\frac{b}{d}\right)^2 \ln \frac{b}{d} - \frac{1}{4\nu} \left(\frac{a}{d}\right)^2 \left(\frac{c}{d}\right)^2 \ln \left(\frac{c}{d}\right)\right] \qquad \text{(F42)}$$

All terms are now available to solve for the stresses at any radial location. The maximum combined or equivalent stress will occur at the inner radius. Therefore, equations for the stresses at radii a and d were determined.

Stresses at inner and outer radii. - Examination of the stress equations shows that, to get the stresses at radii a and d, $F_1(a/d)$, $F_1(1)$, $F_2(a/d)$, $F_2(1)$, $F_3(a/d)$, and $F_3(1)$ must be known. The first two have been obtained (eqs. (F35) and (F39)). From equations (F30) and (F31) and the variation of γ, it can be shown that

$$F_2\left(\frac{a}{d}\right) = \frac{1}{4} \left(\frac{b^2 - R_m^2}{d^2}\right) - \frac{1}{4}\left(\frac{d}{a}\right)^2 \left(\frac{c^2 - R_m^2}{d^2}\right) - \frac{1}{8}\left(\frac{d}{a}\right)^2 \left(\frac{b^4 - c^4}{d^4}\right) \qquad \text{(F43)}$$

Declassified 1-24-1963

$$F_2(1) = 0 \tag{F44}$$

$$F_3\left(\frac{a}{d}\right) = \frac{1-\nu}{2\nu}\left(\frac{b^2 - R_m^2}{d^2}\right)\ln\left(\frac{a}{d}\right) - \frac{1-\nu}{2\nu}\left[\left(\frac{b}{d}\right)^2 \ln\frac{b}{d} - \left(\frac{c}{d}\right)^2 \ln\frac{c}{d} - \frac{1}{2}\left(\frac{b^2 - c^2}{d^2}\right)\right] \tag{F45}$$

$$F_3(1) = 0$$

Making use of all of the foregoing equations, the stresses at the radii mentioned become

$$\sigma_r\left(\frac{a}{d}\right) = -p \tag{F46}$$

$$\sigma_r(1) = -p \tag{F47}$$

$$\sigma_\theta\left(\frac{a}{d}\right) = -W\left[F_2\left(\frac{a}{d}\right) - \frac{2d^2}{a^2 - d^2} F_1\left(\frac{a}{d}\right)\right] - p \tag{F48}$$

$$\sigma_\theta(1) = W\left[\frac{2a^2}{a^2 - d^2} F_1\left(\frac{a}{d}\right)\right] - p \tag{F49}$$

$$\begin{aligned}\sigma_z\left(\frac{a}{d}\right) = -W\nu\Bigg\{&2F_1\left(\frac{a}{d}\right) + F_2\left(\frac{a}{d}\right) + F_3\left(\frac{a}{d}\right) - \frac{2d^2}{d^2 - a^2}\Bigg[\frac{1}{8\nu}\frac{R_m^2 - c^2}{d^2} \\ &+ \frac{1}{8\nu}\left(\frac{a}{d}\right)^2\left(\frac{b^2 - R_m^2}{d^2}\right) + \frac{1}{16\nu}\frac{c^4 - b^4}{d^4} - \frac{1}{8\nu}\left(\frac{a}{d}\right)^2\frac{b^2 - c^2}{d^2} \\ &- \frac{1}{4\nu}\left(\frac{a}{d}\right)^2\left(\frac{b^2 - R_m^2}{d^2}\right)\ln\frac{a}{d} + \frac{1}{4\nu}\left(\frac{a}{d}\right)^2\left(\frac{b}{d}\right)^2 \ln\frac{b}{d} - \frac{1}{4\nu}\left(\frac{a}{d}\right)^2\left(\frac{c}{d}\right)^2 \ln\left(\frac{c}{d}\right)\Bigg]\Bigg\}\end{aligned} \tag{F50}$$

$$\begin{aligned}\sigma_z(1) = -W\nu\Bigg\{&\frac{2d^2}{a^2 - d^2}\Bigg[\frac{1}{8\nu}\frac{R_m^2 - c^2}{d^2} + \frac{1}{8\nu}\left(\frac{a}{d}\right)^2\left(\frac{b^2 - R_m^2}{d^2}\right) \\ &+ \frac{1}{16\nu}\frac{c^4 - b^4}{d^4} - \frac{1}{8\nu}\left(\frac{a}{d}\right)^2\frac{b^2 - c^2}{d^2} - \frac{1}{4\nu}\left(\frac{a}{d}\right)^2\left(\frac{b^2 - R_m^2}{d^2}\right)\ln\left(\frac{a}{d}\right) \\ &+ \frac{1}{4\nu}\left(\frac{a}{d}\right)^2\left(\frac{b}{d}\right)^2 \ln\frac{b}{d} - \frac{1}{4\nu}\left(\frac{a}{d}\right)^2\left(\frac{c}{d}\right)^2 .\ln\left(\frac{c}{d}\right)\Bigg]\Bigg\}\end{aligned} \tag{F51}$$

Declassified 1-24-1963

Declassified 1-24-1963

Equivalent stress. - The radial, tangential, and longitudinal stresses are combined into an "equivalent" stress. The shape of the element being considered does not enter into the equation for equivalent stress, because a point is being considered when the stresses are combined. The equation is

$$\sigma_{eq} = \frac{1}{\sqrt{2}} \sqrt{(\sigma_r - \sigma_\theta)^2 + (\sigma_r - \sigma_z)^2 + (\sigma_\theta - \sigma_z)^2} \qquad \text{(F52)}$$

E-288

The equivalent stress is determined at the inner and outer boundaries of the fuel element.

Adjusted equivalent stress. - The foregoing equivalent stress is greater than the actual stress in the material, because some plastic flow and stress-relieving occurs. A method based on the short-time stress-strain curve of the material as shown in figure 63 is used to get the actual stress to compare with allowable stress values for the material. The short-time curve is plotted as shown in figure 63, and the elastic part of the curve is extended as shown by the dashed line. If the equivalent stress is in the dashed region of the curve, as shown, then a vertical line is dropped from this point to a point on the solid curve (point a). The stress at this point, the adjusted stress σ_{ad}, is the one used to compare with the allowable stress. If σ_{eq} falls on the line Ob, it is not adjusted but is used to compare with the allowable stress.

CA-16

Moderator Block

The foregoing analysis is applicable to the moderator block, if the hexagonal outer boundary is considered to be represented by an equivalent circle of radius f. The maximum temperature in the moderator block occurs at this radius f, and the block is uniformly heated radially. In a sense, it is equivalent to the meat of the fuel element (only one ring), and γ would be 1 throughout from radius e to radius f. Then the following changes are required in the equations to make them applicable to the moderator: Change R_m to f, a to e, b to e, c to f, and d to f. The pressure of the coolant around the moderator block is again equal to p, but no cooling is assumed, as mentioned in appendix E.

Determination of $\overline{Q}$

In the foregoing analysis, the term Q_o is equal to $Q_{mt}(x)$ or $Q_{mod}(x)$ of appendix E, depending on whether the fuel element or moderator block is considered. Combining equations (E37) and (E55) and

Declassified 1-24-1963

Declassified 1-24-1963

equations (E38) and (E56), the following values for $Q_{mt}(x)$ and $Q_{mod}(x)$ result:

$$Q_{mt}(x) = \frac{0.9}{0.95}\, 1.21\, \frac{(w_1 + w_2)c_p(T_{out} - T_{in})}{\pi l(c^2 - b^2)} \cos\left(\frac{2\pi x}{3l} - \frac{\pi}{3}\right) \qquad \text{(F53)}$$

$$Q_{mod}(x) = \frac{0.05}{0.95}\, 1.21\, \frac{(w_1 + w_2)c_p(T_{out} - T_{in})}{\pi l(f^2 - e^2)} \cos\left(\frac{2\pi x}{3l} - \frac{\pi}{3}\right) \qquad \text{(F54)}$$

E-288

Then for the fuel-element stress equations,

$$\overline{Q} = -2Q_{mt}(x) \int_1^{a/d} \gamma\xi \, d\xi = -2Q_{mt}(x) \int_{c/d}^{b/d} \xi \, d\xi \qquad \text{(F55)}$$

Integrating this equation and substituting equation (F53) result in

$$\overline{Q} = 0.365\, \frac{(w_1 + w_2)c_p(T_{out} - T_{in})}{l d^2} \cos\left(\frac{2\pi x}{3l} - \frac{\pi}{3}\right) \qquad \text{(F56)}$$

In like manner, for the moderator-block stress equations,

$$\overline{Q} = -2Q_{mod}(x) \int_1^{e/f} \gamma\xi \, d\xi = -2Q_{mod}(x) \int_1^{e/f} \xi \, d\xi \qquad \text{(F57)}$$

or

$$\overline{Q} = 0.02025\, \frac{(w_1 + w_2)c_p(T_{out} - T_{in})}{l f^2} \cos\left(\frac{2\pi x}{3l} - \frac{\pi}{3}\right) \qquad \text{(F58)}$$

Accuracy of Calculated Stresses

Equations (F48) to (F51) and similar ones for the moderator block are of a form such that the W term is very large and the bracketed or braced term consists of differences between very small numbers. These latter numbers must be carried out to many significant figures for any accuracy to result from the calculations.

In the present calculations the results were carried to eight significant figures on a computing machine, but even then some uncertainty arose as to whether this was accurate enough. As a consequence, one formula (that for the fuel-element tangential stress $\sigma_\theta(a/d)$) was expanded by substitution of series expansions for the log terms and use

Declassified 1-24-1963

Declassified 1-24-1963

of the inner radius plus small increments for the radii of the fuel element to get the formula in a form more accurate to use than the original one. Then a check of the stress using the expanded form was made and compared with the original calculations described. The following shows the expansion of the $\sigma_\theta(a/d)$ formula of equation (F48).

E-288

Expansion of Tangential-Stress Formula

Substituting equations (F32), (F38), (F39), and (F43) into equation (F48), the equation for $\sigma_\theta(a/d)$, and reducing give the following:

CA-16 back

$$\sigma_\theta\left(\frac{a}{d}\right) = \frac{E\alpha\bar{Q}}{8k(1 - \nu)} \frac{d^2}{(d^2 - a^2)} \frac{1}{(c^2 - b^2)} \left[4c^2d^2 \ln\left(\frac{c}{a}\right)\right.$$

$$- 4c^2d^2 \ln\left(\frac{d}{a}\right) - 4b^2d^2 \ln\left(\frac{b}{a}\right) + 4R_m^2d^2 \ln\left(\frac{d}{a}\right)$$

$$\left. -2a^2b^2 + 2a^2R_m^2 - 2R_m^2d^2 - c^4 + b^4 + 2b^2d^2\right] - p \qquad \text{(F59)}$$

Letting $a = R$, $b = R + \beta$, $R_m = R + m$, $c = R + \rho$, $d = R + \delta$, and expanding the log terms in a series expansion,

$$\ln\left(\frac{c}{a}\right) = \ln\left(1 + \frac{\rho}{R}\right)$$

$$= \frac{\rho}{R} - \frac{1}{2}\left(\frac{\rho}{R}\right)^2 + \frac{1}{3}\left(\frac{\rho}{R}\right)^3 - \frac{1}{4}\left(\frac{\rho}{R}\right)^4 + \frac{1}{5}\left(\frac{\rho}{R}\right)^5 - \frac{1}{6}\left(\frac{\rho}{R}\right)^6 + \ldots \qquad \text{(F60)}$$

which converges for $\rho \leq R$. Similar equations are obtained for $\ln(b/a)$ and $\ln(d/a)$, the ρ terms in equation (F60) being replaced by β and δ, respectively.

Substituting these expansion formulas for the log terms and the new nomenclature for the radii in equation (F59), and in turn expanding terms such as $(R + \beta)^4$, substituted for b^4, and finally reducing give

Declassified 1-24-1963

Declassified 1-24-1963

$$\sigma_\theta\left(\frac{a}{d}\right) = \frac{E\alpha\bar{Q}d^2}{8k(1-\nu)(d^2-a^2)(c^2-b^2)} \Bigg\{ 8R\left[-\delta^2(\rho - m) + \delta(\rho^2 - \beta^2) - \frac{1}{3}(\rho^3 - \beta^3)\right] + 4\left[-\frac{2}{3}\delta^3(\rho - m) - \delta^2(\rho^2 - m^2) + \delta^2(\rho^2 - \beta^2) + \frac{2}{3}\delta(\rho^3 - \beta^3) - \frac{1}{3}(\rho^4 - \beta^4)\right]$$

$$+ \frac{2}{3R}\left[\delta^4(\rho - m) - 2\delta^3(\rho^2 - m^2) + 2\delta^2(\rho^3 - \beta^3) - \delta(\rho^4 - \beta^4) + \frac{1}{5}(\rho^5 - \beta^5)\right] + \frac{1}{3R^2}\left[-\frac{4}{5}\delta^5(\rho - m) + \delta^4(\rho^2 - m^2) - \delta^2(\rho^4 - \beta^4) + \frac{4}{5}\delta(\rho^5 - \beta^5) - \frac{1}{5}(\rho^6 - \beta^6)\right]$$

$$+ \frac{2}{15R^3}\left[\delta^6(\rho - m) - \delta^5(\rho^2 - m^2) + \delta^2(\rho^5 - \beta^5) - \delta(\rho^6 - \beta^6) + \frac{2}{7}(\rho^7 - \beta^7)\right] + \ldots \Bigg\} - p \qquad \text{(F61)}$$

This type of equation is more amenable to computation and does not require the large number of significant figures for accuracy needed by the original equation.

Sources of Properties Used in Stress Calculations

The properties needed in the calculation of the fuel-element and moderator stresses are the modulus of elasticity E, the coefficient of thermal expansion α, Poisson's ratio ν, and the thermal conductivity k, of the materials used for the parts. The fuel elements, as mentioned in the body of this report, are considered to be made entirely of molybdenum. The moderator blocks are made of beryllium oxide BeO. The sources for the data mentioned for the two materials are given in table XIV.

Declassified 1-24-1963

E-288

Declassified 1-24-1963

E-288

APPENDIX G

ANALYSIS OF NUCLEAR CRITICAL REQUIREMENTS

The following analysis gives a method for determining the uranium investment required for a given cylindrical reactor to make it critical or to have a required reactivity with and without control rod, distributed boron, and xenon buildup after shutdown effects. The one-dimensional, two-group diffusion method of reference 12 (p. 238) is extended to six groups. A fully reflected cylindrical reactor is approximated by first prescribing values of the axial buckling and solving in a radial direction, and then by prescribing values of radial buckling based on assumed flux levels, solving in an axial direction, and iterating. The method is based on dividing the energy spectrum into six groups and the reactor into three regions, first in a radial direction and then in an axial direction. The core is one region, and the reflector is divided into two regions. It is necessary to obtain the neutron cross section and diffusion coefficients for each energy group before using the diffusion-theory equations. The averaging procedure is similar to that in reference 12 (pp. 227-229). Some details of the method are given herein.

Symbols

The following symbols are used in appendix G:

B^2	buckling, cm^{-2}
d	reactor-core diameter, in.
E	neutron energy, ev
E_o	energy of source neutrons produced by fission = 10^7 ev
k_{eff}	effective multiplication factor
l	length of reactor core, in.
N	concentration of reactor constituent, atoms/cc
$\mathscr{P}$	reactor power, Mw
r	reactor-core radius, d/2, in.
T	average temperature of reactor core, ^oK

Declassified 1-24-1963

Declassified 1-24-1963

u	lethargy of neutrons, $\ln \frac{E_o}{E}$
v	neutron velocity, cm/sec
x	any variable distance used in buckling formula, cm
λ_{tr}	transport mean free path, cm
Σ	macroscopic neutron cross section, $N\sigma$, cm^{-1}
σ	microscopic neutron cross section, cm^2/atom
φ	neutron flux, neutrons/(cm^2)(sec)

Subscripts:

a	absorption
f	fission
n	refers to n^{th} neutron group
r	radial
s	scattering
t	total
th	thermal
z	axial
1,2,3, 4,5,6	denotes the six energy groups into which neutrons are divided (6th group is thermal group)

Superscript:

$\bar{}$	average when used with Σ and φ

Detailed Procedure for Determining Required Uranium Investment

Reactor composition. - The number of nuclei per cubic centimeter N of each material in the reactor is first determined. Enriched uranium

E-288

Declassified 1-24-1963

Declassified 1-24-1963

with 92.5 percent U^{235} and 7.5 percent U^{238} was assumed. The methods of determining the N values are straightforward and will not be discussed. The N of the coolant was determined at an average pressure and temperature of the coolant.

Microscopic neutron cross sections. - The microscopic cross sections σ_a, σ_s, and σ_t of the materials in the reactor are required as well as σ_f of the uranium. They were obtained from reference 32, over the range of lethargy u from 0 to thermal. The thermal values of the 1/v absorbers were averaged for the Maxwell-Boltzmann distribution by multiplying them by $\sqrt{\pi}/2$. For uranium, the thermal values were also multiplied by a factor to account for the non-1/v behavior of the absorption and fission cross sections. The thermal energy used to determine the thermal cross sections was calculated from

$$E_{th} = 8.61 \times 10^{-5}\ T,\ \text{ev} \tag{G1}$$

Average macroscopic cross sections and diffusion coefficients. - The average macroscopic cross sections and diffusion coefficients for each of the six groups are required as mentioned before. These include values for both the reflector and the core. The general method of getting these constants using the N and σ values described is reported in reference 12. The macroscopic cross sections were flux-weighted.

The buckling of the cylinder was computed using estimated values of the axial and radial reflector savings. This buckling could, for example, represent an equivalent bare sphere for purposes of discussion of the results of the constants program, and also leads to an estimate of the neutron leakage from the reactor core. Modifications included in the program from the one mentioned in the reference are computations of the neutron age by Marshak's formula for mixtures of heavy elements (ref. 33) and use of Goertzel-Selengut slowing down for hydrogen and Wigner slowing down for other elements (ref. 34) rather than the simple Fermi approximation.

Determination of multiplication factor, k_{eff}. - Knowing the constants mentioned, the diffusion theory can be used to determine, for a given reactor and uranium investment, the effective multiplication factor k_{eff}. The details of the method for the six-group, three-region case used herein are similar to those fully described for a nine-group four-region reactor in reference 35. In the present case, the method was programmed for an IBM 653 computer. The restrictions used in the six-group theory are as follows:

(1) All fissions occur in the first region, the core.

(2) All fissions are assumed to occur in the lower three energy groups.

Declassified 1-24-1963
E-288

Declassified 1-24-1963

(3) Neutrons may be born only in the upper three energy groups.

The first region, the core, is divided into 20 parts; and the second and third regions, in the reflector, are divided into 10 and 8 parts, respectively. The output of the program consists of the flux and the power distributions for each group at the 38 points just described and k_{eff}.

Determination of k_{eff} for fully reflected reactor. - The program discussed in the previous section can be applied to a cylindrical reactor either radially or axially. As pointed out in the beginning of this appendix, in solving in a given direction, the leakage in the other direction is approximated by using an estimated buckling in that direction. The formulas used for the buckling are

$$B_z^2 = \left[\frac{\pi}{(l + x) + 1.42\ \lambda_{tr}}\right]^2 \qquad \text{(G2)}$$

$$B_r^2 = \left[\frac{2.405}{(r + x) + 0.71\ \lambda_{tr}}\right]^2 \qquad \text{(G3)}$$

where B_z^2 is an estimated axial buckling used with a radial solution, and B_r^2 is an estimated radial buckling used with an axial solution. The term that must be estimated is the reflector savings (not necessarily the same value in the two equations). This puts some reflector on the core in the direction in which the assumed buckling is being determined. In addition, the actual thickness of the reflector on the side or end of the core is put into the programs discussed when either a radial or axial solution, respectively, is being sought. The transport mean free path λ_{tr} in the equations for buckling is a value determined in the constants program for the core. The value of λ_{tr} for the third group is used as being about an average for all of the groups.

The method for getting k_{eff} for the fully reflected reactor is to run the constants program using the B^2 for the equivalent spherical reactor previously described. Then an estimated B_z^2 is calculated using equation (G2), and k_{eff} is found using the six-group program in a radial direction. From the results of the program it is possible to set up a series of coefficients in a matrix, in a manner similar to that described for the nine-group solution of reference 35, and by Crouts rule to determine manually the B_t^2 resulting from the calculations. Knowing B_t^2 and the estimated B_z^2, B_r^2 is calculated from $B_t^2 - B_z^2$. This is then used and the program is solved axially. Again from these

Declassified 1-24-1963

Declassified 1-24-1963

results B_t^2 is determined manually and B_z^2 is calculated from B_t^2 minus the B_r^2 used. This is compared with the original B_z^2 estimated, and if it is different, the procedure is repeated. The fact that the B^2 used in the constants program may not be the same, as it theoretically should be, as the final B_t^2 determined as described is usually of little importance, because the constants for most reactors of the type involved vary very little with B^2.

E-288

The procedure just described will yield k_{eff} for the chosen reactor; but, for machine calculations, it is awkward in that after each machine calculation with an estimated B_z^2 or B_r^2 a manual calculation of B_t^2 is required instead of leaving the calculation on the machine. As a consequence, a method has been worked out that avoids this awkwardness. In addition to running a constants program with B^2 for the equivalent spherical reactor, at least two more are run with widely differing values of B^2. The multiplication factors are then obtained from the programs and are plotted as shown in figure 64(a). The point marked A on this plot is the one for which the buckling is that of the equivalent spherical reactor. Then using the constants from the program in which the equivalent spherical reactor buckling is used, multiplication factors for a radial solution of the diffusion-theory program are obtained using three estimated values of axial buckling. This procedure is repeated for an axial solution using three estimated values of radial buckling. The results are plotted as shown in figure 64(b).

CA-17

There is only one B_t^2 $(= B_r^2 + B_z^2)$ that results in a given k_{eff} for the reactor. So B_t^2 is the same on either the B_z^2 varied curve or B_r^2 varied curve for a k_{eff} such as ① in figure 64(b). Call this $B_{t,①}^2$. Then,

$$B_{t,①}^2 = B_r^2 + B_{z,②}^2 \tag{G4}$$

for the B_z^2 varied curve. In like manner for the other curve,

$$B_{t,①}^2 = B_{r,③}^2 + B_z^2 \tag{G5}$$

Because the left sides of the two equations are identical, B_r^2 in the first equation equals $B_{r,③}^2$ and B_z^2 in the second equation equals $B_{z,②}^2$. Then, for a given k_{eff} on the figure, adding the intercepts of the constant k_{eff} line with the curve, as shown, will give a point on a curve of k_{eff} against B_t^2. This procedure is repeated for other values of k_{eff}, which results in the curve shown in figure 64(c).

Declassified 1-24-1963

Declassified 1-24-1963

The curve just obtained does not give the answer for the reactor specified but gives a curve for many reactors with the chosen core composition. There is some equivalent bare reactor with the chosen core composition whose B_t^2 and k_{eff} are the same as that for the specified reactor. If the results for such a bare reactor were known, the point could be spotted on figure 64(c), and the k_{eff} for the specified reactor would be known. It is not known, so the approach is to take a curve such as in figure 64(a) and plot it on the same sheet with the curve in figure 64(c). The results would be like that shown in figure 64(d). It will be remembered that the results at the B_t^2 of point A in the figure were used to get the results for figure 64(c). Now, if point A had coincided with point B in figure 64(d), the k_{eff} at crossover point B would be the answer for the specified reactor. The fact that the points do not coincide makes the k_{eff} at B an approximate answer. If the fast cross sections are constant over the range of B_t^2 used in the constants program, then, even if A does not coincide with B in figure 64(d), the k_{eff} at the crossover point B is satisfactory. If the constants mentioned do vary some with B_t^2, the calculations are repeated until A and B do coincide, or the constants used in the diffusion theory are at the B_t^2 that results at the crossover point in figure 64(d).

E-288

Average flux in core and percent fissions in each group. - Part of the output of the diffusion-theory program, as mentioned previously, is the distribution of flux for each group through the core and reflector. The flux distribution in the reactor is the product of the radial and axial distributions. The fluxes obtained are of course relative fluxes. The absolute fluxes were determined as follows: For a core diameter of d inches, a core length of l inches, and a reactor power of $\mathcal{P}$ megawatts, the following formula is applicable under the restrictions imposed before (fissions occur only in lower three energy groups):

$$\frac{\mathcal{P}\times 10^6\times 3.1\times 10^{10}}{\frac{\pi d^2}{4}\, l\,(2.54)^3} = \bar{\varphi}_6\left(\bar{\Sigma}_{f,4}\frac{\bar{\varphi}_4}{\bar{\varphi}_6} + \bar{\Sigma}_{f,5}\frac{\bar{\varphi}_5}{\bar{\varphi}_6} + \bar{\Sigma}_{f,6}\right) \qquad (G6)$$

Therefore, the left side gives the number of fissions per second per cubic centimeter of core. The right side gives the same thing. The fluxes $\bar{\varphi}_1$, $\bar{\varphi}_2$, and so forth, determined as described, are relative fluxes to some standard of reference. Dividing one by the other as shown in the formula gives the average flux of one group relative to the other. The $\bar{\varphi}_6$ term outside the parentheses is the absolute flux for the thermal group. Since everything is known in the formula except this value, the equation can be solved for it. The average fission macroscopic

Declassified 1-24-1963

Declassified 1-24-1963

cross sections $\overline{\Sigma}_f$ for the three groups in the formula are obtained from the programs described before.

Knowing one absolute average flux, in this case $\overline{\varphi}_6$, the absolute fluxes for the other groups can be obtained by multiplying this value by the relative flux ratios $\overline{\varphi}_1/\overline{\varphi}_6$, $\overline{\varphi}_2/\overline{\varphi}_6$, and so forth, obtained as described. The percent fissions in the fourth, fifth, and thermal groups are calculated from the following formula:

$$(\text{Percent fissions})_n = \left[\frac{\overline{\Sigma}_{f,n}\,\overline{\varphi}_n}{\sum_{n=4}^{6} \overline{\Sigma}_{f,n}\,\overline{\varphi}_n}\right]100 \qquad (G7)$$

where for the fourth group $n = 4$, and so forth. The fluxes are the absolute values.

The details of analyses that use results obtained by methods described herein to determine xenon effects, amount of distributed boron required at startup, results of burnout of boron and fuel, and control-rod effects are given in the body of this report.

E-288

CA-17 back

Declassified 1-24-1963

Declassified 1-24-1963

APPENDIX H

ANALYSIS OF SIDE-REFLECTOR, THERMAL-SHIELD, AND PRESSURE-SHELL TEMPERATURES

It is assumed that heating is caused principally by primary gammas; and, although radial attenuation of the gammas occurs in each reactor part considered, the attenuation is small enough in each part that a constant heat source (an average of the heat source in the part considered) is assumed in the analysis of the part. The heat source is assumed constant axially in any slab also. The radii of all parts are large enough that the equations for heat flow through slabs are considered valid. Thermal radiation between parts will be neglected. Attenuation of the radiation through the coolant (helium in this project) is also neglected.

The analysis has been made assuming that the coolant flows through the passages will be metered so that the coolant temperature in each passage at a given axial position from the inlet will be equal. This will result in a fixed ratio of coolant weight flows in adjacent passages throughout the length of passage, and the maximum temperature in a part will remain at the same radial position for all axial positions. The particular equations for the shields are developed herein. The fixed position of the maximum temperature simplifies the analysis.

Symbols

The following symbols are used in appendix H:

A cross-sectional area of shield normal to gamma radiation, sq in.

c_p specific heat of coolant, Btu/(lb)(°R)

d reactor-core diameter, in.

h convective heat-transfer coefficient, Btu/(sec)(°R)(sq in.)

I heat flux, Btu/(sec)(sq in.)

k thermal conductivity, Btu/(in.)(sec)(°R)

l reactor-core length, in.

$\mathscr{P}$ reactor power, Mw

Declassified 1-24-1963

E-288

Declassified 1-24-1963

E-288

Q volumetric heat source, Btu/(sec)(cu in.)

$\overline{Q}$ average volumetric heat source, Btu/(sec)(cu in.)

r radius, in.

T temperature, $^{\circ}R$

t thickness, in.

w coolant-flow rate, lb/sec

x distance from inner radius of a shield, in. (see fig. 65)

Δy incremental axial distance from coolant entrance in passage, in. (see fig. 65)

μ_a absorption coefficient for gamma radiation, in.$^{-1}$

Subscripts:

A slab A

B slab B

C slab C

con container around reactor core

i inner

in coolant into reactor

max maximum

o when used with I, denotes core flux; when used with r, denotes outer radius (away from core)

$r_{A,i}$ inner radius of slab A

$r_{B,i}$ inner radius of slab B

t total

w,eff effective wall

x any position x in a shield as shown in fig. 65

Declassified 1-24-1963

Declassified 1-24-1963

1 passage 1; when used with T only, refers to coolant temperature in passage 1 at any axial position; when used with T and another subscript, refers to temperature on surface near passage

2 passage 2 with same other connotation as subscript 1

3 passage 3

E-288

General Equations

Temperatures. - In figure 65 are shown three slab cross sections that are representative of a series of thermal shields. Coolant flows in the passages between the slabs, and heat flows from a slab to the coolant on either side. Equations for the coolant temperatures and the temperatures for the middle slab, a representative one, will be developed.

In a small increment of coolant-passage length Δy (see fig. 65), the following equations are applicable with the maximum temperature occurring at x_A, x_B, and x_C:

$$T_1(\Delta y) = T_{in} + \frac{\left[2\pi r_{A,o}\bar{Q}_A(t_A - x_A) + 2\pi r_{B,i}\bar{Q}_B x_B\right]\Delta y}{w_1 c_p} \tag{H1}$$

$$T_2(\Delta y) = T_{in} + \frac{\left[2\pi r_{B,o}\bar{Q}_B(t_B - x_B) + 2\pi r_{C,i}\bar{Q}_C x_C\right]\Delta y}{w_2 c_p} \tag{H2}$$

where $T(\Delta y)$ is the temperature Δy distant from the inlet, and

$$h_1\left[T_{B,1}(\Delta y) - T_1(\Delta y)\right](\Delta y \times 1) = \bar{Q}_B x_B(\Delta y \times 1)$$

where $\Delta y \times 1$ is the surface area transmitting heat to the coolant for a depth of 1 inch. From this equation,

$$T_{B,1}(\Delta y) = T_1(\Delta y) + \frac{\bar{Q}_B x_B}{h_1} \tag{H3}$$

In like manner,

$$T_{B,2}(\Delta y) = T_2(\Delta y) + \frac{\bar{Q}_B(t_B - x_B)}{h_2} \tag{H4}$$

Declassified 1-24-1963

Declassified 1-24-1963

E-288

From reference 15 (p. 657), the general differential equation for heat flow through a slab with a constant heat source is

$$-k \frac{d^2T}{dx^2} = Q$$

which when integrated results in the equation shown in reference 15 (p. 658), which in the notation used herein is

$$T_B(\Delta y,x) = -\frac{\overline{Q}_B x^2}{2k_B} + \left[\frac{T_{B,2}(\Delta y) - T_{B,1}(\Delta y)}{t_B} + \frac{\overline{Q}_B t_B}{2k_B}\right] x + T_{B,1}(\Delta y) \quad \text{(H5)}$$

where $T(\Delta y,x)$ is the temperature of slab B at some axial point Δy from the coolant entrance and some radial point x from the left side of the slab.

Differentiating this equation,

$$\frac{dT_B(\Delta y,x)}{dx} = -\frac{2\overline{Q}_B x}{2k_B} + \frac{T_{B,2}(\Delta y) - T_{B,1}(\Delta y)}{t_B} + \frac{\overline{Q}_B t_B}{2k_B} \quad \text{(H6)}$$

For the position x_B, $dT_B(\Delta y,x)/dx = 0$, for which equation (H6) results in

$$x_B = \frac{t_B}{2} + \frac{T_{B,2}(\Delta y) - T_{B,1}(\Delta y)}{t_B} \frac{k_B}{\overline{Q}_B} \quad \text{(H7)}$$

From equations (H5) and (H7),

$$T_{B,max}(\Delta y) - T_{B,1}(\Delta y) = -\frac{\overline{Q}_B}{2k_B}\left[\frac{t_B}{2} + \frac{T_{B,2}(\Delta y) - T_{B,1}(\Delta y)}{t_B}\frac{k_B}{\overline{Q}_B}\right]^2$$

$$+ \left[\frac{T_{B,2}(\Delta y) - T_{B,1}(\Delta y)}{t_B} + \frac{\overline{Q}_B t_B}{2k_B}\right]\left[\frac{t_B}{2} + \frac{T_{B,2}(\Delta y) - T_{B,1}(\Delta y)}{t_B}\frac{k_B}{\overline{Q}_B}\right] \quad \text{(H8)}$$

If x_B is at the center of the slab, $T_{B,2}(\Delta y) - T_{B,1}(\Delta y) = 0$, and equation (H8) becomes

$$T_{B,max}(\Delta y) - T_{B,1}(\Delta y) = \frac{\overline{Q}_B}{2k_B}\left(\frac{t_B}{2}\right)^2 \quad \text{(H9)}$$

Declassified 1-24-1963

Declassified 1-24-1963

From equations (H3) and (H4), if w_1 and w_2 are metered so that $T_1(\Delta y) = T_2(\Delta y)$,

$$T_{B,2}(\Delta y) - T_{B,1}(\Delta y) = \frac{\overline{Q}_B}{h_1}\left(\frac{t_B - x_B}{h_2/h_1} - x_B\right) \tag{H10}$$

Putting this in equation (H7) and solving for x_B,

$$x_B = \frac{(t_B/2) + (k_B/h_2)}{1 + \frac{k_B}{t_B}\left(\frac{1}{h_2} + \frac{1}{h_1}\right)} \tag{H11}$$

If $T_1(\Delta y) = T_2(\Delta y)$, equations (H1) and (H2) show that

$$\frac{w_2}{w_1} = \frac{r_{B,o}\overline{Q}_B(t_B - x_B) + r_{C,i}\overline{Q}_C x_C}{r_{A,o}\overline{Q}_A(t_A - x_A) + r_{B,i}\overline{Q}_B x_B} \tag{H12}$$

Finally,

$$\frac{h_2}{h_1} = \left(\frac{w_2}{w_1}\right)^{0.8} \tag{H13}$$

Now, equations similar to equation (H11) can be set up for x_A and x_C. If the values of k_B, h, and $\overline{Q}$ are assumed constant axially, by inspection of equations (H11), (H12), and (H13), it can be seen that x_B would be constant axially if x_A and x_C were constant. Since x_A and x_C depend on the same type of equations as x_B, they would be constant.

Since the maximum shield temperatures occur at the passage exits if $\overline{Q}$ is assumed constant axially, and since x values are constant, Δy in the equations can be replaced by the axial length of the passages to find the outlet coolant temperatures from equations (H1) and (H2) and then the shield temperatures from equations (H3), (H4), and (H8).

Volumetric heat sources. - Five percent of the energy generated in the core is assumed to be dissipated as heat outside the core, as mentioned previously in appendix E. Then the heat flux or intensity coming from the core to the reflectors and shields per unit area of core surface is

$$I_o = \frac{0.05\mathscr{P} \times 948.1}{\pi d^2\left(\frac{l}{d} + \frac{1}{2}\right)} \tag{H14}$$

Declassified 1-24-1963

Declassified 1-24-1963

where $\mathscr{P}$ is the power of the reactor in megawatts. Because the container is so very thin, the gamma flux can be considered constant, and the value of the heat-source strength in it due to the absorption of gammas is

$$\overline{Q}_{con} = (I_o)(\mu_a)_{con} \tag{H15}$$

Reverting to figure 65, if slab A is considered to be the one next to the core container with a coolant passage between, and attenuation through the coolant is neglected, then the flux at the entrance to slab A will be

$$(I_A)_{r_{A,i}} = I_o\left(\frac{r_{con,o}}{r_{A,i}}\right)^2 \tag{H16}$$

The factor, ratio of radii squared, is the allowance for the geometric attenuation.

The volumetric heat source at this face will be

$$(Q_A)_{r_{A,i}} = (I_A)_{r_{A,i}}(\mu_a)_A \tag{H17}$$

Now at any point x in slab A,

$$(Q_A)_x = (Q_A)_{r_{A,i}} e^{-(\mu_a)_A(x)}$$

in which it is assumed that omitting the geometric attenuation $\left[r_{A,i}/(r_{A,i} + x)\right]^2$ compensates for omission of an energy buildup factor within the slab:

$$\overline{Q}_A A t_A = \int_0^{t_A} (Q_A)_x A \, dx$$

where A is the cross-sectional area of the slab normal to the gamma ratiation. Integrating the latter equation after inserting the preceding expression for $(Q_A)_x$ results in the following equation for the average volumetric heat source:

$$\overline{Q}_A = (Q_A)_{r_{A,i}} \frac{1 - e^{-(\mu_a)_A t_A}}{(\mu_a)_A t_A} \tag{H18}$$

Declassified 1-24-1963

E-288
CA-18

Declassified 1-24-1963

In similar manner, but with attenuation being assumed in slab A, formulas for slab B would be as follows:

$$(I_B)_{r_{B,i}} = (I_A)_{r_{A,i}} e^{-(\mu_a)_A t_A} \left(\frac{r_{A,o}}{r_{B,i}}\right)^2 \tag{H19}$$

where $e^{-(\mu_a)_A t_A}$ is the attenuation for the material, and $(r_{A,o}/r_{B,i})^2$ is the geometrical attenuation of the flux at the radius $r_{A,o}$. As before, omission of $(r_{A,i}/r_{A,o})^2$ is assumed to compensate for the lack of an energy buildup factor:

$$(Q_B)_{r_{B,i}} = (I_B)_{r_{B,i}} (\mu_a)_B \tag{H20}$$

and

$$\overline{Q}_B = (Q_B)_{r_{B,i}} \frac{1 - e^{-(\mu_a)_B t_B}}{(\mu_a)_B t_B} \tag{H21}$$

Equations similar to the foregoing can be set up for all the slabs.

Convective heat-transfer coefficients. - Equation (E57) for the fuel-element heat-transfer coefficients was also used to determine the coefficients in the coolant passages between the shields. For the hydraulic diameter, the value for an annulus was used which, for the present case, is twice the space between the shields or twice the coolant-passage thickness. As in the case of the fuel elements, the coefficients depend on the shield temperatures, which in turn depend on the coefficients, so that iteration is required.

General design method. - The steps in the design are as follows:

(1) Values of x where the maximum temperatures in each shield occur are assumed.

(2) Coolant-flow-rate ratios in adjacent passages are calculated using equations of the type of equation (H12).

(3) Since the total coolant-flow rate through the reactor is known, w_1 can be determined from

$$w_t = w_1 \left(1 + \frac{w_2}{w_1} + \frac{w_3}{w_1} + \ldots\right)$$

and the ratios calculated from step (2).

Declassified 1-24-1963

E-288

Declassified 1-24-1963

(4) When w_1 and the coolant-flow ratios are known, w_2, w_3, and so forth, can be calculated.

(5) The heat-transfer coefficient h_1 is calculated using an assumed effective wall temperature and w_1.

(6) The heat-transfer-coefficient ratios are calculated from the approximate formula (eq. (H13)).

(7) The coefficients h_2, h_3, and so forth are calculated using steps (5) and (6).

(8) The coolant outlet temperature is calculated using equation (H1). (This is the same for all passages because of the type of analysis made, as brought out previously.)

(9) Values of x are calculated for the slabs where maximum temperatures occur with equations like equation (H11).

(10) The procedure is repeated until x in step (9) nearly equals values used in step (1). On second trial, step (6) is changed to calculating h for each passage using equation (E57) and iterating on $T_{w,eff}$ as in appendix E for the fuel-element coefficients.

(11) The shield temperatures are calculated using equations like equations (H3), (H4), and (H8).

E-288

CA-18 back

Declassified 1-24-1963

Declassified 1-24-1963

APPENDIX I

REACTOR COMPONENTS AND ASSEMBLY PROCEDURE

By D. W. Drier

A discussion of the various parts of the reactor is given in the body of this report. This appendix summarizes the various reactor parts and outlines the suggested assembly procedure.

Components

Core. - The core consists of the following members:

(a) Two outer support plates (OSP1 and 2, fig. 5)

(b) Five inner support plates (ISP1, 2, 3, 4, and 5, fig. 5)

(c) 2632 Moderator blocks (figs. 5 and 25)

(d) 1316 Reflector blocks (figs. 5 and 25)

(e) 640 Fuel-element tubes (figs. 5 and 25)

(f) 18 Tie bolts (fig. 5)

(g) 3872 Support bushings (figs. 5 and 25)

(h) 3912 Spring spacers (figs. 5 and 25)

(i) Flow-dividing container (fig. 5)

(j) 120 1/8-Inch-diameter radial support pins (figs. 5 and 47)

(k) 48 1/4-Inch-diameter radial support pins (fig. 5)

(l) Circular side reflector (AR1, fig. 5)

Side reflector. - In addition to the side-reflector piece included in the core components, there are three circular side-reflector pieces, AR2, AR3, and AR4 (fig. 5).

Inner shield. - The components of what may be called the inner biological shield, some components of which form the thermal shield, too, are:

(a) Pressure vessel (fig. 5)

Declassified 1-24-1963

Declassified 1-24-1963

(b) Five frontal shields (FS1, 2, 3, 4, and 5, fig. 5)

(c) Four radial centering vanes

(d) Four $1\frac{1}{2}$-inch-diameter bolts

(e) Four annular flow dividers (AFD1, 2, 3, and 4, fig. 5)

(f) Six annular thermal shields (AS1, 2, 3, 4, 5, and 6, fig. 5)

E-288

Rear reactor shield. - The components of the rear reactor shield are:

(a) Pressure-vessel head (fig. 5)

(b) Four rear shields (RS1, 2, 3, and 4, fig. 5)

(c) Four radial vanes (fig. 49)

(d) Four clamping bars (fig. 5)

(e) Annular support (AS, fig. 5)

(f) Five rear annular shields, RAS1, 2, 3, 4, and 5, fig. 5)

(g) 72 1/2-Inch-diameter radial support pins (fig. 5)

(h) 96 3/8-Inch-diameter spacer plugs (fig. 5)

(i) Flow container and ducts (fig. 5)

(j) Flow-distributing shell (fig. 5)

Control rod and actuators. - The components of the control-rod and actuator assemblies are:

(a) Three pairs of shim rods (fig. 7)

(b) Three pairs of housing tubes for shim rods (fig. 7)

(c) Three sets of electrically controlled servo actuators used for shim rods

(d) One pair of central regulating rods (fig. 7)

(e) One pair of housing tubes for central regulating rods (fig. 7)

(f) One pair of electrically controlled servo actuators for regulating rods

Declassified 1-24-1963

Declassified 1-24-1963

(g) Three single shim-scram rods (fig. 7)

(h) Three housing tubes for single shim-scram rods (fig. 7)

(i) Three sets of hydraulically controlled servo actuators for single regulating rods

(j) Two scram rods (fig. 7)

(k) Two housing tubes for scram rods (fig. 7)

(l) Two sets of pneumatically controlled servo actuators for scram rods

(m) Nine split positioning rings (fig. 5)

Assembly Procedure

Core. - The procedure for assembling the reactor core follows:

(1) Insert the bolts through OSP1.

(2) Turn tie bolts vertically with bolt heads supporting the assembly.

(3) Slide flow-dividing container and AR1 over OSP1.

(4) Insert 24 1/4-inch-diameter support pins radially through AR1 and flow-dividing container and into OSP1.

(5) Insert 18 reflector blocks over the 18 tie bolts, fitting the circular ends in OSP1.

(6) Insert spring spacers and support bushings into 640 front reflector blocks used for fuel elements.

(7) Insert the 640 front reflector blocks into OSP1.

(8) Insert odd-shaped reflector blocks surrounding control-rod openings and filling spaces on outside diameter. These blocks are held in place with end pins.

(9) Place ISP1 over reflector blocks.

(10) Insert 18 support bushings with spring spacers over tie bolts and through ISP1 into reflector blocks.

Declassified 1-24-1963

Declassified 1-24-1963

(11) Insert 640 support bushings with spring spacers through ISP1 into reflector blocks.

(12) Insert 24 1/8-inch-diameter support pins radially through AR1 and flow-dividing container and into ISP1.

(13) Assemble first layer of moderator blocks over tie bolts and support bushings.

E-288

(14) Fill in spaces surrounding control-rod openings and spaces on outside diameter with odd-shaped moderator blocks, and insert end pins.

(15) Place ISP2 over reflector blocks and continue assembly of core in a repetitive manner, as described in the previous steps, to OSP2.

(16) Place OSP2 over the rear layer of assembled reflector blocks and insert 24 1/4-inch-diameter support pins radially.

(17) Tighten tie-bolt nuts in place.

Side reflector and inner shield. - The five frontal shields (FS1, 2, 3, 4, and 5) and four radial centering vanes are assembled externally with the four annular flow dividers acting as spacers. The assembly of the shields, reflectors, and core is accomplished by lowering these members into the pressure vessel. The pressure vessel is supported in a fixture attached to its central support pin with its axis of symmetry vertical. The assembly procedure follows:

(1) The four radial centering vanes are positioned vertically in an assembly fixture with the rear straight edge down.

(2) The five frontal shields are then slid over the radial vanes beginning with FS1 and separated by the four annular flow dividers.

(3) After FS5 is lowered into place, it is bolted to each of the four radial centering vanes. This completes the external assembly of the five frontal shields, clamping them positively together.

(4) The externally assembled frontal shields are lowered into the pressure vessel. They are positioned by the centering pin and the four pads with the torque pins fitting in corresponding slots in the radial vanes. A cross section of this construction is shown in figure 66, section F-F of figure 5.

(5) The annular shields are then lowered into the pressure vessel beginning with AS5. The forward end of AS5 is positioned by the four radial vanes over which it slides and the rearward end by radial splines mating with the pressure vessel. AS4, 3, 2, and 1 are positioned by the four radial vanes.

Declassified 1-24-1963

Declassified 1-24-1963

(6) Three annular reflectors (AR4, 3, and 2) are then lowered into place, also being positioned by the four frontal radial vanes.

(7) The assembled core, with several control rods already inserted, is then lifted vertically by attaching to the threaded tie-bolt ends and lowered into position with the extending radial pins sliding in the internal grooves in AR2.

(8) The 640 fuel-element tubes can then be vertically lowered into the core, being guided by the spring spacers.

E-288

Rear reactor shield. - The rear-shield assembly procedure follows:

(1) The four radial vanes and the flow-distributing shell are bolted to RS4 with four bolts.

(2) RS4 Is supported in a fixture with its axis vertical and its rear face down.

(3) RS1 Is laid flat with its front face down.

(4) The flow container with ducts and the annular support are lowered over RS1.

(5) 24 1/2-Inch-diameter radial support pins are then inserted through AS and the flow container into RS1.

(6) RS2 And RS3 are then lowered into position, and the remaining 48 1/2-inch-diameter radial support pins are inserted.

(7) This assembly is then lowered into RS4.

(8) RAS5, 4, 3, 2, and 1 are then lowered into position, being guided by the four radial vanes and each being separated from the preceding by 24 3/8-inch-diameter spacer plugs.

(9) The entire rear reactor shield assembly is then clamped tight by bolting the four clamping bars to the four radial vanes.

(10) The rear reactor shield assembly is lowered on the main assembly containing the core. The four radial slots in the protruding annular shields guide the rear reactor shield assembly into position by mating with its four radial vanes.

(11) The pressure-vessel head is lowered over the rear assembly and rotated to secure positively the clamping bars that position the rear assembly.

Declassified 1-24-1963

Declassified 1-24-1963

Control rods and actuators. - The control-rod and actuator assembly is accomplished as follows:

(1) The remaining control rods with their respective housings are externally assembled and inserted into the reactor through the pressure-vessel head.

(2) The split positioning rings are inserted around their respective housings in the pressure-vessel head.

(3) The servo actuators are mechanically attached to their respective control rods, and the housing flanges for these actuators are secured to the pressure-vessel head.

(4) The reactor is now ready to be installed in the fuselage of the airplane.

E-288

CA-19

Declassified 1-24-1963

Declassified 1-24-1963

APPENDIX J

REACTOR BIOLOGICAL SHIELD

In order to calculate the biological-shield weight, it is necessary to know the reactor power, reactor-core size, reflector thicknesses, thermal-shield thicknesses, pressure-shell dimensions, and the materials to be used. These items are assumed to be known. The biological-shield problem then reduces to the determination of the gamma- and neutron-shield thicknesses that result in a shaped unit shield of minimum weight for a prescribed total radiation dose rate at a specified distance from the reactor center. Such calculations currently depend upon the use of various assumptions and approximations, and at best only an approximate shield weight can be obtained at this time. A brief description of the method employed is given herein.

E-288

The leakages of the various gamma energy groups and of the neutrons out of the reactor are evaluated. The reactor is then replaced by an isotropic point source having a source strength equal to this leakage. The reactor and shield assembly is divided into n conical shell sectors (see fig. 54). The radiation that emerges from each sector contributes to the prescribed total dose rate at the crew compartment as direct and single air-scattered radiation. The gamma- and neutron-shield thicknesses external to the pressure shell are determined for each sector by the use of Lagrange multipliers so that a minimum total shield weight will result.

Symbols

The following symbols are used in appendix J:

a	distance from reactor center to exterior of reflector, cm
B	buildup factor
b	distance from reactor center to exterior of pressure shell, cm
D	dose rate, rem/hr
d	distance from reactor center to crew compartment, cm
E_o	average energy of gamma rays, Mev/photon
H	height of reactor core, cm

Declassified 1-24-1963

Declassified
1-24-1963

E-288

CA-19 back

K	factor for conversion from neutrons/(cm^2)(sec) to rem/hr
K'	factor for conversion from photons/(cm^2)(sec) to rem/hr
L	total leakage from reactor core, neutrons/sec or photons/sec
La	Lagrange multiplier
l	leakage from reactor core per cm^2, neutrons/(cm^2)(sec) or photons/(cm^2)(sec)
n	number of sectors
$\mathscr{P}$	reactor power, Mw
$p(\xi)$	scattered gamma dose rate per unit energy emitted from isotropic source for various shadow-shield angles, (rems/hr)/(Mev)/sec)
R	radius of reactor, cm
r	radial variable, cm
S	source strength, neutrons/(cc)(sec) or photons/(cc)(sec)
s	leakage from shield through solid angle $d\Omega$, neutrons/sec or photons/sec
t	thickness, cm
t_{ths}	actual metal thickness of thermal shields and pressure shell, cm
V	volume, cc
v	void fraction, $(b - a - t_{ths})/(b - a)$
W	weight, g
θ	angle of distribution of radiation from shield with normal to surface, radians
θ'	angle from which neutrons can emerge from shield and enter detector directly (see fig. 67)
μ	absorption coefficient, cm^{-1}
ξ	shadow-shield angle, radians

Declassified 1-24-1963

Declassified 1-24-1963

ρ	density, g/cc
Σ	macroscopic cross section, cm^{-1}
φ	neutron flux, neutrons/(cm^2)(sec)
ψ	sector angle, radians
$\Delta \cos_k \psi$	$\cos \psi_1 - \cos \psi_2$
$d\Omega$	solid angle, radians

Subscripts:

c	reactor core
in	inside of pressure shell
k	sector
N	neutron
out	outside of pressure shell
R	reflector
S	shield
s	refers to thermal shield modified to account for void
T	total for all sectors
t	total for any one sector
ths	thermal shield
V	volume
γ	gamma
1,2	sector angle limits

Superscripts:

A	attenuated through biological shield
D	direct

Declassified 1-24-1963

Declassified 1-24-1963

m exponent of neutron distribution from shield

n exponent of gamma distribution from shield

s scattered

Sources and Leakages

E-288

The fast-neutron and gamma leakages from the reactor were evaluated and the reactor was then replaced by an isotropic point source giving these leakages. Assuming a uniform power generation, the number of fast neutrons produced per unit volume becomes

$$S_{V,N} = \frac{7.75(10^{16})\mathscr{P}}{V}, \frac{\text{neutrons}}{(\text{cc})(\text{sec})} \tag{J1}$$

Assuming that five 3-Mev photons are emitted per fission, the number of photons produced per unit volume becomes

$$S_{V,\gamma} = \frac{1.55(10^{17})\mathscr{P}}{V}, \frac{\text{photons}}{(\text{cc})(\text{sec})} \tag{J2}$$

The average energy of the neutrons and gammas was assumed to be 3 Mev.

The uncollided leakages out of the reactor core were assumed to be the same as those out of the surface of a semi-infinite slab. These leakages are good approximations along most of a cylindrical surface if the radius of the cylinder is sufficiently large. Near the ends these leakages exceed those out of a cylinder.

These leakages are

$$l_N = \frac{S_{V,N}}{4\Sigma_c}, \frac{\text{neutrons}}{(\text{cm}^2)(\text{sec})} \tag{J3}$$

and

$$l_\gamma = \frac{S_{V,\gamma}}{4\mu_c}, \frac{\text{photons}}{(\text{cm}^2)(\text{sec})} \tag{J4}$$

and the total leakages are

$$L_N = l_N(2\pi R^2 + 2\pi RH), \frac{\text{neutrons}}{\text{sec}} \tag{J5}$$

Declassified 1-24-1963

Declassified 1-24-1963

$$L_\gamma = l_\gamma(2\pi R^2 + 2\pi RH), \ \frac{\text{photons}}{\text{sec}} \tag{J6}$$

Dose Rates

The radiation leaking out of the surface of the shield was taken to be that coming from the reactor core only. Capture gammas, inelastic scattering gammas, and other gamma radiation originating outside the core were not considered. Of the radiation leaking out of the shield, the amount reaching the detector (or crew compartment) directly and the amount reaching the detector after single air scattering were determined. These radiation amounts were obtained for a number of sectors into which the reactor and shield were divided.

E-288

Direct neutron dose rate. - The neutrons entering a sector of solid angle $d\Omega$ were attenuated through the known thicknesses of the reflector, the thermal shields, and the pressure shell. Allowance was made for the amount of void within the pressure shell. The neutrons were further attenuated through gamma and neutron shields of unknown thicknesses external to the pressure shell. The neutron leakage out of the kth sector of the shield was thus expressed as

$$s_{k,N} = L_N \frac{d\Omega}{4\pi} \left(e^{-\Sigma_R t_{k,R}}\right)\left(e^{-\Sigma_{ths} t_{k,ths}}\right)\left[e^{-(\Sigma_\gamma t_{k,\gamma} + \Sigma_N t_{k,N})}\right] \tag{J7}$$

where the only unknowns are $t_{k,\gamma}$ and $t_{k,N}$ after the shielding materials are selected. The factor $e^{-\Sigma_R t_{k,R}}$ accounts for the neutron attenuation through the kth sector of the reflector. The factor $e^{-\Sigma_{ths} t_{k,ths}}$ accounts for the neutron attenuation through the kth sector thermal shields and pressure shell. If the thermal shields and the pressure shell are made of different materials, this factor must be replaced by the product of two exponentials, one for attenuation through the thermal shields and the other through the pressure shell. The void within the pressure shell is accounted for as follows: $t_{k,s} = t_{k,ths}/(1 - v_k)$ and $\Sigma_s = \Sigma_{ths}(1 - v_k)$, where v_k is the void fraction and $t_{k,ths}$ is the actual metal thickness of the thermal shields and pressure shell. The factor $e^{-(\Sigma_\gamma t_{k,\gamma} + \Sigma_N t_{k,N})}$ accounts for the neutron attenuation through the biological shield exterior to the pressure shell.

The neutron leakage out of the shield surface is assumed to have an angular distribution proportional to $\cos^m\theta$, where θ is the angle

Declassified 1-24-1963

Declassified 1-24-1963

the emergent neutron makes with the normal to the surface. If $s_{k,N}$ neutrons leaking out of the surface have this distribution, there will be $\left[(m + 1)/2\pi\right]\left(s_{k,N} \cos^m\theta\right)$ neutrons per unit solid angle in direction θ. From figure 67 it can be seen that only those neutrons that emerge at an angle θ' will enter the detector directly. For large separation distances as encountered here, θ' is approximately equal to ψ.

E-288

The total flux into a detector at a distance d from the reactor center, for the kth sector, was then found by integration over the angular width of the sector (ψ_1 to ψ_2). Introduction of a factor K for converting neutrons/(cm^2)(sec) to dose-rate units rem/hr finally produced the equation for the direct neutron dose rate into the crew compartment from the kth reactor sector:

$$D^D_{k,N} = \frac{1}{4}\frac{L_N}{4\pi d^2}\left(e^{-\Sigma_R t_{k,R}}\right)\left(e^{-\Sigma_{ths} t_{k,ths}}\right) \times \left[e^{-(\Sigma_\gamma t_{k,\gamma} + \Sigma_N t_{k,N})}\right]\left(\cos^{m+1}\psi_1 - \cos^{m+1}\psi_2\right) \quad \text{(J8)}$$

Scattered neutron dose rate. - Consider an isotropic source emitting L^A_N neutrons per second, and consider only those neutrons emitted into the solid angle $d\Omega$ contained in the conical shell bounded by angles ψ_1 and ψ_2. The single scattered flux into a detector at distance d from the source due to the neutrons in $d\Omega$ is

$$\varphi = \frac{L^A_N \Sigma^s}{8\pi d}\left(\pi\psi - \frac{\psi^2}{2}\right)_{\psi_1}^{\psi_2} \quad \text{(J9)}$$

where Σ^s is the total macroscopic scattering cross section for air evaluated at the appropriate altitude (see ref. 36).

Now $s_{k,N}$ represents the neutrons entering the solid angle $d\Omega$. To facilitate scattering calculations, assume that these neutrons are emitted radially from the shield surface (instead of with a $\cos^m\theta$ distribution). The corresponding isotropic source becomes

$$L^A_N = s_{k,N}\frac{4\pi}{d\Omega} \quad \text{(J10)}$$

Declassified 1-24-1963

Declassified 1-24-1963

Insertion of equations (J7) and (J10) into (J9) and introduction of the conversion factor K finally yields the scattered neutron dose rate at the crew compartment as

$$D^{s}_{k,N} = \frac{L_N}{8\pi dK}\left(e^{-\Sigma_R t_{k,R}}\right)\left(e^{-\Sigma_{ths} t_{k,ths}}\right) \times \left[e^{-(\Sigma_\gamma t_{k,\gamma}+\Sigma_N t_{k,N})}\right] \Sigma^s \left(\pi\psi - \frac{\psi^2}{2}\right)_{\psi_1}^{\psi_2} \quad \text{(J11)}$$

Direct gamma dose rate. - The direct gamma dose rate at the detector at a distance d from the reactor center is calculated in a manner analogous to that used for the direct neutron dose rate. In the case of gammas, however, the gamma leakage L_γ replaces the neutron leakage L_N, a new conversion factor K' to convert photons/(cm^2)(sec) to rems per hour is used, reflector and shield buildup factors are incorporated, μ replaces Σ, and a new distribution at the shield surface ($\cos^n\theta$) is assumed. The direct gamma dose rate can then be written as

$$D^{D}_{k,\gamma} = \frac{L_\gamma}{4\pi K' d^2}\left(e^{-\mu_R t_{k,R}}\right)\left(e^{-\mu_{ths} t_{k,ths}}\right)\left[e^{-(\mu_\gamma t_{k,\gamma}+\mu_N t_{k,N})}\right] \times (B_R B_S)(\cos^{n+1}\psi_1 - \cos^{n+1}\psi_2) \quad \text{(J12)}$$

Scattered gamma dose rate. - The total isotropic source, obtained as for neutrons, is

$$L^{A}_{\gamma} = s_{k,\gamma}\frac{4\pi}{d\Omega}$$

$$= L_\gamma\left(e^{-\mu_R t_{k,R}}\right)\left(e^{-\mu_{ths} t_{k,ths}}\right)\left[e^{-(\mu_\gamma t_{k,\gamma}+\mu_N t_{k,N})}\right] B_R B_S \quad \text{(J13)}$$

Reference 37 presents data for evaluating $p(\xi)$, the scattered gamma dose rate per unit energy emitted from an isotropic source for various shadow-shield angles ξ. An approximate analytical expression for $p(\xi)$ for 3-Mev photons was found to be

$$p(\xi) = \frac{\rho_{altitude}}{0.0765}\,\frac{1500}{d}\,\frac{2}{10^{15}}\,e^{\left[3.898(10^{-8})\xi^2 - 9.41(10^{-4})\right]} \quad \text{(J14)}$$

Declassified 1-24-1963

Declassified 1-24-1963

The scattered dose rate from any sector bounded by angles ψ_1 and ψ_2 will be $p(\psi_1) - p(\psi_2)$ (rems/hr)/(Mev/sec). Hence, the dose rate from the kth sector is

$$D^s_{k,\gamma} = \left[p(\psi_1) - p(\psi_2)\right] E_o L^A_\gamma \tag{J15}$$

where $E_o L^A_\gamma$ is the energy emission from the source. Substitution for L^A_γ leads to the equation

$$D^s_{k,\gamma} = E_o L_\gamma \left(e^{-\mu_R t_{k,R}}\right)\left(e^{-\mu_{ths} t_{k,ths}}\right)\left[e^{-(\mu_\gamma t_{k,\gamma} + \mu_N t_{k,N})}\right] B_R B_S p_{k,\gamma} \tag{J16}$$

E-288

Total dose rate. - The total radiation dose rate reaching the crew compartment is the sum of the individual dose rates for all sectors, or

$$D_T = \sum_{k=1}^{n} \left(D^D_{k,N} + D^s_{k,N} + D^D_{k,\gamma} + D^s_{k,\gamma}\right) \tag{J17}$$

CA-20

Weight

An element of volume of one of the conical-shell sectors of the shield is

$$\left.\begin{aligned} dV &= 2\pi r \sin\psi \; r \, d\psi \, dr \\ \text{Therefore} \qquad & \\ dW &= \rho 2\pi r^2 \sin\psi \, d\psi \, dr \end{aligned}\right\} \tag{J18}$$

where ρ is the density of the shield material considered. The weight of the kth sector can now be found by double integration between the appropriate limits:

$$\begin{aligned} W &= 2\pi\rho \int_{r_1}^{r_2} \int_{\psi_1}^{\psi_2} r^2 \, dr \sin\psi \, d\psi \\ &= 2\pi\rho(\cos\psi_1 - \cos\psi_2) \int_{r_1}^{r_2} r^2 \, dr \\ &= \frac{2\pi\rho}{3} \Delta \cos\psi_k (r_2^3 - r_1^3) \end{aligned} \tag{J19}$$

Declassified 1-24-1963

Declassified 1-24-1963

where r_1 and r_2 are the radial limits for the particular piece of shield under consideration, and $\Delta \cos \psi_k$ represents the difference in $\cos \psi$ evaluated at the angular limits of the sector under consideration.

Gamma-shield weight inside pressure shell and including pressure-shell weight. - In this case, the lower radial limit is the distance from the reactor center to the outer edge of the reflector a_k. This distance increased by the thermal-shield thickness adjusted to account for the void is used for the upper radial limit. Measurements are made along the centerline of the sector under consideration. To account for the void in this region, the density ρ_γ is replaced by $\rho_\gamma(1 - v_k)$, and the thermal-shield thickness $t_{k,s}$ is replaced by $t_{k,ths}/(1 - v_k)$. Hence,

$$W_{k,\gamma,in} = \frac{2\pi}{3} \rho_\gamma (1 - v_k) \Delta \cos \psi_k \left[\left(a_k + \frac{t_{k,ths}}{1 - v_k}\right)^3 - a_k^3\right] \qquad (J20)$$

Gamma shield exterior to pressure shell. - The lower limit in this case is the distance from reactor center to the outer edge of the pressure shell denoted by b_k, and the upper limit is this distance increased by the gamma-shield thickness yet to be determined. Again, measurements are made along the centerline of the sector. The result is

$$W_{k,\gamma,out} = \frac{2\pi\rho_\gamma}{3} \Delta \cos \psi_k \left[(b_k + t_{k,\gamma})^3 - b_k^3\right] \qquad (J21)$$

Weight of neutron shield. - The neutron shield is located exterior to the outer gamma shield. The inner radial limit is therefore equal to the outer radial limit for $W_{k,\gamma,out}$; the outer radial limit is this value increased by the yet to be determined neutron-shield thickness. The neutron-shield weight is given by

$$W_{k,N} = \frac{2\pi\rho_N}{3} \Delta \cos \psi_k \left[(b_k + t_{k,\gamma} + t_{k,N})^3 - (b_k + t_{k,\gamma})^3\right] \qquad (J22)$$

Total shield weight. - The total shield weight is the sum of the over-all sectors of the three weights just described, or

$$W_T = \sum_{k=1}^{n} (W_{k,\gamma,in} + W_{k,\gamma,out} + W_{k,N}) \qquad (J23)$$

E-288

Declassified 1-24-1963

Declassified 1-24-1963

E-288

CA-20 back

Gamma- and Neutron-Shield Thicknesses

For a given reactor power and size, the number and thicknesses of the thermal shields and the thickness and size of the pressure shell are known. Hence, $W_{\gamma,in}$ also remains fixed. The gamma- and neutron-shield thicknesses for those parts of the shield exterior to the pressure shell must be determined. Use of Lagrange multipliers permits the calculation of these thicknesses that will give a minimum-weight shield for a prescribed total dose rate at a specified location. The known necessary conditions are

$$\frac{\partial W_T}{\partial t_{k,\gamma}} + \frac{1}{La}\frac{\partial D_T}{\partial t_{k,\gamma}} = 0 \tag{J24}$$

and

$$\frac{\partial W_T}{\partial t_{k,N}} + \frac{1}{La}\frac{\partial D_T}{\partial t_{k,N}} = 0 \tag{J25}$$

In conjunction with the subsidiary condition imposed by the prescribed total dose rate D_T, these equations serve to determine the gamma- and neutron-shield thicknesses and the constant of proportionality La.

From equations (J24) and (J25), the value of La can be written as

$$La = -\frac{\dfrac{\partial D_T}{\partial t_{k,\gamma}}}{\dfrac{\partial W_T}{\partial t_{k,\gamma}}} = -\frac{\dfrac{\partial D_T}{\partial t_{k,N}}}{\dfrac{\partial W_T}{\partial t_{k,N}}} \tag{J26}$$

as shown in reference 34. Differentiation of equations (J8), (J11), (J12), and (J16) with respect to $t_{k,\gamma}$ and $t_{k,N}$, but assuming that the buildup factors remain constant, results in the following:

Declassified 1-24-1963

Declassified 1-24-1963

$$\left.\begin{aligned}
\frac{\partial D^D_{k,N}}{\partial t_{k,\gamma}} &= -\Sigma_\gamma D^D_{k,N} \\
\frac{\partial D^S_{k,N}}{\partial t_{k,\gamma}} &= -\Sigma_\gamma D^S_{k,N} \\
\frac{\partial D^D_{k,\gamma}}{\partial t_{k,\gamma}} &= -\mu_\gamma D^D_{k,\gamma} \\
\frac{\partial D^S_{k,\gamma}}{\partial t_{k,\gamma}} &= -\mu_\gamma D^S_{k,\gamma}
\end{aligned}\right\} \qquad \text{(J27)}$$

$$\left.\begin{aligned}
\frac{\partial D^D_{k,N}}{\partial t_{k,N}} &= -\Sigma_N D^D_{k,N} \\
\frac{\partial D^S_{k,N}}{\partial t_{k,N}} &= -\Sigma_N D^S_{k,N} \\
\frac{\partial D^D_{k,\gamma}}{\partial t_{k,N}} &= -\mu_N D^D_{k,\gamma} \\
\frac{\partial D^S_{k,\gamma}}{\partial t_{k,N}} &= -\mu_N D^S_{k,\gamma}
\end{aligned}\right\} \qquad \text{(J28)}$$

If D_t designated the total dose rate for any one sector, then

$$\begin{aligned}
\frac{\partial D_T}{\partial t_{k,\gamma}} &= \frac{\partial D_t}{\partial t_{k,\gamma}} \\
&= -\Sigma_\gamma \left(D^D_{k,N} + D^S_{k,N}\right) - \mu_\gamma \left(D^D_{k,\gamma} + D^S_{k,\gamma}\right)
\end{aligned} \qquad \text{(J29a)}$$

and

$$\begin{aligned}
\frac{\partial D_T}{\partial t_{k,N}} &= \frac{\partial D_t}{\partial t_{k,N}} \\
&= -\Sigma_N \left(D^D_{k,N} + D^S_{k,N}\right) - \mu_N \left(D^D_{k,\gamma} + D^S_{k,\gamma}\right)
\end{aligned} \qquad \text{(J29b)}$$

Declassified 1-24-1963

E-288

Declassified 1-24-1963

Also, if W_t designates the total weight for any one sector, then

$$\frac{\partial W_T}{\partial t_{k,\gamma}} = \frac{\partial W_t}{\partial t_{k,\gamma}}$$

$$= \left\{2\pi\rho_\gamma(t_{k,\gamma} + b_k)^2 + 2\pi\rho_N\left[(t_{k,N} + t_{k,\gamma} + b_k)^2 - (t_{k,\gamma} + b_k)^2\right]\right\}\Delta \cos \psi_k \quad \text{(J30a)}$$

E-288

and

$$\frac{\partial W_T}{\partial t_{k,N}} = \frac{\partial W_t}{\partial t_{k,N}}$$

$$= 2\pi\rho_N(t_{k,N} + t_{k,\gamma} + b_k)^2 \Delta \cos \psi_k \quad \text{(J30b)}$$

Therefore, from equations like (J26) for each individual sector,

$$La = \frac{\Sigma_\gamma\left(D^D_{k,N} + D^s_{k,N}\right) + \mu_\gamma\left(D^D_{k,\gamma} + D^s_{k,\gamma}\right)}{\left\{2\pi\rho_\gamma(t_{k,\gamma} + b_k)^2 + 2\pi\rho_N\left[(t_{k,N} + t_{k,\gamma} + b_k)^2 - (t_{k,\gamma} + b_k)^2\right]\right\}\Delta \cos \psi_k} \quad \text{(J31)}$$

and

$$La = \frac{\Sigma_N\left(D^D_{k,N} + D^s_{k,N}\right) + \mu_N\left(D^D_{k,\gamma} + D^s_{k,\gamma}\right)}{2\pi\rho_N(t_{k,N} + t_{k,\gamma} + b_k)^2 \Delta \cos \psi_k} \quad \text{(J32)}$$

If equations (J31) and (J32) are equated for any sector, the only unknowns are the gamma- and neutron-shield thicknesses $t_{k,\gamma}$ and $t_{k,N}$. For a series of assumed values for $t_{k,\gamma}$, corresponding values of $t_{k,N}$ can then be found, and a relation between $t_{k,\gamma}$ and $t_{k,N}$ can be determined.

From either equation (J31) or (J32), values of La can be found for the corresponding pairs of values of $t_{k,\gamma}$ and $t_{k,N}$ previously determined. A relation between La and either $t_{k,\gamma}$ or $t_{k,N}$ can then be established for each sector.

By use of these values of La and the corresponding values of $t_{k,\gamma}$ and $t_{k,N}$, equations (J31) and (J32) can be solved simultaneously for $\left(D^D_{k,N} + D^s_{k,N}\right)$ and $\left(D^D_{k,\gamma} + D^s_{k,\gamma}\right)$ for each sector. The sum of these

Declassified

Declassified 1-24-1963

quantities then yields D_t for each sector, and the sum of the D_t gives the total dose rate D_T. When such calculations are completed for a series of values of La, a relation between La and D_T can be established. From this relation, the value of La corresponding to the prescribed allowable total dose rate at the crew compartment can be found. The values of $t_{k,\gamma}$ and $t_{k,N}$ corresponding to this La can then be found, and the shield weights can then be calculated for each sector. Finally, the sum of the individual sector shield weights gives the desired total weight W_T.

Tables XV and XVI give some material properties and constants used in the shielding calculations. The values of the final shield thicknesses and weights are given in tables XI and XII.

E-288

Declassified 1-24-1963

Declassified 1-24-1963

E-288

APPENDIX K

ADDITIONAL SHIELD WEIGHTS TO COMPENSATE FOR DUCTS

The previous discussion of the biological-shield calculations did not account for the presence of ducts in the shield. Allowances must be made for additional shielding in order to compensate for radiation streaming through the ducts and for the voids in the shielding caused by the presence of ducts. A simplified method for incorporating these effects is described herein.

Only fast-neutron shielding must be considered for streaming and void effects; such neutron shielding is generally believed sufficient to shield against gamma rays, too. A method of calculating these additional shield weights will be described. The additional shield weights will be determined on the assumption that hemispherical bumps will be added to the previously calculated biological shield. These bumps are to be tanks of decalin, which will also provide additional chemical fuel for emergency use.

Symbols

The following symbols are used in appendix K:

d duct diameter, cm

l length of duct leg, cm

α reflection coefficient (assumed $\equiv 1$)

θ angle variation from elbow corner to elbow corner of duct-leg exit, radians

φ_i fast-neutron flux at duct-leg inlet, neutrons/(cm^2)(sec)

φ_o fast-neutron flux leaving duct-leg exit, neutrons/(cm^2)(sec)

Subscript:

m duct leg

Calculation Method

A method was derived that would yield the optimum lengths of ducts and an accompanying minimum additional shield weight. However, the

Declassified 1-24-1963

Declassified 1-24-1963

geometry of the reactor discussed herein prevented the use of optimum-length ducts. As a consequence, the method of optimization could not be used, and calculations were made for the particular duct configuration of the present reactor. Using the biological-shield procedure (appendix J), it is possible to determine the flux at the inlet of each duct leg; these calculated fluxes are the fluxes that would exist at the specified locations if there were no ducts (e.g., for a solid shield). An additional flux due to streaming through each duct must also be considered. The streaming fluxes were determined by use of the equation on page 278 of reference 38:

$$\frac{\varphi_o}{\varphi_i} = \frac{1}{8}\left(\frac{d_1}{l_1}\right)^2 \frac{1}{8}\left(\frac{d_2}{l_2}\right)^2 \frac{\alpha}{\sec\ \theta_1} \frac{1}{8}\left(\frac{d_3}{l_3}\right)^2 \frac{\alpha}{\sec\ \theta_2} \cdot \cdot \cdot \frac{1}{8}\left(\frac{d_m}{l_m}\right)^2 \frac{\alpha}{\sec\ \theta_m}$$

The values of d_m, l_m, d_m/l_m, and θ_m for the reactor considered herein are as follows:

Leg	Duct diameter, d, cm	Duct length, l, cm	d/l	θ_m, deg
1	1.27	12.70	1/10	90
2	20.32	30.48	2/3	60
3	27.94	50.80	11/20	90
4	27.94	121.92	11/48	45
5	27.94	137.16	11/54	--

The value of φ_i used in the determination of the streaming fluxes of each leg was taken as the sum of the solid-shield flux and the streaming flux of the preceding leg. The total flux for each leg was the sum of this calculated streaming flux plus the so-called direct or solid-shield flux at the leg outlet.

The sum of the two fluxes (that for the solid shield plus that for the streaming) was then attenuated through the remaining biological-shield lengths. The thickness of the additional shielding required to attenuate this flux to the allowable flux was then determinable; the allowable flux was found from the biological-shield calculations of the neutron dose rates in the appropriate sector of the shield. The weight of the additional shield required because of streaming was then determined under the assumption that it would be added as a hemispherical bump.

Declassified 1-24-1963

Declassified 1-24-1963

These bumps would then be placed on the exterior of the biological shield in direct line with the respective duct under consideration.

Additional shielding due to the voids in the biological shield caused by the presence of ducts is also required. The volume of each duct was calculated, and its weight was determined. This weight was then projected to the outside of the biological shield, and the additional shielding required because of the presence of ducts was thereby determined.

E-288

CA-21

REFERENCES

1. Johnson, P. G., and Smith, R. L.: A Comparison of Three Nuclear Propulsion Systems for a Logistic Type Aircraft. NASA MEMO 3-16-59E, 1959.

2. Cleveland Laboratory Staff: Performance and Ranges of Application of Various Types of Aircraft-Propulsion System. NACA TN 1349, 1947.

3. Cavicchi, Richard H.: Analysis of Limitations Imposed on One-Spool Turboprop-Engine Designs by Compressors and Turbines at Flight Mach Numbers of 0, 0.6, and 0.8. NACA RM E56I05, 1956.

4. Voit, Charles H.: Investigation of a High-Pressure-Ratio Eight-Stage Axial-Flow Research Compressor with Two Transonic Inlet Stages. I - Aerodynamic Design. NACA RM E53I24, 1953.

5. Cavicchi, Richard H.: Analysis of Limitations Imposed on One-Spool Ducted-Fan-Engine Designs by Compressors and Turbines at Flight Mach Numbers of 0, 0.6, and 0.8. NACA RM E57E14, 1957.

6. Cavicchi, Richard H., and English, Robert E.: A Rapid Method for Use in Design of Turbines Within Specified Aerodynamic Limits. NACA TN 2905, 1953.

7. Eckert, E. R. G.: Introduction to the Transfer of Heat and Mass. McGraw-Hill Book Co., Inc., 1950.

8. McAdams, William H.: Heat Transmission. Third ed., McGraw-Hill Book Co., Inc., 1954.

9. Kays, W. M., and London, A. L.: Compact Heat Exchangers. The Nat. Press, Palo Alto (Calif.), 1955.

10. Thompson, A. S.: Gas Cooled Nuclear Reactor Study. AECU-3559, Nuclear Power Dept., Studebaker-Packard Corp., July 31, 1956.

Declassified 1-24-1963

Declassified 1-24-1963

11. Anon.: Arc-Cast Molybdenum and Its Alloys. Climax Molybdenum Co., 1955.

12. Glasstone, Samuel, and Edlund, Milton C.: The Elements of Nuclear Reactor Theory. D. Van Nostrand Co., Inc., 1952.

13. Webster, J. W.: The Low Cross-Section Fission Product Poisons. IDO 16100, Phillips Petroleum Co., June 8, 1953.

14. Webster, J. W.: Practical Reactor Theory. AECD-4083, AEC, Oct. 21, 1953.

15. Glasstone, Samuel: Principles of Nuclear Reactor Engineering. D. Van Nostrand Co., Inc., 1955.

16. Hogerton, J. F., and Grass, R. C., eds.: The Reactor Handbook. Vol. 3 - General Properties of Materials. AECD-3647, AEC, Mar. 1955.

17. Schultz, M. A.: Control of Nuclear Reactors and Power Plants. McGraw-Hill Book Co., Inc., 1955.

18. Hughes, Donald J., and Harvey, John A.: Neutron Cross Sections. BNL 325, Brookhaven Nat. Lab., July 1, 1955.

19. Wood, Karl D.: Technical Aerodynamics. McGraw-Hill Book Co., Inc., 1935.

20. Tucker, Maurice: Approximate Calculation of Turbulent Boundary-Layer Development in Compressible Flow. NACA TN 2337, 1951.

21. English, Robert E., and Wachtl, William W.: Charts of Thermodynamic Properties of Air and Combustion Products from 3000° to 3500° R. NACA TN 2071, 1950.

22. Holden, F. R.: A Statistical Study of Turbojet Engine Component Weights. Rep. No. NADC-AC-5310, U. S. Naval Air Dev. Center, Dec. 1953.

23. Eckert, E. R. G., and Diaguila, Anthony J.: Method of Calculating Core Dimensions of Crossflow Heat Exchanger with Prescribed Gas Flows and Inlet and Exit States. NACA TN 3655, 1956.

24. Akin, S. W.: Thermal Conductivity and Viscosity of Helium. Supp. Rep. 55141, Gen. Eng. and Consulting Lab., General Electric Co., July 1947.

Declassified 1-24-1963

Declassified 1-24-1963

25. Keenan, Joseph H., and Kaye, Joseph: Thermodynamic Properties of Air. John Wiley & Sons, Inc., 1945.

26. Schwenk, Francis C., Lieblein, Seymour, and Lewis, George W., Jr.: Experimental Investigation of an Axial-Flow Compressor Inlet Stage Operating at Transonic Relative Inlet Mach Numbers. III - Blade-Row Performance of Stage with Transonic Rotor and Subsonic Stator at Corrected Tip Speeds of 800 and 1000 Feet per Second. NACA RM E53G17, 1953.

27. Lieblein, Seymour, Schwenk, Francis C., and Broderick, Robert L.: Diffusion Factor for Estimating Losses and Limiting Blade Loadings in Axial-Flow-Compressor Blade Elements. NACA RM E53D01, 1953.

28. Lieblein, Seymour: Analysis of Experimental Low-Speed Loss and Stall Characteristics of Two-Dimensional Compressor Blade Cascades. NACA RM E57A28, 1957.

29. Members of the Staff: Course Outlines and Engineering Problems. TID-5261, U. S. Atomic Energy Comm., July 1955.

30. Humble, Leroy V., Lowdermilk, Warren H., and Desmon, Leland G.: Measurements of Average Heat-Transfer and Friction Coefficients for Subsonic Flow of Air in Smooth Tubes at High Surface and Fluid Temperatures. NACA Rep. 1020, 1951. (Supersedes NACA RM's E7L31, E8L03, E50E23, and E50H23.)

31. Thompson, A. Stanley, and Rodgers, Oliver E.: Thermal Power from Nuclear Reactors. John Wiley & Sons, Inc., 1956.

32. Hughes, Donald J., and Schwartz, Robert B.: Neutron Cross Sections. BNL 325, Brookhaven Nat. Lab., Jan. 1, 1957.

33. Marshak, Robert E.: Theory of Slowing Down of Neutrons by Elastic Collision with Atomic Nuclei. Rev. Modern Phys., vol. 19, no. 3, July 1947, pp. 185-238.

34. Hogerton, J. F., and Grass, R. C., eds.: The Reactor Handbook. Vol. 1 - Physics. AECD-3645, AEC, Mar. 1955.

35. Miser, James W., Hyland, Robert E., and Fieno, Daniel: Computer Program for Solving Nine-Group Diffusion Equations for Cylindrical Reactors. NASA MEMO 12-24-58E, 1959.

36. Stephenson, Richard: Introduction to Nuclear Engineering. McGraw-Hill Book Co., Inc., 1954.

E-288

CA-21 back

Declassified 1-24-1963

Declassified 1-24-1963

SECRET

37. Lynch, R. E., Benoit, J. W., Johnson, W. P., and Zerby, C. D.: A Monte Carlo Calculation of Air-Scattered Gamma Rays. ORNL 2292, vol. 4, Oak Ridge Nat. Lab., Feb. 12, 1958.

38. Rockwell, Theodore, III, ed.: Reactor Shielding Design Manual. TID-7004, AEC, Mar. 1956.

39. Anon.: Modern Flange Design. Bull. 502, Taylor Forge and Pipe Works, Third ed., 1950.

40. Osborn, R. H.: Thermal Conductivity of Tungsten and Molybdenum at Incandescent Temperature. Jour. Optical Soc. Am., vol. 31, June 1941, pp. 428-431.

41. Campbell, E.: High Temperature Technology. John Wiley & Sons, Inc., 1956.

E-288

Declassified 1-24-1963

SECRET

Declassified 1-24-1963

E-288

TABLE I. - PRINCIPAL ASSUMPTIONS, DESIGN, AND OPERATING CONDITIONS FOR TYPICAL AIRPLANE

Airplane:	
Gross weight, lb	400,000
Flight Mach number	0.72
Altitude, ft	30,000
Wing:	
Area, sq ft	6250
Span, ft	250
Sweep, leading edge, deg	18.5
Design lift coefficient	0.28
Tail area, sq ft	2500
Fuselage:	
Length, ft	175
Diameter (nominal), ft	15
Lift-drag ratio (including nacelles)	19.7
Engines:	
Number	8
Airflow, each engine at flight conditions, lb/sec	57.0
Nacelle diameter, ft	4.0
Compressor pressure ratio	11.0
Turbine-inlet temperature, °R	1800
Propeller shaft horsepower, each engine at flight conditions	3410
Ratio of turbine-inlet to compressor-exit pressure	0.85
Reactor:	
Power to coolant, Mw	98.5
Helium:	
Flow, lb/sec	74
Inlet pressure, lb/sq ft	180,000
Inlet temperature, °R	1250
Outlet pressure, lb/sq ft	172,800
Outlet temperature, °R	2250
Heat exchanger:	
Number	8
Helium:	
Inlet pressure, lb/sq ft	170,200
Inlet temperature, °R	2250
Inlet Mach number	0.024
Outlet pressure, lb/sq ft	168,500
Outlet temperature, °R	1200
Air:	
Inlet pressure, lb/sq ft	9070
Inlet temperature, °R	985
Inlet Mach number	0.063
Outlet pressure, lb/sq ft	8330
Outlet temperature, °R	1200
Helium pump:	
Pressure ratio	1.085
Efficiency	0.80
Temperature rise, °R	50
Horsepower per engine	872

Declassified 1-24-1963

Declassified 1-24-1963

TABLE II. - WEIGHTS OF TYPICAL AIRPLANE COMPONENTS

Aircraft structure, lb		108,000
Fuselage, lb	28,000	
Wing, lb	41,000	
Tail, lb	9,000	
Landing gear, lb	30,000	
Equipment, lb		22,000
Engines, pumps, and nacelles, lb		58,000
Heat exchangers and lines, lb		25,000
Reactor and shield, lb		120,000
Core, lb; Reflector, lb	4,500	
Thermal shield, lb; Pressure shell, lb	36,000	
Gamma shield, lb	30,500	
Neutron shield:		
Lithium hydride, lb	18,500	
Decalin (chemical fuel), lb	30,500	
Decalin for takeoff and landing, lb		4,000
Payload, lb		63,000
Gross weight, lb		400,000

TABLE III. - DESIGN CONDITIONS HELD CONSTANT

Efficiencies:	
Compressor polytropic	0.88
Turbine polytropic	.85
Reduction gear (propeller and helium pump)	.95
Propeller	.80
Inlet total-pressure ratio	.95
Exhaust-nozzle velocity coefficient	.96
Compressor rotor inlet relative Mach number at tip	.95
Turbine rotor inlet Mach number at hub	.60
Turbine rotor exit axial Mach number at hub	.47
Hub-tip radius ratio:	
Compressor inlet	.50
Turbine exit	.60
Turbine blade centrifugal stress at rotor exit hub, psi	30,000
Turbine blade material density, lb/cu ft	500
Blade taper factor, ψ	.70
Compressor equivalent tip speed, ft/sec	1000
Ratio of turbine-exit to compressor-inlet pressure	1.038

Declassified 1-24-1963

E-288

Declassified 1-24-1963

E-288

TABLE IV. - FINAL REACTOR-CORE VOLUMES

Power = 100 Mw
Number of fuel elements = 640
Core length = 24 in.
Side reflector thickness = 3.75 in.
End reflector thickness = 4 in.
Uranium = 140.5 lb of 92.5 percent U^{235} and 7.5 percent U^{238}
Fuel element "meat": UC-Mo mixture
Core radius = 17.36 in.

Item	Volume, cu in.	Volume, percent
UC in fuel elements meat	312	1.4
Mo in fuel elements tubes	320	
Mo in fuel elements spacers	21.6	1.72
Mo in fuel elements sleeves	48	
Mo in moderator-block support plates	265	1.53
Mo in core container	81.8	Structure
Mo in control rods	635.8	2.80
Inconel in through-bolts (70 percent Ni)	47.8	.21
He in core (void)	3094	13.61 Void
BeO in moderator blocks	17,598	77.30
BeO in control rods (rods out)	326	1.43
Total	22,750	100.00

Flow area, 118 sq in.
Frontal area, 947 sq in.

$$\frac{\text{Flow area}}{\text{Frontal area}} = 0.125$$

Declassified 1-24-1963

Declassified 1-24-1963

TABLE V. - REACTOR DATA FOR TWO OPERATING CONDITIONS

		Loaded core for initial startup		Partially depleted core 37.4 days at 100 Mw	
W_U, lb		140.5		130.0	
k_{eff} (cold clean)		1.18		-----	
k_{eff} (hot clean)		1.12		1.11	
k_{eff} (hot dirty)		-----		1.08	
Group	Energy	Neutron flux, neutrons / (sec)(cm^2)	Fissions, percent	Neutron flux, neutrons / (sec)(cm^2)	Fissions, percent
1	10 Mev - 2.46 Mev	1.57×10^{13}	-----	1.48×10^{13}	-----
2	2.46 Mev - 0.908 Mev	16.40	-----	16.18	-----
3	0.908 Mev - 25 Kev	65.86	-----	65.52	-----
4	25 Kev - 50.6 ev	62.19	31.13	63.58	29.58
5	50.6 ev - 0.411 ev	18.02	34.50	19.31	34.28
6	0.102 ev	3.22	34.37	3.66	36.13

Declassified 1-24-1963

Declassified 1-24-1963

E-288

CA-22

TABLE VI. - WEIGHTS AND DENSITIES

OF CONSTITUENTS IN CORE

Constituent	Weight, lb	Weight, percent
UC	153.1	6.1
He	.5	Negligible
Mo	506	20.1
BeO	1845	73.2
Ni	15.4	.6
Weight of core	2520	100.0

Constituent	N, atoms/cc core
He	8.6×10^{19}
Mo	387.5
Be	5401
O	5401
U^{235}	40.39
U^{238}	3.28
C	43.67
Ni	19.19

Declassified 1-24-1963

Declassified 1-24-1963

SECRET

TABLE VII. - VOLUMES AVAILABLE AND REQUIRED IN FUEL ELEMENTS FOR FUEL

[Uniform radial power distribution.]

Reactor sector	Volume available, cu in.	Volume required for UO_2, cu in.	Volume required for UC, cu in.
1	0	[a]2.47	[a]1.85
2	13.09	7.48	5.58
3	20.37	12.82	9.56
4	40.72	18.82	14.04
5	34.18	25.89	19.32
6	40.72	34.69	25.88
7	61.8	46.16	34.44
8	87.3	61.79	46.09
9	77.1	[a]83.57	62.34
10	90.2	[a]108.87	81.22

[a]Available volume insufficient.

E-288

TABLE VIII. - PROPOSED CONTROL-ROD SYSTEM COMPONENTS AND WORTH

Control rods		Worth, δk/rod	Actuating mechanism
Number	Type		
2	Regulating	0.005	Linear reluctance motor
3 (Pairs)	Shim	.04	Synchronous reluctance motor
3	Shim-scram	.04	Hydraulic or pneumatic
2	Scram	.02	Pneumatic
Total 10	----------	Total 0.285+	----------

SECRET

Declassified 1-24-1963

Declassified 1-24-1963

SECRET

TABLE IX. - REACTOR STRESSES

[In psi. Loading, 3 g's.]

Pressure vessel	Core	Rear shield assembly	Control rod housing tubes	Front centering pin
1. Wall (1.75 in.) Hoop membrane 22,400 Average longitudinal 11,200	1. Supporting bushings Longitudinal bending Negligible Bearing 57 Shear 58 Hoop bending 3780	1. Fin positioning Shear 5133	Max. bending[a] 1970 Max. deflection, in. 0.015	Shear 2100 Bending 2700
2. Flange[b] (without gussets) Longitudinal hub 31,200 Radial flange 17,220 Tangential flange 10,700 Maximum equivalent 26,435	2. Spring spacers Tensile 176	2. Fin bolt Tensile 13,410		
3. Bolt Tensile 19,400	3. Pins for fuel-element support plates[c] (angular acceleration = 6 radians/sec^2) Max. shear 8900 Max. bearing 3850 Max. bending 5030			

[a]In most unfavorable position.

[b]Method of computation given in reference 39.

[c]It is assumed that support plates are at uniform temperature throughout and no thermal stresses are generated.

SECRET

Declassified 1-24-1963

Declassified 1-24-1963

TABLE X. - SHIELD WEIGHTS FOR VARIOUS

COMBINATIONS OF MATERIALS

[100 Mw, 100 ft, 0.025 rem/hr, 0.72 Mach number, 30,000 ft.]

Inner gamma shield material	Outer gamma shield material	Six 15° neutron shield material	Four $22\frac{1}{2}$° neutron shield material	Weight, lb
*U **F77 W	*U **F77 W	LiH Decalin Decalin	LiH ↓ ↓	73,000 89,000 91,000
Fe ↓	W F77 Pb	Decalin ↓ ↓	LiH ↓ ↓	96,000 96,000 97,000
	Fe ↓	LiH Decalin LiH	LiH LiH Decalin	98,000 103,000 (Design) 107,000
	Pb Fe Fe	H_2O Decalin H_2O	H_2O Decalin H_2O	111,000 112,000 121,000

*Depleted.

**Fansteel 77 metal (89 percent W).

Declassified 1-24-1963

Declassified 1-24-1963

E-288

TABLE XI. - EXTERIOR SHIELDING IN EACH SECTOR

[100 Mw, 100 ft, 0.025 rem/hr, 0.72 Mach number, 30,000 ft.]

Sector	Angle, deg	Gamma-shield thickness (Fe), in.	Neutron-shield thickness, in.	
			Decalin	LiH
1	15	4.8	35.8	----
2	↓	5.7	35.8	----
3		7.0	36.7	----
4		10.7	38.4	----
5		7.2	40.3	----
6		6.0	39.7	----
7	22.5	5.0	----	36.8
8	↓	1.3	----	37.8
9		.7	----	38.2
10		0	----	37.1

TABLE XII. - SHIELD WEIGHTS FOR VARIOUS REACTOR POWERS AND SEPARATION DISTANCES

[0.025 rem/hr, 0.72 Mach number, 30,000-ft altitude, Fe-Fe-decalin-LiH.]

Reactor power, Mw	Distance, ft	W_n, lb	$W_{\gamma,i}$, lb	$W_{\gamma,o}$, lb	W_t, lb	W_D, lb
50	50	35,000	28,000	25,000	88,000	21,000
	100	31,000	28,000	18,000	77,000	18,000
	150	29,000	28,000	15,000	72,000	16,000
100	50	45,000	35,000	38,000	118,000	26,000
	100	40,000	35,000	28,000	103,000	23,000 (Design)
	150	37,000	35,000	24,000	96,000	21,000
150	50	50,000	38,000	45,000	133,000	30,000
	100	45,000	38,000	36,000	119,000	26,000
	150	42,000	38,000	30,000	110,000	24,000
200	50	55,000	41,000	52,000	148,000	32,000
	100	49,000	41,000	42,000	132,000	29,000
	150	46,000	41,000	38,000	125,000	27,000

Declassified 1-24-1963

Declassified 1-24-1963

SECRET

TABLE XIII. - FACTORS REQUIRED IN SOLUTION OF FUEL-ELEMENT AND MODERATOR TEMPERATURES

Selected temperature	A, $(ft^3)(sec)(^oR)/Btu$	B, $(ft^3)(sec)(^oR)/Btu$	D, ^oR	E, ^oR	F, ^oR
T_m	$\frac{\pi l}{w_2 c_p}\left[c^2 - R_m^2 + (f^2 - e^2)\frac{\overline{Q}_{mod}}{\overline{Q}_{mt}}\right]$	$\frac{1}{2}\left[\frac{(c^2 - R_m^2)}{2k_{mt}} - \frac{R_m^2}{k_{mt}}\ln\frac{c}{R_m} + \frac{c^2 - R_m^2}{U_2 d}\right]$	$T_m\left(\frac{l}{2}\right) - T_{2,in} - \left(\frac{A}{2} + B\right)\left(\frac{F - T_{in}}{B}\right)$	$T_m(l) - T_{in} - (A + B)\left(\frac{F - T_{in}}{B}\right)$	$T_m(0)$
T_a	$\frac{\pi l}{w_1 c_p}(R_m^2 - b^2)$	$\frac{R_m^2 - b^2}{2h_1 a}$	$T_a\left(\frac{l}{2}\right) - T_{1,in} - \left(\frac{A}{2} + B\right)\left(\frac{F - T_{in}}{B}\right)$	$T_a(l) - T_{in} - (A + B)\left(\frac{F - T_{in}}{B}\right)$	$T_a(0)$
T_d	$\frac{\pi l}{w_2 c_p}\left[c^2 - R_m^2 + (f^2 - e^2)\frac{\overline{Q}_{mod}}{\overline{Q}_{mt}}\right]$	$\frac{c^2 - R_m^2}{2h_2 d}$	$T_d\left(\frac{l}{2}\right) - T_{2,in} - \left(\frac{A}{2} + B\right)\left(\frac{F - T_{in}}{B}\right)$	$T_d(l) - T_{in} - (A + B)\left(\frac{F - T_{in}}{B}\right)$	$T_d(0)$
T_e	$\frac{\pi l}{w_2 c_p}\left[\frac{\overline{Q}_{mt}}{\overline{Q}_{mod}}(c^2 - R_m^2) + (f^2 - e^2)\right]$	$\frac{f^2 - e^2}{2h_2 e}$	$T_e\left(\frac{l}{2}\right) - T_{2,in} - \left(\frac{A}{2} + B\right)\left(\frac{F - T_{in}}{B}\right)$	$T_e(l) - T_{in} - (A + B)\left(\frac{F - T_{in}}{B}\right)$	$T_e(0)$
T_f		$\frac{1}{2}\left[\frac{f^2}{k_{mod}}\ln\frac{f}{e} + \frac{e^2 - f^2}{2k_{mod}} + \frac{f^2 - e^2}{h_2 e}\right]$	$T_f\left(\frac{l}{2}\right) - T_{2,in} - \left(\frac{A}{2} + B\right)\left(\frac{F - T_{in}}{B}\right)$	$T_f(l) - T_{in} - (A + B)\left(\frac{F - T_{in}}{B}\right)$	$T_f(0)$

SECRET

Declassified 1-24-1963

Declassified 1-24-1963

E-288

TABLE XIV. - SOURCES OF PROPERTIES USED IN STRESS CALCULATIONS

Material	E	α	ν	k
Mo	Ref. 16 (pp. 195-198) Ref. 11 (fig., p. 17)	Ref. 16 (p. 193)	Ref. 11	Ref. 16 (p. 193) Ref. 40
BeO	Ref. 15 (table A-3) Ref. 41 (table IX)	Ref. 15 (table A-3) Ref. 41 (p. 50)	Ref. 15 (table A-3)	Ref. 41 (p. 51)

TABLE XV. - MATERIAL PROPERTIES

USED IN SHIELD ANALYSIS

Material	Density, ρ, g/cc	Σ, cm^{-1}	μ, cm^{-1}
Core BeO	2.20	0.1111	0.0714
Reflector BeO	2.20	.1111	.0714
Thermal- and gamma-shield Fe	7.8	.1667	.2703
Pressure-shell Fe	7.8	.1667	.2703
Neutron-shield LiH	.79	.1160	.0280
Neutron-shield decalin	.895	.1019	.0349

Declassified 1-24-1963

Declassified 1-24-1963

SECRET

TABLE XVI. - CONSTANTS USED IN SHIELD ANALYSIS

[Reactor power, 100 Mw; reactor-core height, H, 60.96 cm; reactor-core radius, R, 44.02 cm; reflector thickness, t_R, 10.16 cm; distance from reactor center to crew compartment, d, 3048 cm.]

Sector	Range of sector, deg	a_k, cm	b_k, cm	$t_{k,ths}^{Fe}$, cm	$v_k = \frac{b_k - a_k - t_{k,ths}}{b_k - a_k}$
1	0-15	40.44	108.80	55.36	0.190
2	15-30	43.30	109.80	50.54	.240
3	30-45	50.34	106.70	42.00	.255
4	45-60	68.10	99.16	23.78	.234
5	60-75	61.60	88.62	21.74	.195
6	75-90	57.38	82.56	20.30	.194
7	90-112$\frac{1}{2}$	57.80	83.24	20.54	.193
8	112$\frac{1}{2}$-135	68.00	100.50	27.40	.157
9	135-157$\frac{1}{2}$	47.80	110.00	27.64	.556
10	157$\frac{1}{2}$-180	40.92	109.00	42.78	.372

SECRET
Declassified 1-24-1963

Declassified 1-24-1963

SECRET

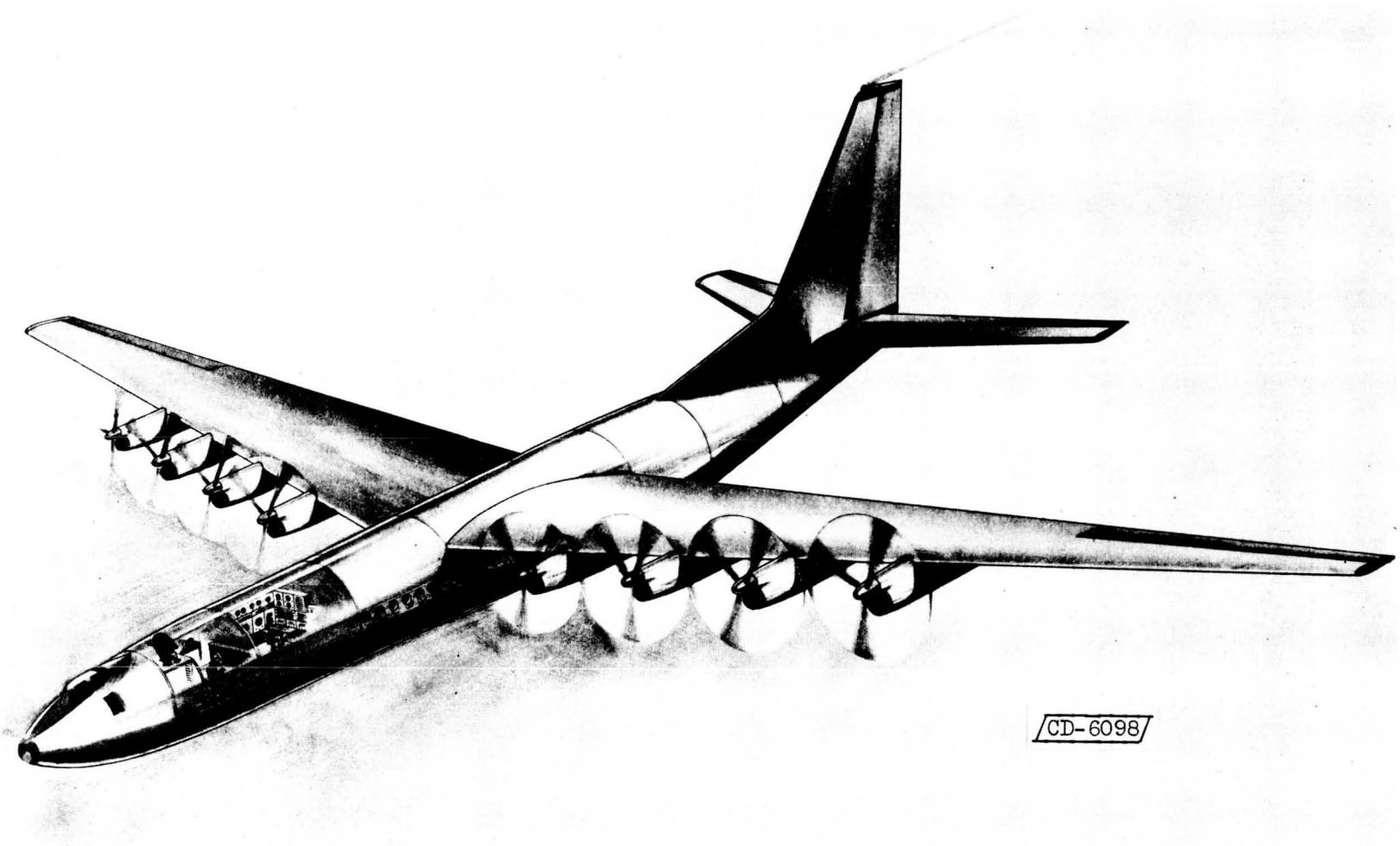

Figure 1. - Artist's sketch of reference airplane.

SECRET

Declassified 1-24-1963

CONFIDENTIAL

Declassified 1-24-1963

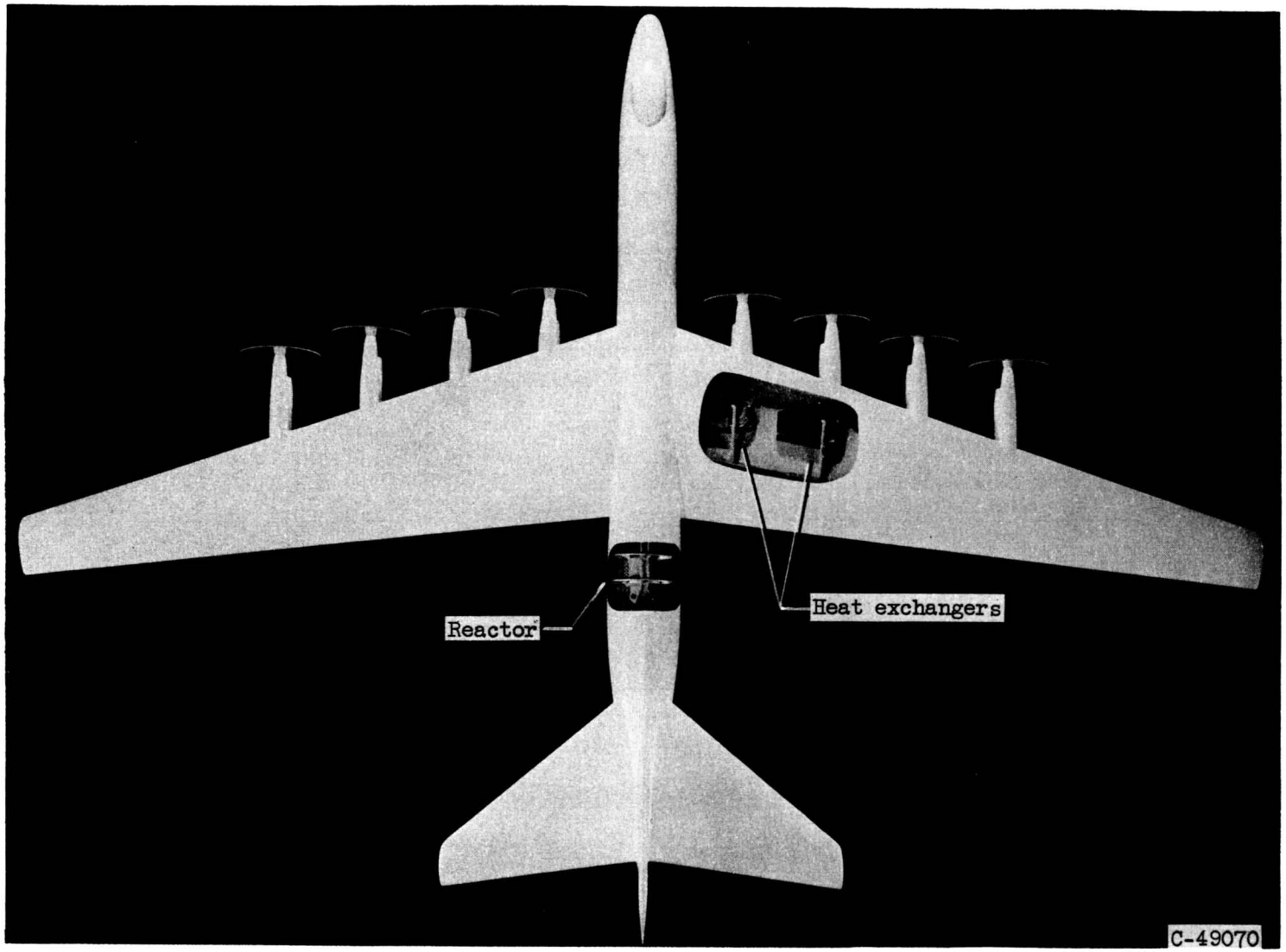

Figure 2. - Picture of airplane model showing location and arrangement of equipment.

CONFIDENTIAL

Declassified 1-24-1963

Declassified 1-24-1963

SECRET

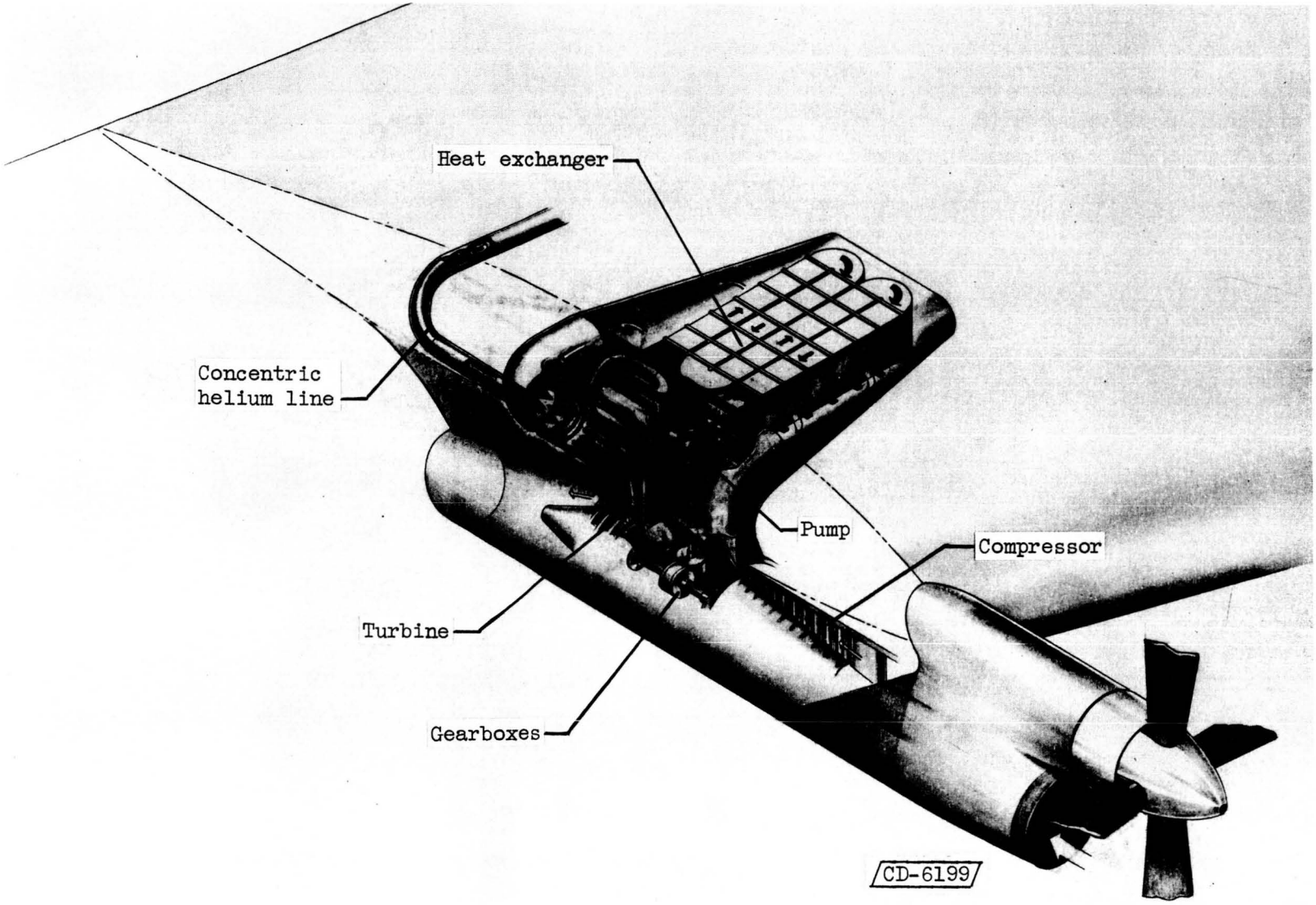

Figure 3. - Layout of engine, heat exchanger, pump, and headers.

Declassified 1-24-1963

Declassified 1-24-1963

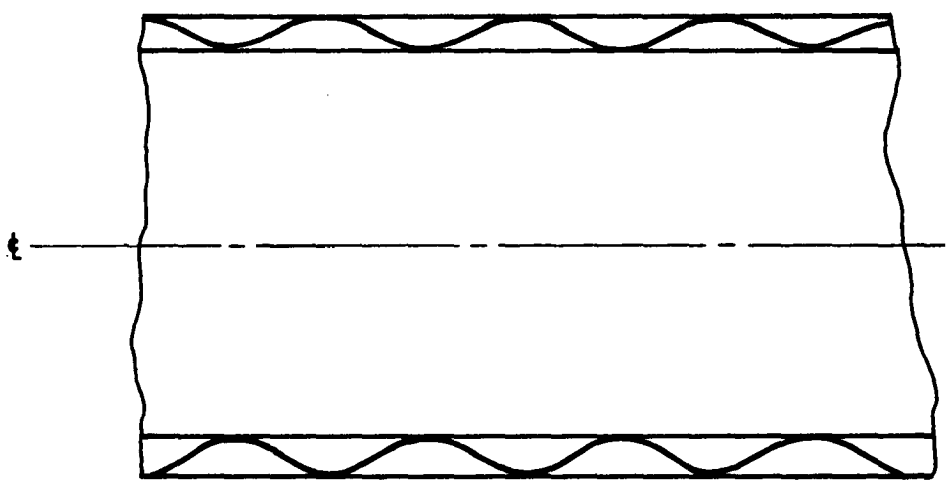

Figure 4. - Schematic cross section of inner pipe of the concentric helium lines.

Declassified 1-24-1963

Declassified 1-24-1963

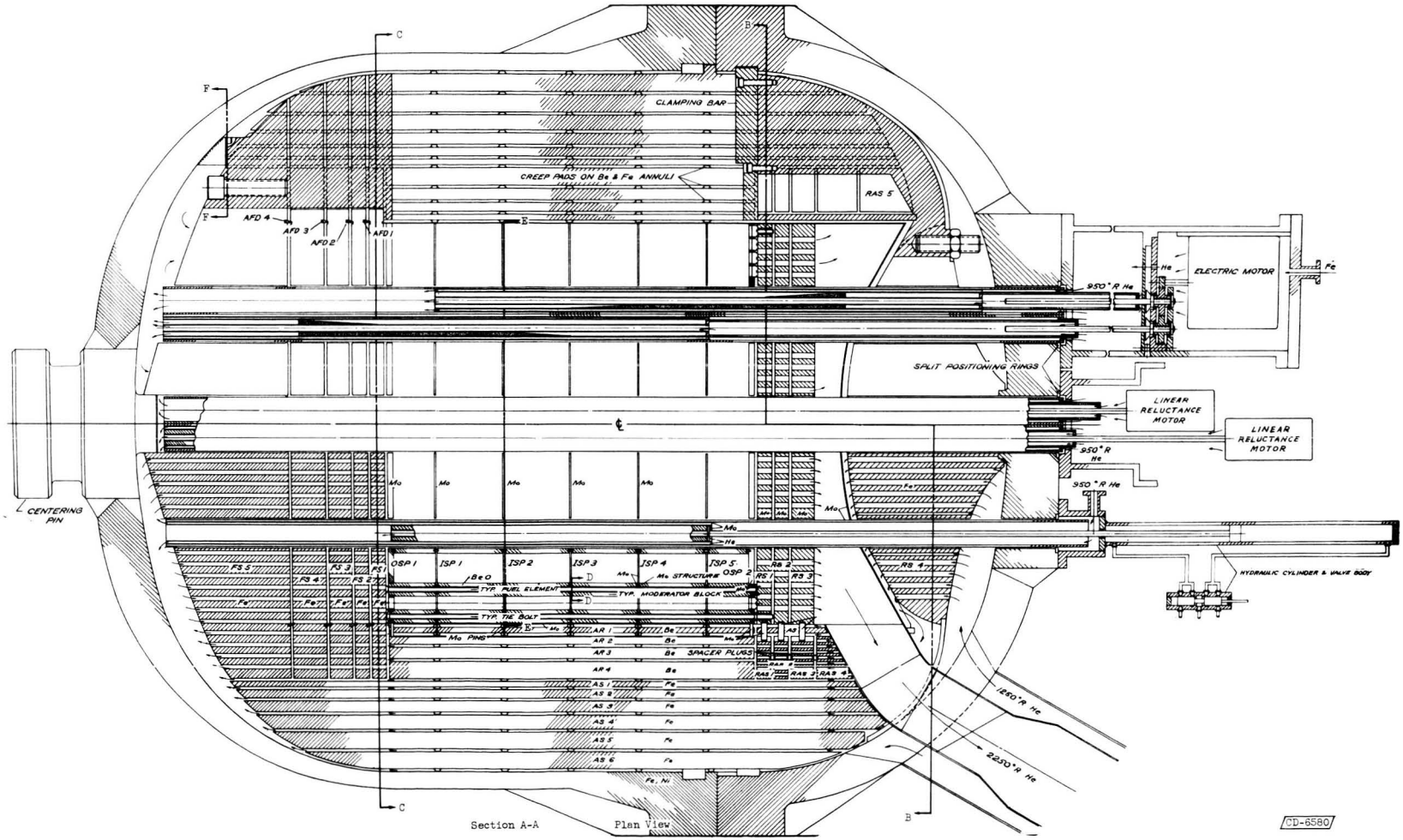

Figure 5. - Plan view of reactor showing control and mechanism (section A-A of fig. 52). (A large copy of this figure may be obtained by using the request card bound in the back of the report.)

Declassified 1-24-1963

Declassified 1-24-1963

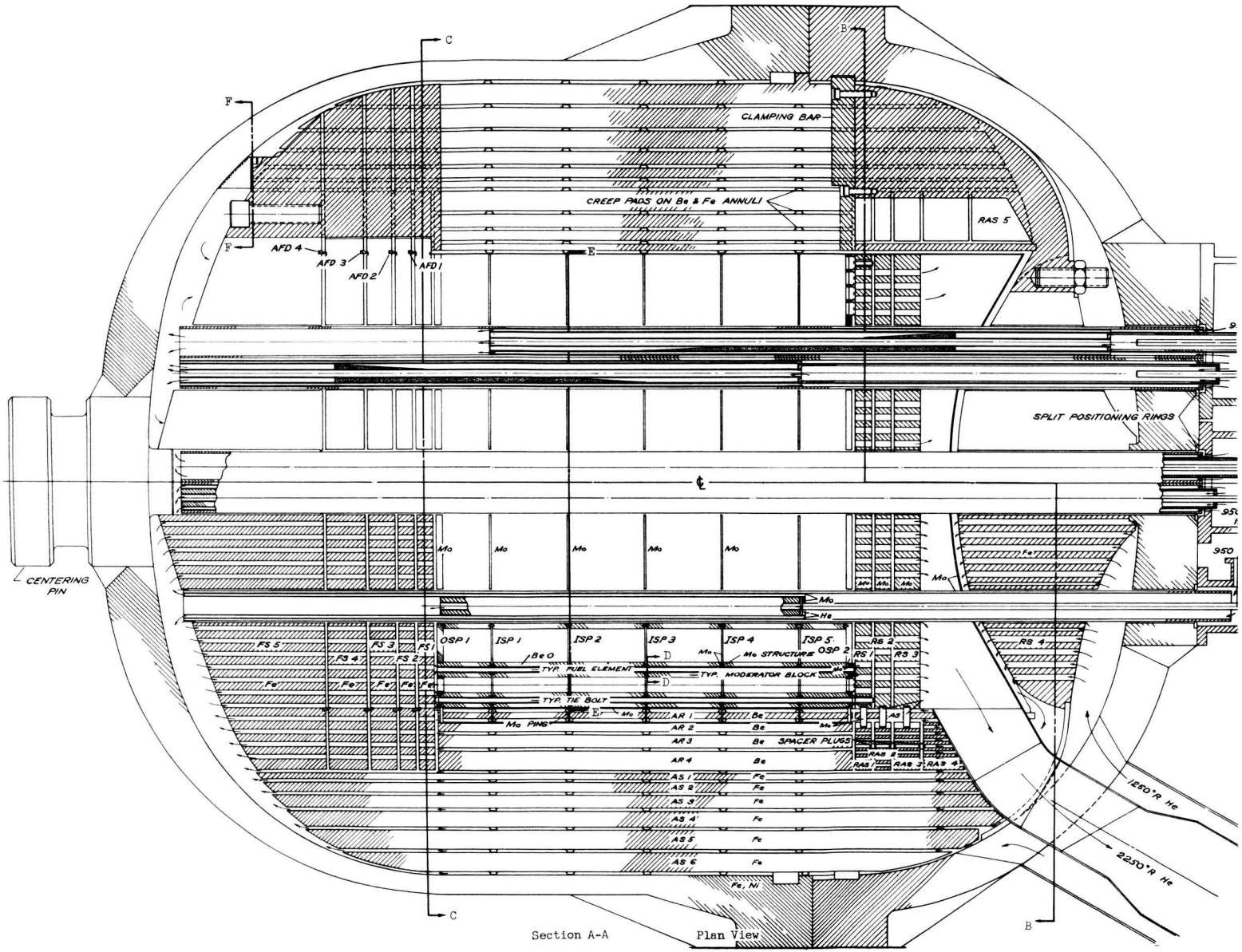

Figure 6. - Enlarged plan view of reactor (section A-A of fig. 52).

Declassified 1-24-1963

Declassified 1-24-1963

E-288

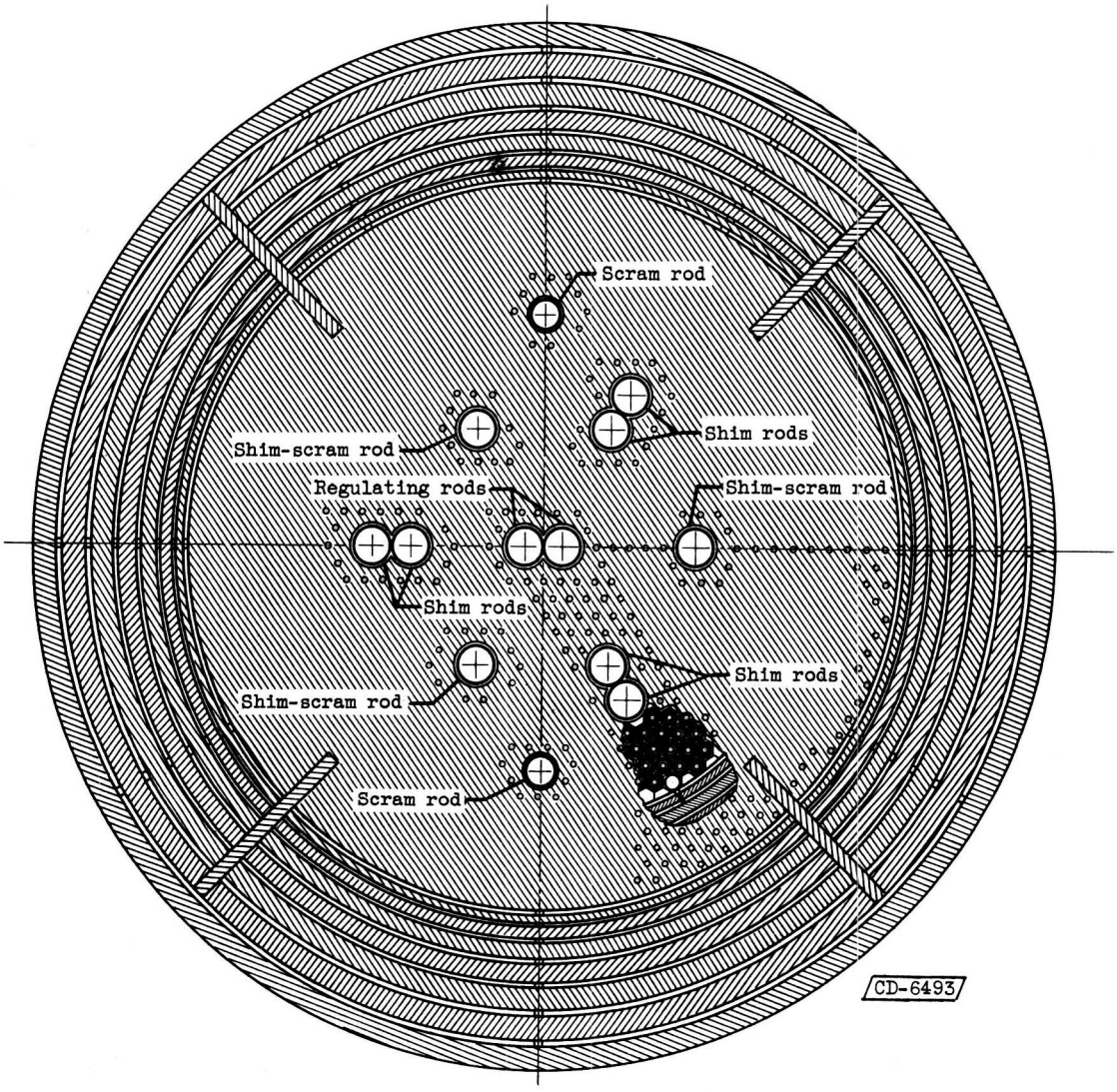

Figure 7. - Section C-C of figure 5.

Declassified 1-24-1963

Declassified 1-24-1963

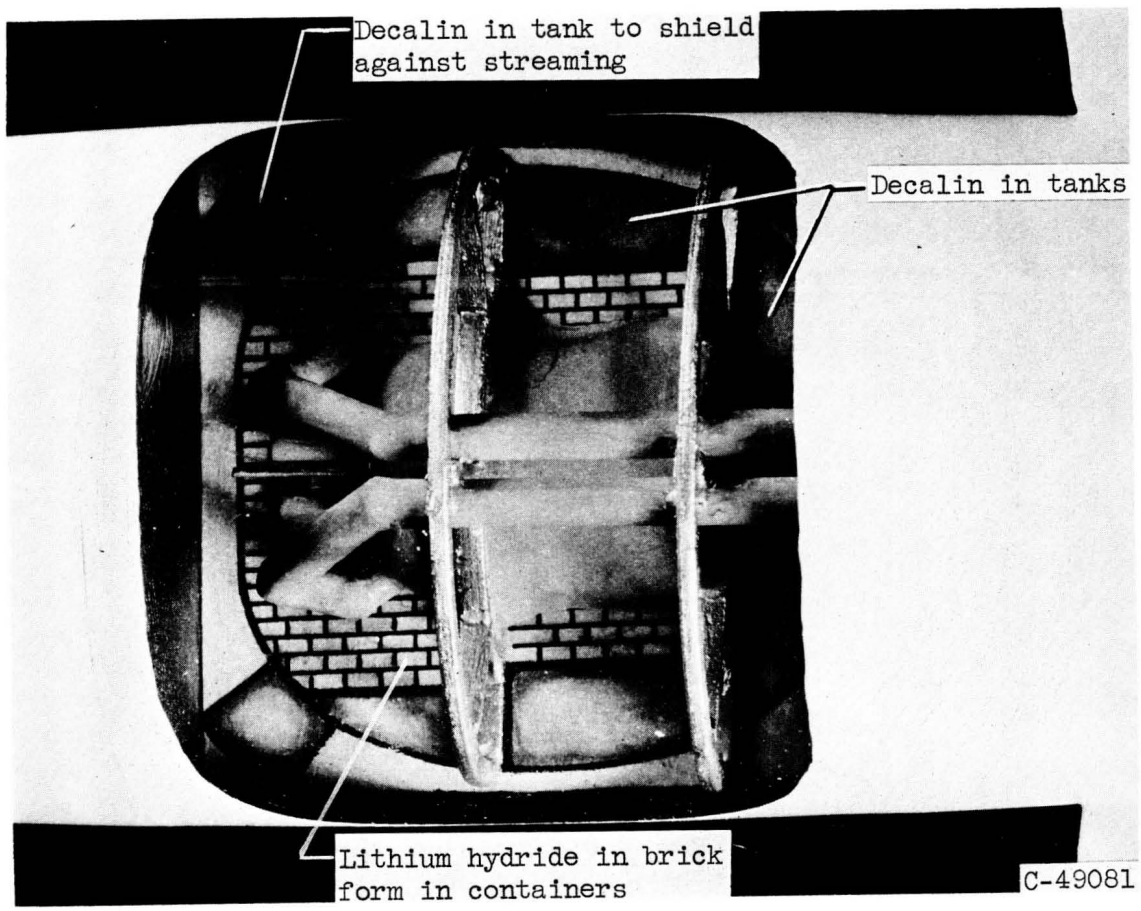

Figure 8. - Closeup plan view of reactor pressure shell in airplane model with shield indicated.

Declassified 1-24-1963

Declassified 1-24-1963

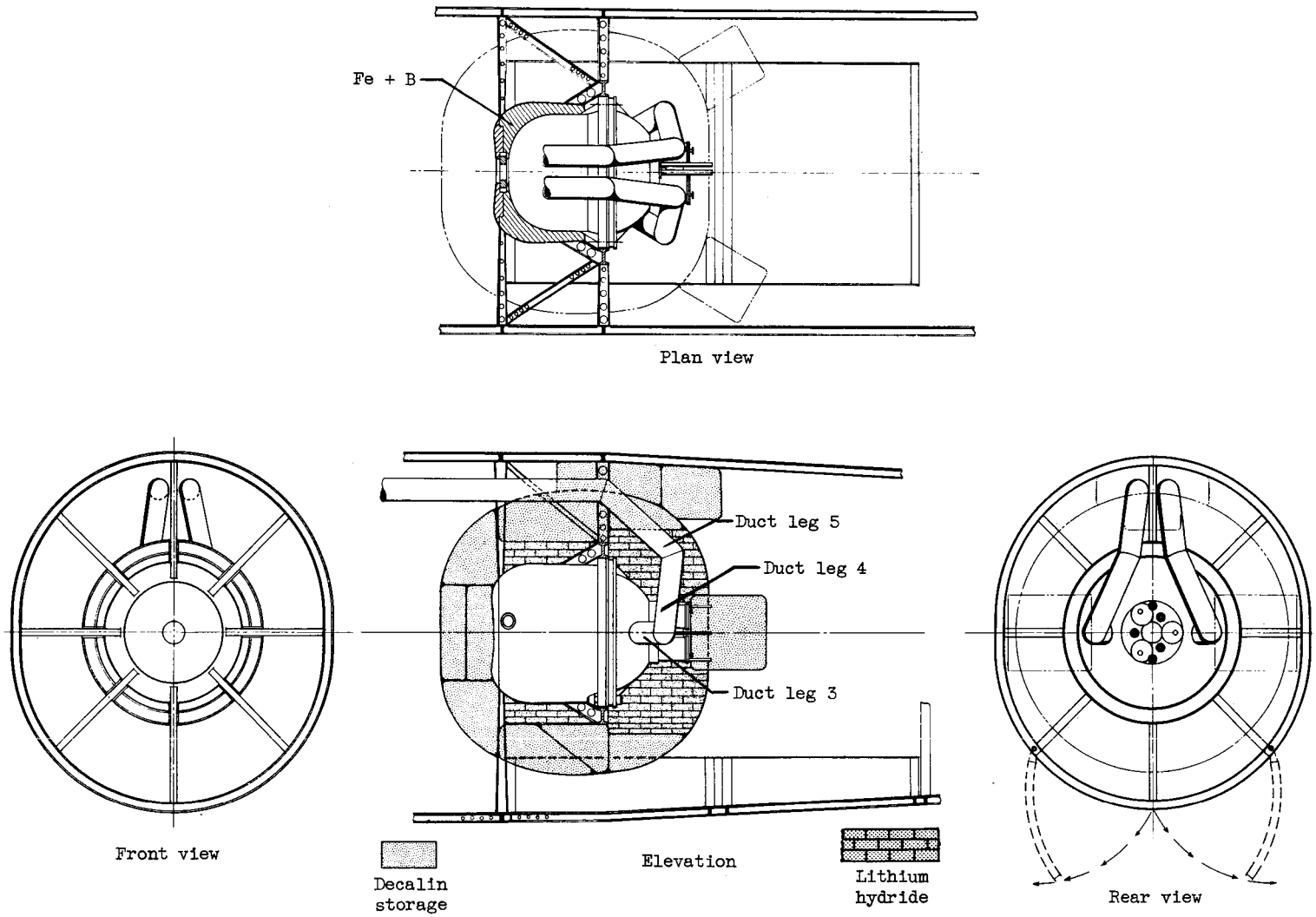

Figure 9. - Details of mounting reactor and shield in airplane fuselage.

Declassified 1-24-1963

Declassified 1-24-1963

SECRET

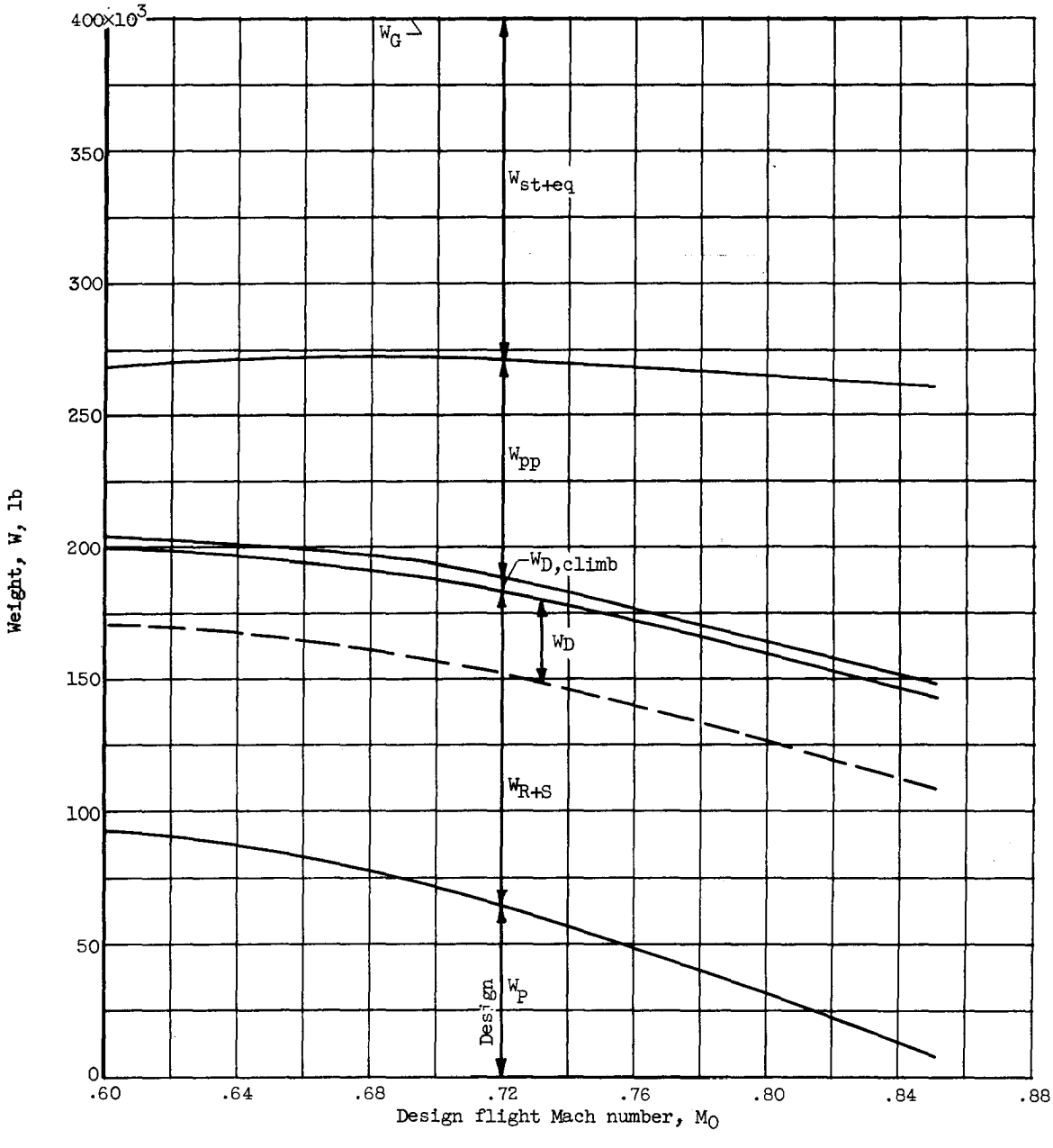

Figure 10. - Effect of design flight Mach number on airplane component weights. Altitude, 30,000 feet.

SECRET

Declassified 1-24-1963

Declassified 1-24-1963

E-288

CA-24 back

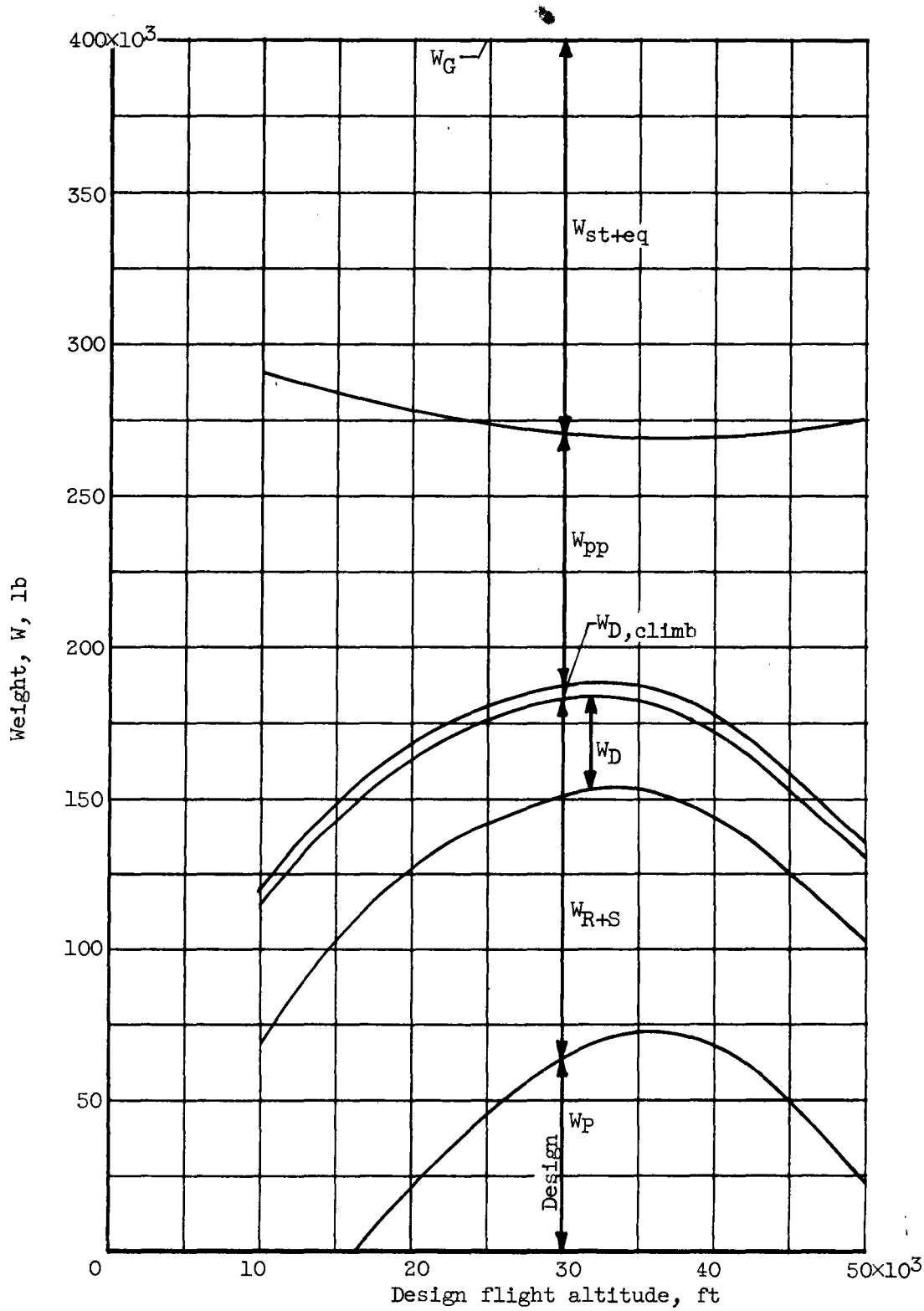

Figure 11. - Effect of design flight altitude on airplane component weights. Flight Mach number, 0.72.

Declassified 1-24-1963

Declassified 1-24-1963

SECRET

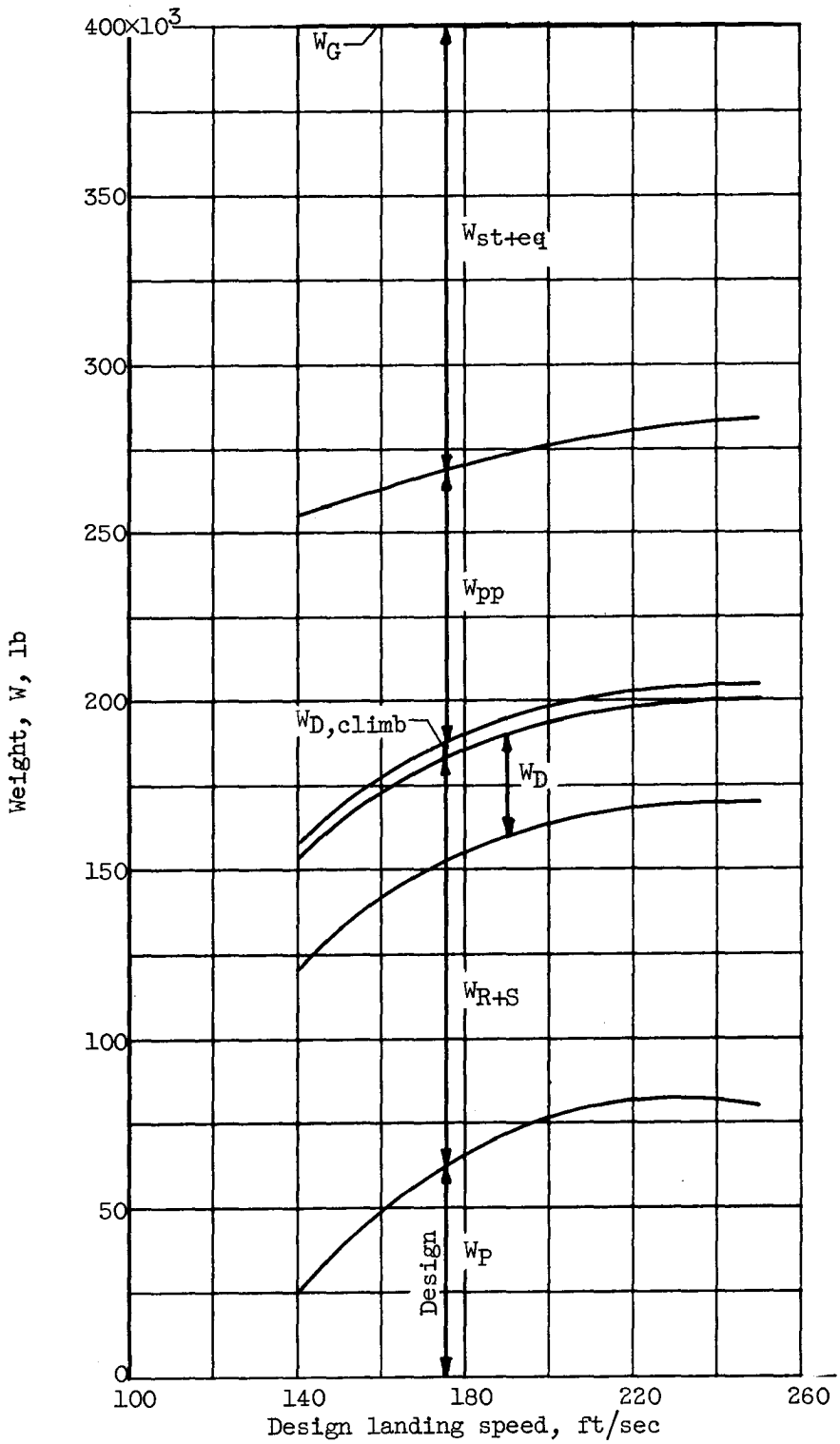

Figure 12. - Effect of design landing speed on airplane component weights. Flight Mach number, 0.72; altitude, 30,000 feet.

SECRET

Declassified 1-24-1963

E-288

Declassified 1-24-1963

E-288

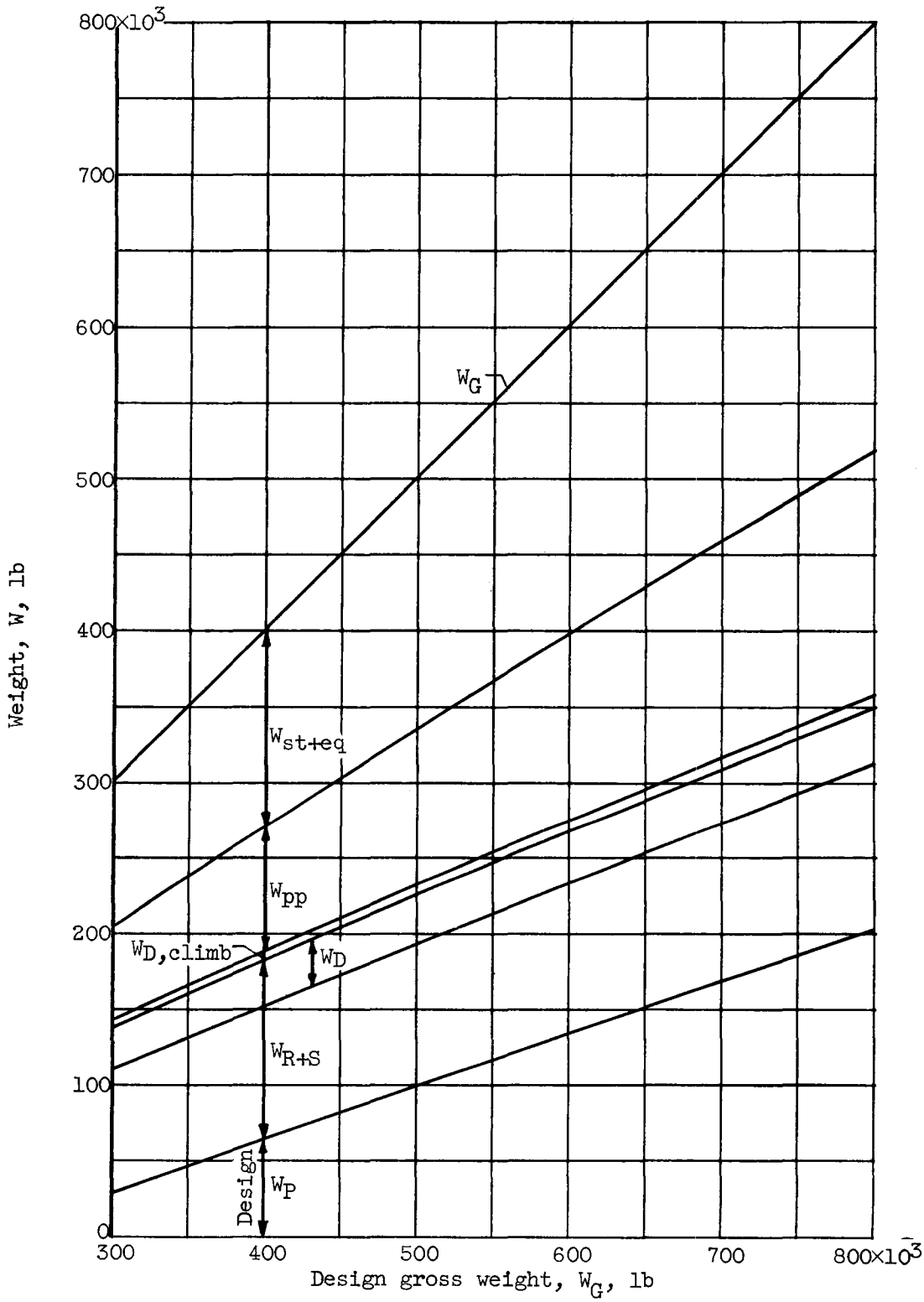

Figure 13. - Effect of design gross weight on airplane component weights. Flight Mach number, 0.72; altitude, 30,000 feet.

Declassified 1-24-1963

Declassified 1-24-1963

SECRET

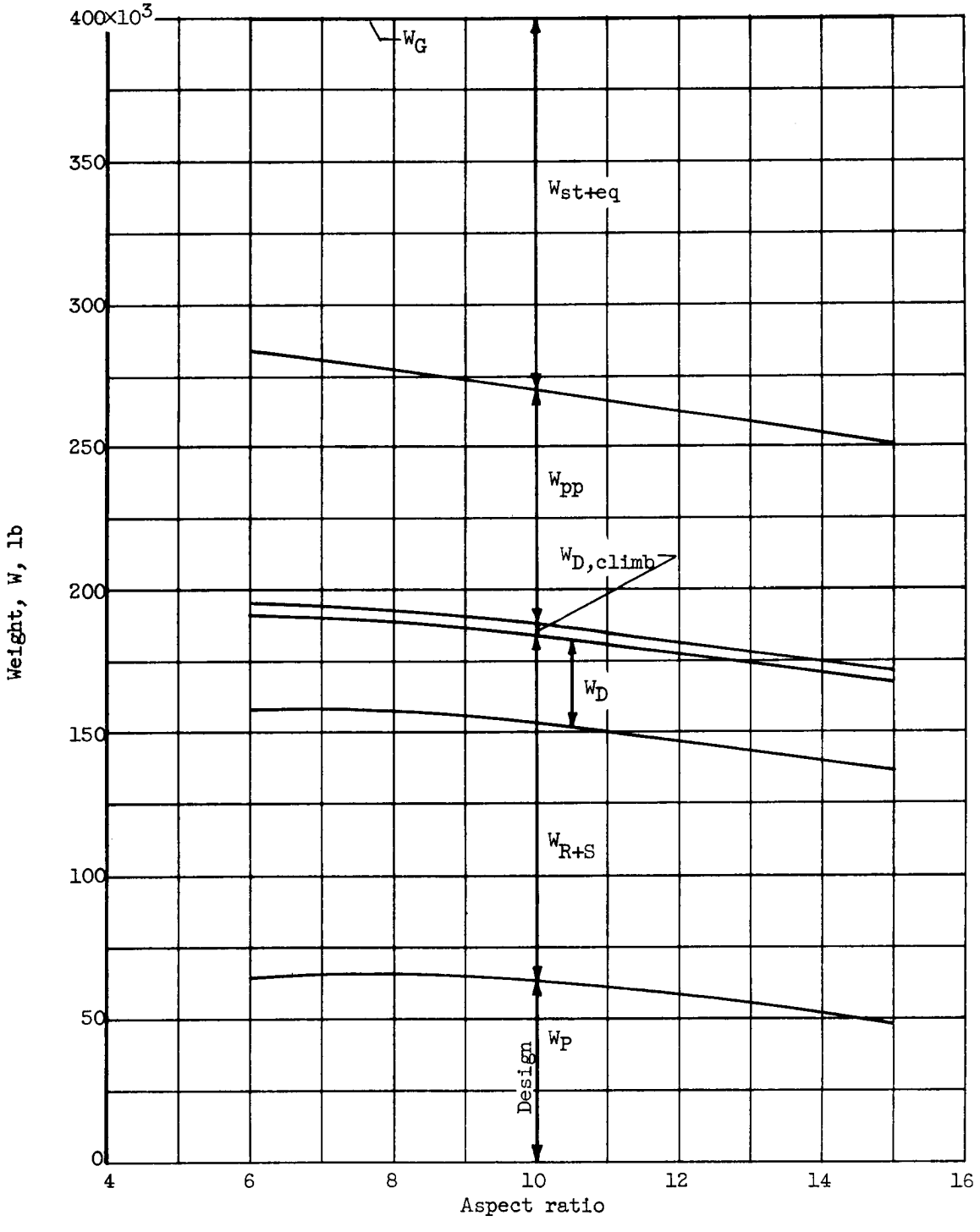

Figure 14. - Effect of aspect ratio on airplane component weights. Flight Mach number, 0.72; altitude, 30,000 feet.

E-288

SECRET

Declassified 1-24-1963

Declassified 1-24-1963

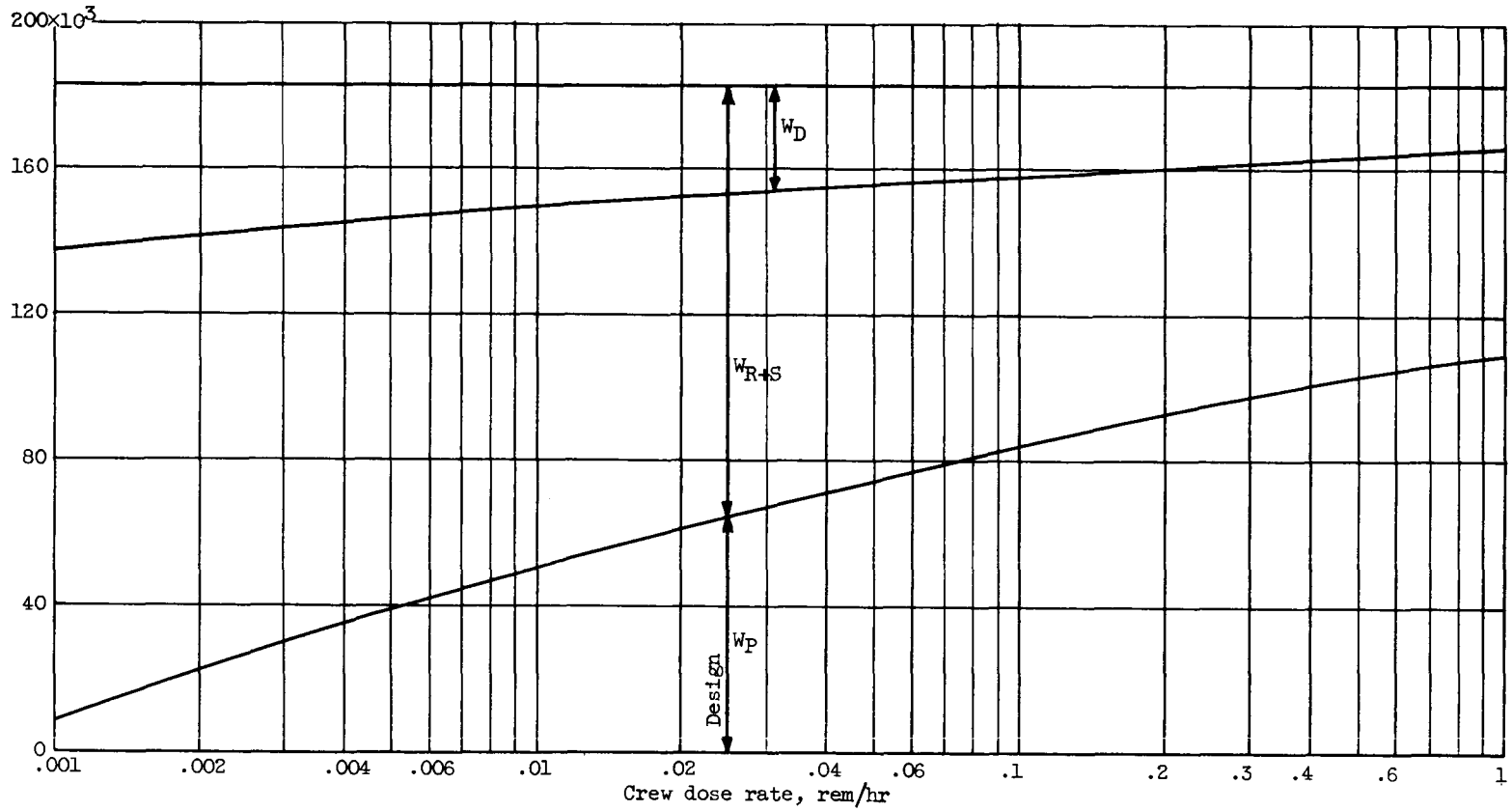

Figure 15. - Effect of crew dose rate on shield and payload weights. Flight Mach number, 0.72; altitude, 30,000 feet.

Declassified 1-24-1963

Declassified 1-24-1963

SECRET

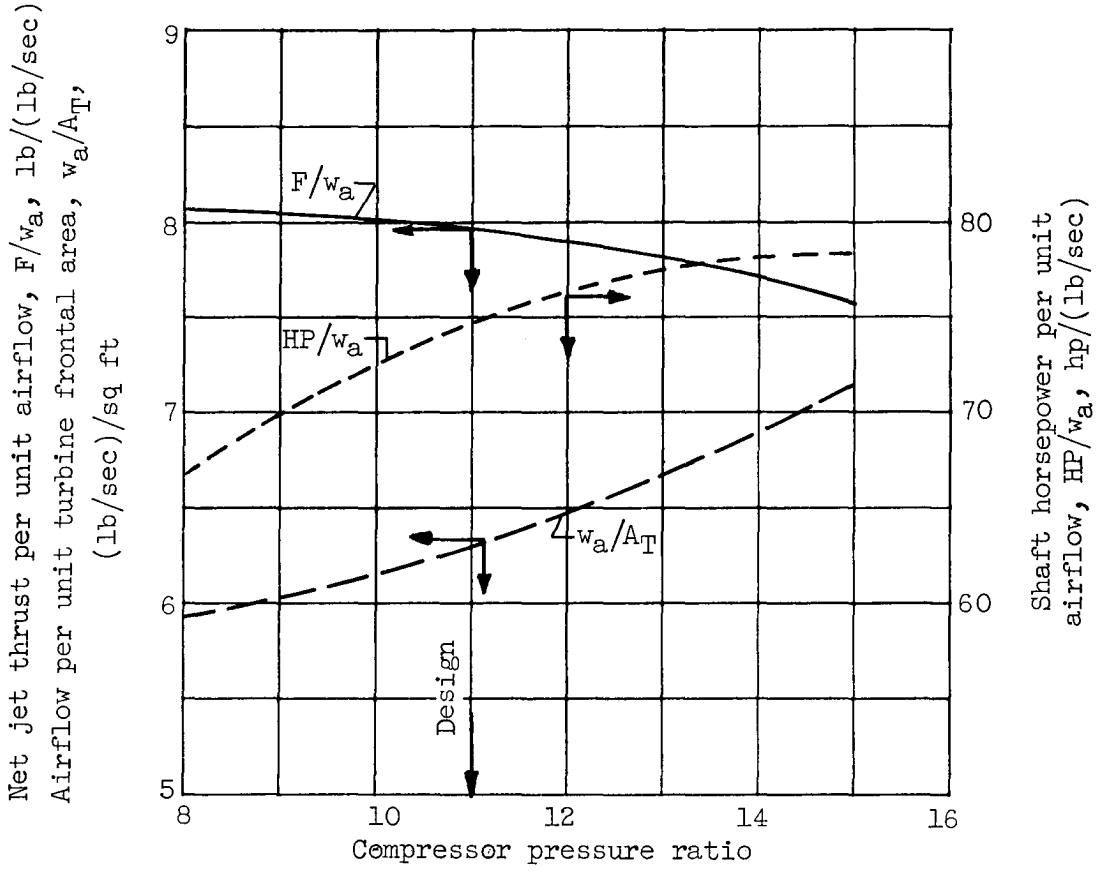

Figure 16. - Variation in F/w_a, w_a/A_T, and HP/w_a with compressor pressure ratio. Flight Mach number, 0.72; altitude, 30,000 feet; turbine-inlet temperature, 1800° R.

SECRET
Declassified 1-24-1963

Declassified 1-24-1963

E-288

CA-25

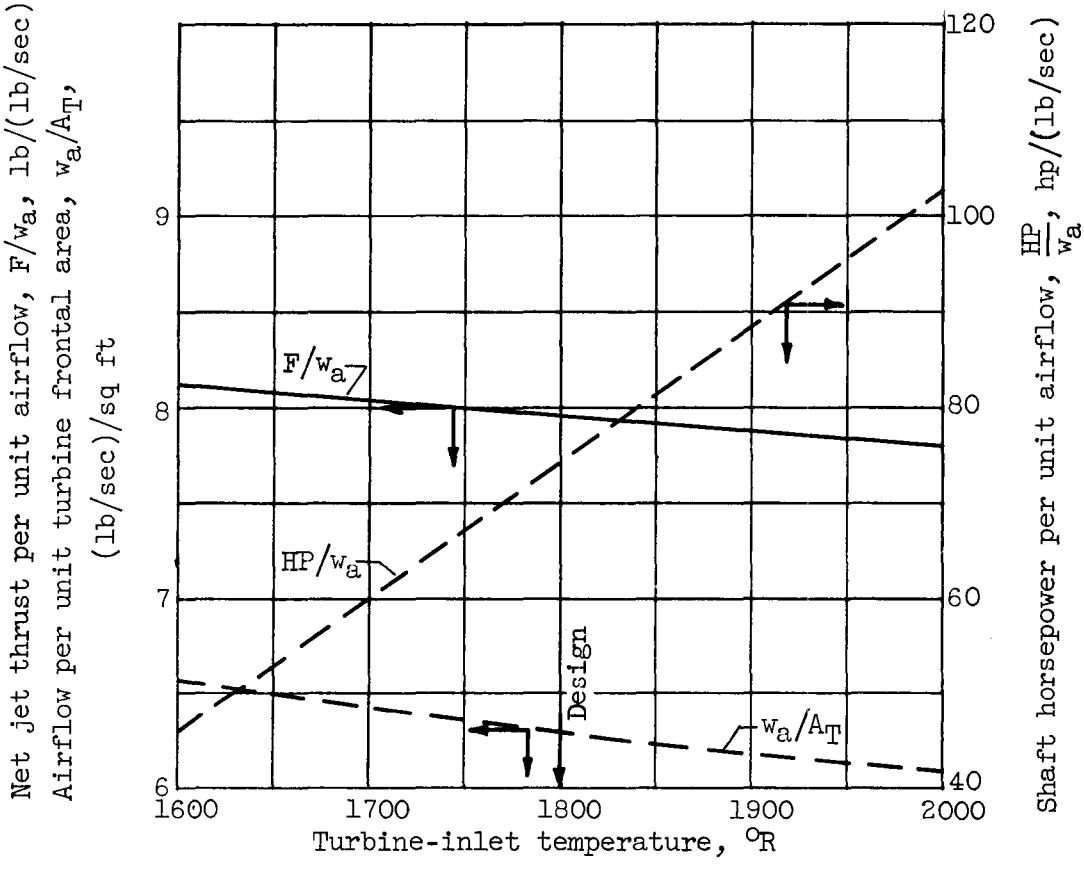

Figure 17. - Variation in F/w_a, w_a/A_T, and HP/w_a with turbine-inlet temperature. Flight Mach number, 0.72; altitude, 30,000 feet; compressor pressure ratio, 11.

Declassified 1-24-1963

Declassified 1-24-1963

SECRET

E-288

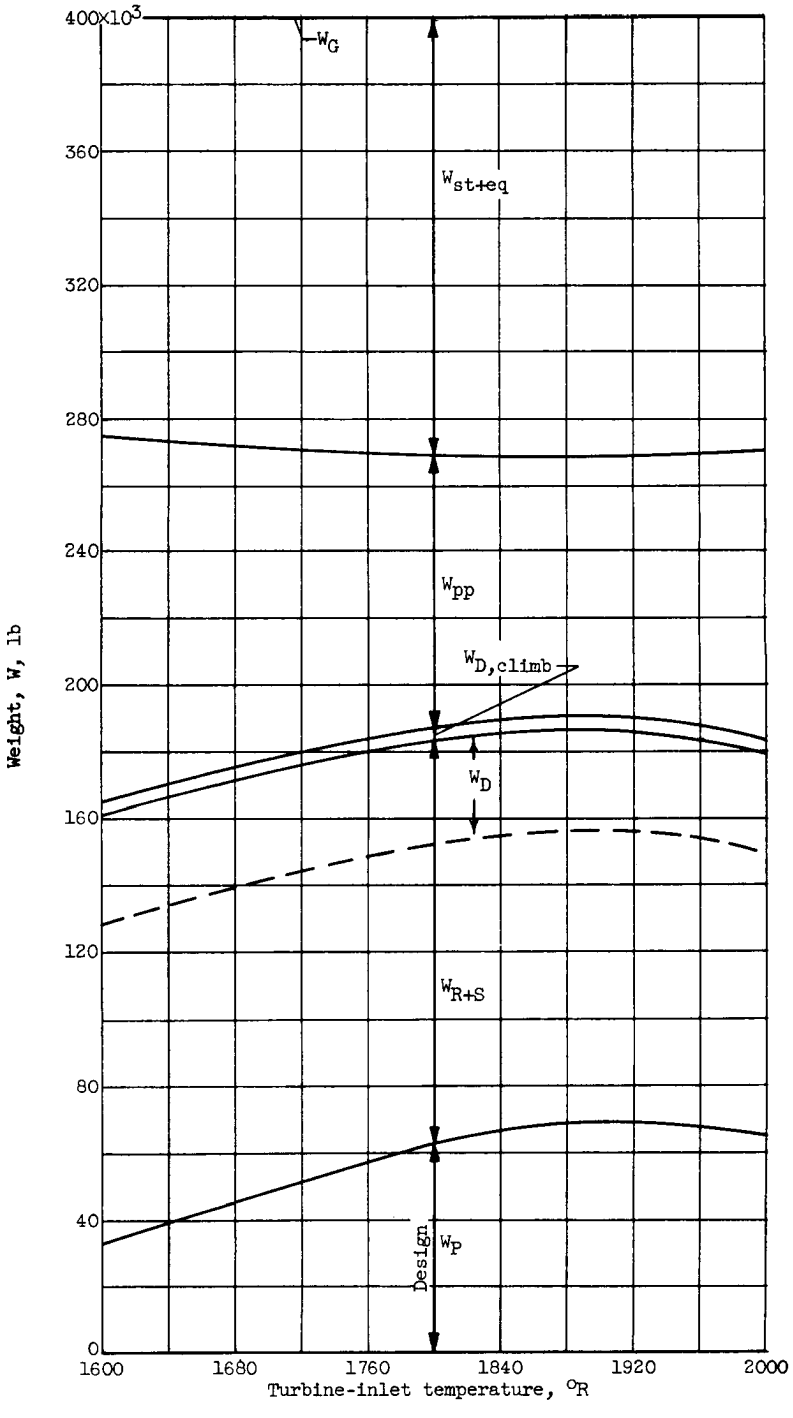

(a) Breakdown of airplane component weights.

Figure 18. Effect of turbine-inlet temperature on component weights. Flight Mach number, 0.72; altitude, 30,000 feet; compressor pressure ratio, 11.

SECRET

Declassified 1-24-1963

Declassified 1-24-1963

E-288

CA-25 back

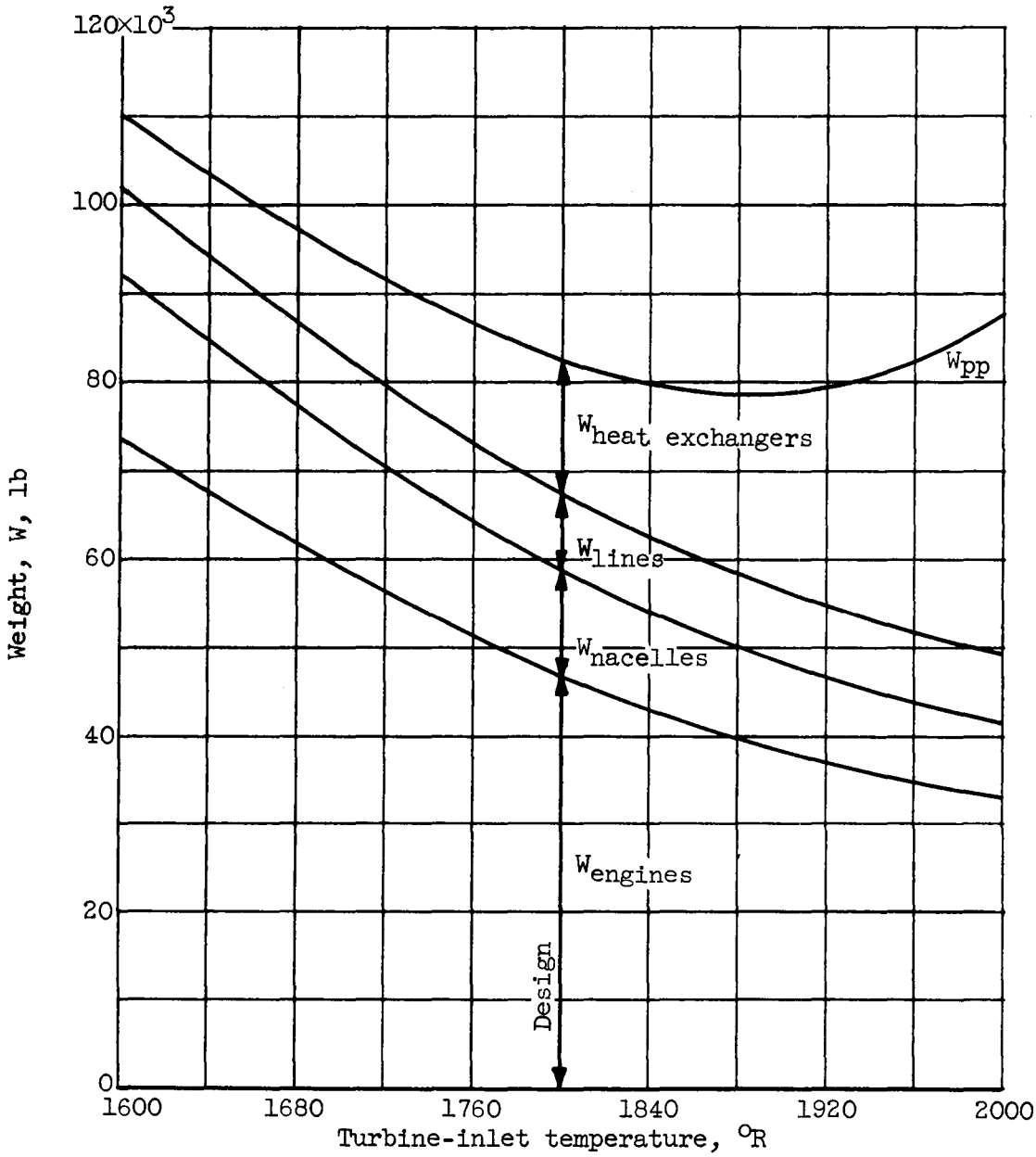

(b) Breakdown of powerplant component weights.

Figure 18. - Concluded. Effect of turbine-inlet temperature on component weights. Flight Mach number, 0.72; altitude, 30,000 feet; compressor pressure ratio, 11.

Declassified 1-24-1963

Declassified 1-24-1963

SECRET

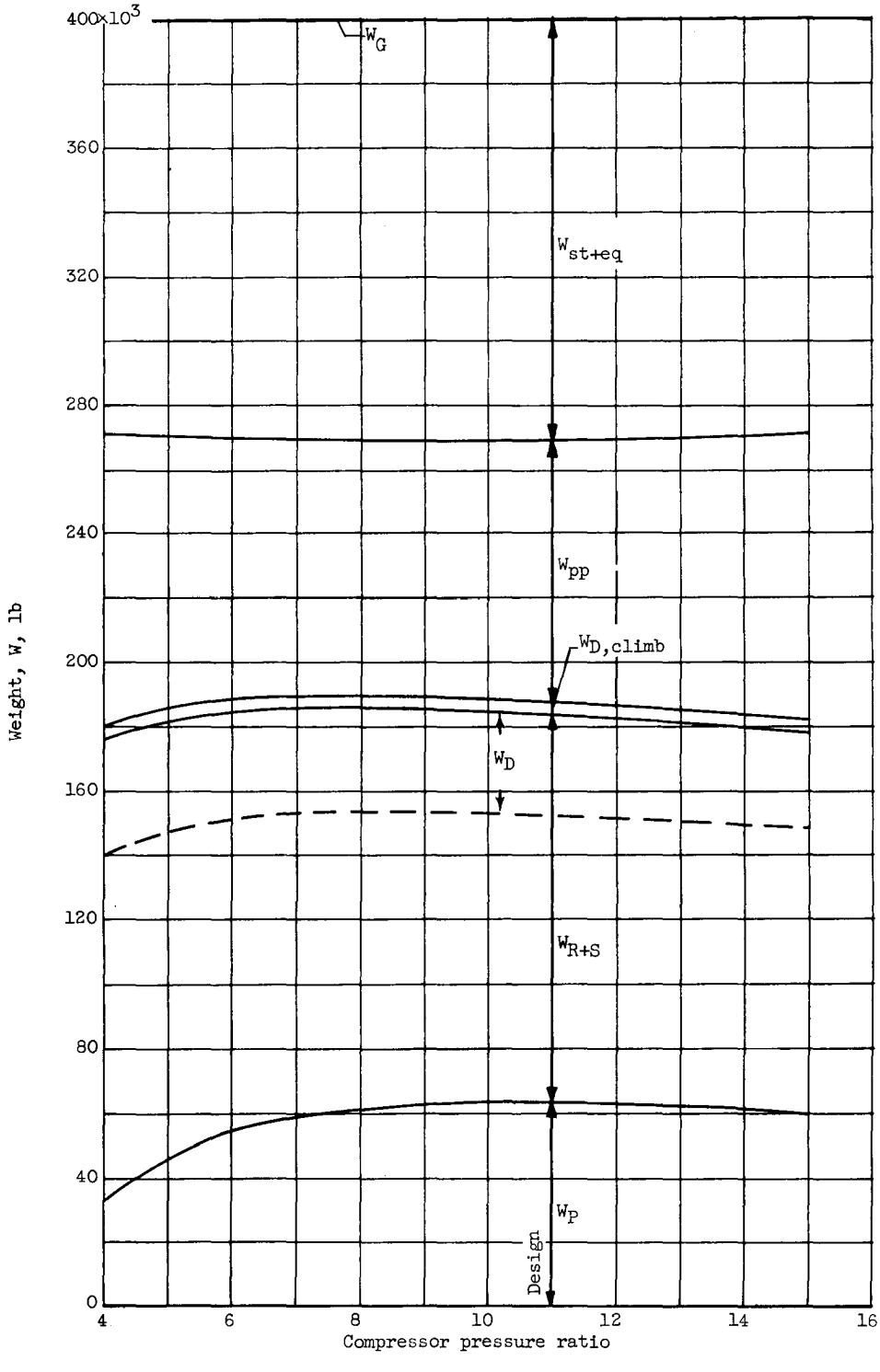

(a) Breakdown of airplane component weights.

Figure 19. - Effect of compressor pressure ratio on component weights. Flight Mach number, 0.72; altitude, 30,000 feet; turbine-inlet temperature, 1800° R.

E-288

SECRET

Declassified 1-24-1963

Declassified 1-24-1963

E-288

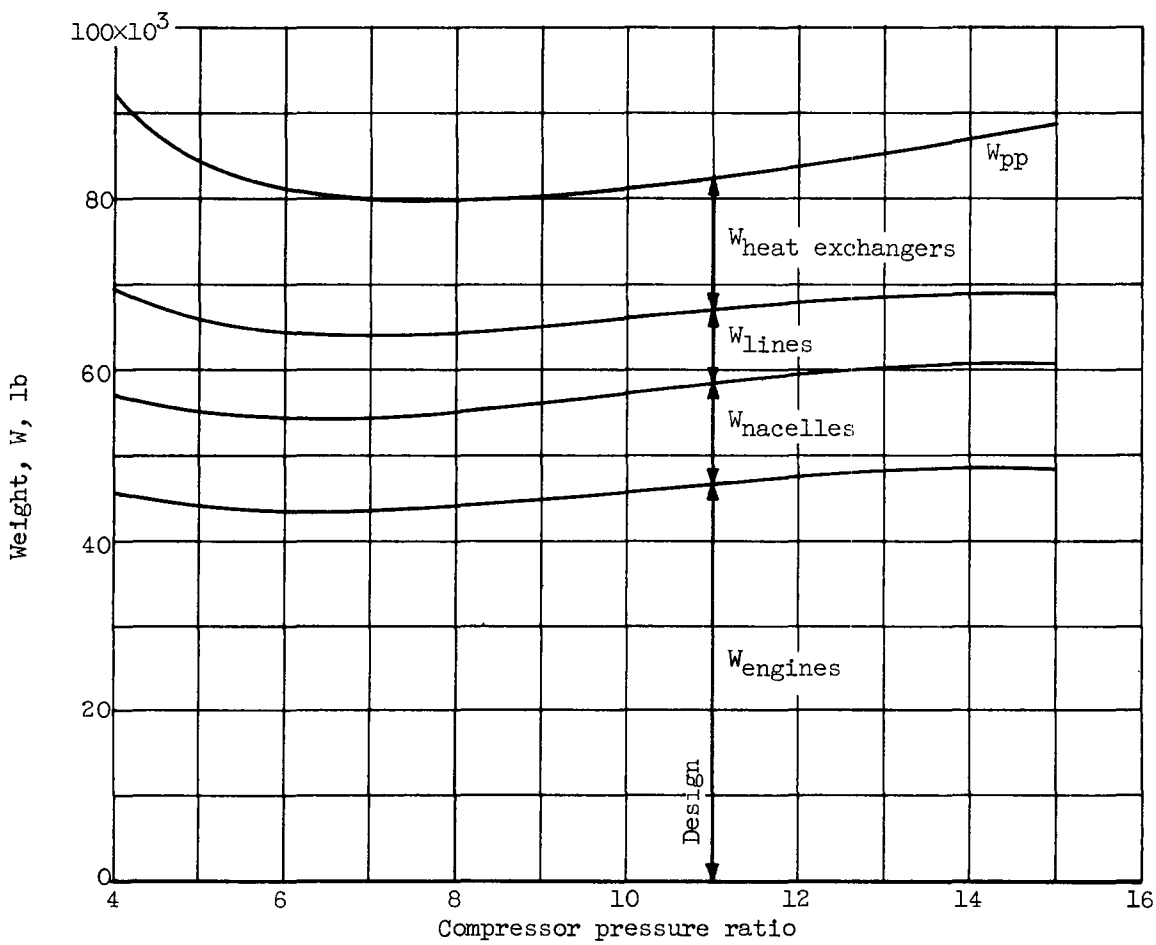

(b) Breakdown of powerplant component weights.

Figure 19. - Concluded. Effect of compressor pressure ratio on component weights. Flight Mach number, 0.72; altitude, 30,000 feet; turbine-inlet temperature, 1800° R.

Declassified 1-24-1963

Declassified 1-24-1963

SECRET

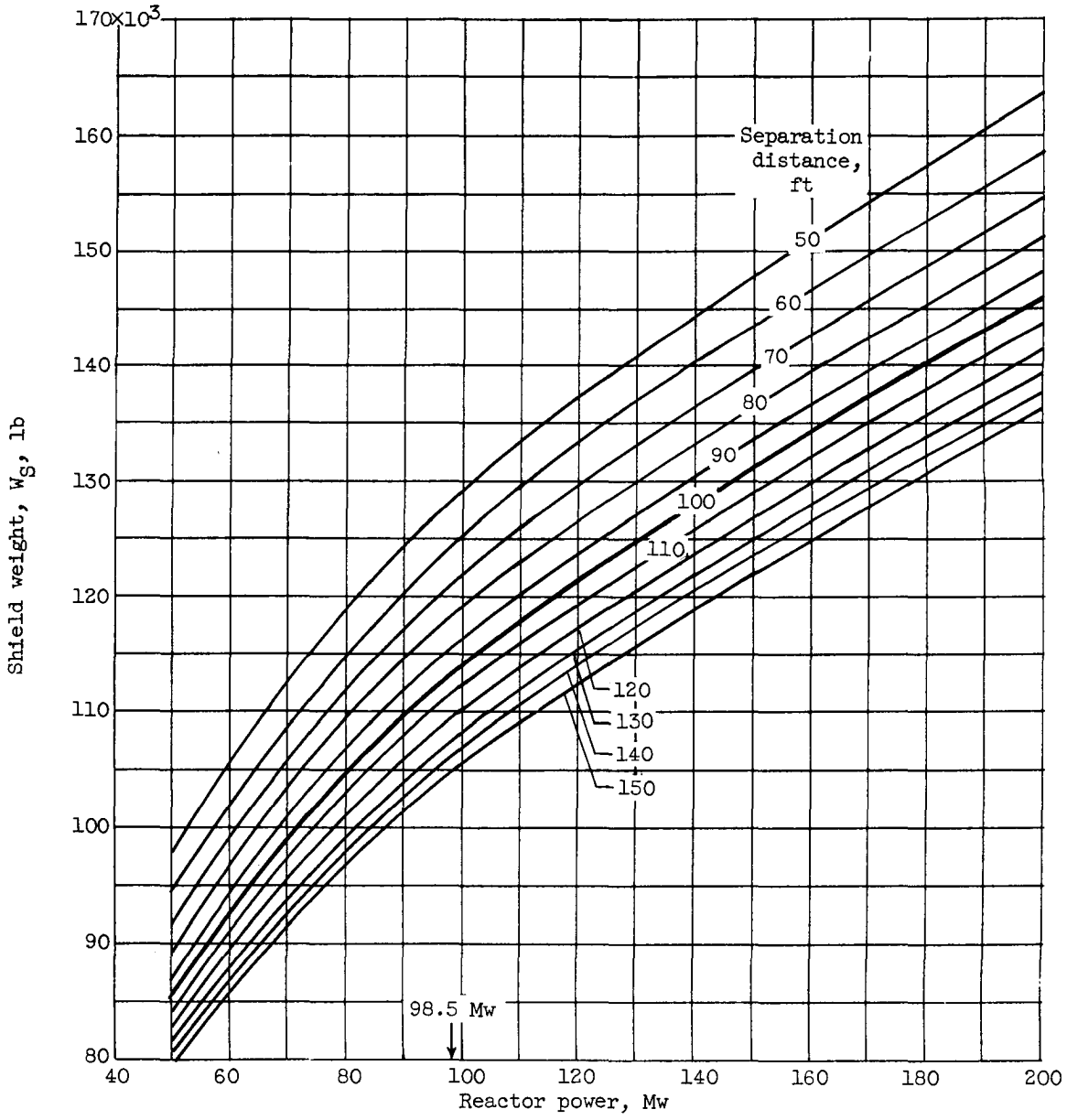

Figure 20. - Variation of weight (shield + ducts + cooling) with reactor power. Flight Mach number, 0.72; altitude, 30,000 feet; dose rate, 0.025 rem per hour.

E-288

SECRET

Declassified 1-24-1963

Declassified 1-24-1963

E-288

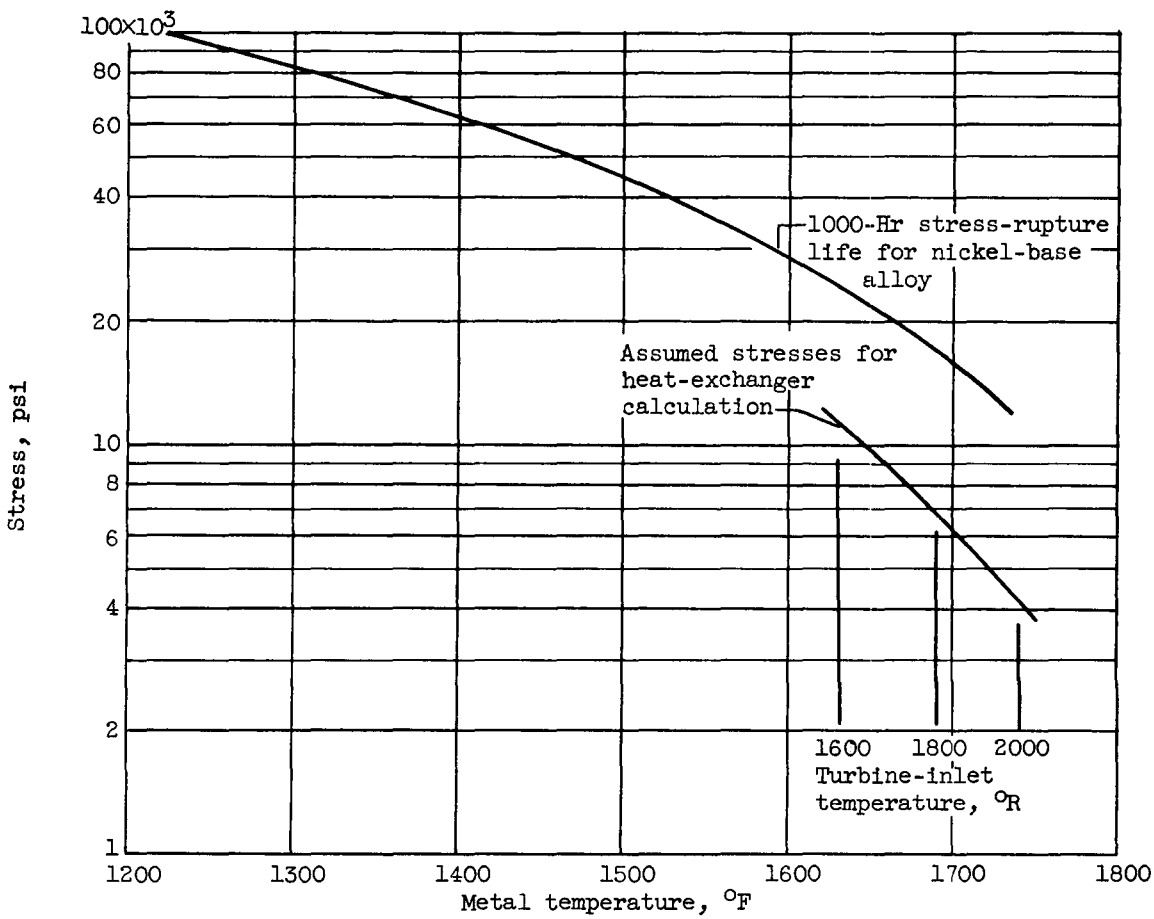

Figure 21. - Stress data employed in heat-exchanger studies.

Declassified 1-24-1963

Declassified 1-24-1963

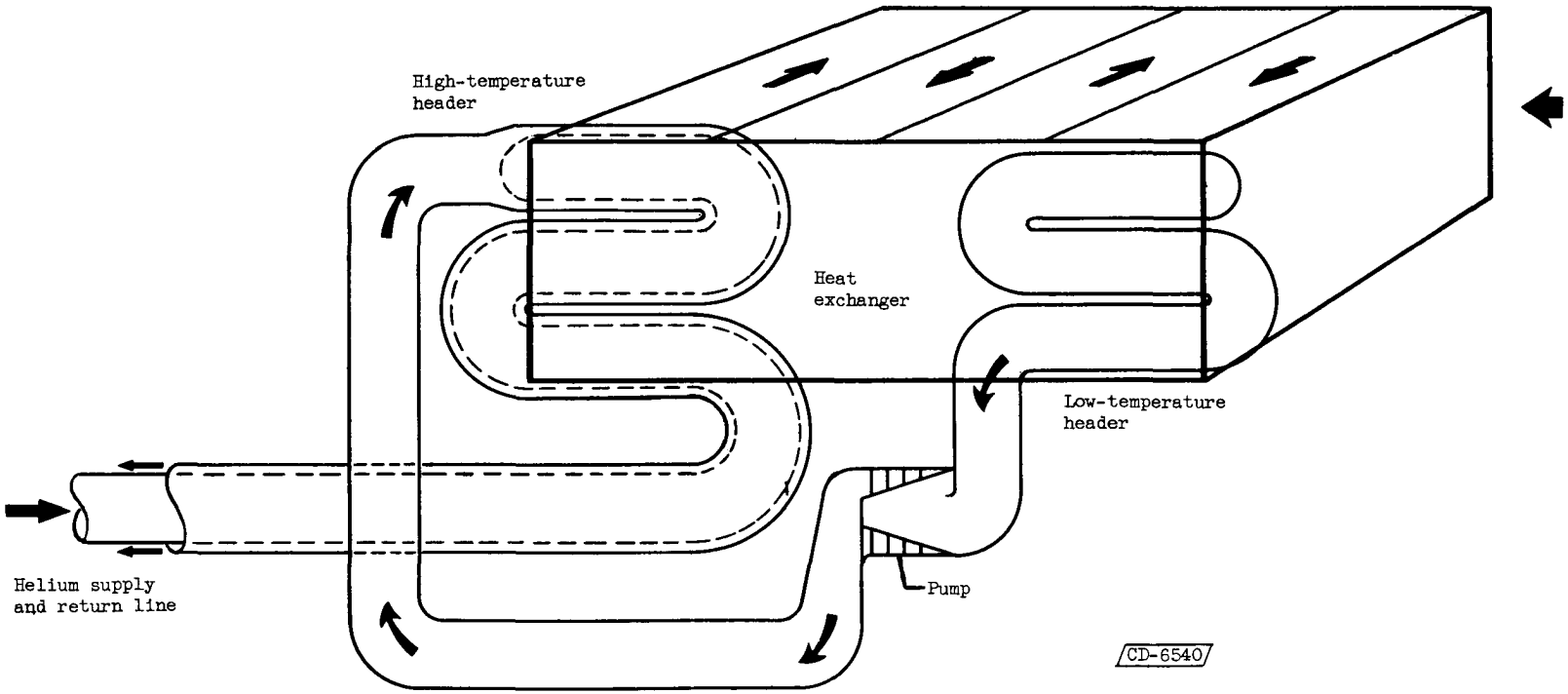

Figure 22. - Schematic sketch of end view of header arrangement for heat exchanger.

Declassified 1-24-1963

Declassified 1-24-1963

E-288

CA-26

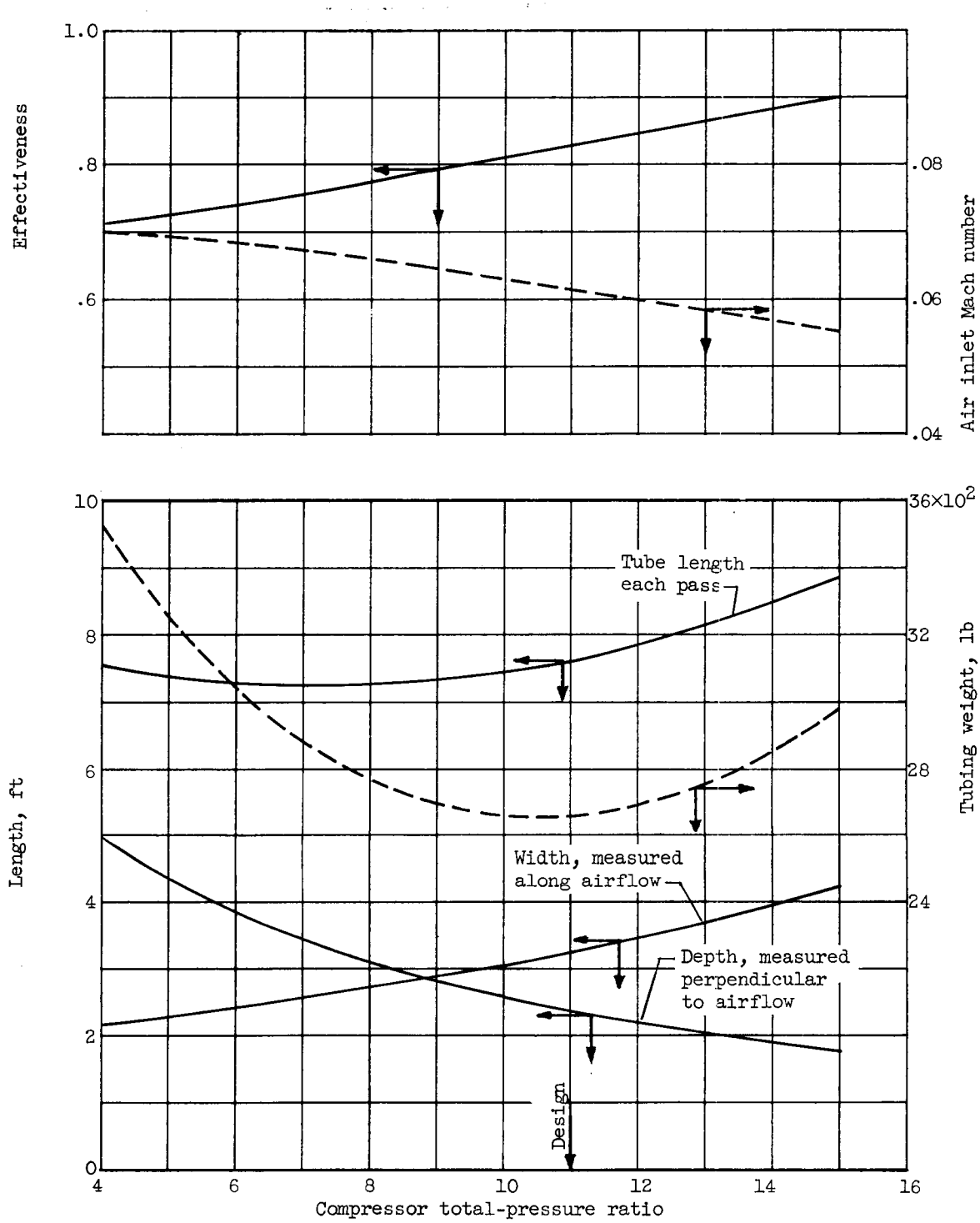

Figure 23. - Effect of compressor total-pressure ratio (inlet pressure) on heat-exchanger dimensions and weight for reference airflow rate of 100 pounds per second.

Declassified 1-24-1963

Declassified 1-24-1963

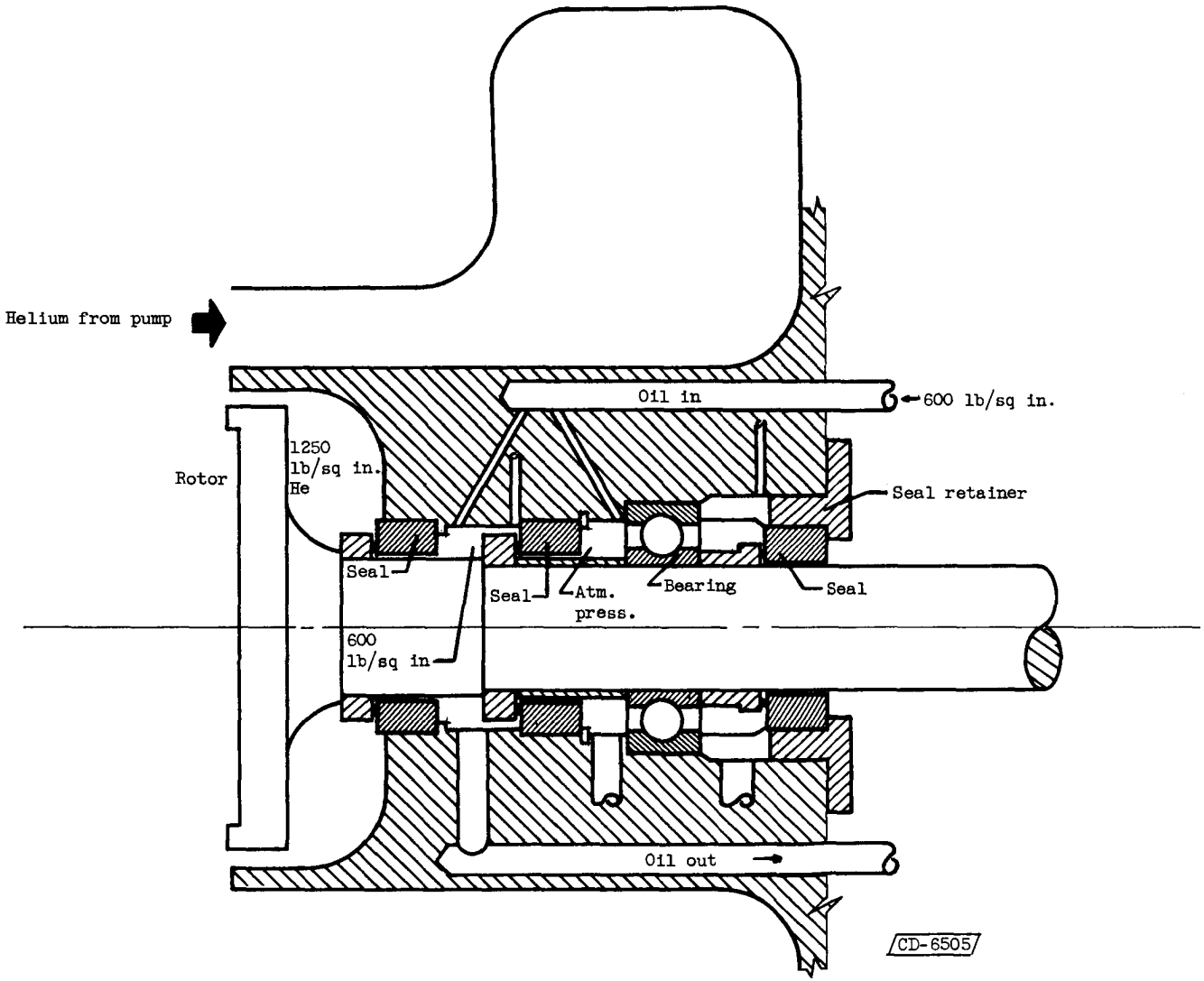

Figure 24. - Proposed design of pump bearings and seals.

Declassified 1-24-1963

Declassified 1-24-1963

E-288
CA-26 back

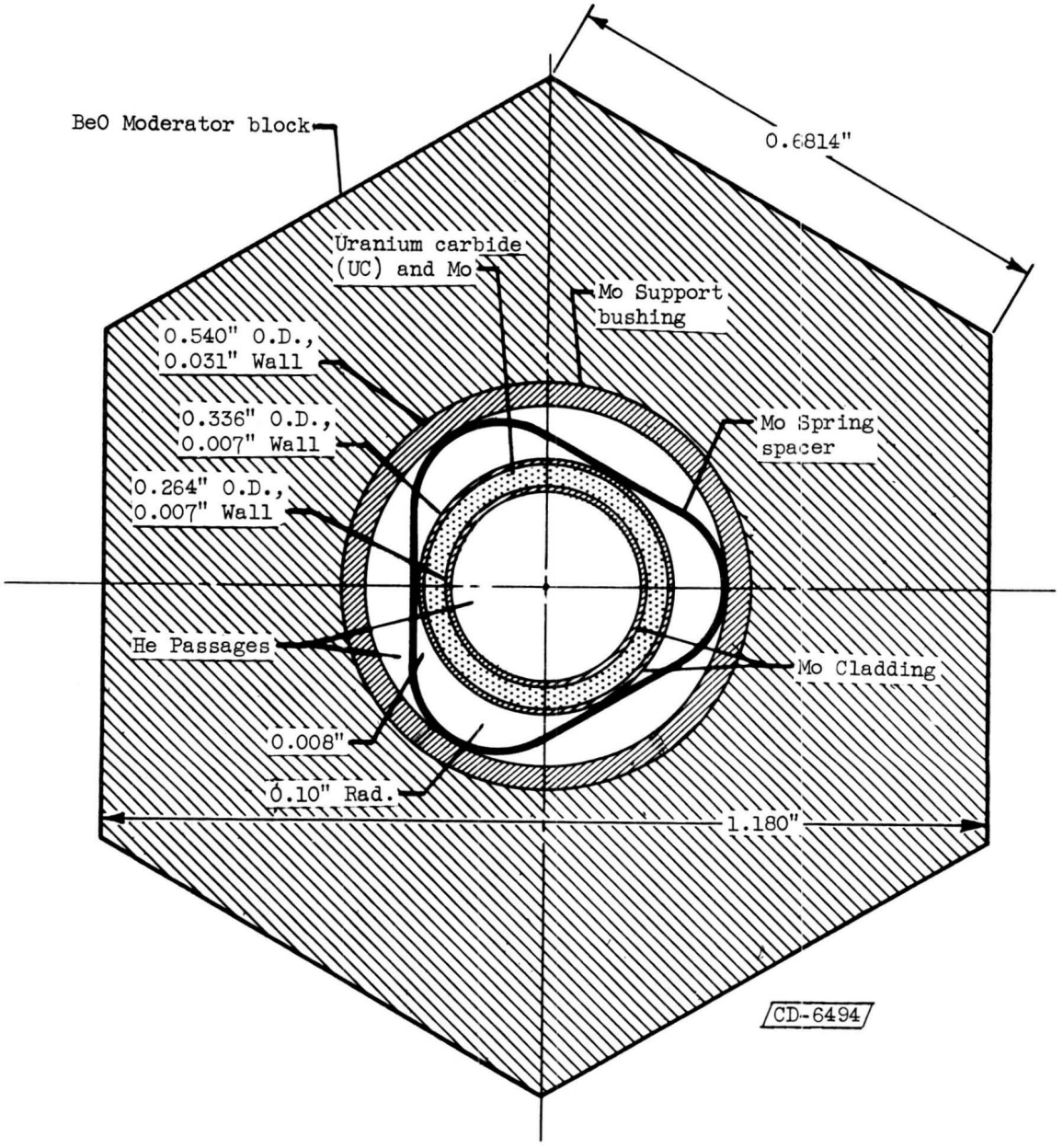

Figure 25. - Section D-D of figure 5, through support bushing for moderator block.

Declassified 1-24-1963

Declassified 1-24-1963

SECRET

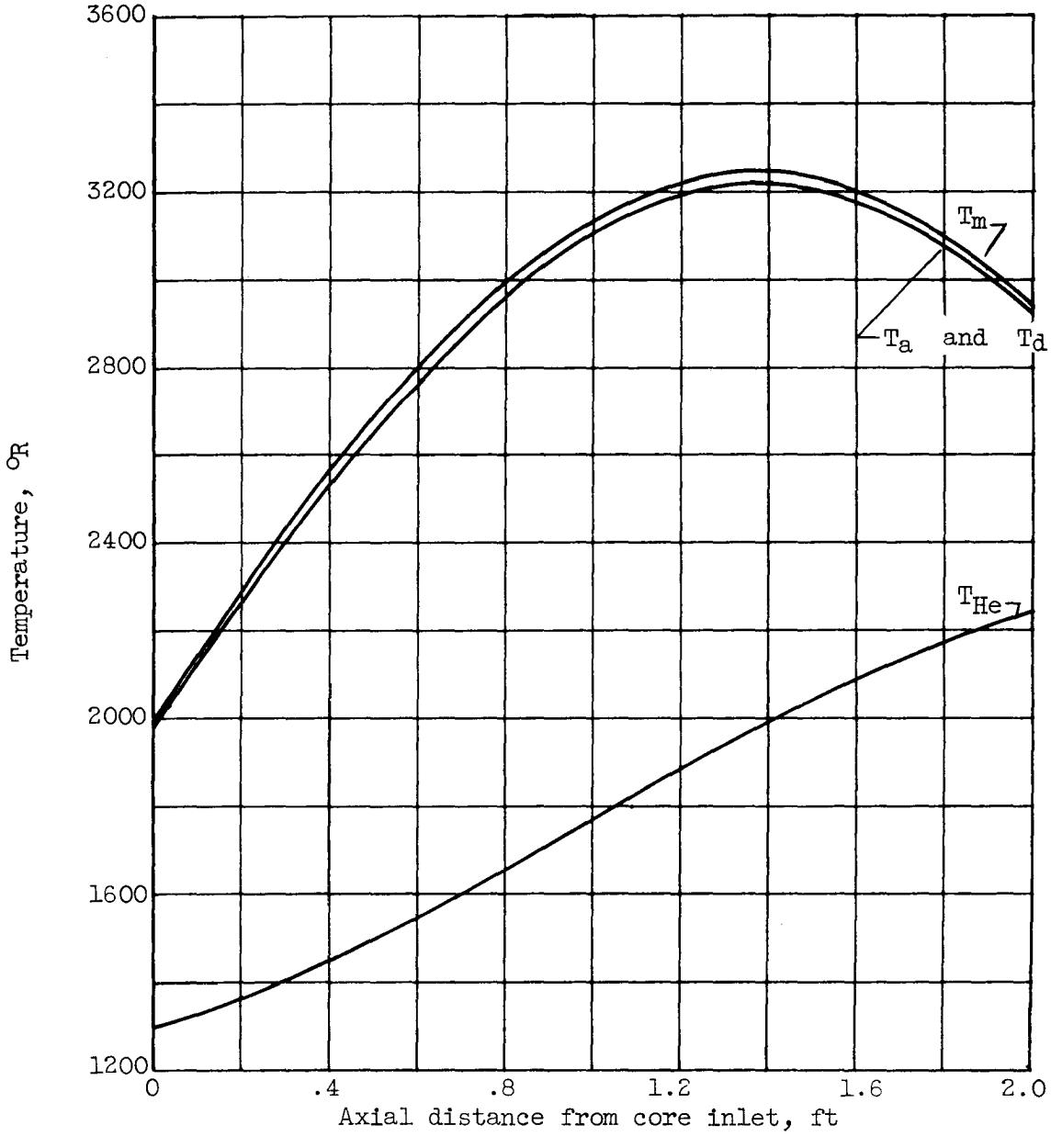

Figure 26. - Temperatures of two-coolant-passage fuel element and of helium in axial direction for 100-megawatt reactor (for "chopped" 2/3-cosine axial distribution of heat). (w_h = 0.0459 lb/sec; w_{an} = 0.0684 lb/sec; $\Delta P_{passages}$ = 2.6% of initial pressure.)

SECRET

Declassified 1-24-1963

Declassified 1-24-1963

E-288

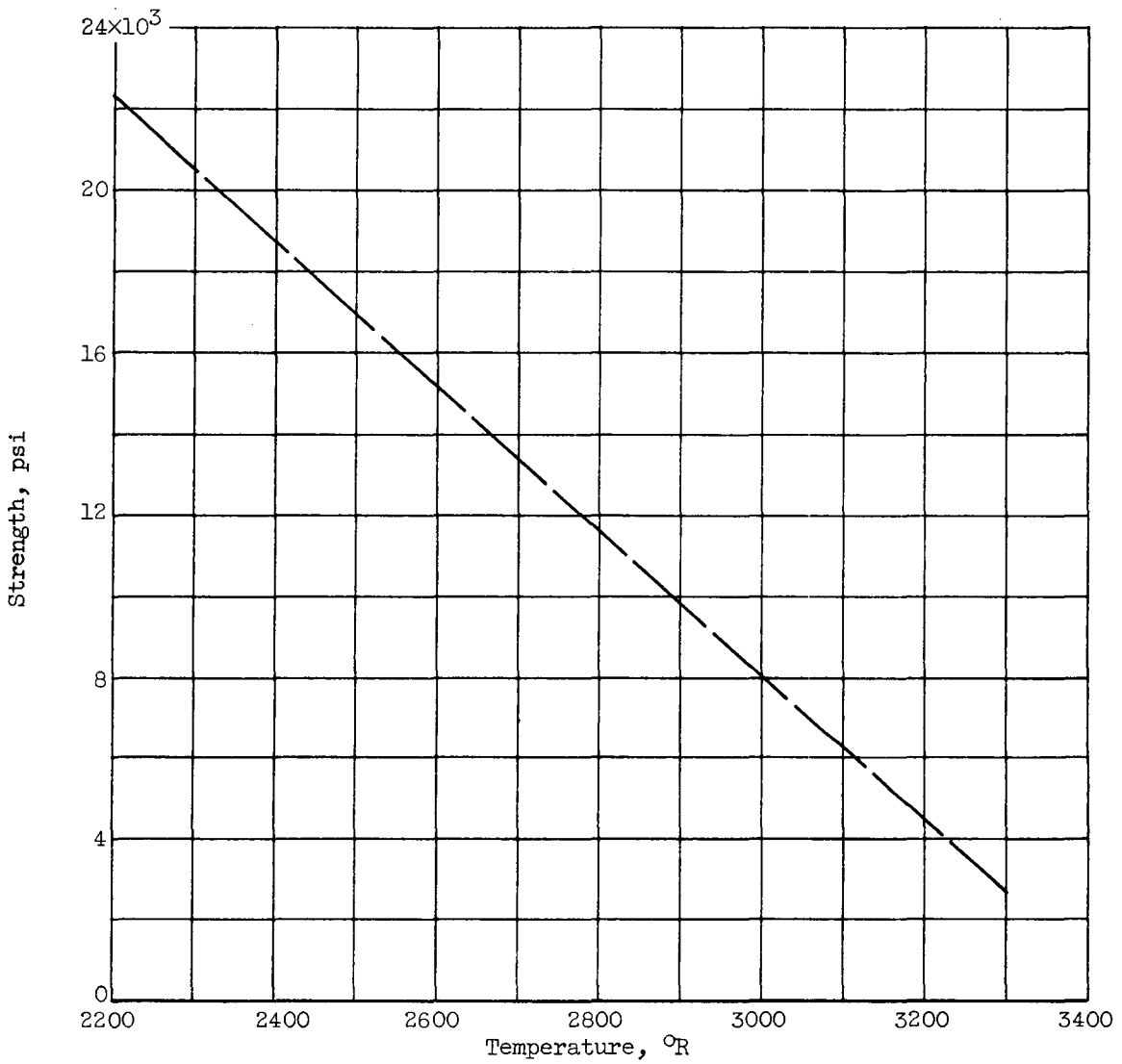

Figure 27. - Stress-rupture strength of molybdenum + 0.45 percent titanium for 1000-hour rupture life (extrapolated data).

Declassified 1-24-1963

Declassified 1-24-1963

SECRET

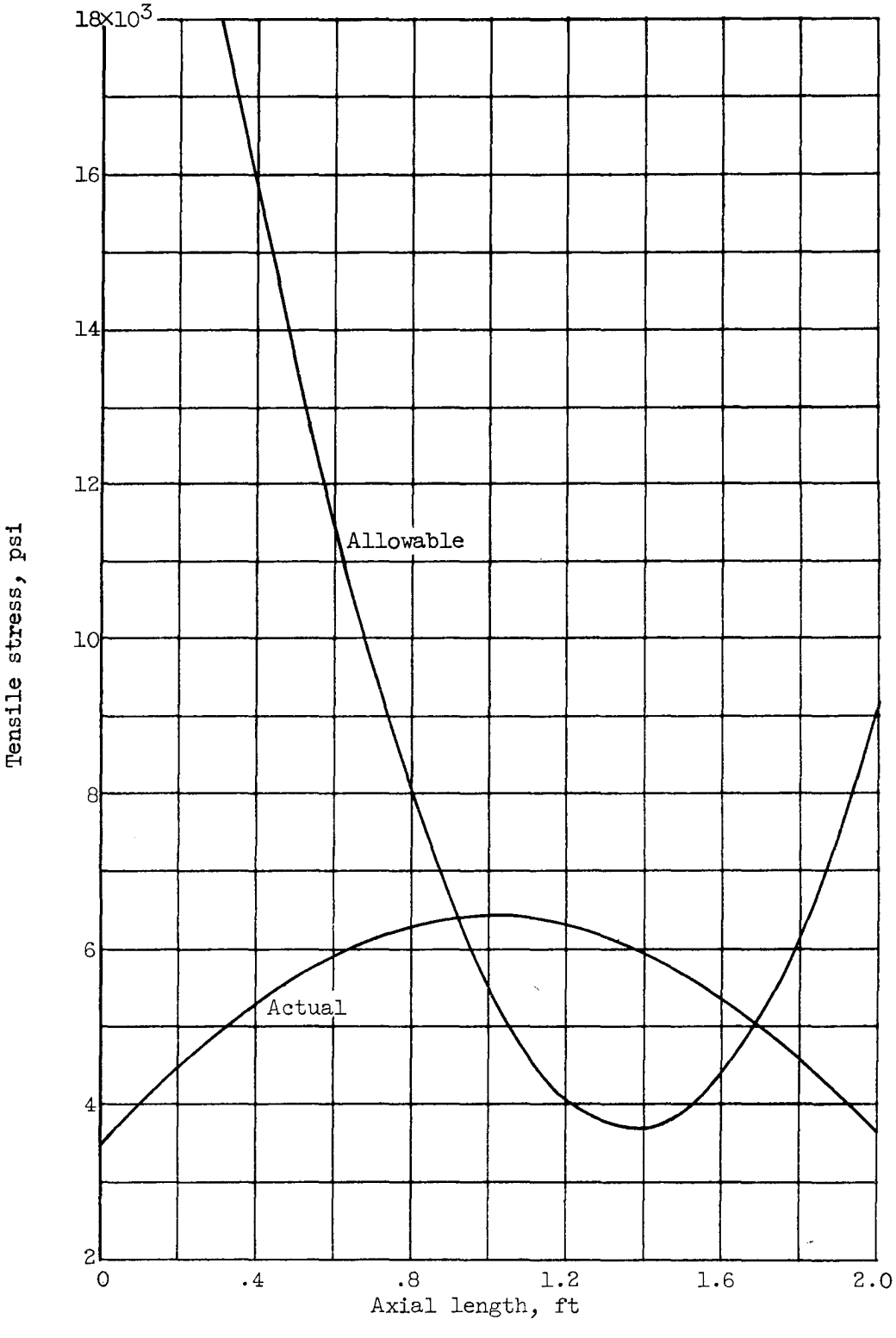

Figure 28. - Allowable and actual fuel-element stresses at outer radius (for "chopped" 2/3-cosine axial distribution of heat).

E-288

SECRET
Declassified 1-24-1963

Declassified 1-24-1963

E-288

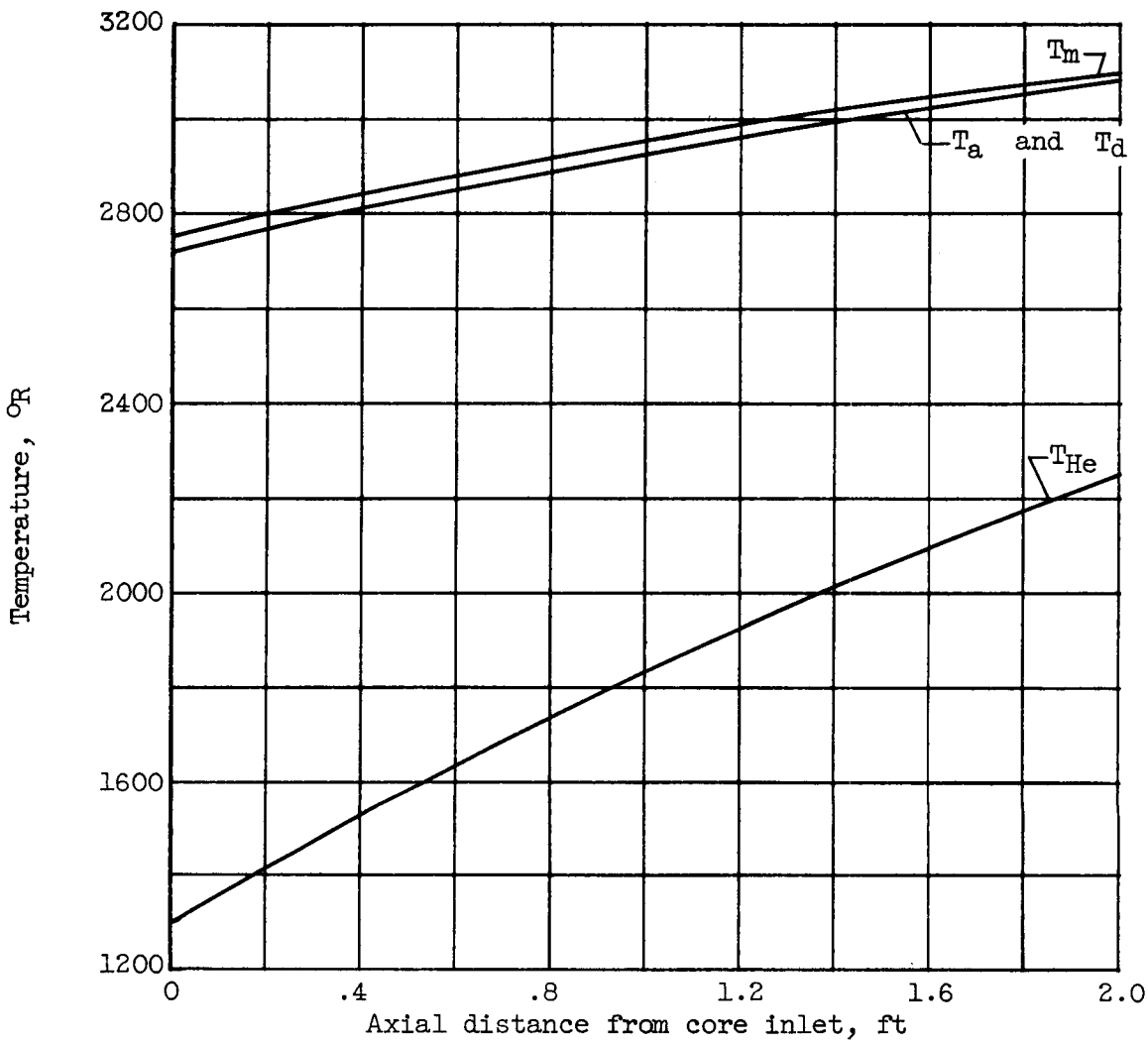

Figure 29. - Temperatures of two-coolant-passage fuel element and of helium in axial direction for 100-megawatt reactor (for axial distribution of heat resulting in satisfactory fuel-element stresses). (w_h = 0.0459 lb/sec; w_{an} = 0.0684 lb/sec; $\Delta P_{passages}$ = 2.6% of initial pressure.)

Declassified 1-24-1963

Declassified 1-24-1963

SECRET

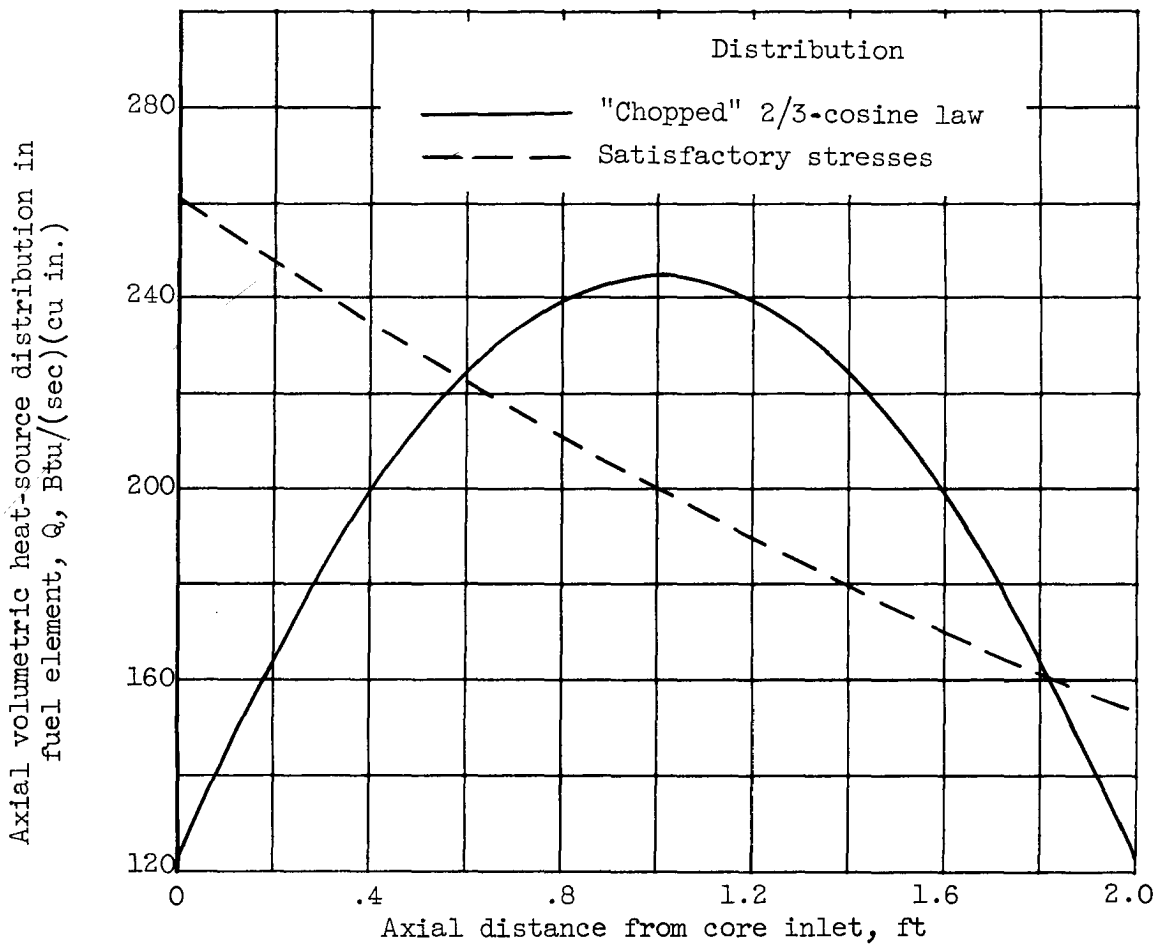

Figure 30. - Variations of volumetric heat-source distribution in fuel element.

SECRET
Declassified 1-24-1963

Declassified 1-24-1963

E-288

CA-27

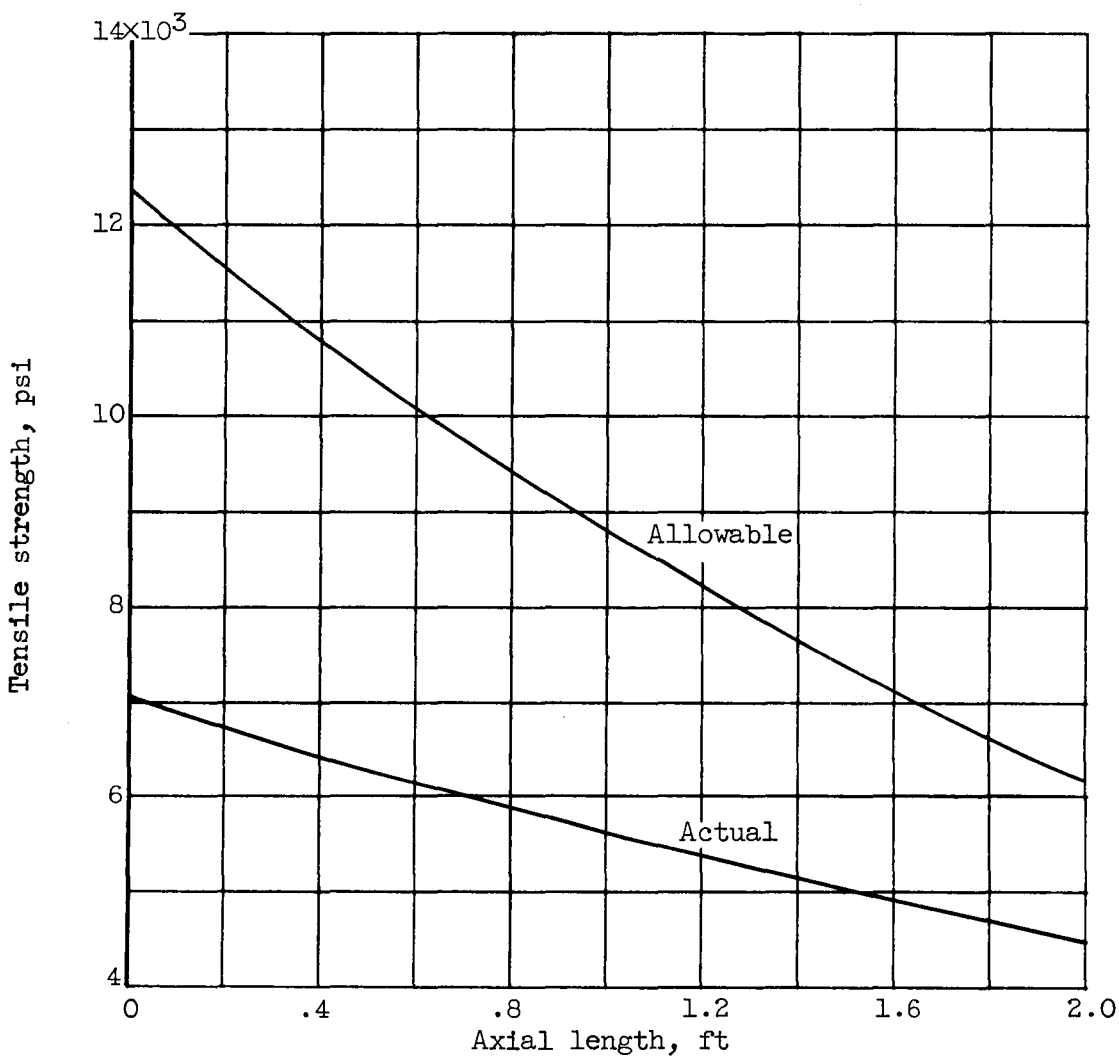

Figure 31. - Allowable and actual fuel-element stresses at outer radius (for conditions resulting in satisfactory fuel-element stresses).

Declassified 1-24-1963

SECRET
Declassified 1-24-1963

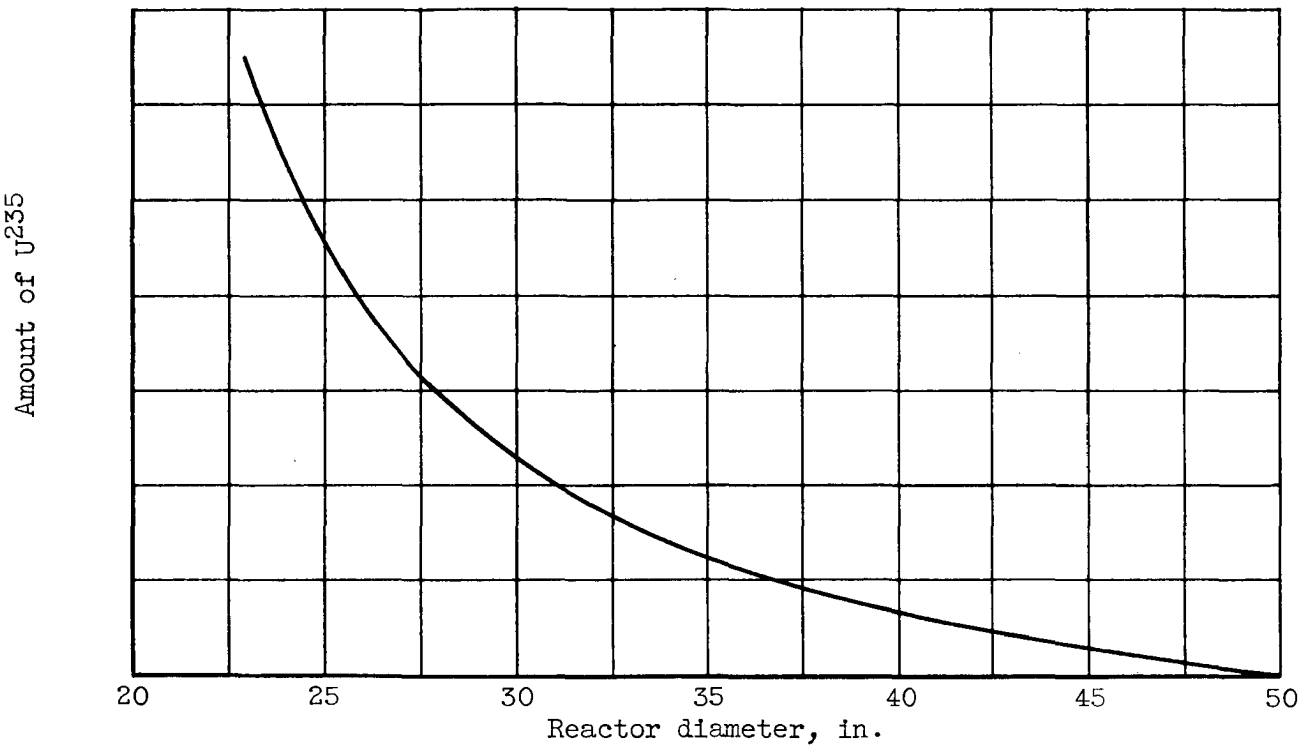

Figure 32. - Effect of reactor diameter (core diam. plus twice reflector thickness) on amount of U^{235} required for constant effective multiplication factor.

SECRET
Declassified 1-24-1963

Declassified 1-24-1963

SECRET

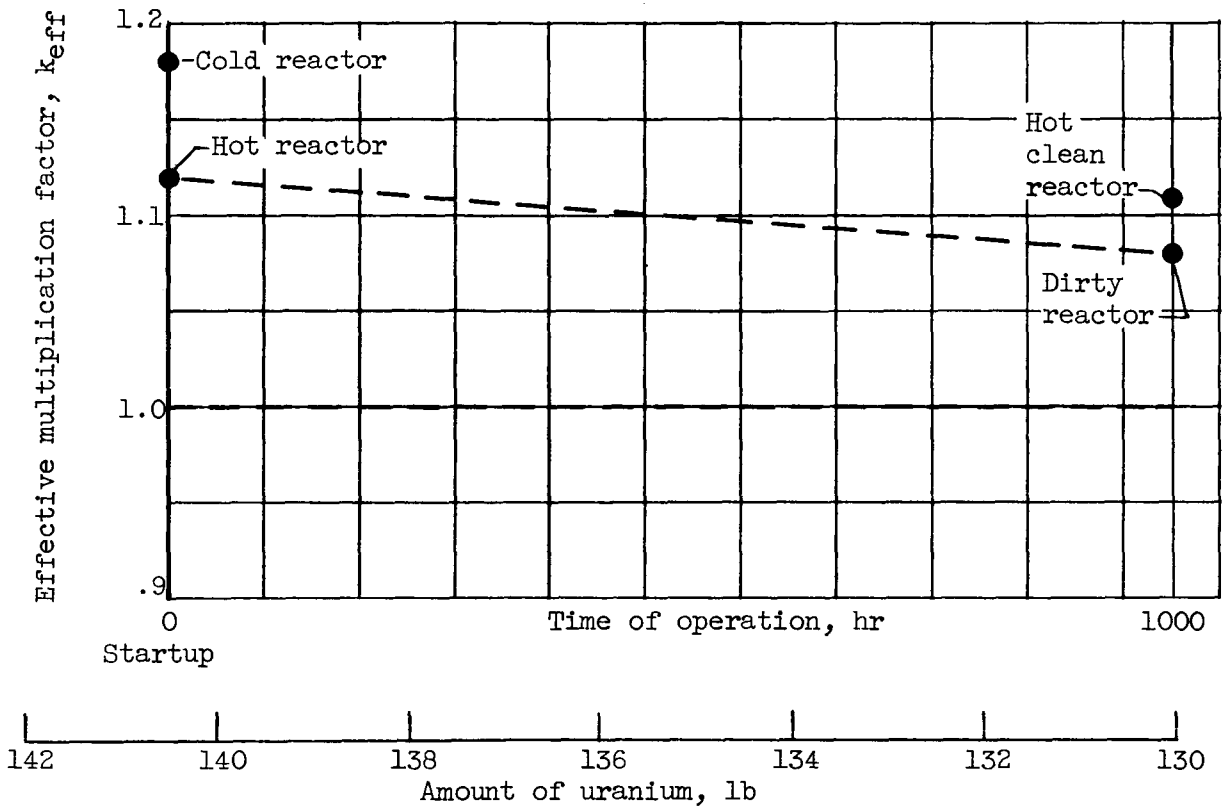

Figure 33. - Effective multiplication factor for reactor for various operating conditions.

Declassified 1-24-1963

SECRET

Declassified 1-24-1963

SECRET

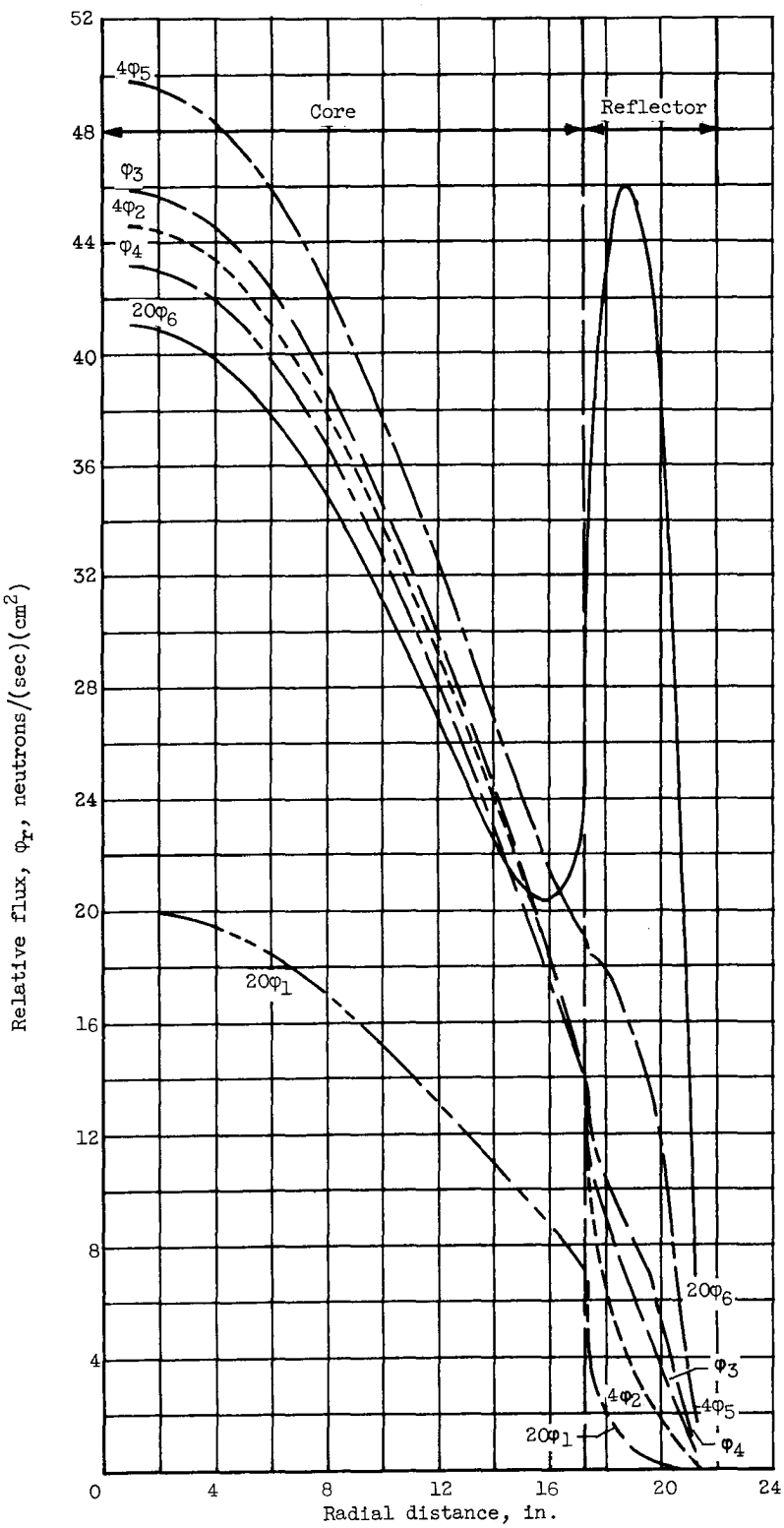

Figure 34. - Variation of flux radially along reactor center-line for six groups. (Startup, 140.5 lb of uranium.)

SECRET

Declassified 1-24-1963

Declassified 1-24-1963

E-288

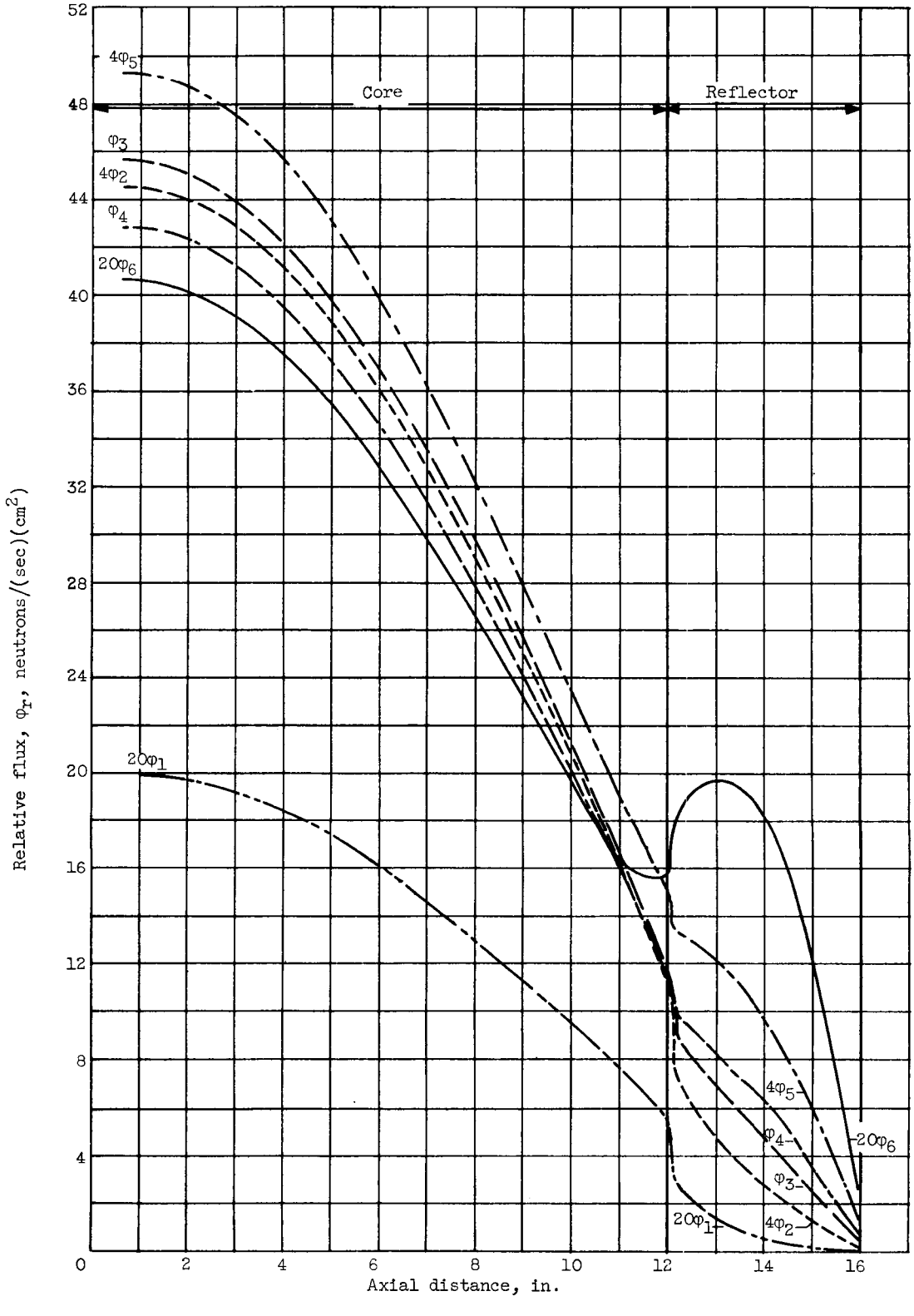

Figure 35. - Variation of flux axially along reactor centerline for six groups. (Startup, 140.5 lb of uranium.)

Declassified 1-24-1963

Declassified 1-24-1963

SECRET

F-288

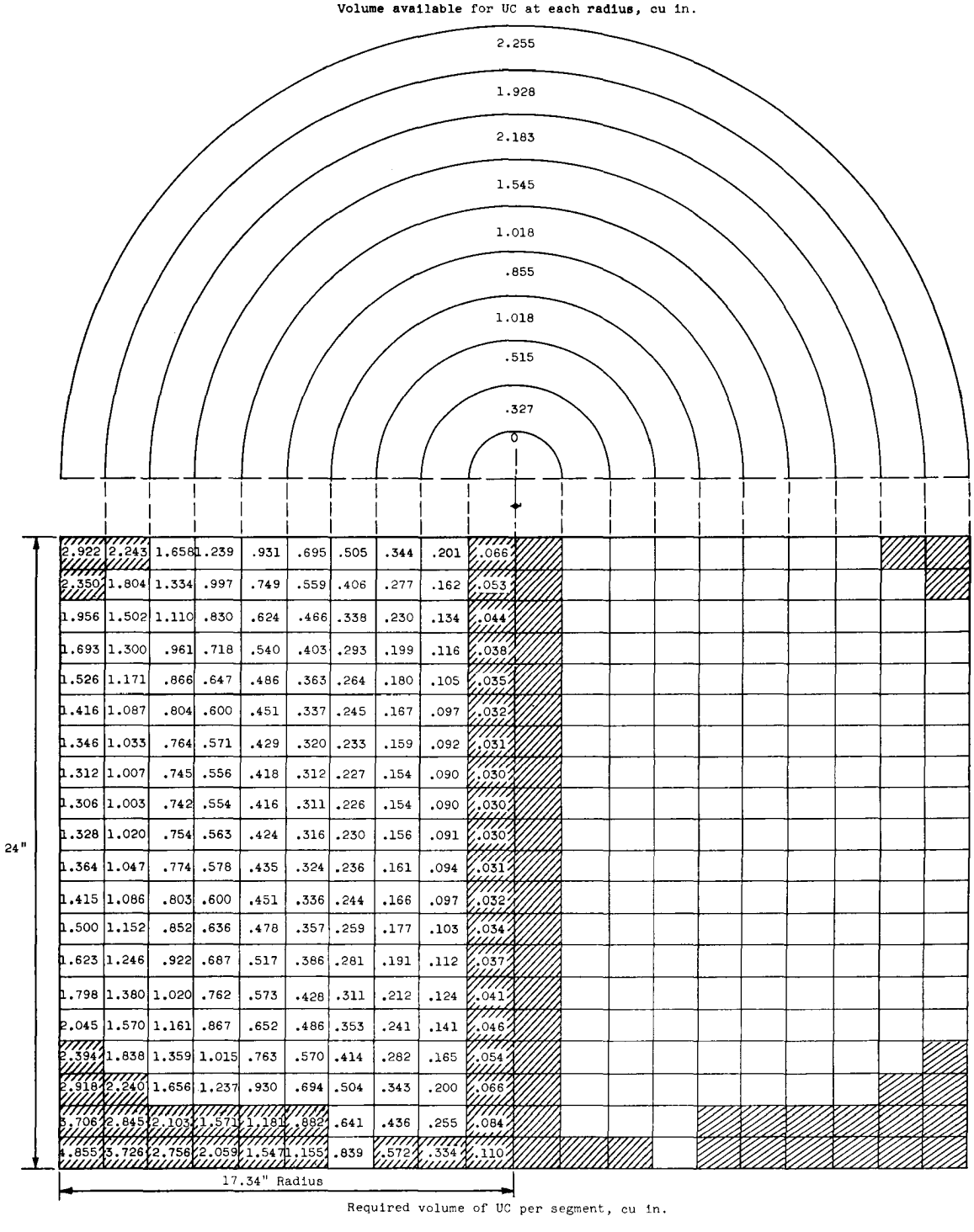

2.922	2.243	1.658	1.239	.931	.695	.505	.344	.201	.066
2.350	1.804	1.334	.997	.749	.559	.406	.277	.162	.053
1.956	1.502	1.110	.830	.624	.466	.338	.230	.134	.044
1.693	1.300	.961	.718	.540	.403	.293	.199	.116	.038
1.526	1.171	.866	.647	.486	.363	.264	.180	.105	.035
1.416	1.087	.804	.600	.451	.337	.245	.167	.097	.032
1.346	1.033	.764	.571	.429	.320	.233	.159	.092	.031
1.312	1.007	.745	.556	.418	.312	.227	.154	.090	.030
1.306	1.003	.742	.554	.416	.311	.226	.154	.090	.030
1.328	1.020	.754	.563	.424	.316	.230	.156	.091	.030
1.364	1.047	.774	.578	.435	.324	.236	.161	.094	.031
1.415	1.086	.803	.600	.451	.336	.244	.166	.097	.032
1.500	1.152	.852	.636	.478	.357	.259	.177	.103	.034
1.623	1.246	.922	.687	.517	.386	.281	.191	.112	.037
1.798	1.380	1.020	.762	.573	.428	.311	.212	.124	.041
2.045	1.570	1.161	.867	.652	.486	.353	.241	.141	.046
2.394	1.838	1.359	1.015	.763	.570	.414	.282	.165	.054
2.918	2.240	1.656	1.237	.930	.694	.504	.343	.200	.066
3.706	2.845	2.103	1.571	1.181	.882	.641	.436	.255	.084
4.855	3.726	2.756	2.059	1.547	1.155	.839	.572	.334	.110

Figure 36. - Required and available volume distribution of uranium carbide in reactor core. (Shaded regions indicate that required volume exceeds available volume.)

SECRET

Declassified 1-24-1963

Declassified 1-24-1963

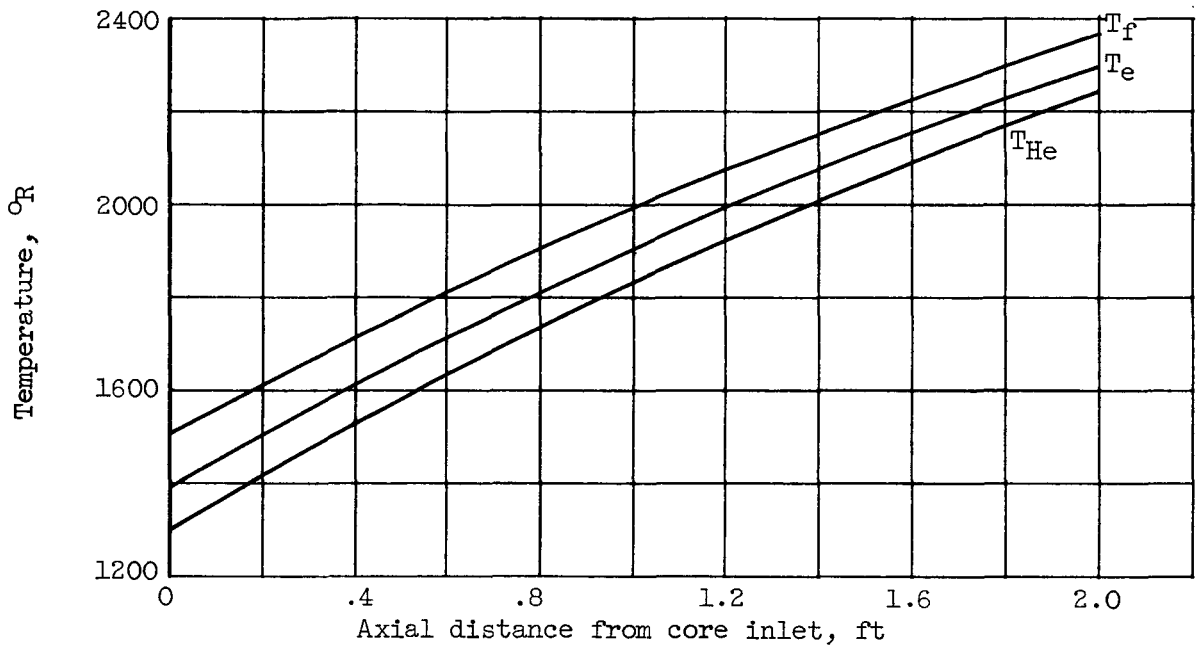

Figure 37. - Temperatures of moderator block and helium in axial direction for 100-megawatt reactor (for axial distribution of heat resulting in satisfactory fuel-element stresses). (w_h = 0.0459 lb/sec; w_{an} = 0.0684 lb/sec; $\Delta P_{passages}$ = 2.6% of initial pressure.)

Declassified 1-24-1963

Declassified 1-24-1963

SECRET

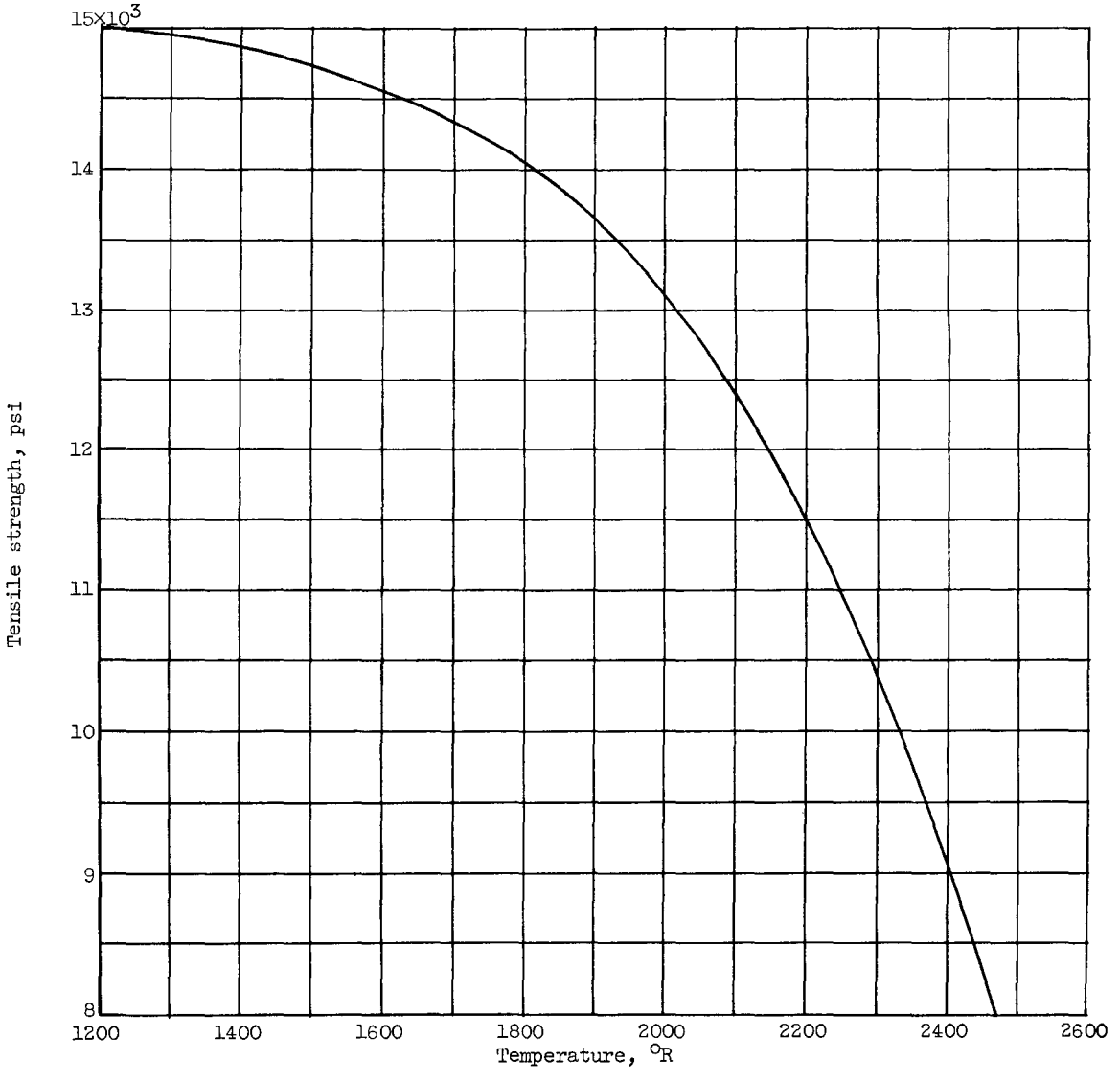

Figure 38. - Tensile strength of beryllium oxide.

SECRET

Declassified 1-24-1963

Declassified 1-24-1963

E-288
CA-28

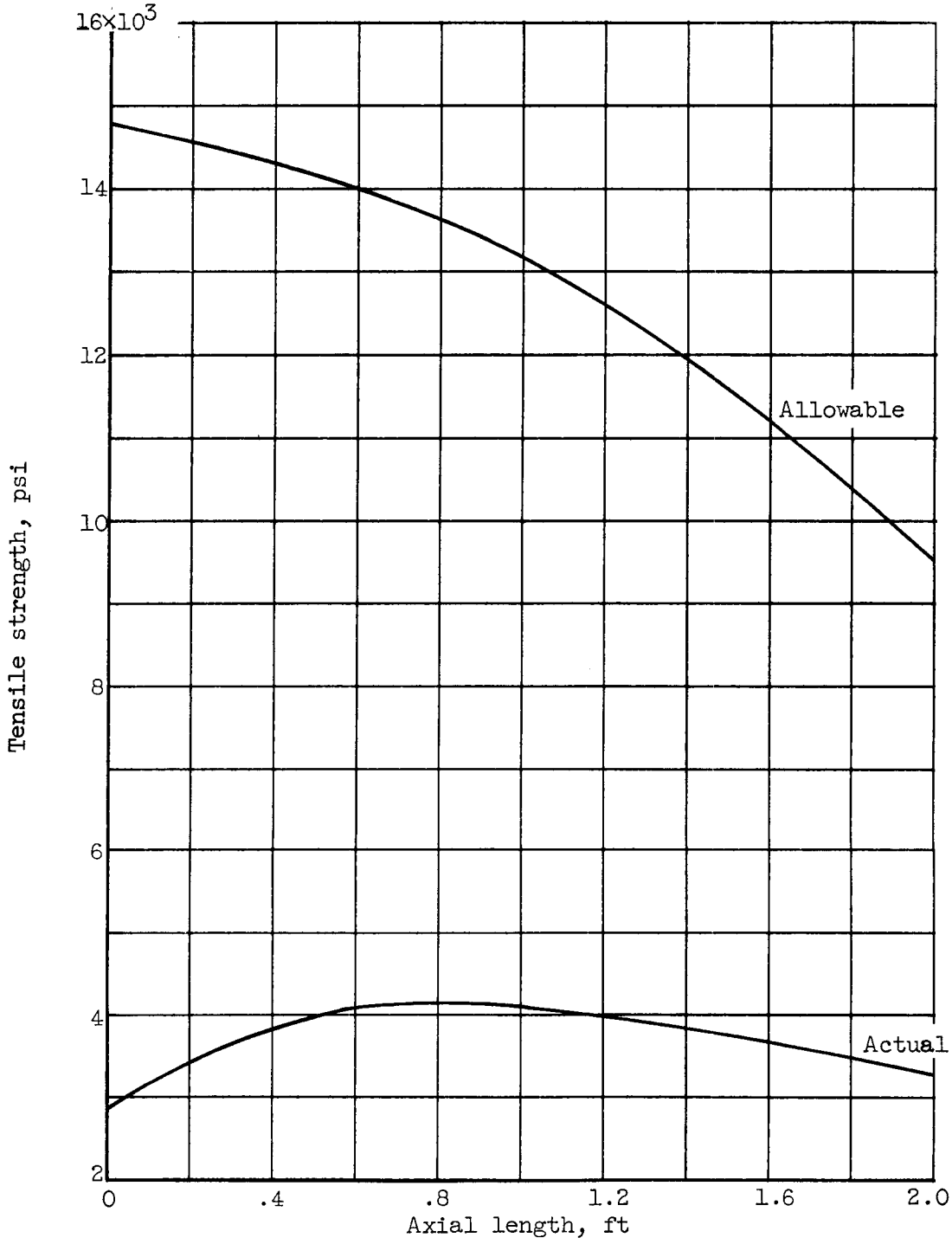

Figure 39. - Variation of allowable and actual moderator-block stresses at outer radius with axial length of block (for conditions resulting in satisfactory fuel-element stresses).

Declassified 1-24-1963

Declassified 1-24-1963

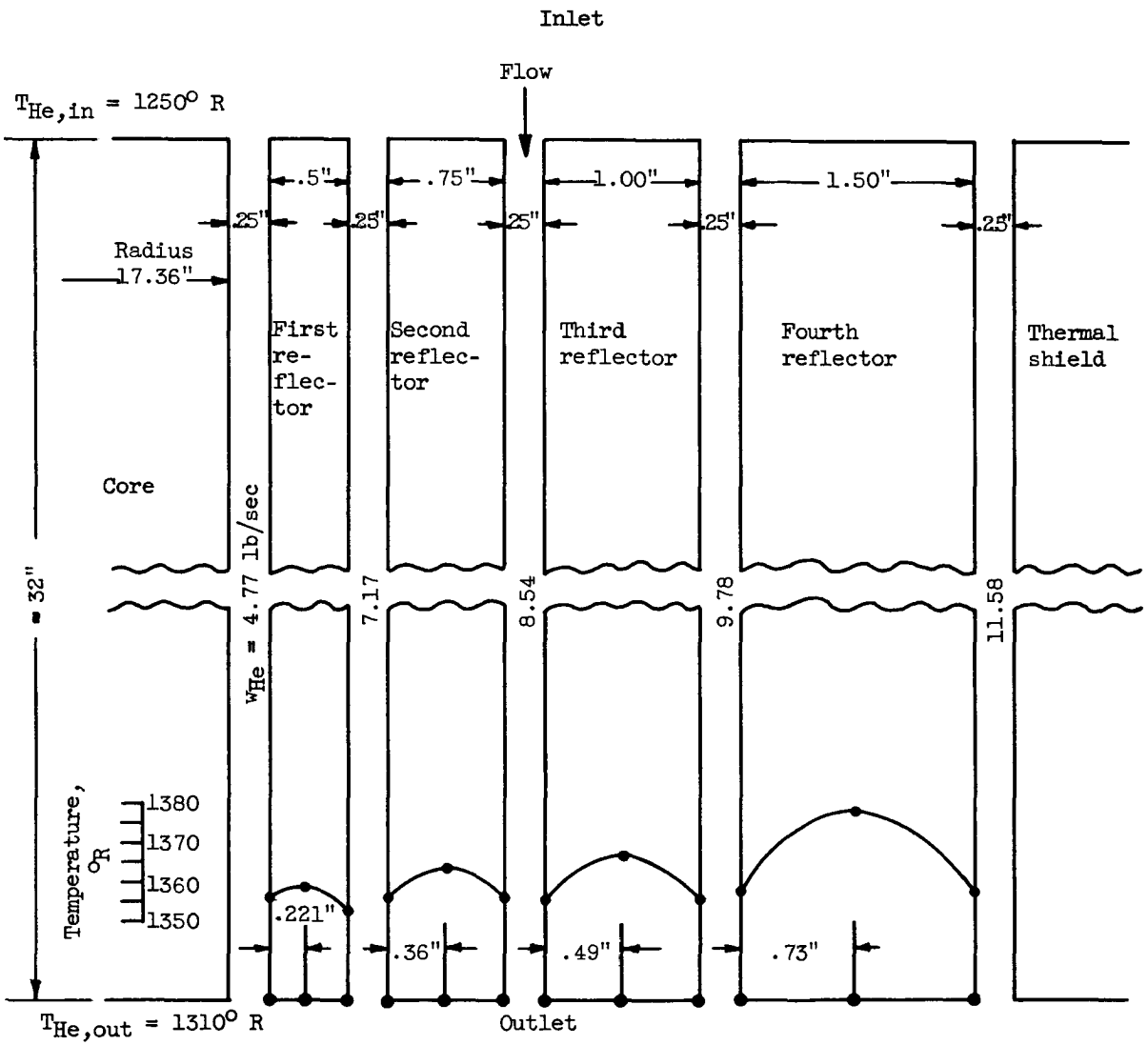

Figure 40. - Side-reflector temperatures and flow rates in passages between reflector shells.

Declassified 1-24-1963

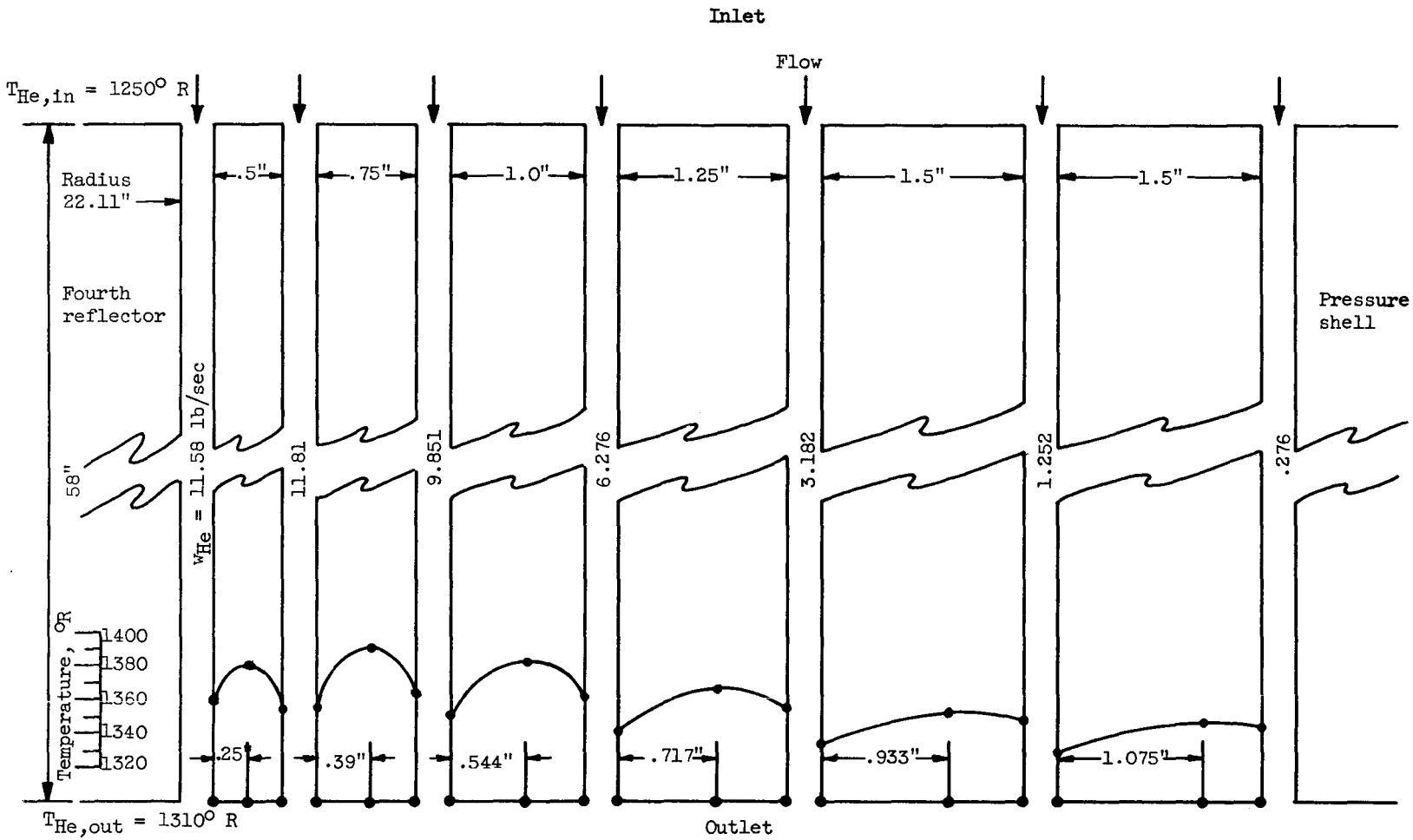

Figure 41. - Thermal-shield temperatures and flow rates through passages.

Declassified 1-24-1963

Declassified 1-24-1963

Declassified 1-24-1963

SECRET

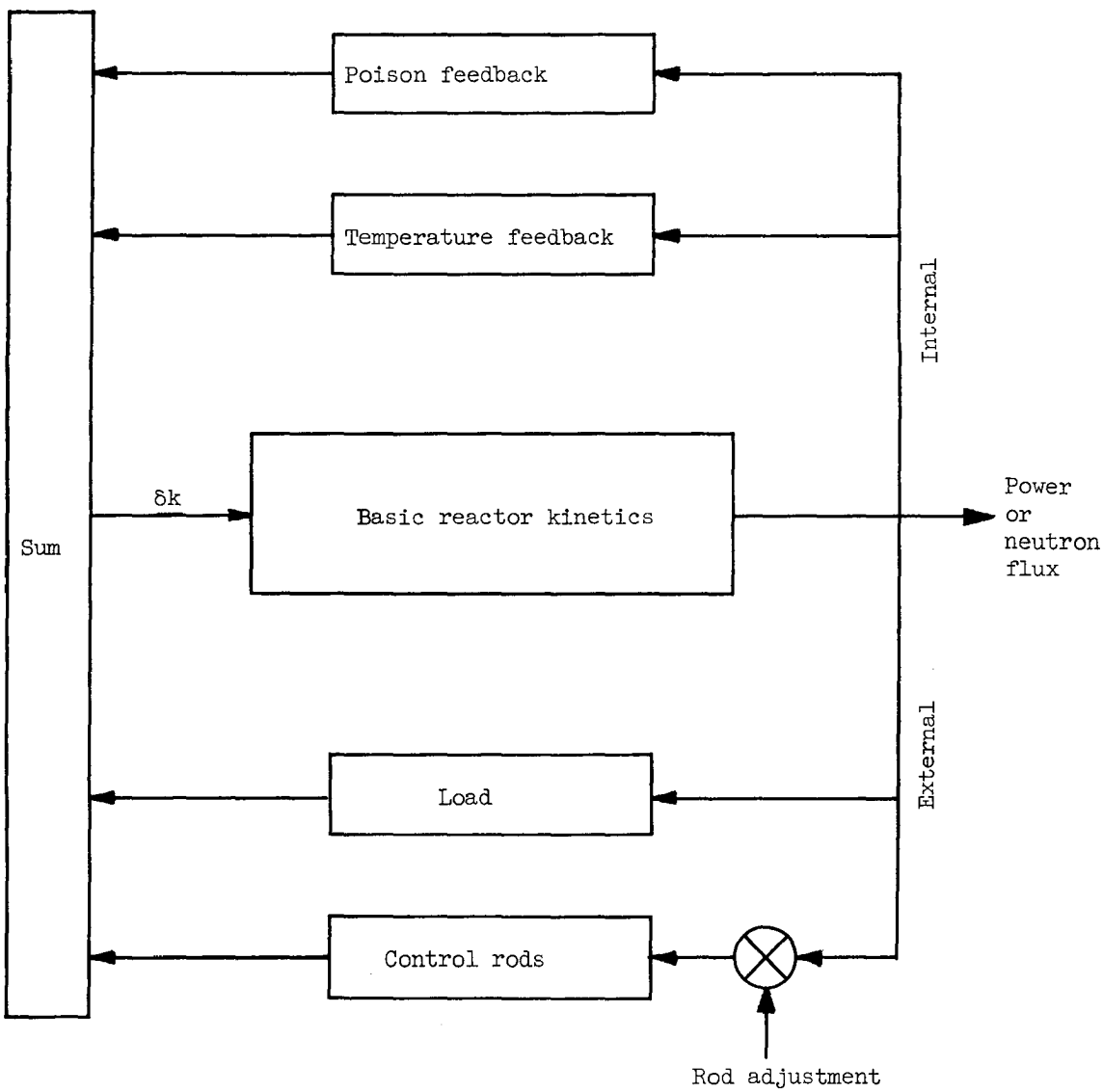

Figure 42. - Block diagram showing power or neutron-flux variations that affect reactivity.

SECRET
Declassified 1-24-1963

Declassified 1-24-1963

E-288

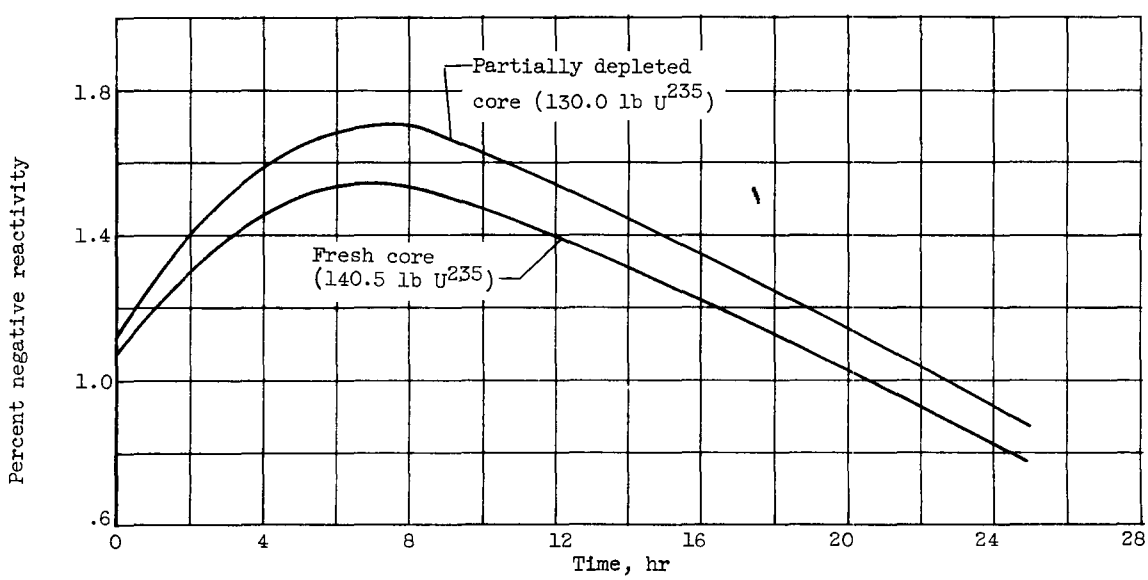

Figure 43. - Xenon buildup in response to step decrease in neutron flux from equilibrium xenon.

Declassified 1-24-1963

Declassified 1-24-1963

SECRET

E-288

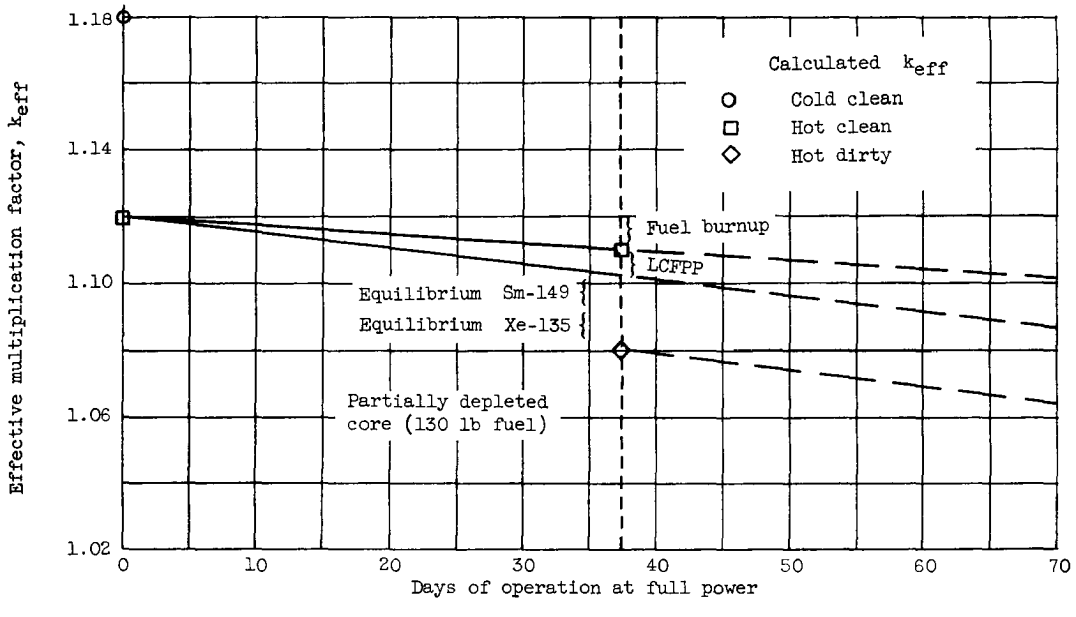

Figure 44. - Reactivity variations with time of operation at full power.

SECRET

Declassified 1-24-1963

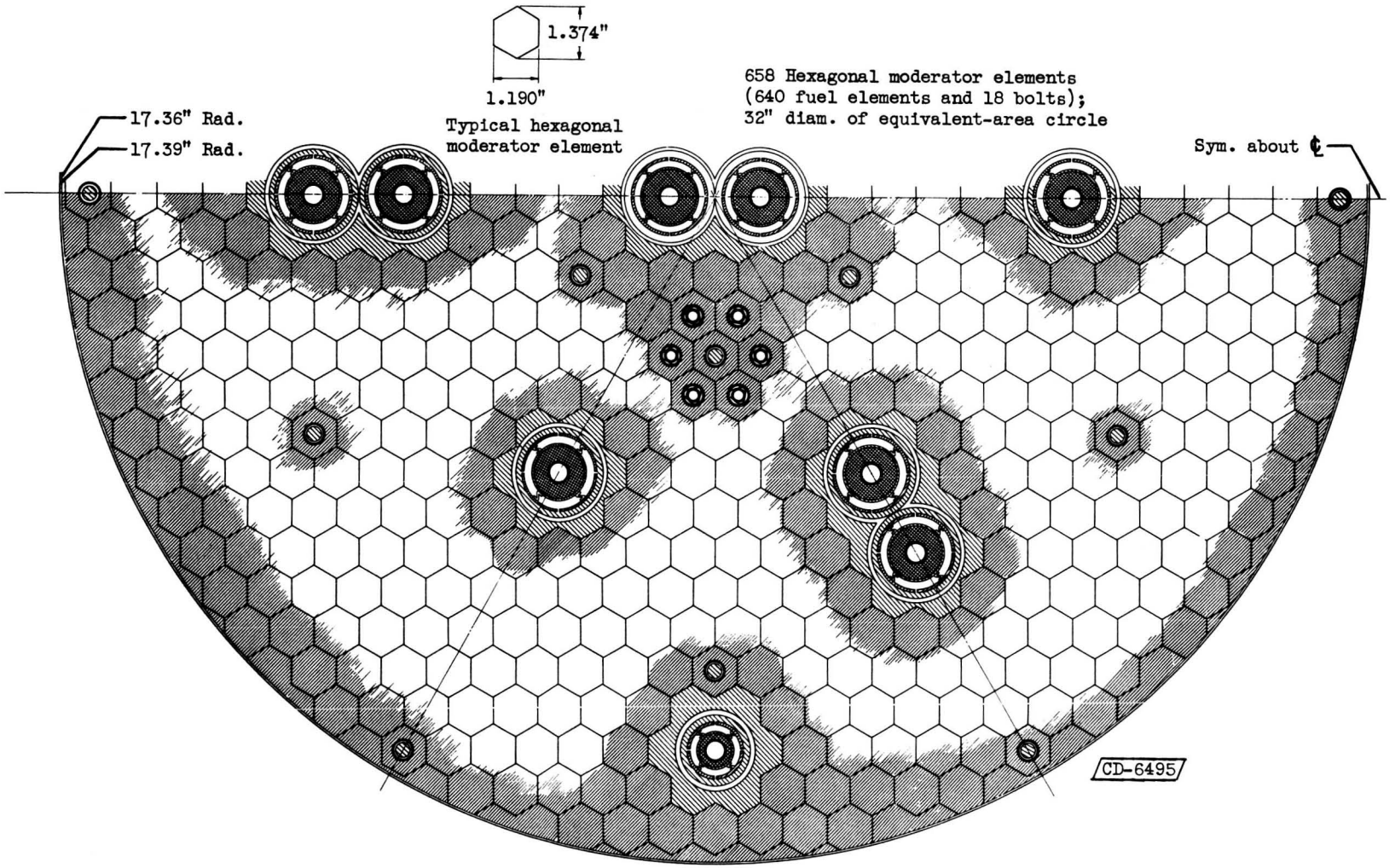

Figure 45. - Section E-E of figure 5.

Declassified 1-24-1963
Declassified 1-24-1963

Declassified 1-24-1963

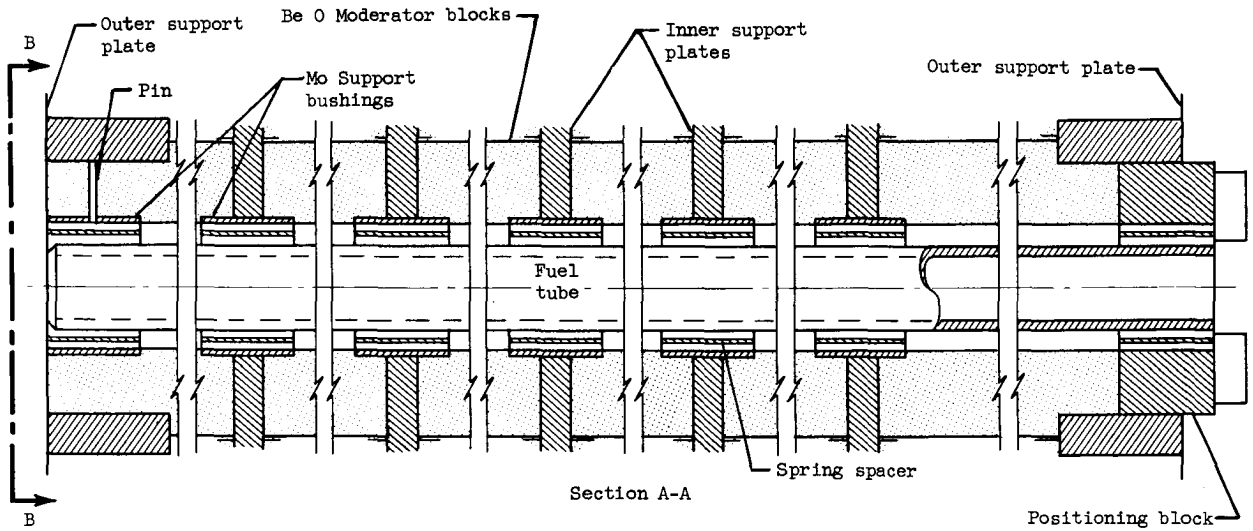

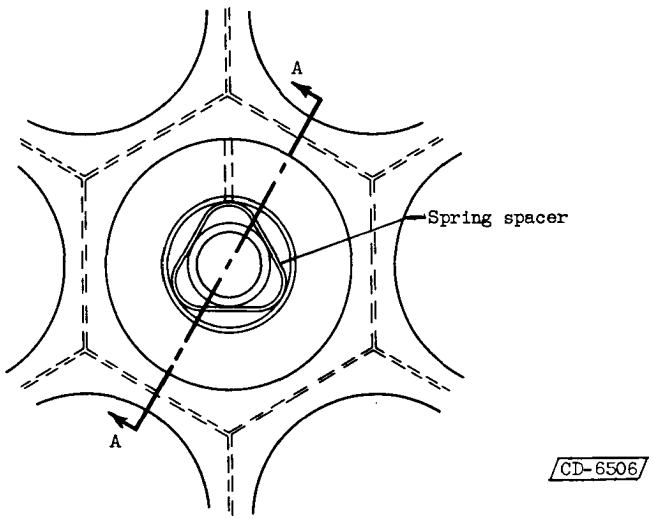

View B-B

Figure 46. - Fuel tube in reactor core.

Declassified 1-24-1963

Declassified 1-24-1963

E-288

CA-29

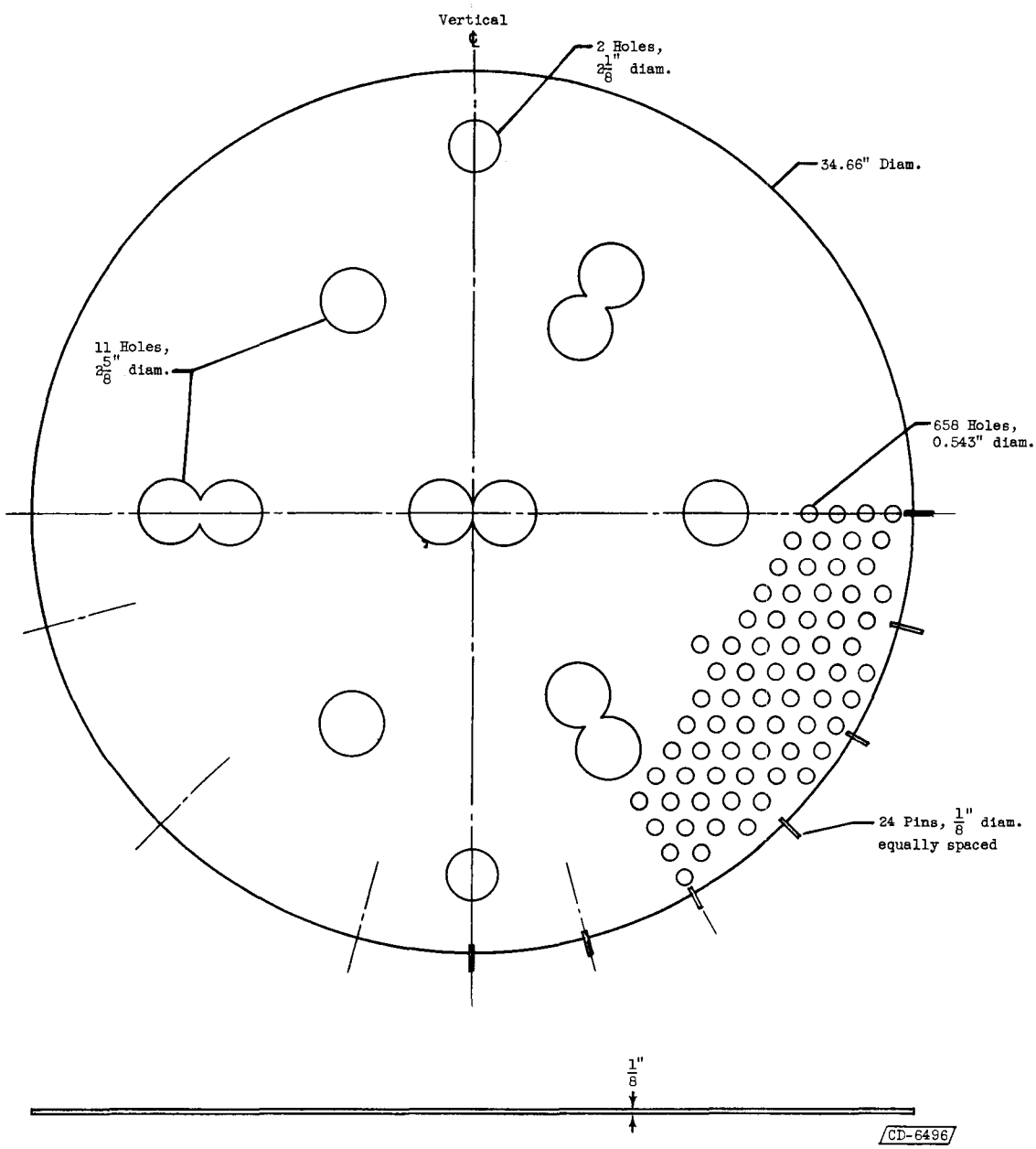

Figure 47. - Inner moderator block and fuel-element support plate; five required.

Declassified 1-24-1963

Declassified 1-24-1963

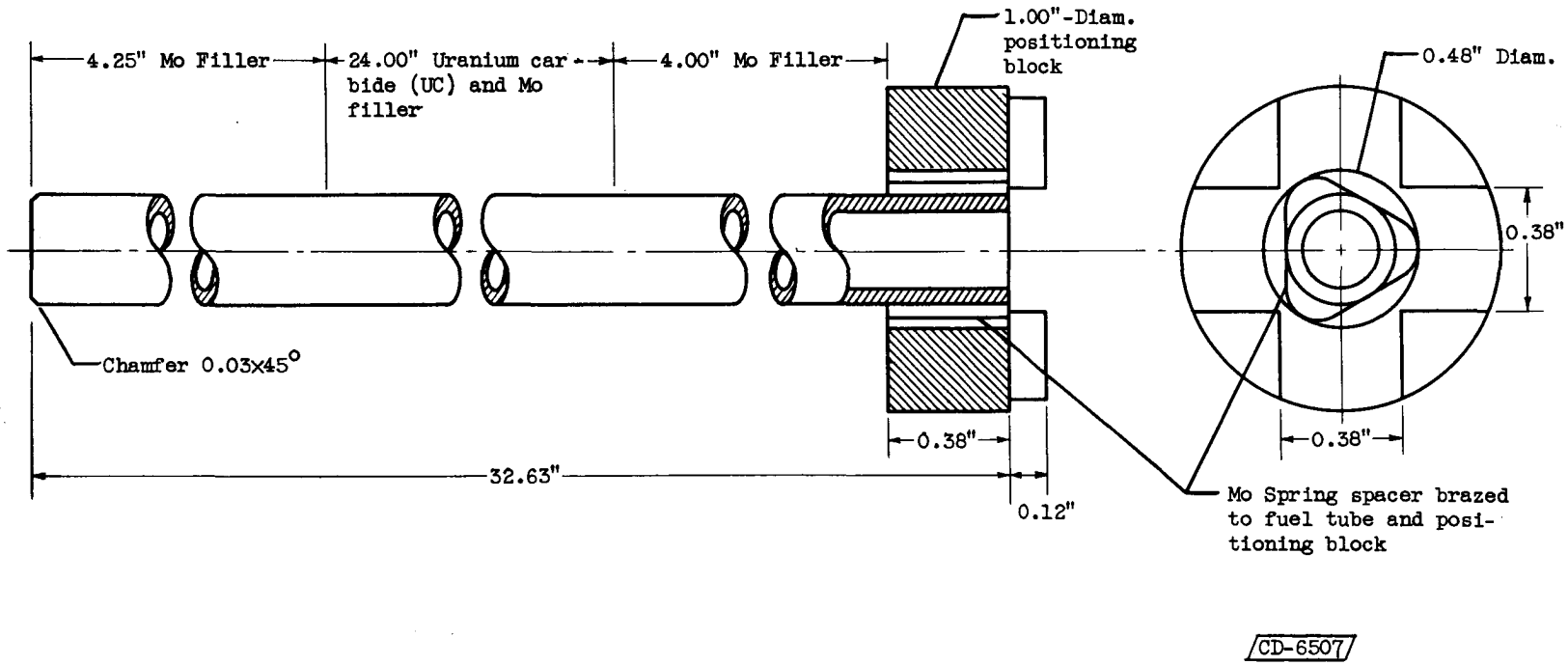

Figure 48. - Fuel tube and positioning block.

Declassified 1-24-1963

Declassified 1-24-1963

E-288

CA-29 back

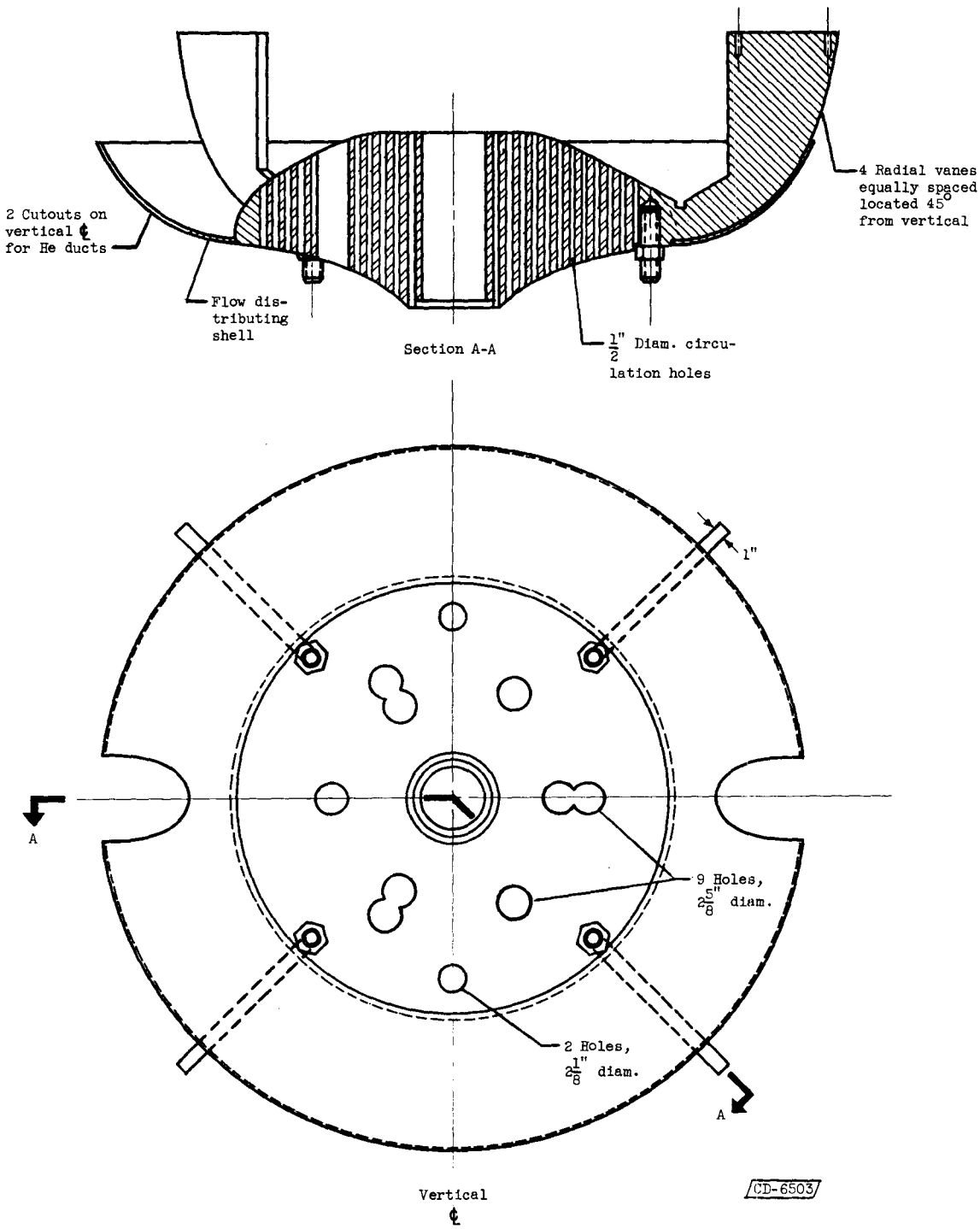

Figure 49. - Rear support shield RS 4.

Declassified 1-24-1963

Declassified 1-24-1963

SECRET

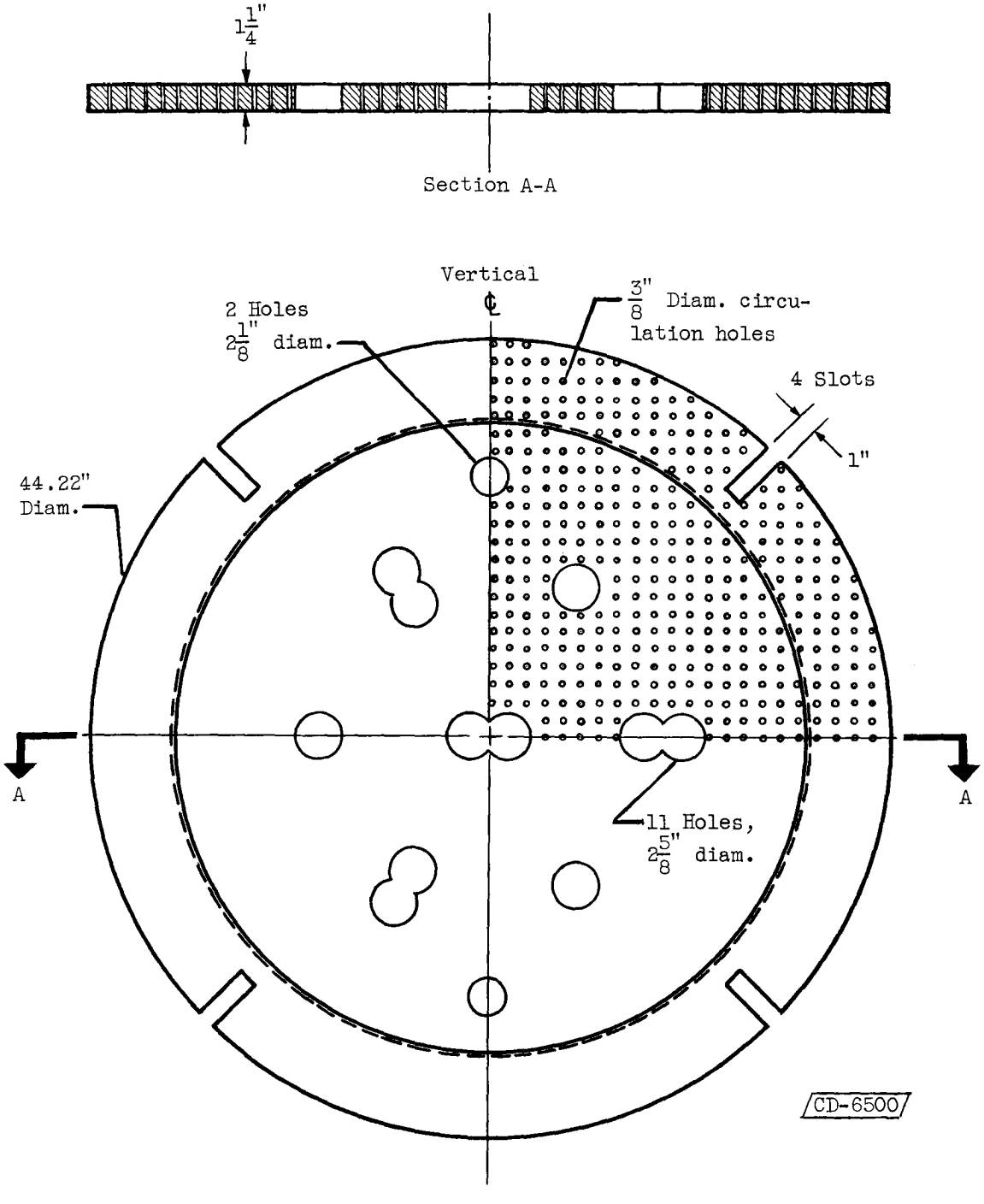

Figure 50. - First front shield plate FS1.

SECRET
Declassified 1-24-1963

Declassified 1-24-1963

SECRET

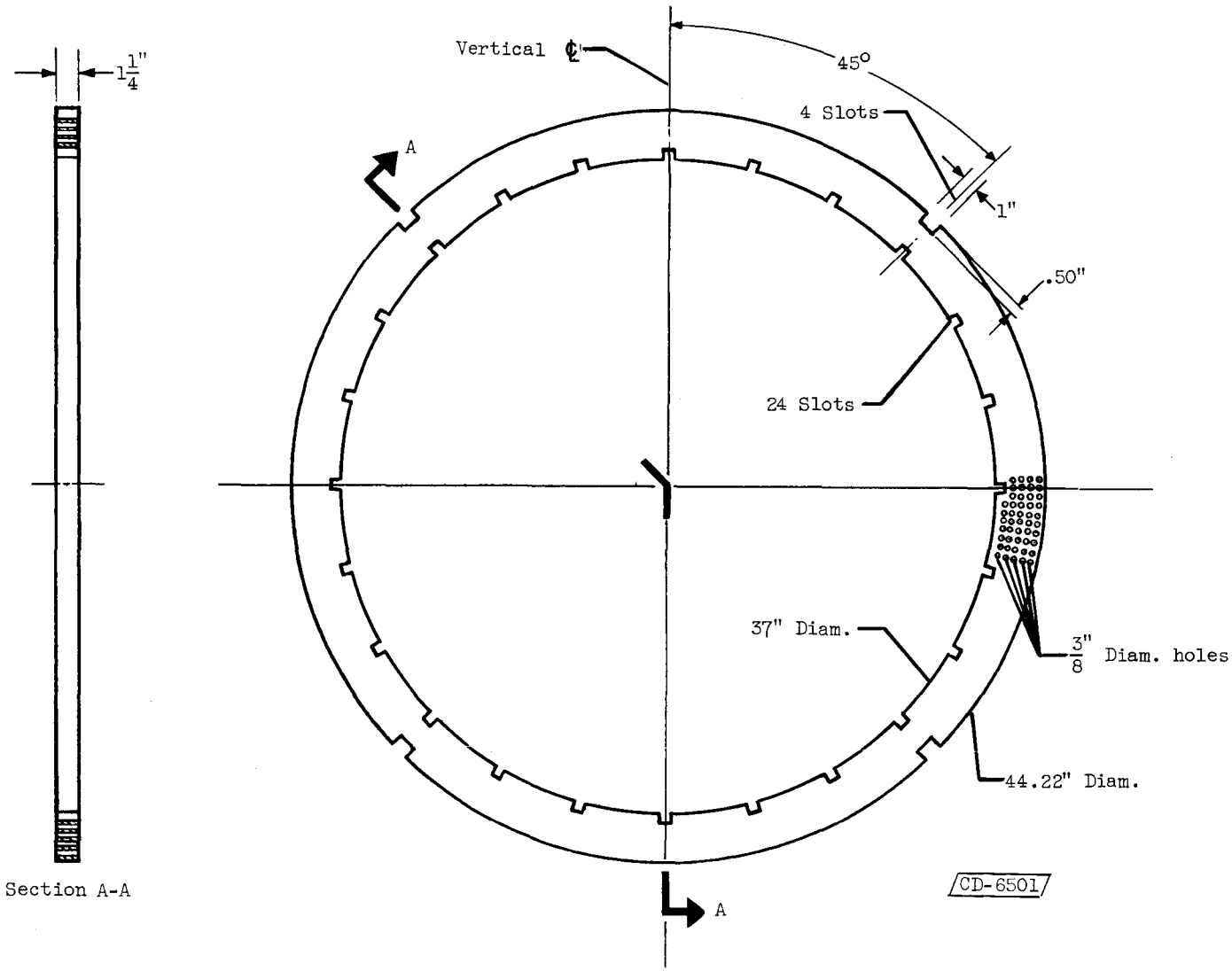

Figure 51. - First rear annular shield plate RAS1.

Declassified 1-24-1963

SECRET

Declassified 1-24-1963

SECRET

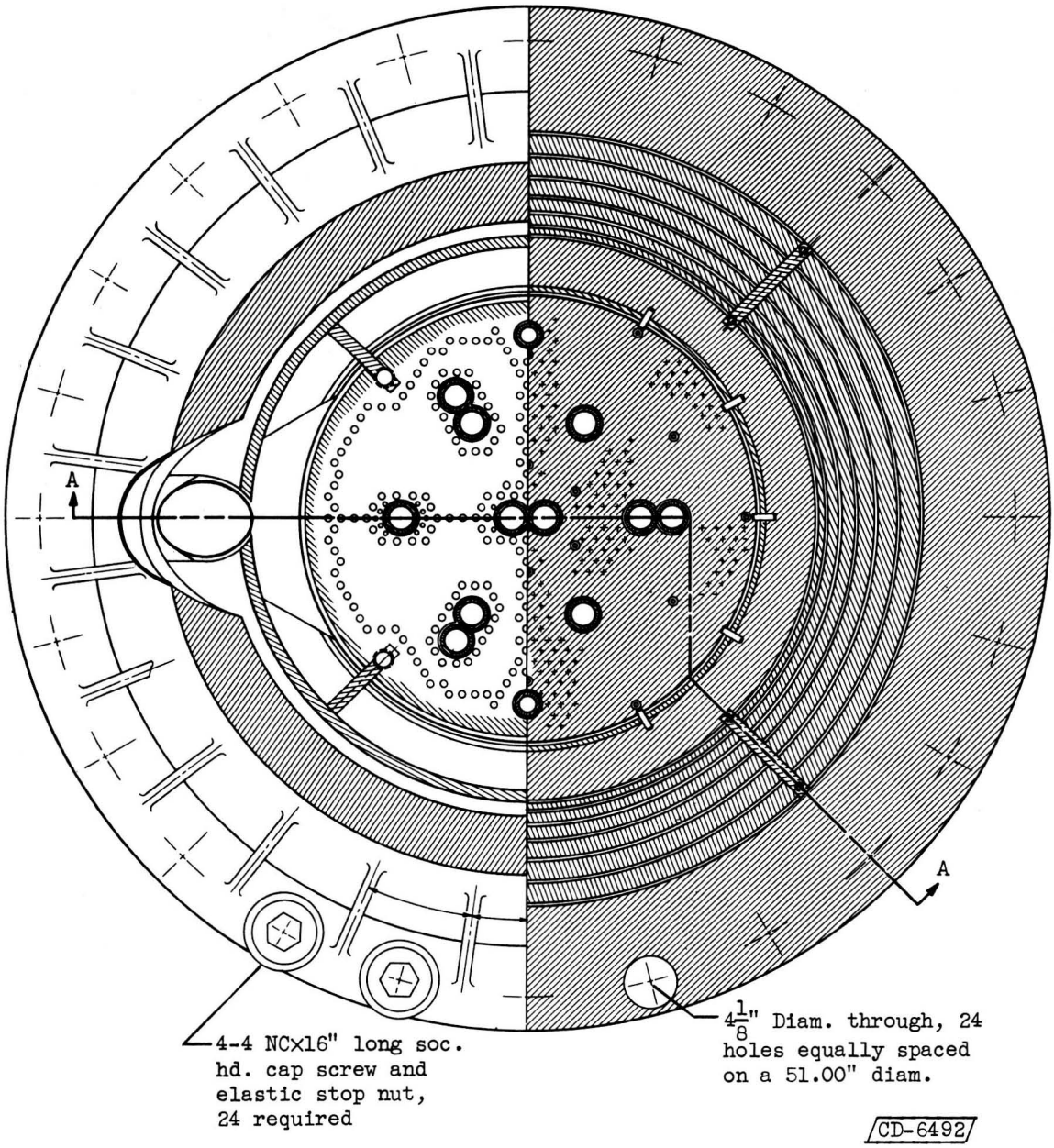

Figure 52. - Section B-B of figure 5.

SECRET

Declassified 1-24-1963

Declassified 1-24-1963

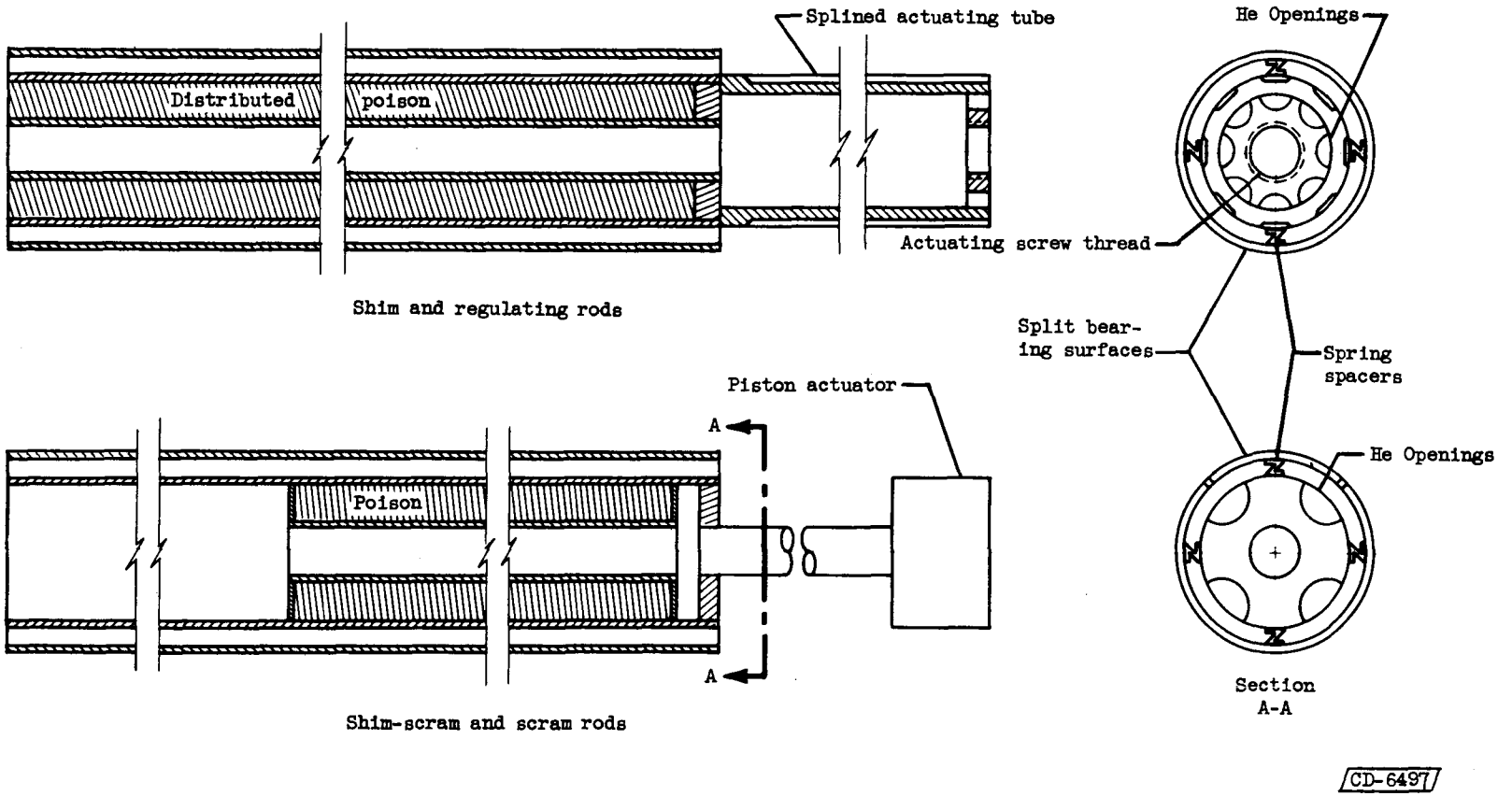

Figure 53. - Control-rod details.

Declassified 1-24-1963

Declassified 1-24-1963

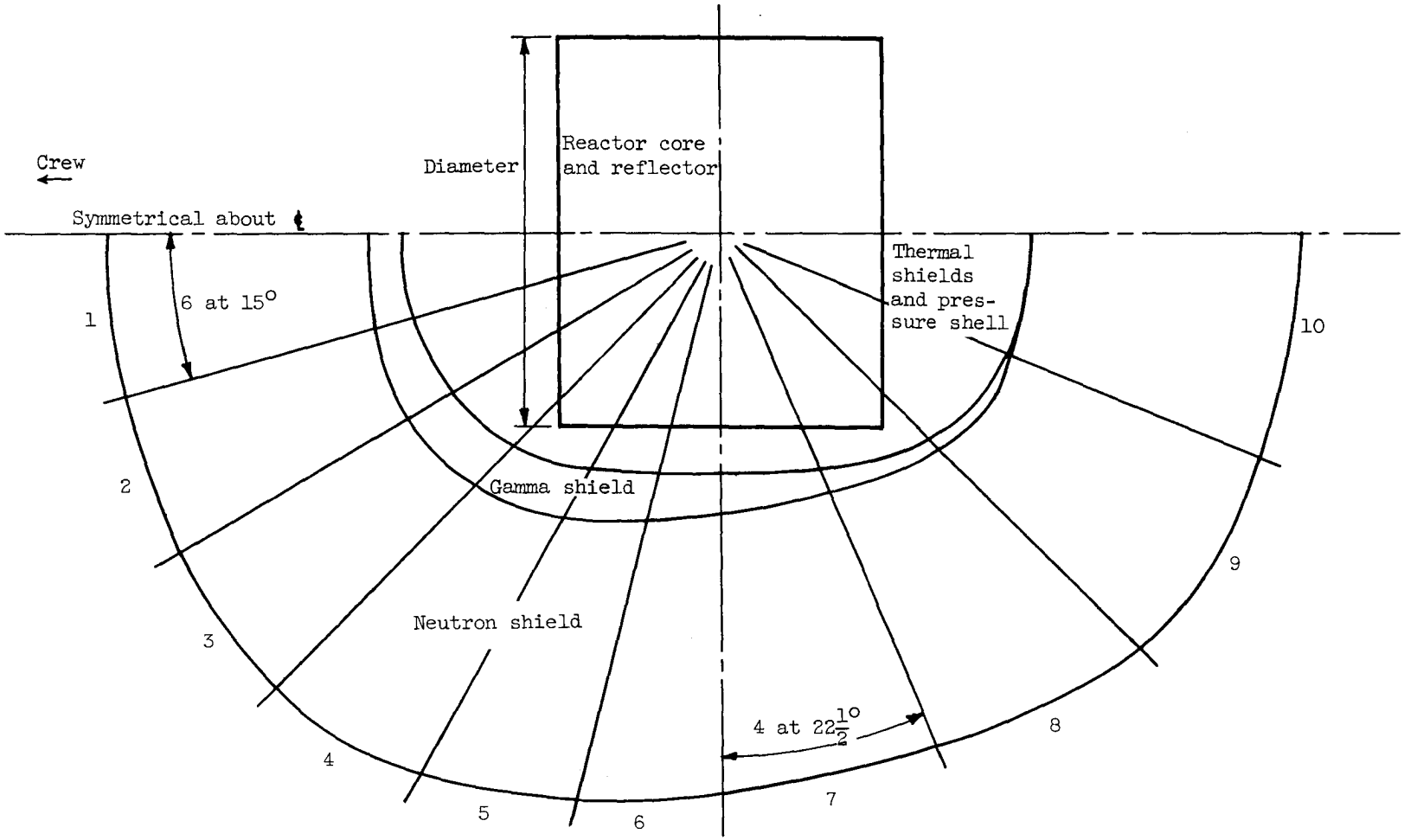

Figure 54. - Schematic elevation showing shaping of biological shield.

SECRET

Declassified 1-24-1963

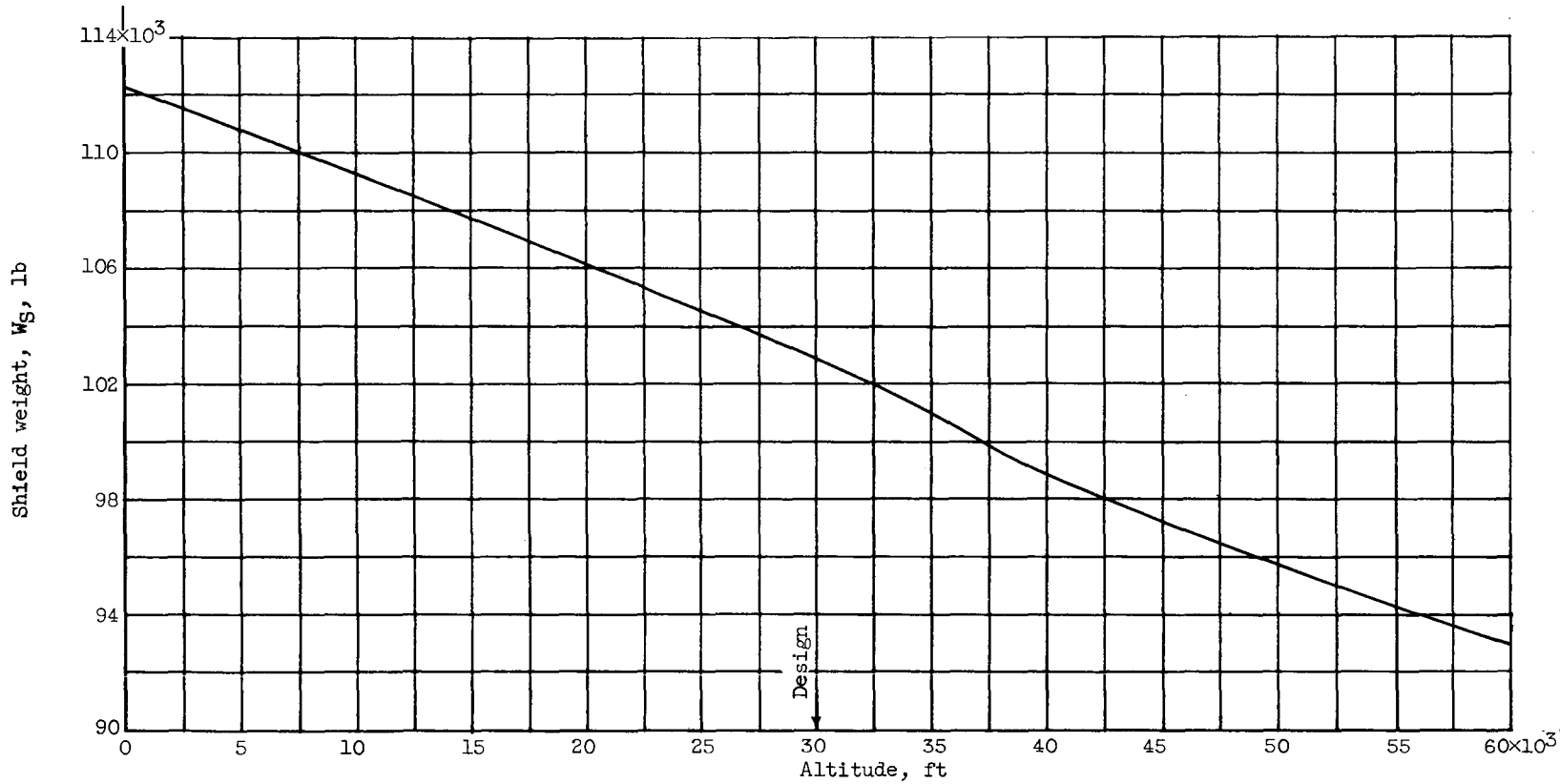

Figure 55. - Variation in shield weight with altitude. Reactor power, 100 megawatts; dose rate, 0.025 rem per hour at 100-foot distance. (Additional weights for streaming, voids, and cooling not included.)

Declassified 1-24-1963

Declassified 1-24-1963

Declassified 1-24-1963

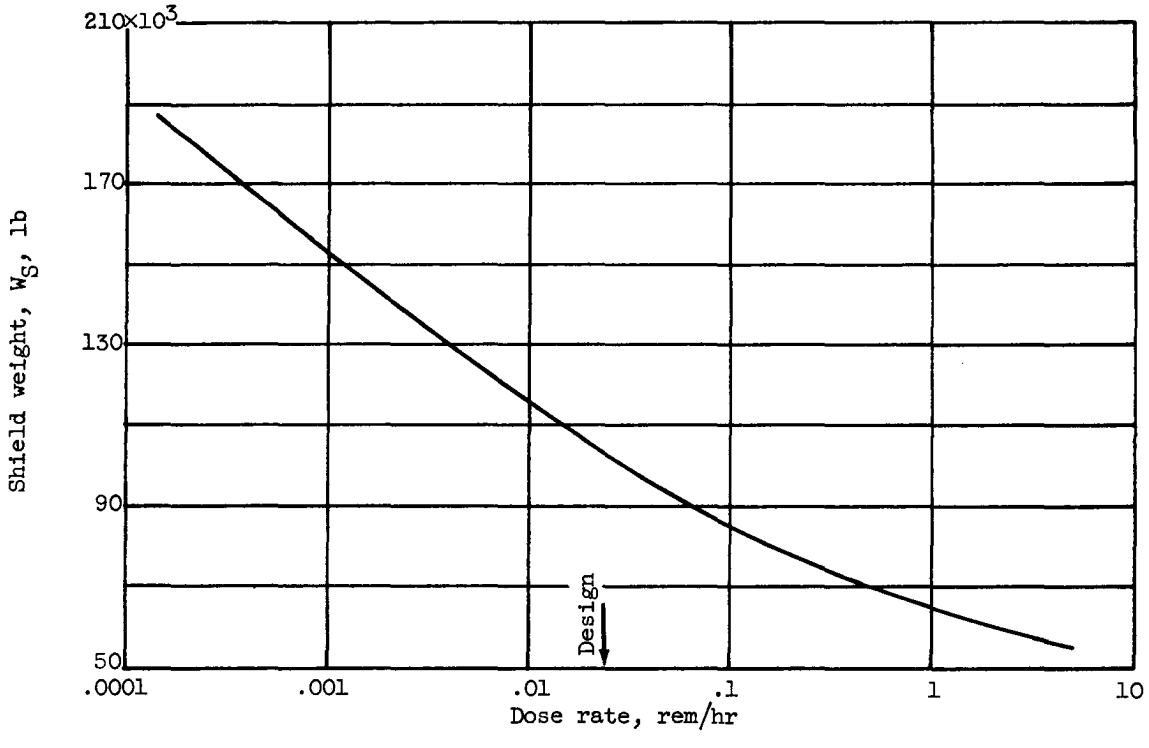

Figure 56. - Variation of shield weight with dose rate at 100-foot distance. Altitude, 30,000 feet; reactor power, 100 megawatts. (Additional weights for streaming, voids, and cooling not included.)

Declassified 1-24-1963

Declassified 1-24-1963

E-288

CA-30 back

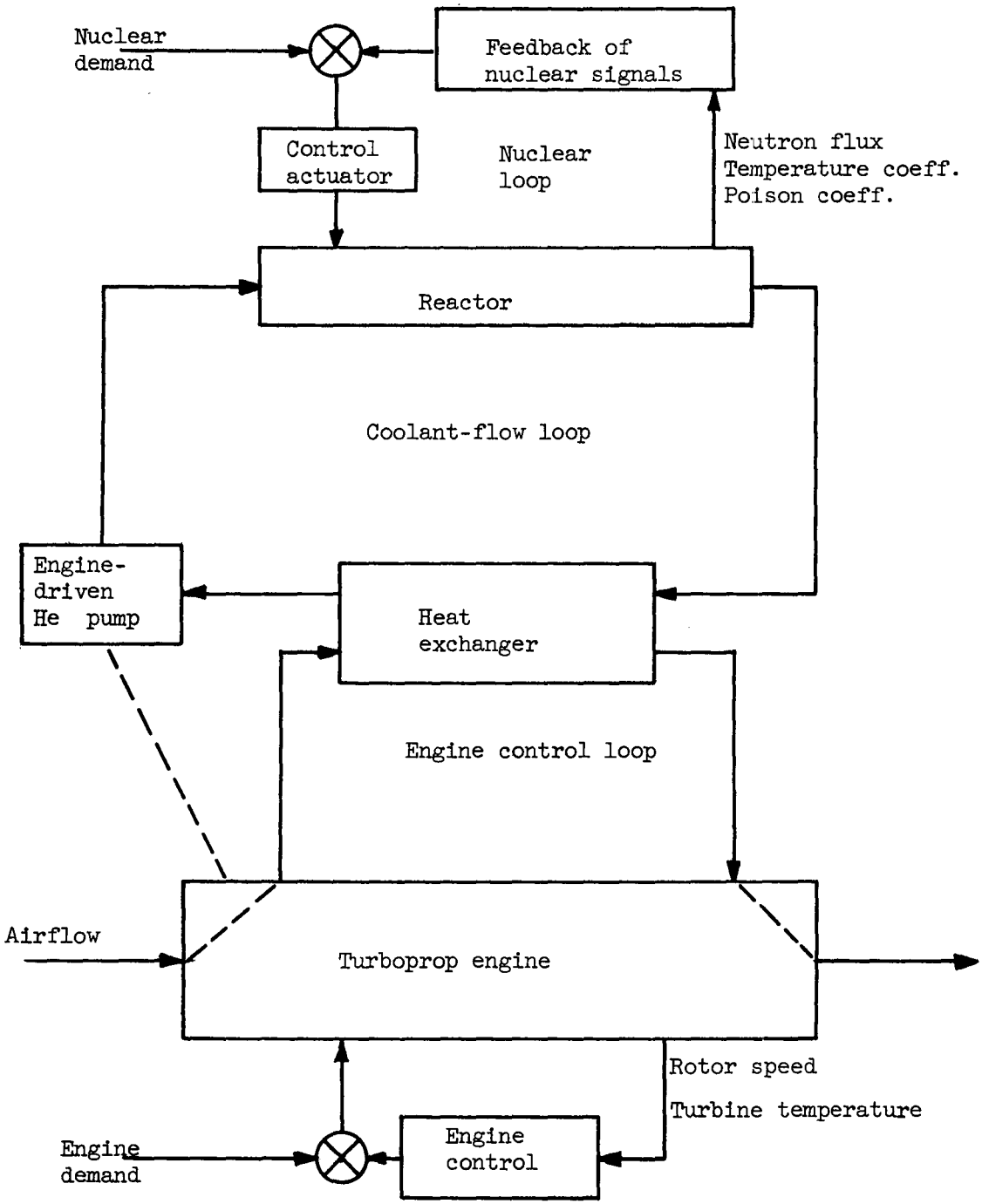

Figure 57. - Block diagram of basic nuclear-powered turboprop control loops.

Declassified 1-24-1963

Declassified 1-24-1963

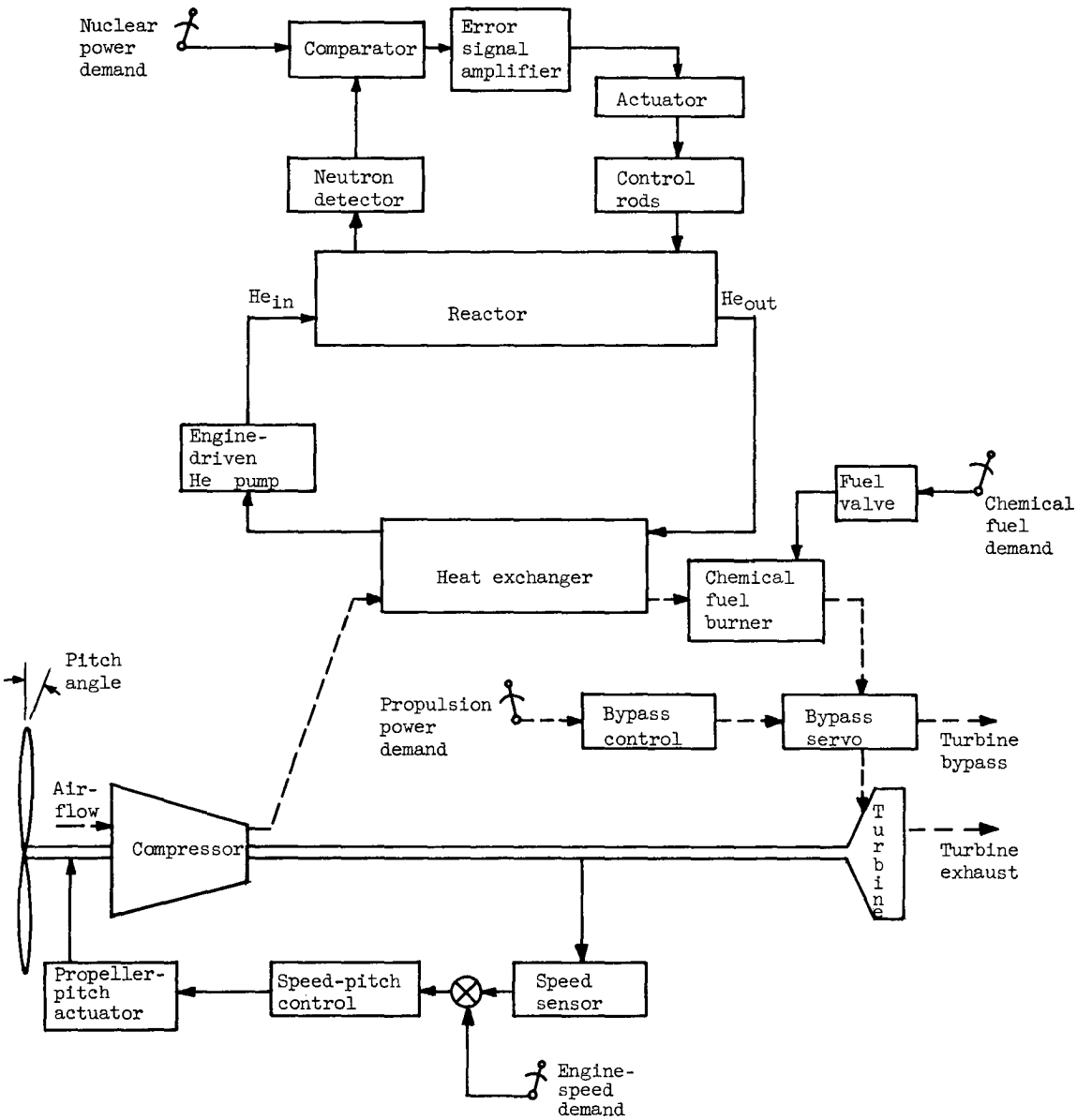

Figure 58. - Turboprop control scheme utilizing turbine bypass power modulation.

Declassified 1-24-1963

Declassified 1-24-1963

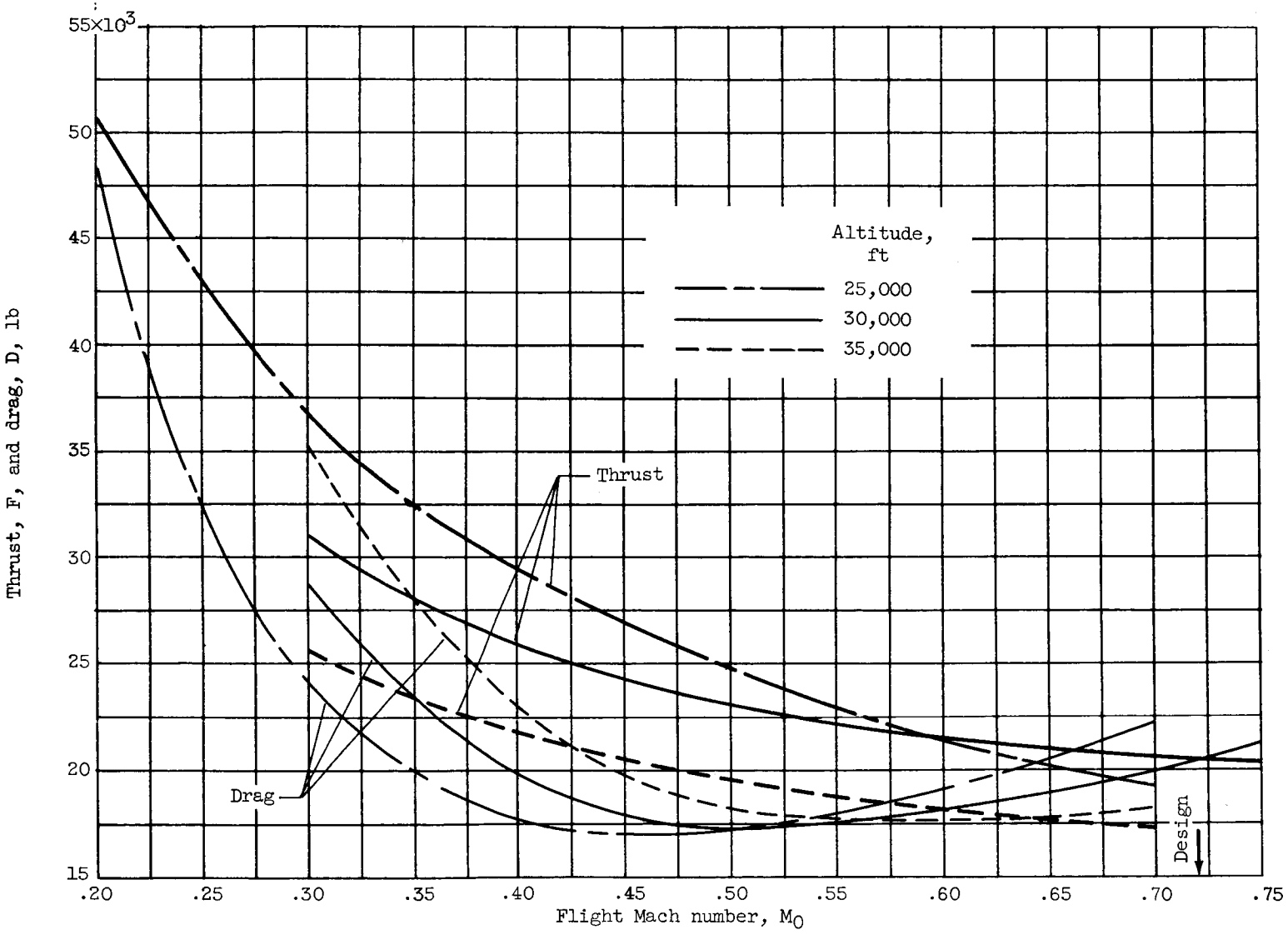

Figure 59. - Variations of thrust and drag with Mach number and altitude.

Declassified 1-24-1963

Declassified 1-24-1963

SECRET

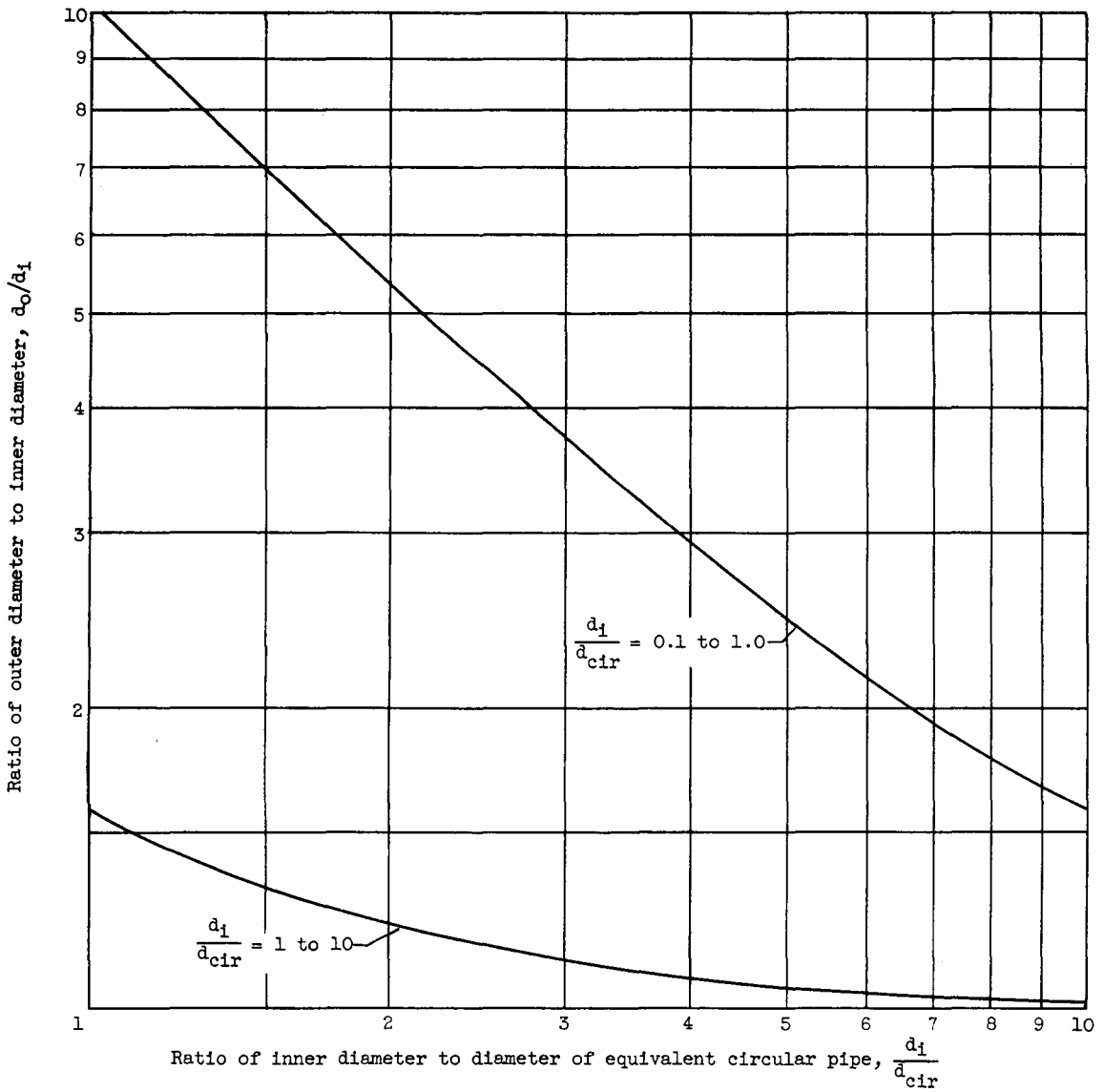

Figure 60. - Curve used to determine sizes of concentric lines (eq. (C27)).

SECRET

Declassified 1-24-1963

Declassified 1-24-1963

E-288

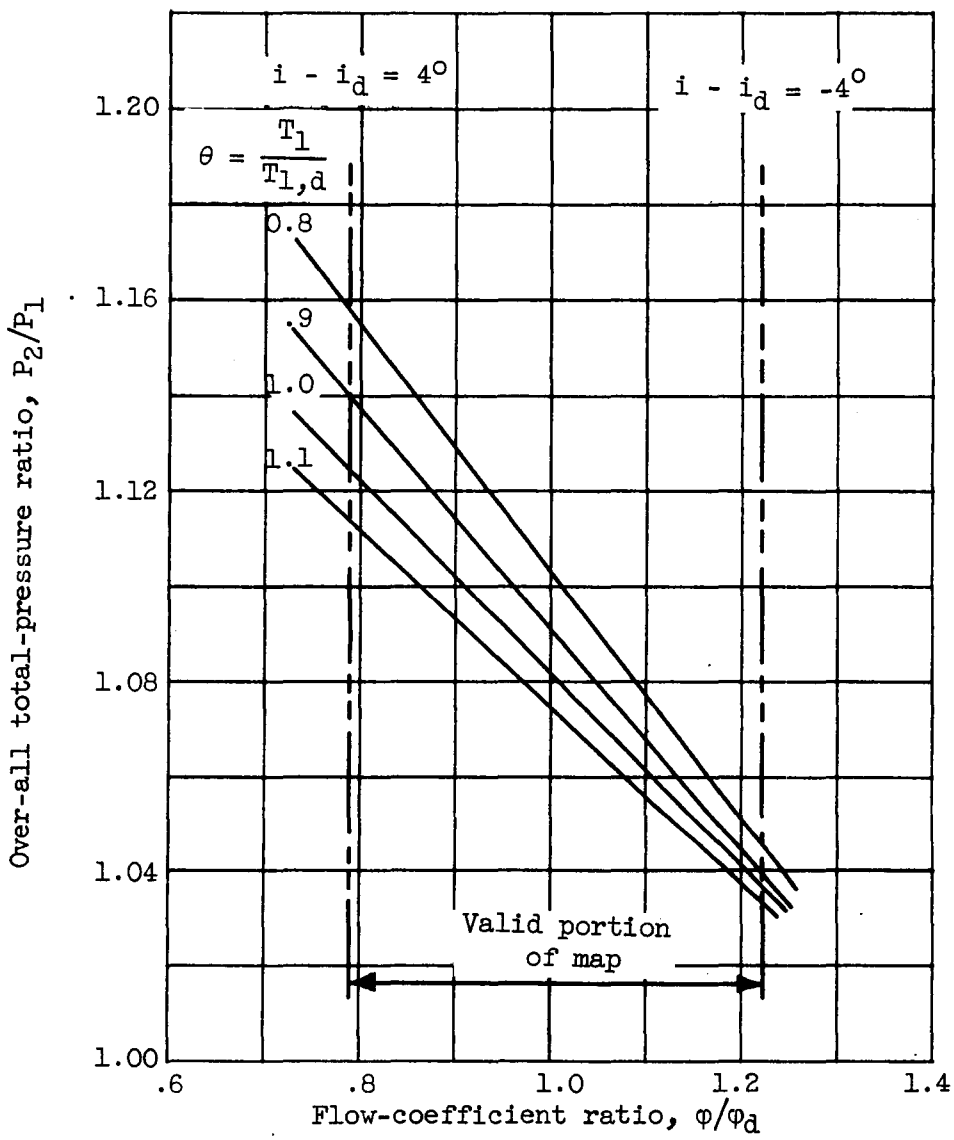

Figure 61. - Estimated performance map of axial-flow helium pump assuming operation at constant actual blade speed.

Declassified 1-24-1963

Declassified 1-24-1963

SECRET

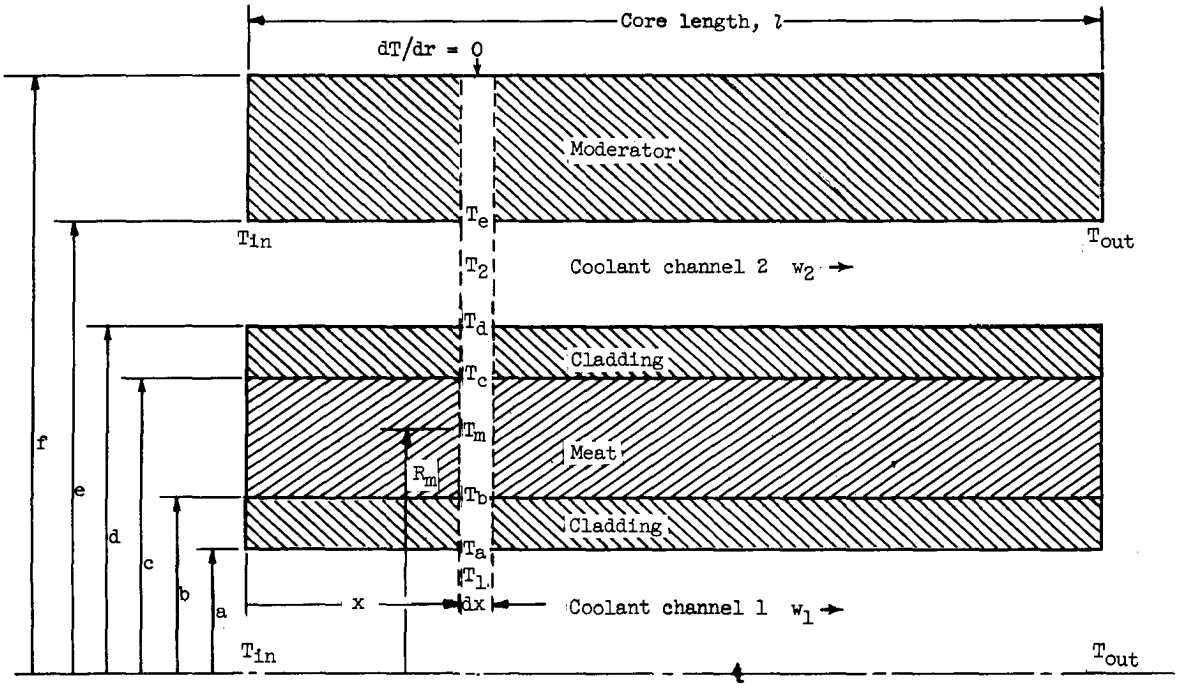

Figure 62. - Axial cross section of fuel element.

Declassified 1-24-1963

SECRET

Declassified 1-24-1963

E-288

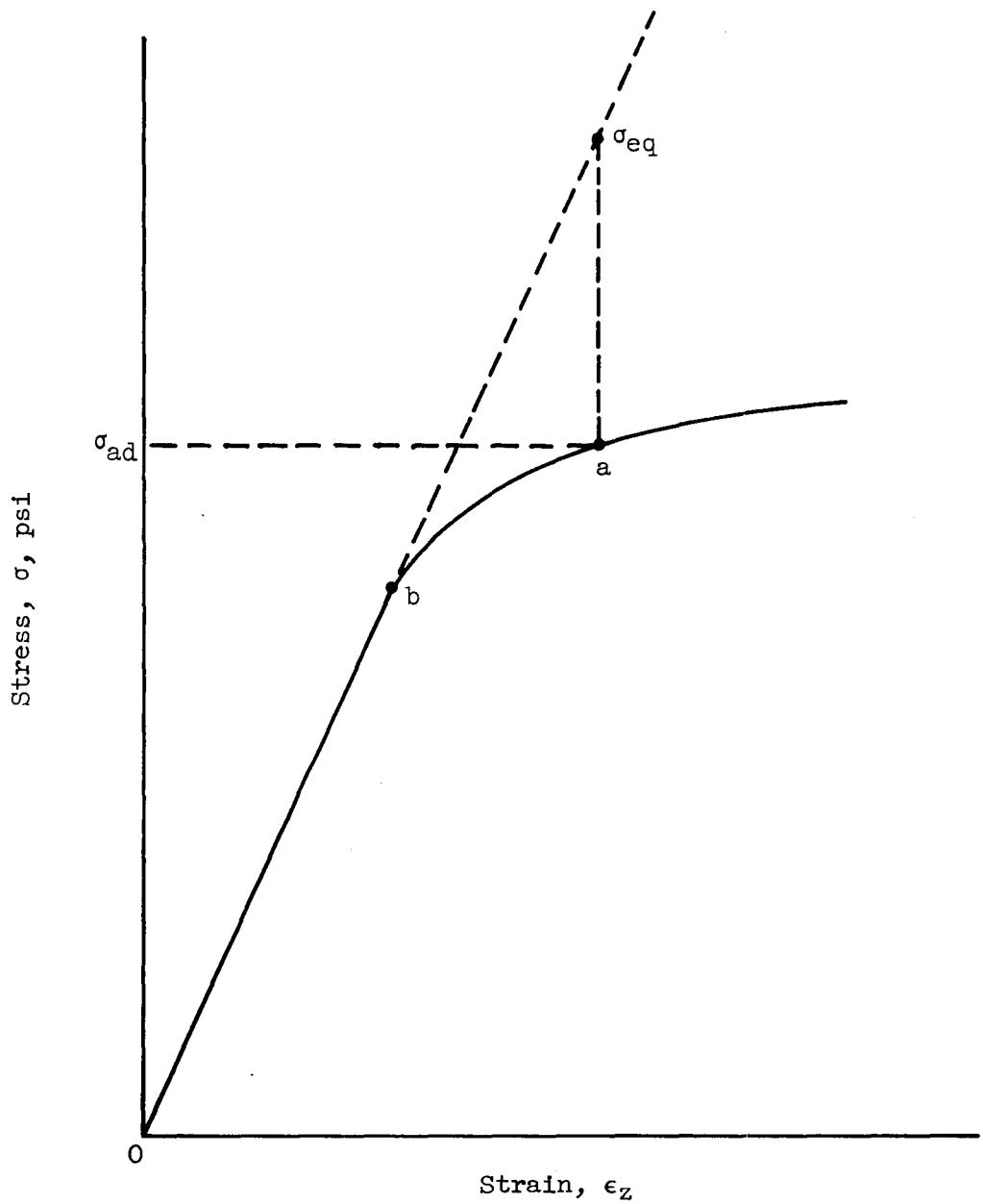

Figure 63. - Illustration of method of determining adjusted equivalent stress σ_{ad}.

Declassified 1-24-1963

Declassified 1-24-1963

SECRET

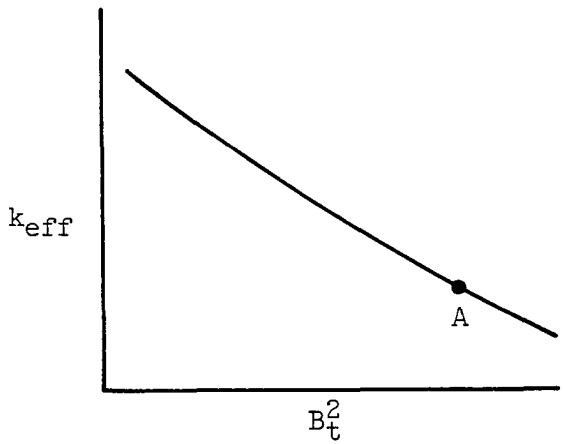

(a) Results from constants program for core.

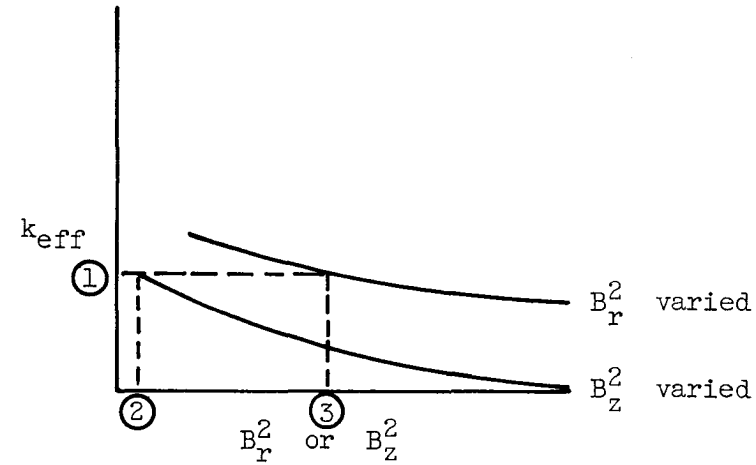

(b) Results from diffusion-theory program.

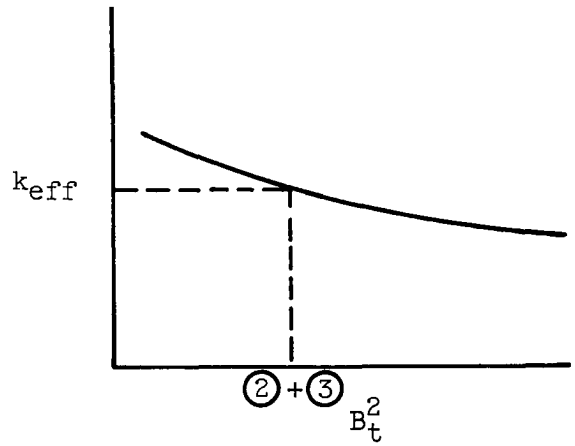

(c) Combined results.

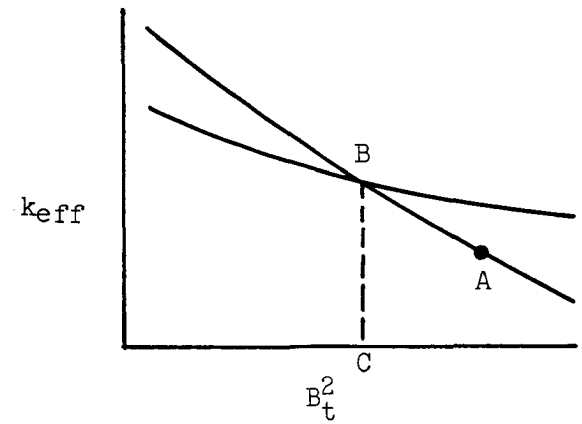

(d) Final curves.

Figure 64. - Method of determining effective multiplication factor k_{eff}.

Declassified 1-24-1963

SECRET

Declassified 1-24-1963

E-288

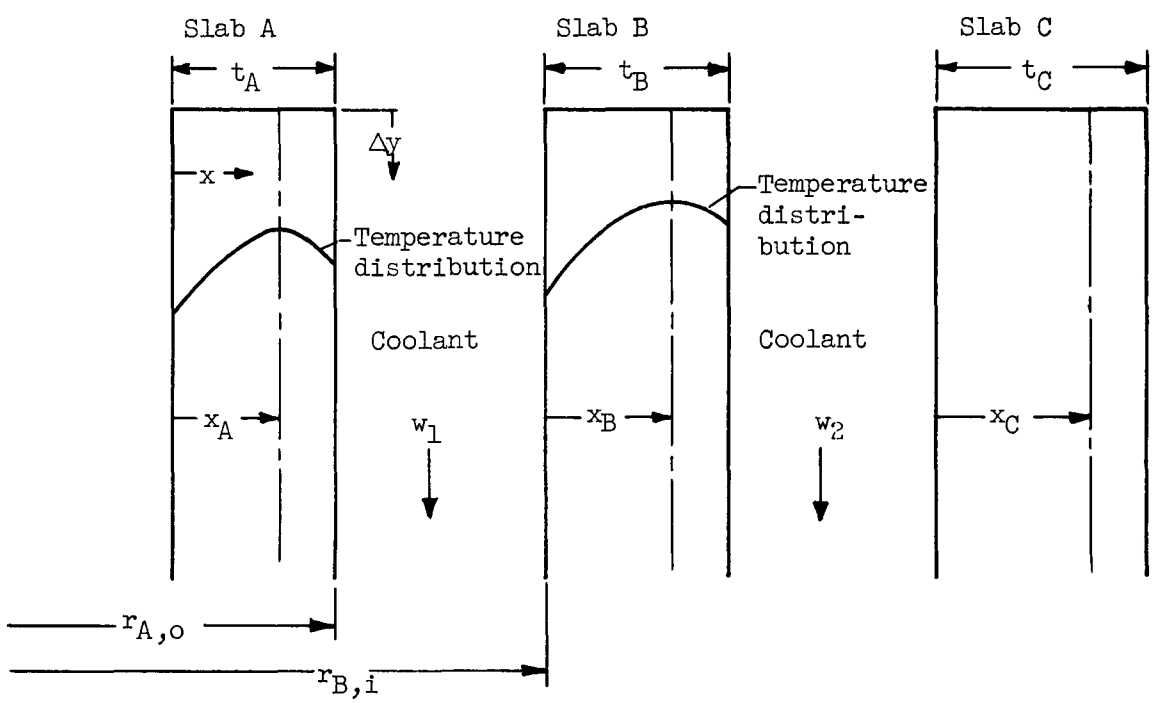

Figure 65. - Schematic cross section of thermal shield.

Declassified 1-24-1963

Declassified 1-24-1963

SECRET

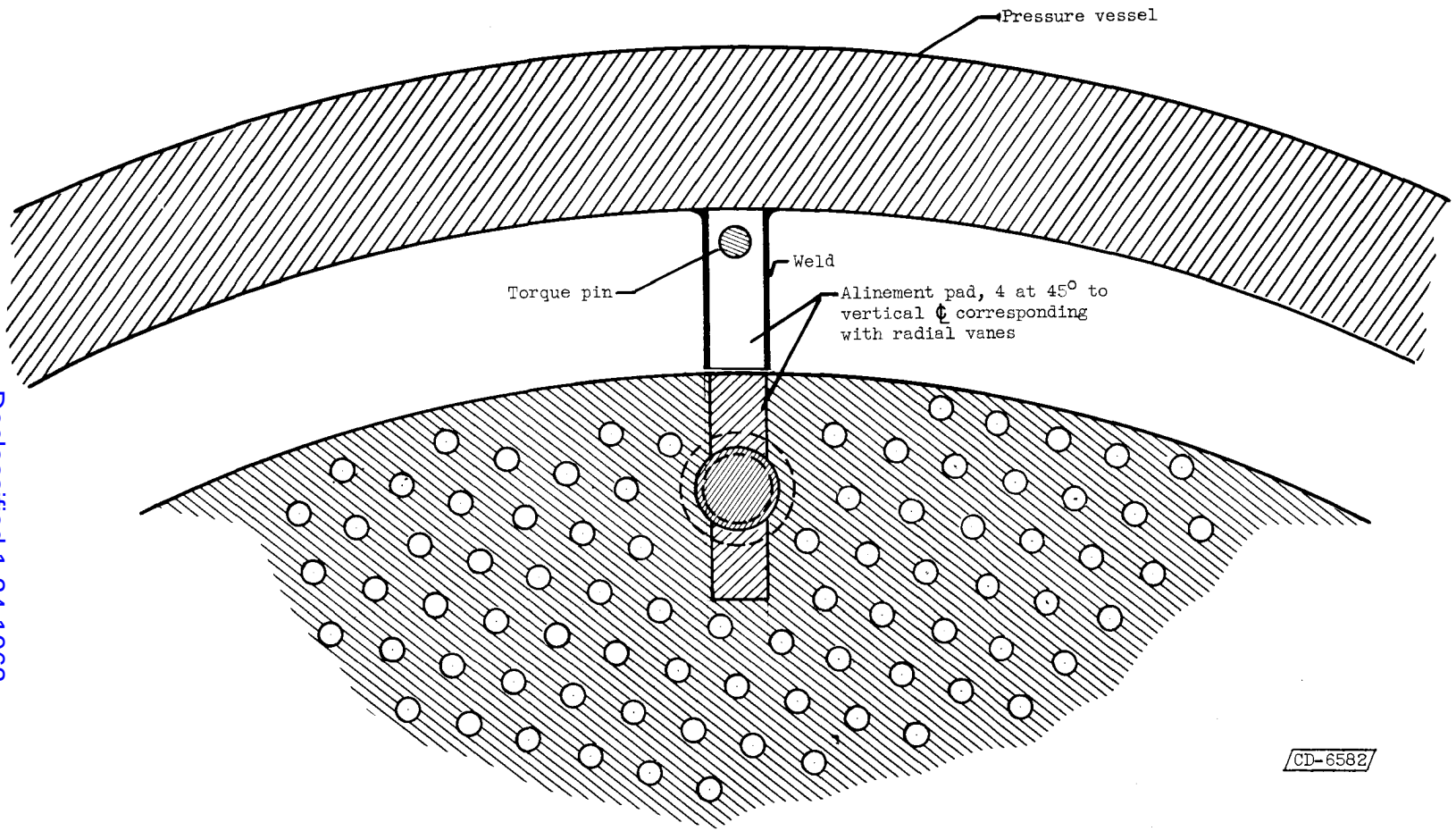

Figure 66. - Section F-F of figure 5.

Declassified 1-24-1963

SECRET

Declassified 1-24-1963

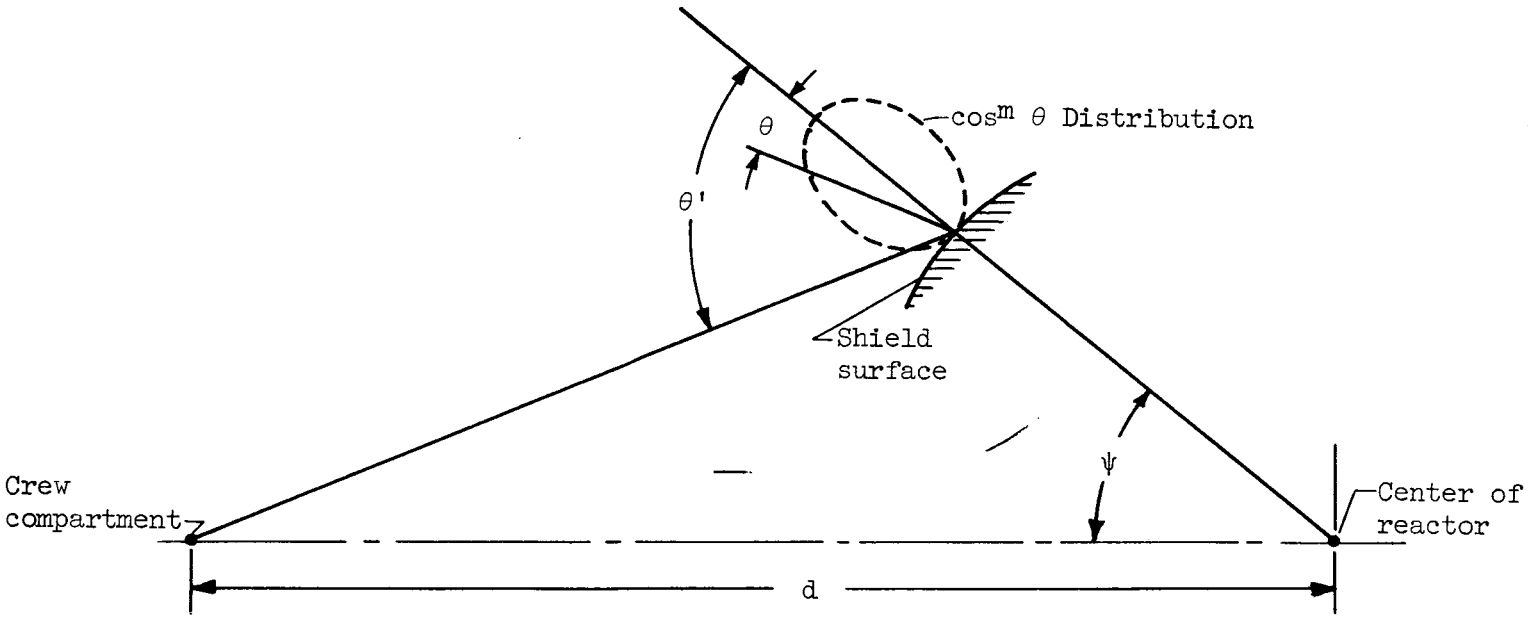

Figure 67. - Sketch used in determining direct neutron dose rate at detector.

Declassified 1-24-1963

CLASSIFICATION CANCELLED

SECRET

SEP 19 1963

CLASSIFICATION CANCELLED

SECRET